Adduct Compounds of late transition metal halides with arseno-chalcogenide cage molecules

Dissertation

zur Erlangung des Doktorgrades
der Naturwissenschaften (Dr. rer. nat.)
der Fakultät für Chemie und Pharmazie
der Universität Regensburg

vorgelegt von

Salil Bal

aus Pune / Indien

August 2022

Dedicated to my parents

From the Unreal to the Real!
From the Darkness to the Light!
From Death to Immortality!

Aus dem Unwirklichen zum Wirklichen!
Aus der Dunkelheit zum Licht!
Vom Tod zur Unsterblichkeit!

Brihadaranyaka Upanishad (1.3.28)

Acknowledgement

The experimental work presented here was carried out between September 2019 and May 2022 at the chair of Professor Arno Pfitzner at the Institute of Inorganic Chemistry, University of Regensburg.

The making of the present work would have not been possible without the help and support of many people.

Prof. Dr. Arno Pfitzner for giving me the opportunity to carry out this work, the freedom to choose the topic, the discussions, and numerous friendly conversations, even outside the daily work routine. Thank you so much for always having an open ear and supervising me through this journey.

Dr.Marc Schlosser for always being there for discussions, for the help in all questions regarding powder X-ray diffraction. Thank you for the help in organising the graduate and undergraduate practical courses and lab courses.

Ms.Bianca Frömel and Mrs.Katharina Trögl – a big thank you for the help from the very beginning and many conversations during the coffee breaks.

Dr. Michael Bodensteiner, Ms.Birgit Hischa, Ms .Sabine Stempfhuber as well as the staff of the ZA-X-ray of the University of Regensburg for the good cooperation in organising the measuring time at the single crystal diffractometer.

Mrs.Ulirike Schießl for helping me out with so many samples for thermal analysis and electron microscopy. Thank you for the many friendly conversations even outside work routine.

Mr. Florian Truksa – Thank you so much Flo for the great willingness to always help and for the support with many different problems. Also thank you for the many friendly discussions.

Dr. Christian Klimas and Dr. Christoph Meier for their great support and help at the start and during the experimental work.

Dr. Ria Mandal and Dr. Igor Plokhikh for their support and always having an open mind for discussions.

Dr. Christoph Meier, Ms. Susan Rank and Mr. Michael Kulschar for being so nice to share laboratory with.

Special thanks to Dr. Gabor Balaz and Ms. Lisa Zimmerman for their time and effort in organising the setup for Raman spectroscopy.

All students whose bachelor's theses and research projects I supervised contributed to the success of this work, for their preparative support.

To all other current and former members of Prof. Dr. Arno Pfitzner's chair for the great atmosphere, the entertaining coffee rounds, and the pleasant working day: Dr. Clauidia De Giorgi, Dr. Maximilian Sehr, Dr.Florian Wisser, Dr. Florian Pielnhofer, Dr. Sebastian Faeth, Mr. Maximillian Obermeier, Mr. Philip Schmid, Mr. Florian Wegner, Ms. Franziska Kamm, Mr. Rafal Samp, Mr. Martin Schmid, Mr.Ferninand Gigl, Mr. Sven Schedlowski, Mr. Martin Rosenhammer, Ms. Elisabeth Huf, Mr. Julian Schiller, Mr. Michael Stammler, Ms. Lea Huber, Ms. Daniela Garcia, Ms. Heidi Paulus, Ms. Elisabeth Bauer.

My very special thanks go to my mother, Smita Bal, who supported me in all situations and always gave me good advice and my brother, Sumeet Bal, without their support this work would not have been possible.

Eidesstattliche Erklärung

Ich erkläre hiermit an Eides statt, dass ich die vorliegende Arbeit ohne unzulässige Hilfe Dritter und ohne Benutzung anderer als der angegebenen Hilfsmittel angefertigt habe. Die aus anderen Quellen direkt oder indirekt übernommenen Daten und Konzepte sind unter Angabe des Literaturzitats gekennzeichnet. Die Arbeit wurde bisher weder im In- noch im Ausland in gleicher oder ähnlicher Form einer anderen Prüfungsbehörde vorgelegt. Ich versichere an Eides statt, dass ich nach bestem Wissen die reine Wahrheit gesagt und nichts verschwiegen habe.

I hereby confirm that I have completed this thesis independently; that I have used only those sources and aids cited; and that I have not already submitted the work to another university to obtain an academic degree.

Regensburg den

Salil Bal

This work was supervised by Prof. Dr. Arno Pfitzner

Submission of doctoral application:

Date of oral examination:

Examination Committee:

Chairman	Prof. Dr. Alkwin Slenczka
1. Reviewer	Prof. Dr. Arno Pfitzner
2. Reviewer	Prof. Dr. Richard Weihrich (University of Augsburg)
Further examiner	Prof. Dr. Frank-Michael Matysik

Abstract

The main aim of this thesis was the synthesis of new adduct compounds of late transition metal halides with pnicogen chalocogenide cage molecules, PnQ_x , where Pn = As, *Q* = S/Se, n = 3/4. It is an established fact that the pnicogen chalocogenide cages have a tendency to disintegrate when coordinated to transition metal halide matrix. In this work we were able to synthesise adduct compounds via solid state synthesis and hydrothermal synthesis in which the pnicogen chalocogenide cages remain intact. Furthermore, we were the first to synthesize adduct compounds of Ag*X* (*X* = Cl/Br/I) with molecular As_4S_4 cages. Noteworthy here was the fact that silver does not show any special preference towards As and S/Se, thus presenting a rare example of compound containing Ag-As bond. The adduct chemistry of Cu*X* (*X* = Br/I) was taken a step further by synthesising new adduct compounds with As_4S_4 and As_4Se_3.

Three new host/guest compounds, viz $(CuI)_7(MI_2)_3(As_4Se_3)$, *M* = Zn/Cd/Hg were synthesised. These are similar to a known family of compounds $(ZnI2)_6(ZnS)(P_4S_x)$ and $Cd_7I_{12}S\cdot(As_4S_x)$ and hence show structural similarity. These are adduct compounds where highly disordered As_4Se_3 cage molecules are embedded in a CuI matrix connected through MI_4 tetrahedron.

In the last part of the thesis we report two new compounds – In $[(Hg_2I_6)\ (HgI_2)][Cu(MeCN)_4]_2$ we see both the polymorphs of HgI_2, the red and the meta-stable yellow in a matrix of Cu-MeCN. Cu_2AsS_2I was a synthesised via solvothermal synthesis and presents copper in both tetrahedral and trigonal coordination mode.

Abstrakt

Das Hauptziel dieser Arbeit war die Synthese neuer Adduktverbindungen von Halogeniden später Übergangsmetalle mit Pnicogen-Chalocogenid-Käfigmolekülen, As_4Q_x , Q = S/Se, x = 3/4. Es ist eine erwiesene Tatsache, dass die Pnicogen-Chalocogenid-Käfige dazu neigen, sich aufzulösen, wenn sie an eine Übergangsmetallhalogenid-Matrix koordiniert werden. In dieser Arbeit konnten wir Adduktverbindungen durch Festkörpersynthese und Hydrothermalsynthese synthetisieren, bei denen die Pnicogen-Chalocogenid-Käfige intakt bleiben. Darüber hinaus waren wir die ersten, die Adduktverbindungen von AgX (X = Cl/Br/I) mit molekularen $A_{s4}S_4$-Käfigen synthetisierten. Bemerkenswert war hier die Tatsache, dass Silber keine besondere Präferenz gegenüber As und S/Se zeigt, wodurch ein seltenes Beispiel für eine Verbindung mit Ag-As-Bindung präsentiert wird. Die Adduktchemie von CuX (X = Br/I) wurde einen Schritt weitergeführt, indem neue Adduktverbindungen mit As_4S_4 und As_4Se_3 synthetisiert wurden.

Drei neue Einschlussverbindungen, nämlich $(CuI)_7(MI_2)_3(As_4Se_3)$, M = Zn/Cd/Hg, wurden synthetisiert. Diese ähneln einer bekannten Familie von Verbindungen $(ZnI2)_6(ZnS)(P_4S_x)$ und $Cd_7I_{12}S\cdot(As_4S_x)$ und zeigen daher strukturelle Ähnlichkeiten. Dies sind Adduktverbindungen, bei denen hoch fehlgeordnete As_4Se_3-Käfigmoleküle in eine CuI-Matrix eingebettet sind, die durch einen MI_4-Tetraeder verbunden ist.

Im letzten Teil der Arbeit berichten wir über zwei neue Verbindungen – In $[(Hg_2I_6)(HgI_2)][Cu(MeCN)_4]_2$ sehen wir beide Polymorphe von HgI_2, das Rot und das metastabile Gelb in einer Matrix aus Cu-MeCN. Cu_2AsS_2I wurde durch Solvothermalsynthese synthetisiert und präsentiert Kupfer sowohl im tetraedrischen als auch im trigonalen Koordinationsmodus.

Table of Contents

1. Introduction ……1

2. Experimental ……4

2.1 Starting Materials ……4

2.1.1 Purification of elemental arsenic ……4

2.1.2 Synthesis of realgar (As_4S_4) …… 4

2.1.3 Synthesis of As_4Se_3 and As_4Se_4 ……5

2.1.4 Purification of Cu(I) halides ……5

2.1.5 Used Chemicals …….. 6

2.2 Preparation Methods ……7

2.2.1 Preparation in ampoules ……7

2.2.2 Solvothermal Synthesis ……7

2.3 Characterisation Methods ……8

2.3.1 X- Ray Powder Diffraction ……8

2.3.2 Single Crystal X- Ray Diffraction ……10

2.3.3 Raman Spectroscopy ……12

2.3.4 UV Visible Spectroscopy ……13

2.3.5 Scanning Electron Microscopy/EDX ……14

2.3.6 Thermal Analysis ……15

2.3.7 Impedance Spectroscopy ……15

3. Adduct compounds of As_4S_4 with Ag*X* and Cu*X* (*X*= Cl/Br/I) 17

3.1 Literature Overview and Theoretical Aspects 17

3.2. Adduct compounds of As_4Q_n with Ag*X* and Cu*X* (*X* = Cl/Br/I, *Q* = S/Se, n = 3/4) 23

3.2.1 The Adduct $(AgI)_2 \cdot (As_4S_4)$ 23

3.2.1.1 Synthesis 23

3.2.1.2 Single Crystal X- Ray Diffraction Analysis 24

3.2.1.3 Powder X -Ray Diffraction Analysis 32

3.2.1.4 SEM and EDX Analysis 35

3.2.1.5 Raman Spectroscopy 36

3.2.1.6 UV Visible Spectroscopy 38

3.2.1.7 Thermal Analysis 39

3.2.1.8 Impedance Spectroscopy 40

3.2.1.9 Structural aspects and reactivity of As_4S_4 as neutral ligand 42

3.2.2 The Adduct $(AgI)_2 \cdot (As_4Se_4)$ 43

3.2.2.1 Synthesis 43

3.2.2.2 Single Crystal X- Ray Diffraction Analysis 43

3.2.2.3 SEM and EDX Analysis 52

3.2.3 The Adduct $(AgBr) \cdot (As_4S_4)$ 54

3.2.3.1 Synthesis 54

3.2.3.2 Single Crystal X- Ray Diffraction Analysis 55

3.2.3.3 Powder X -Ray Diffraction Analysis 64

3.2.3.4 UV Visible Spectroscopy 65

3.2.2.5 Thermal Analysis 67

3.2.4 The Adduct $(AgCl)\cdot(As_4S_4)$ 68

3.2.4.1 Synthesis 68

3.2.4.2 Single Crystal X- Ray Diffraction Analysis 69

3.2.5 The Adduct $(CuI)_3\cdot(As_4S_4)$ 79

3.2.5.1 Synthesis 79

3.2.5.2 Single Crystal X- Ray Diffraction Analysis 80

3.2.5.3 Powder X -Ray Diffraction Analysis 88

3.2.5.4 SEM and EDX Analysis 88

3.2.6 The Adduct $(CuBr)_2\cdot(As_4S_4)$ 90

3.2.6.1 Synthesis 90

3.2.6.2 Single Crystal X- Ray Diffraction Analysis 90

3.2.6.3 SEM and EDX Analysis 98

3.2.7 The Adduct $(CuBr)_2\cdot(As_4Se_3)$ 100

3.2.7.1 Synthesis 100

3.2.7.2 Single Crystal X- Ray Diffraction Analysis 100

3.2.7.3 SEM and EDX Analysis 108

4. Host/Guest Compounds 110

4.1 Introduction 110

4.2 The Adducts $(CuI)_7(MI_2)_3(As_4Se_3)$, *M* = Zn/Cd/Hg 110

4.2.1 Synthesis 110

4.2.2 Single Crystal X- Ray Diffraction Analysis 112

4.2.3 SEM and EDX Analysis 118

5. Serendipitous Compounds 120

5.1 The Compound $[(Hg_2I_6)(HgI_2)][Cu(MeCN)_4]_2$ 122

5.1.1 Introduction 122

5.1.2 Synthesis 122

5.1.3 Single Crystal X- Ray Diffraction Analysis 123

5.2 The Compound Cu_2AsS_2I 125

5.2.1 Synthesis 128

5.2.2 Single Crystal X- Ray Diffraction Analysis 128

5.2.3 SEM and EDX Analysis 132

6. Summary and Outlook 132

7. References 134

8. Appendix 144

1.Introduction

Solid state chemistry deals with the synthesis and characterisation of new inorganic materials, along with investigation and optimisation of the physical properties[1]. As an interdisciplinary science it lies at the interface of chemistry, physics, and materials science. The classical solid-state reaction (solid-solid reaction) involves heating finely powdered and homogeneous starting compounds to high temperatures which leads to product which is thermodynamically more stable[2,3]. However, the main concern in this route is the large amount of reaction time required, which is the direct consequence of the extremely slow diffusion rate of the atoms or ions in solid state. Reactions are found to run quicker when they are carried out in melt conditions. Here, either the starting compounds are melted, or a flux is employed in which the starting compounds are soluble. The reaction conditions are then similar to that of solution state chemistry. This leads in a multi-fold increase in the reaction rate. Another method is the solvothermal synthesis. Here, the starting compounds are reacted together with a suitable solvent in a closed container. The temperature of the reaction is in the supercritical region of the concerned solvent, and hence a high pressure is created in the container. Under these solvothermal conditions, the otherwise not so soluble starting compounds are soluble as complexes in the solvent[4]. Further commonly used method which try to address the problem of slow diffusion in the solid-state chemistry are reactions in the gas phase (the chemical transport reactions) or the precursor method[5,6]. Here, the thermally labile precursor decomposes at relatively low temperatures with product formation. A very useful advantage of this low temperature route is the access to the otherwise labile thermodynamically metastable connections. Along with theses standard methods there are also methods which are developed to cater the needs of individual cases. Thus, the development of new synthesis routes often leads to the synthesis of entirely new compounds.

The word “adduct” comes from the latin word “*adducere*” which means bringing together or leading two individual entities together. Thus, adduct compounds can be visualized as compounds that are made up of two distinct sub-structures and thus having two distinct subunits. Therefore, these compounds are often also known as “nanocomposites”.

Adduct compounds have been the area of active research since many years. Based on the works of Milius and Rabenau[7], Möller and Jeitschko[8] and Pfitzner and Freudenthaler[9] a

whole series of adduct compounds containing Cu(I) halides and neutral or low valent molecules of group 15 and 16 of the periodic table was synthesised and characterised. Interesting observation with this this approach is the characterisation of very unusual molecules or polymers, which were until then unknown in their free form. To this class belong the phosphorus polymer $_{\infty}^{1}[P_{12}]$ or $_{\infty}^{1}[P_{14}]$ in $(CuI)_3P_{12}$[9] and $(CuI)_2P_{14}$[10](See Figure 1.1), the conventionally not accessible cage molecule β-P_4Se_4 which is stabilised in the $(CuI)_3 \cdot P_4Se_4$ adduct compound[11] or the P_8Se_3 molecule in the adduct $(CuX)_2 \cdot P_8Se_3$ X = Br, I[12,13].

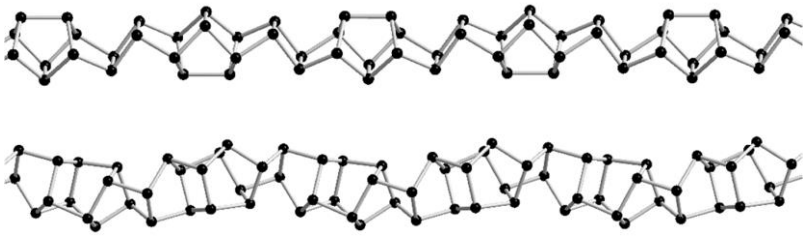

Figure 1.1: rods of phosphorus obtained after extraction of adduct compound $(CuI)_8P_{12}$ and $(CuI)_3P_{12}$.

A major reason for the success of this approach stems from the structural flexibility of Cu(I) ion exhibiting a plethora of structural motifs – the zig-zag chains, the columnar rod like variation, the split- chair chain. Thus, in a sense the Cu(I) halide matrix function as a "solid solvent" making a three-dimensional packing of the embedded molecule feasible.

In the previous dissertation, *Bräu*[14] and *Rödl*[15] was able to show that this synthetic approach can be generally applied to other transition metal halides also. Especially the iodides and bromides of the electron rich, soft d^{10} cations – Cu^{1+}, Au^{1+}, Zn^{2+}, Cd^{2+}, Hg^{2+}. They form adduct compounds with the soft pnictogen chalcogenides. Thus the Pearson concept of hard-soft acid bases probably could play a role to explain the overall reactivity, however this does not explain all of the previous observations[16].

The aim of the current work, in addition to synthesis and structural characterisation and elucidation of new adduct compounds, is to provide more insights into the comprehensive chemistry of this class of compounds. Characterisation was mainly carried by single crystal X-ray diffraction and powder X -ray diffraction. Other techniques viz. DTA, Raman spectroscopy, UV-Visible spectroscopy, Impedance spectroscopy and electron microscopy were also employed to get a comprehensive understanding of the bonding situation and structural dynamics.

The dissertation is structured as follows: Chapter 2 begins with the general information on the experimental procedure followed and the instruments used. Chapter 3 deals with the new adduct compounds of silver halides with arseno-chalcogenide cages. Along with that this chapter includes adduct compounds of copper halides with arseno-chalcogenide cages. Chapter 4 deals with the boracite type inclusion compounds of the type $(Pn_4Q_3)@Cu_7M_3I_{13}$, where Pn = As, Q= Se and M = Zn/Cd/Hg. Chapter 5 consists of two new compounds - Cu_2AsS_2I - an arsenic sulphide bridged by copper iodide and $[(HgI_2)_3]$ $[Cu(MeCN)_4]_2$.

Table 1.1: Overview of the synthesised compounds and the conditions for synthesis

Compound	Conditions for Synthesis
$(AgI)_2{\cdot}(As_4S_4)$	Solvothermal Synthesis – 160 °C, 5 days
	Solid State Synthesis – 220 °C, 14 days
$(AgI)_2{\cdot}(As_4Se_4)$	Solvothermal Synthesis – 160 °C, 5 days
$(AgBr){\cdot}(As_4S_4)$	Solvothermal Synthesis – 160 °C, 5 days
	Solid State Synthesis – 210 °C, 14 days
$(AgCl){\cdot}(As_4S_4)$	Solvothermal Synthesis – 160 °C, 5 days
	Solid State Synthesis – 210 °C, 14 days (no phase pure product)
$(CuI)_3{\cdot}(As_4S_4)$	Solvothermal Synthesis – 160 °C, 5 days
	Solid State Synthesis – 170 °C, 14 days (no phase pure product)
$(CuBr)_2{\cdot}(As_4S_4)$	Solvothermal Synthesis – 160 °C, 5 days
$(CuBr)_2{\cdot}(As_4Se_3)$	Solvothermal Synthesis – 160 °C, 7 days
$(Pn_4Q_3)@Cu_7M_3I_{13}$ Pn = As, Q= Se, M =Zn/Cd/Hg	Solid State Synthesis, tempering for 2 weeks followed by several weeks after grinding.
$[(Hg_2I_6)(HgI_2)][Cu(MeCN)_4]_2$	Solvothermal Synthesis – 160 °C, 5 days (Step 1)
	Crystallisation in MeCN – 16 weeks
Cu_2AsS_2I	Solid State Synthesis – 170 °C, 14 days

2. Experimental

2.1. Starting Materials

2.1.1 Purification of elemental Arsenic

Elemental arsenic often contains As_2O_3 as an impurity which needs to be got rid of before any further use. This is conveniently done by sublimation method. Arsenic is filled in a Schlenk tube and evacuated and put in an oven with a temperature gradient. The oven is heated to 300° C for 3 days. The fact that arsenic sublimes at 616 °C while As_2O_3 at 313 °C is taken to advantage. Thus, white As_2O_3 sublimates on the colder end while pure arsenic remains at the hot end yield a physical separation of the arsenic from its oxide. This pure arsenic was employed for further synthesis.

Figure 2.1.1: Purification of arsenic: Purchased arsenic was purified by sublimation in a Schlenk tube – pure arsenic is seen on the right-hand side while sublimated As_2O_3 is seen on the left-hand side.

2.1.2 Synthesis of As_4S_4

As_4S_4 (Realgar) was synthesized by high temperature synthesis in evacuated quartz ampoules. Elemental arsenic and sulphur were melted together at 350 °C and kept at this temperature for 1 day to get an orange melt. The melt was tempered at 300 °C for 4 days. The amorphous mass was filled in a Schlenk flask and evacuated and put in an oven at 300 °C with a temperature gradient. Pure As_4S_4 was harvested from the cool end of the Schlenk flask. Purity of the synthesized As_4S_4 was evaluated by X- Ray powder diffraction. This was used for further synthesis.

Figure 2.1.2: Sublimation of melt of realgar (As_4S_4) to yield pure realgar crystals (seen as bright yellow on the left-hand side of the Schlenk tube).

2.1.3 Synthesis of As_4Se_3 and As_4Se_4

As_4Se_3 was also synthesized by high temperature synthesis in evacuated quartz ampoules. Stoichiometric amounts of arsenic and sulphur were weighed and melted together at 350 °C for 1 day. The orange- yellow melt was tempered at 290 °C for 6 days. The amorphous mass was then sublimated at 280 °C in an oven with temperature gradient. As_4Se_3 was deposited on the cold end, the purity of which was evaluated by X- Ray powder diffraction. For synthesis of As_4Se_4, As_4Se_3 and Se were melted together at 280 ° C in sealed quartz ampoule and annealed at this temperature for 14 days. The purity was verified using powder X- Ray powder diffraction.

2.1.4 Purification of Cu(I) halides

Since the commercially available copper halides typically contain impurities, it was purified before it was used. The Cu(I) halides were dissolved in corresponding hot concentrated hydrohalic acids and subsequently quenched several times with deionised water and filtered under argon. At this stage any contact with atmospheric oxygen should be avoided in order to supress any renewed oxidation of Cu^{1+}. The purity of so obtained Cu(I) halides was inspected with X-ray powder diffraction experiment. All the Cu(I) halides were stored under a protective argon atmosphere in a glove box[17].

2.1.5 Used Chemicals

Following table shows the chemicals used for performing the experiments. Arsenic and copper halides were purified before use.

Table 2.1 1: Chemicals used with purity and producer

Compound	Formula	Producer	Purity
Arsenic	As	Chempur	Purified by sublimation
Selenium (grey)	Se	Chempur	99.999 %
Copper chloride	CuCl	Merck	Recryst. from conc. HCl
Copper bromide	CuBr	Merck	Recryst. from conc. HBr
Copper iodide	CuI	Merck	Recryst. from conc. HI
Silver chloride	AgCl	Merck	99.99 %
Silver bromide	AgBr	Heraueus	99.99 %
Silver iodide	AgI	Sigma Aldrich	99.99 %
Hydrochloric acid	HCl	VWR	p.A
Hydrobromic acid	HBr	Merck	p.A
Hydroiodic acid	HI	Merck	p.A
Zinc iodide	ZnI_2	Sigma Aldrich	99.9 %
Cadmium iodide	CdI_2	Merck	99.99 %
Mercuric iodide	HgI_2	Merck	99.99 %
Sulphur	S	Merck	99.999 %
Realgar	As_4S_4	In house synthesis	
Arsenic selenide	As_4Se_4	In house synthesis	
Tetraarsenic trisulphide	As_4Se_3	In house synthesis	
Tin iodide	SnI_4	In house synthesis	
Toluene	C_7H_8	VWR	100 % ; $H_2O \leq 0.02$ %
Acetonitrile	C_2H_3N	Sigma Aldrich	≥ 99.9 %

2.2 Preparation Methods

2.2.1 Preparation in ampoules

The samples were prepared in evacuated silica glass ampoules, which in laboratory jargon are called quartz ampoules. The empty ampoules were heated at 120 °C to get rid of the any possible water. The starting materials were then weighed (Analytical balance, Kern, accuracy; 0.1 mg) and transferred carefully to the ampules. Care was taken that no part of the educts was stuck on the sides of the ampoules. The ampoules were then flushed with argon several times to remove the air completely and finally evacuated to a pressure of $< 0.2 \cdot 10{-}3$ bar. Finally, the ampoules were melted and sealed with hydrogen-oxygen draft burner. Annealing and tempering of the samples was carried out in tube furnaces according to the reaction profile and specific reaction conditions. After cooling to room temperature, the ampoules were cut open either in air or under inert gas atmosphere, if necessary.

2.2.2 Solvothermal Synthesis

In analogy to the traditional solid-state approach, the educts were weighed in Duran glass ampoules followed by the addition of the appropriate amount of the desired solvent(s). The solvent(s) were then frozen in liquid nitrogen to enable to melt and seal the ampoules under vacuum. By heating the reaction mixture above the boiling point of the solvent, considerable amount of pressure is developed in the system. Hence the ampoules were transferred to a stainless-steel autoclave and a suitable solvent or water was added to the sides of the autoclave which serves to counter the pressure. After cooling to room temperature, considerable amount of pressure can remain in the ampoule. Hence, before opening the ampoule, the solvent(s) were frozen in order to avoid any explosion.

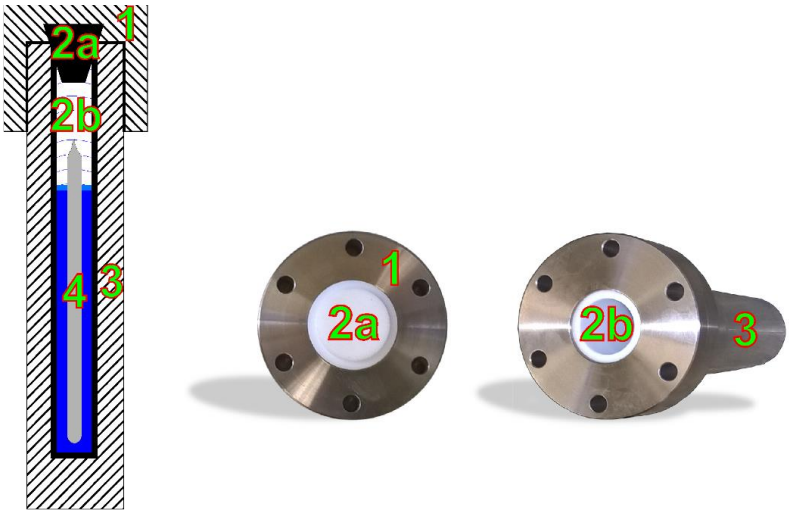

Figure 2.2.1 : (Left): Typical experimental setup for a solvothermal synthesis as per Rabenau. (Right): Experimental setup used in the following work. The stainless autoclave consists of a lid (1) with a Teflon seal (2a). The other part consists of a hollow Teflon pod/case (2b) enclosed in a stainless-steel mantel (3). The schematic representation by Rabenau shows the sealed ampoule (4) in the autoclave surrounded by water to counter the generated pressure (painted in blue)[18].

2.3 Characterization Methods

The purpose and aim of the following work were the structural elucidation of compounds which were newly synthesized. Therefore, it was always the effort to have a crystal structure analysis using single crystal X-Ray crystallography. Powder X-Ray diffraction patterns were also recorded. Both of these techniques were instrumental in knowing the exact atomic constitutions of the new compounds. Phase pure compounds were further analysed with Raman spectroscopy, thermal analysis and elemental analysis using scanning electron microscopy.

2.3.1 X-Ray Powder Diffraction

The exact unit cell parameters were calculated using powder X-Ray diffraction, which coincide with those from the single crystal measurement. This reflects the fact that the sample for the powder diffraction in fact contains many micro-crystals in all possible orientations. **Fig 2.2.2** represents the schematic diagram for a typical powder diffraction experiment. For precise results, the incoming X-Rays must be monochromatized (done by the monochromator).

Typically, the characteristic Kα1 radiation of the corresponding radiation source was used for the measurements.

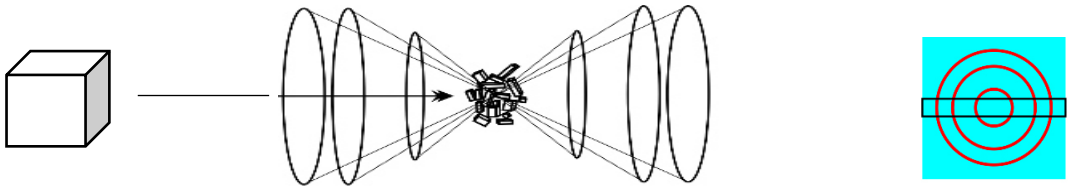

X-Ray Source multi-crystalline sample typical diffraction pattern

Figure 2.2 2: Left: A schematic representation of a powder diffraction experiment shown with the Laue cones. Right: A theoretical diffraction pattern with concentric rings[18].

Thus, with powder diffraction one gets a one-dimensional image of the diffracted X-Rays. It is usually plotted as intensity versus the diffraction angle, 2θ. From this we can know the unit cell parameters and the symmetry of the unit cell. Moreover, the Bravias type can be known from the study of the extinction patterns. To get the diffractograms, two diffractometers from STADI-P, viz. STOE and Cie were employed. Both diffractometers are equipped with Mythen K1 Detector (PSD) from Dectris. One diffractometer was operated with Cu Kα1 wavelength (λ = 1.54 Å), while the other was with Mo Kα1 wavelength (λ = 0.709 Å). The radiation was monochromatized by means of a germanium single crystal. LaB_6 and silicon were used as external standards for calibration. All measurements were done in the Debye- Scherrer (transmission)geometry. A small amount of neatly homogenised sample was place in between two Mylar foils and then clamped in a flatbed carrier and loaded on to the instrument. For analysing the recorded diffraction pattern, the WinXPOW program from Stoe and Cie were used[19]. All the powder diffraction experiments mentioned in this work were conducted at room temperature.

2.3.2 Single Crystal X-Ray Diffraction

To know the exact structures of the compounds, single crystal X-Ray analysis of selected single crystals were carried out. **Figure 2.2.3** shows a schematic diagram for a typical single crystal diffraction experiment[18].

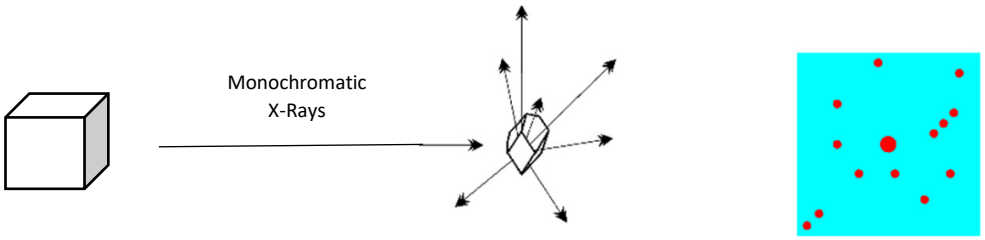

Figure 2.2 3 : Experimental setup for a single crystal diffraction experiment with theoretical diffraction pattern.

When the X-Rays are diffracted by a single crystal, we get a 3-dimensional diffraction pattern (unlike powder, where we get only one-dimensional view), from which we can assign the exact 3-dimensional orientation of the compound under investigation. The reflexes are located at certain point in space on the Ewaldsphere (named in honour of German physicist Paul Peter Ewald). Suitable crystals were chosen and put in Fomblin and fished on to the nylon loop and mounted on to Super Nova from Rigaku Oxford Diffraction to measure. Mo Kα1 wavelength (λ = 0.709 Å) was employed for all measurements, unless until stated with an EOS CCD detector. The crystal cooled down to 123 °K during the measurement in order to avoid possible decomposition by contact with air. Crysalis Pro program was used for data collection, integration and absorption correction[20]. The solving of the crystal structure and the subsequent refinement was done with the help of programme Olex2[21] with SHELXT[22](charge flipping method) and SHELXL-2014[23] (least square method) . Jana2006[24] software was also used along with Olex2 in some cases. In order to know the degree of agreement between the crystallographic model and the experimental X-Ray diffraction data, the R-factor is calculated.

$$R\text{-}factor = \frac{\sum_{(h,k,l)} \| F_{obs}(h,k,l) | - | F_{calc}(h,k,l) \|}{\sum_{(h,k,l)} | F_{obs}(h,k,l) |}$$

Where F is the structure factor. It is usually calculated during each cycle of least-square refinement to evaluate the progress. Thus, the R factor serves as a measure of structure quality. R factor of 0 means the perfect match of the calculated and the observed intensities.

For further analysis the program PLATON[25] was used for examining additional symmetry elements (ADDSYM) and twinning (TwinRotMat) and structures were transformed into standard setting (Structure Tidy) . The measurement parameters and the data of the resulting

structure were summarised in a crystallographic information file (cif). The visualisation of the structures was done with Diamond[26] with displacement ellipsoids shown with a probability factor of 90 % unless stated otherwise.

2.3.3 Raman Spectroscopy

Raman spectroscopy, like IR spectroscopy, is a vibrational spectroscopic method. As like any other spectroscopic method, it based of the interaction of the electromagnetic radiation with matter. IR spectrum is observed when energy corresponding to the vibrational transitions in a molecule is absorbed. But there is yet another manner in which the molecular vibrations can be excited. The radiation employed is of higher energy than of molecular vibration, usually lying in the visible range. The molecule is exited to a 'virtual' state after absorbing energy from the incident photon. The lifetime of this excited state is so short that there is almost immediate re-emission of a photon, with the molecule left in a different vibrational energy. This process is very weak with the resulting signals being only about one millionth of the starting exciting radiation. The resulting Raman spectrum has vibrational frequencies which differ from the incident radiation. Those to the lower end are the so called Stoke lines and to the higher end are the anti-Stoke lines. Usually, the Stokes lines are more important because the anti-Stoke lines arise from the small number of molecules in vibronically excited state. Along with Stoke and anti -Stoke lines, there is the Rayleigh scattering, which unlike Raman, corresponds to the elastic scattering. A vibration in a molecule will give rise to a Raman spectrum if it leads to a change in its polarizability. Thus, the polarization of the electron cloud of the molecule by the electric vector of the incident quantum of photon ultimately is responsible for the Raman spectrum and hence deeming polarizability as the most important property which a molecule should possess in order to be Raman active.

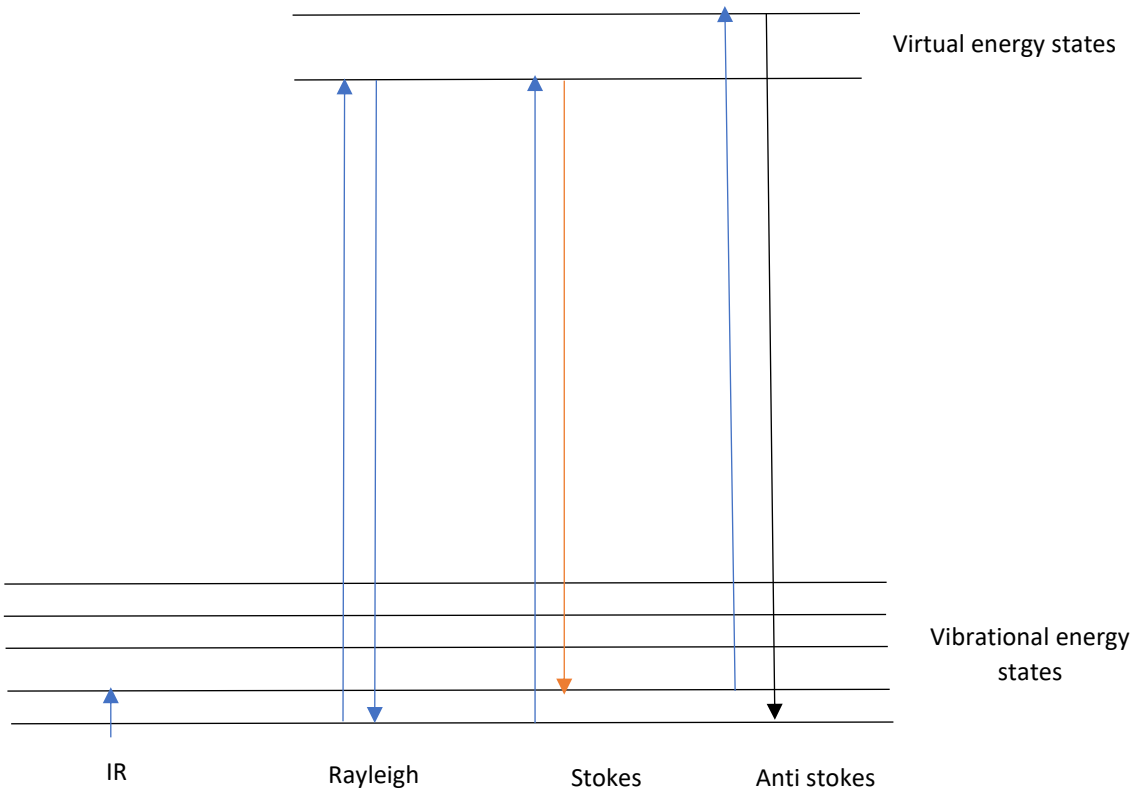

Figure 2.2.4 : Schematic diagram of the energy levels involved in a Raman experiment.

For the preparation of the sample, the compound was ground and filled in a melting point determination capillary eventually sealing the capillary with hydrogen – oxygen flame. The measurements were done on a DXTTM SmartRaman spectrometer (Thermoscientific) with 780 nm as the excitation wavelength and 0.5 cm-1 resolution. OMNIC[27] was used for baseline correction and smoothening of the spectra.

2.3.4 UV - Visible Spectroscopy

For recording the solid-state UV-Visible spectra an Omega 20 spectrophotometer from Bruins Instruments[28] was employed. Initially a reflectance spectrum was recorded using an Ulbricht sphere, which was subsequently transformed to absorption using the Kubelka Munk theory[29] (See Equation below), where A stands for absorption and R for reflectance.

$$A = \sqrt{R \times E \frac{\left(\frac{1-R}{100}\right)^2}{200}}$$

$BaSO_4$ was used a white reference material. The resolution was 0.5 nm with a detection range from 380 nm to 1100 nm. The spectra were further worked upon and plotted with OMEGA program. The intersection of linear extrapolation of the baseline and the absorption edge indicated the optical band gap of the sample under consideration.

2.3.5 Scanning Electron Microscopy/Energy Dispersive X-Ray Spectroscopy

A Scanning Electron Microscope (SEM) consists of an electron source, electromagnetic lenses and an electron detector. It employs an electron beam instead of light, based on the wave – particle duality. The electron beam is accelerated and focussed on a sample using the lenses. The sample emits secondary electrons, which are detected. The number of detected electrons depends on the variation of the sample's surface. By scanning the beam and detecting the variation of the number of the emitted electrons, the surface topography of the sample can be reconstituted. Secondary electrons have very low energies (of the order of 50 eV) limiting their mean free path. Consequently, the secondary electrons can escape only from the top few nanometers of the sample surface. The signals from the secondary electrons are highly localized at the point of impact of the primary electron beam, thus rendering it possible to collect the images of the surface of the sample with a resolution below 1 nm. When the inner shell electrons of the sample are removed by bombardment with the primary electron beam, characteristic X-Rays are emitted. This characteristic X-Ray radiation can be measured by Energy Dispersive X-ray Spectroscopy (EDX) and hence can serve as a tool for elemental analysis of the sample under consideration.

The SEM images were taken on EVO MA15 scanning electron microscope from Zeiss. LaB_6 was used as the radiation source. The program SmartSEM[30] was used to manipulate the machine and subsequently to acquire images. A Quantax200 – Z30 EDX detector from Bruker with a resolution of 129 eV (Mn Kα) was used for the EDX analysis. The Quantax ESPIRIT[31] program from Bruker was used for the qualitative evaluation and analysis.

2.3.6 Thermal Analysis

For thermal analysis of the samples, DTA (Differential Thermal Analysis) measurements were performed using Setaram DTA-TG 92-16.18. Finely powdered sampled was filled in evacuated quartz ampoule of 2 mm diameter and melted and sealed under vacuum so the length of the ampoule was approximately 10 mm. Aluminium oxide was used as an external standard for all measurements. Two cycles (heating and cooling) were measured with a heating rate of 10 °C/min.

2.3.7 Impedance Spectroscopy

Impedance measurements were carried out using a Zahner Zennium impedance system. Of the total system, the tube furnace and a measuring cell was located in a glove box under argon atmosphere. The configuration and control of the measurements were carried out with the help of Thales Flink software[32]. A Eurotherm2404 controller was available outside the glovebox which could be programmed and controlled via the NETVI programme from the Thales Flink software, allowing the measurement of temperature dependent spectra. A detailed description of the set-up used is found in the dissertations of Huber[33] and De Giorgi[34]. In order to carry out temperature-dependent conductivity measurements of the synthesised compounds, the samples were triturated into fine powders using an agate mortar and then were pressed into a pellet using a hydraulic press. The samples were filled into steel press (inner diameter - eight millimetres) and pressed with a pressure of about six tons over a period of ten minutes after which the pressure was released slowly. The pellet was then carefully removed, and thickness and mass were measured. From these two values, the density factor, ρPl, was determined. ρPl should be taken into account as a correction factor when calculating conductivity. Along with the X-ray density ρx of the compound, the total correction factor ρtot was calculated. Following scheme was used for the contacting of the pellet:

$$Al_2O_3 \,|\, \text{Pt- Electrode} \,|\, \text{Au-plate} \,|\, \text{Substance} \,|\, \text{Au Plate} \,|\, \text{Pt- Electrode} \,|\, Al_2O_3$$

A schematic diagram of the cell used is shown in the **Figure 2.2.5**. It was assembled at the glassblowing and electronic workshop at the university of Regensburg based on the model of Freudenthaler (Dissertation, University of Siegen,1997).

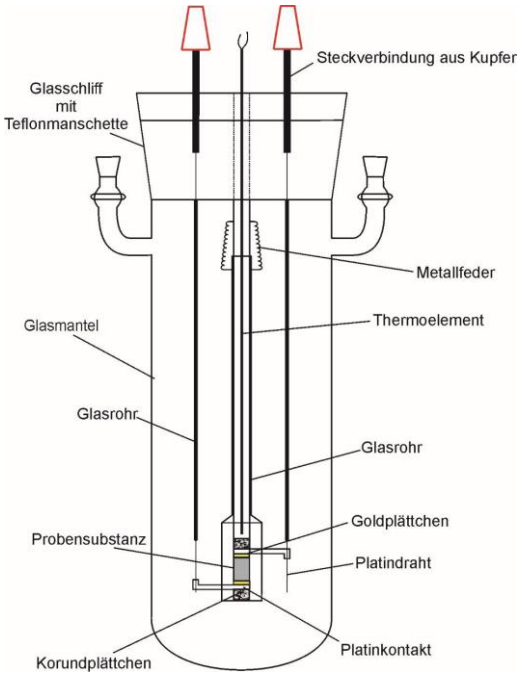

Figure 2.2 5: Schematic diagram of the measuring cell with installed sample.

Each measurement consisted of two heating and cooling cycles respectively in 1Hz – 300 Hz frequency range. The temperature range was 40 °C – 200 °C. The temperature was rose by a step of 20 °C. In between each step the waiting rest time was 20 minutes to ensure that the sample was in thermal equilibrium. The holding time started as soon as the target temperature was achieved with a tolerance window of ± 2.0 °C. The first cycle usually served to reduce the microcracks in the pellet, ensuring a better contact in the second cycle. Data visualisation and subsequent evaluation was done with the Thales Flink programme from Zahner. Suitable circuit diagrams were created using this software and adapted to the data. Subsequently a Nyquist plot (real vs imaginary part of the impedance) was plotted. The values of resistance determined in this way were then imported in an Excel template to calculate the specific resistance which was calculated using the values of the measured resistance, density factor and the sample geometry of pellet. From the value of specific resistance, specific conductivity is easily calculated as they are inversely proportional to each other. Lastly, the activation energy of charge transport can be calculated with the help of Arrhenius equation once since we have the value of specific conductivity in hand.

3. Adduct Compounds of As_4S_4 with Ag*X* and Cu*X* (*X* = Cl/Br/I)

3.1 Literature Overview and theoretical aspects

As shortly touched upon in Chapter 1, in the last two decades the role of copper halides as "preparative tools" for the synthesis of neutral or low charged molecules of group 15 and 16 of the periodic table is well established[35–37]. One of reasons for this plethora of compounds involving copper halides is the high structural diversity of the Cu^{1+} ions, coordinating in linear, planar and tetrahedral environment. For adduct compounds of Cu(I) halides with pnicogenchalcogenide cages, until now eight coordination modes are known which are depicted in the following figure adopted from *Vitzthumecker*[18]

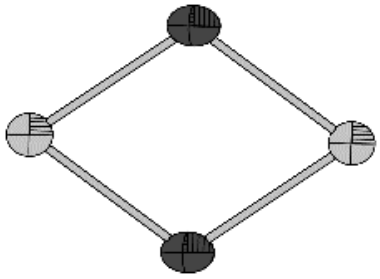

$[Cu_2X_2]$ dimer

$(CuCl)_2{\cdot}(As_4S_3)$[38]; $(CuBr){\cdot}(P_4S_3)$[39]

$(CuBr){\cdot}(As_4S_4)$[15]; $(CuI){\cdot}(P_4S_3)$[40]

$(CuI){\cdot}(P_4Se_3)$[41]; $(CuI){\cdot}(P_4Se_4)$[42]

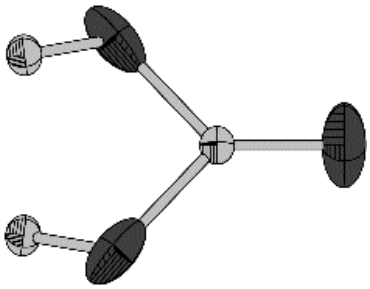

Cu_3X_3 trimer

$(CuI)_3{\cdot}(As_4S_4)_2$[15]

$(CuI)_3{\cdot}(As_4Se_4)_2$[15]

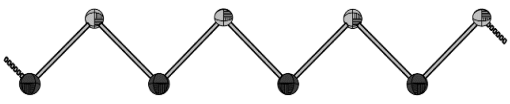

$^1_\infty[CuX]$ zick – zack chains

$(CuCl){\cdot}(As_4S_3)$[38]

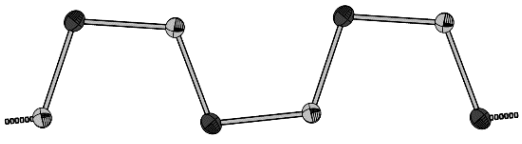

$^1_\infty[CuX]$ wave – like chains

$(CuI)_3{\cdot}(P_4S_3)_2$[40]; $(CuCl){\cdot}(P_4Se_3)$ [41]

$(CuCl)_3{\cdot}(P_4Se_3)_2$[41]; $(CuBr)_2{\cdot}(P_4S_3)_2$[43]

$(CuBr)_3{\cdot}(P_4Se_3)_2$[41]; $(CuI)_3{\cdot}(P_4Se_3)_2$[41]

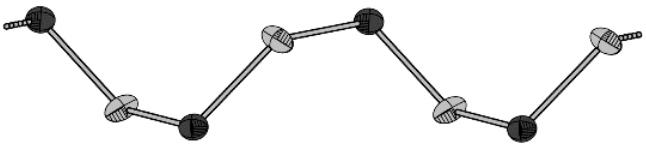

$^{1}_{\infty}[\mathrm{Cu}X]$ screws

$(CuCl)\cdot(As_4S_4)$[18]; $(CuBr)\cdot(As_4Se_4)$ [15]

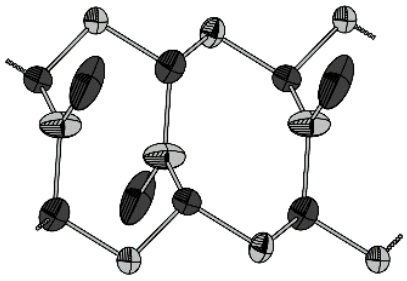

$^{1}_{\infty}[\mathrm{Cu}X]$ ladders

$(CuBr)_3\cdot(As_4Se_4)$ [15]

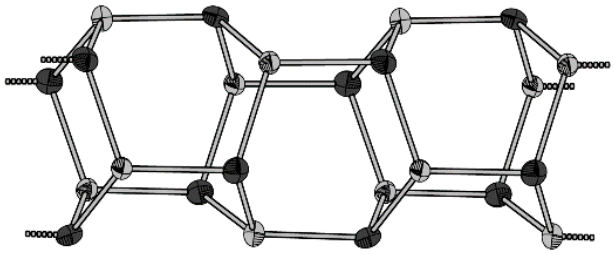

$^{1}_{\infty}[\mathrm{Cu}X]$ rods

$(CuCl)_7\cdot(P_4S_3)_3$[40]; $(CuBr)_7\cdot(P_4S_3)_3$)[39]

$(CuBr)_3\cdot(P_4Se_4)$[44]; $(CuI)_3\cdot(P_4S_4)$[45]

$(CuI)_3\cdot(P_4Se_4)$[46]

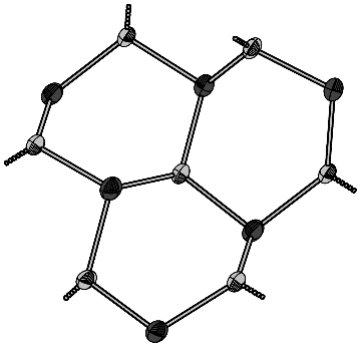

$^{2}_{\infty}[\mathrm{Cu}X]$ layers

$(CuBr)_3\cdot(P_4S_3)$ [39]; $(CuI)_3\cdot(P_4S_3)$ [40]

Figure 3.1.1 : Overview of known coordination modes of Cu(I) halides (CuX)(Pn_4Qx) type adduct compounds (X = Cl/Br/I; Pn = P/As; Q =S/Se). Cu atoms are indicated in dark grey and halide atoms in light grey as adopted from Vitzthumecker.[18]

A number of new phosphorus polymers, thiometallates, phosphorus chalcogenides, polychalcogenides and arsenic chalcogenides were successfully embedded in Cu(I) halide matrix. In the course of time many new formerly unknown (which were assumed to be too stable for an independent existence) polymers and oligomers containing main group elements, of the like $^{1}_{\infty}[\mathrm{P}_{14}]$, $^{1}_{\infty}[\mathrm{P}_{12}]$, $^{1}_{\infty}[\mathrm{P}_{16}\mathrm{S}]$, $^{1}_{\infty}[\mathrm{P}_4\mathrm{Se}_4]$ were stabilized within a Cu(I) halide matrix[8,10,14,42]. Along with polymers and oligomers, a number of new formerly unknown binary phosphorus chalcogenides like P_8Se_3 or β-P_4Se_4 or P_4S_4, P_4S_3 which were stabilized in

Cu(I) halide matrix were synthesised and characterised, like, for instance in the adduct compound $(CuI)\cdot(P_4S_3)$[12,13,40,47]. In all these adduct compounds, Cu^{1+} is exclusively bound with sulphur and halide atoms. Coordination through phosphorus atom was not observed. After successful synthesis and characterisation of adduct compounds with phosphorus chalcogenides, arsenic chalcogenides were a subject of further investigation. Earlier studies showed that the incorporation of As_4Q_n(Q = S, Se; n = 3,4) in a transition metal halide matrix leads to fragmentation of the arseno-chalcogenide cage molecules[48] (J. Wachter**,** *Abstr. Pap. Am. Chem. S***. 1995,** *209***, 231**). There could be many possible reasons for this observation. Among others is the formation of minerals like Cu_3AsS_4 (enargite)[49][50], CuAsS (lautite)[51,52] or also quaternary argyrodites, like, for example Cu_6PS_5I[53,54] or the formation of arsenic trihalides. However, *Pfitzner* and *Bräu*[14,55,56] were successful in incorporation of undistorted cage molecules in mercury(II) halide matrices using solid state synthesis. With this many new adduct compounds with arsenochalcogenide cages were synthesised and characterised. To enhance the solubility of the cage molecule, diffusion technique was preferred. To increase the reactivity and solubility of As_4Q_n cage molecules, *Biegerl*[57] employed diffusion technique where the cages were available in the form of a precursor with their more soluble and reactive pentacarbonyl complexes, $As_4S_3\cdot M(CO)_5$ (M = Cr, W). Thus, by layering the pentacarbonyl complexes of arsenochalcogenide cages with the solution of respective copper(I) halide solutions *Biegerl* was able to attain adduct compounds of P_4S_3 with Cu(I) halides at room temperature[39–41]. Further, also with the diffusion technique, *Schwarz et. al* synthesised several adduct compounds with As_4S_3 and PAs_3S_3[38,58]. Later Rödl, for the first time, was able to synthesise adduct compounds of arseno-chalcogenide cages with copper(I) halides with the cage remaining intact. Rödl was also successful in synthesising adduct compounds of neutral layers of As_2Q_3 (Q = S, Se) with copper(I) halides using solid state method[15,59]. In these compounds also the coordination of copper atom was seen exclusively preferred to chalcogen atom. Yet another facet of these adduct compounds is the high ionic conductivity owing to the high polarizability and mobility of Cu^+ ions which was also seen in one of the first adduct compounds synthesised by *Möller* and *Jeitschko*[8]

Table 3.1.1: Overview of known copper(I) halide adducts with phosphorus polymers, (poly)chalcogenides, phosphorus chalcogenides, arsenic chalcogenides, and arsenic chalcogenide layers.

Compound	Space group	Stabilised Entity	Literature
Phosphorus Polymers			
$(CuI)_2P_{14}$	*P2₁/c*	$^1_\infty[P_{14}]$	[10]
$(CuI)_3P_{12}$	*P2₁*	$^1_\infty[P_{12}]$	[9]
$(CuX)_8P_{12}$ *X* = I,Br	*P2₁/c*	$^1_\infty[P_{12}]$	8,60
$(CuI)_2CuP_{15}$	*P2₁/n*	$^1_\infty[P_{15}]$	61
$(CuBr)_{10}Cu_2P_{20}$	$P\bar{1}$	$^1_\infty[P_{20}]$	62
Polychalcogens			
(CuX)Te; X = I,Br,Cl	*I4₁/amd*	$^1_\infty[Te]$	63–69
$(CuX)Se_2$ X = Br, Cl	*P2₁/n*	$^1_\infty[Se]$	70,71
$(CuX)Te_2$ X = Br, Cl ,I	*P2₁/c*	$^1_\infty[Te]$	72,73
(CuX)STe; X = Br, Cl	*P2₁/n*	$^1_\infty[STe]$	74
(CuX)SeTe; X = I,Br, Cl	*P2₁/n*	$^1_\infty[SeTe]$	75
$(CuI)_3Se_3$	$R\bar{3}m$	Se_6	7
$(CuBr)Se_3$	*Pnma*	Se_6	76,77
$(CuX)(Q_1/Q_2)_3$ X = I,Br Q_1 = Se Q_2 = S, Te	$R\bar{3}m$	$(Q_1/Q_2)_6$	78
Thiometalates			
$(CuI)_3Cu_2TeS_3$	*P3₁21*	TeS_3^{2-}	79
$(CuI)_2Cu_3SbS_3$	*Pnnm*	SbS_3^{2-}	80
$(CuCl)Cu_2TeS_3$	*R3m*	TeS_3^{2-}	81
$(CuBr)Cu_{1.2}TeS_2$	*I4₁/c*	TeS_2^-	82
Phosphorus Chalcogenides			
$(CuI)_3(P_4Q_4)$; Q = S,Se	*P6₃cm*	P_4Q_4	83,84
$(CuBr)_3(P_4Se_4)$;	*P2₁*	P_4Se_4	85
$(CuBr)_5(P_{16}S)$	*P2₁*	$^1_\infty[P_{16}S]$	14
$(CuBr)_5(P_{16}Se)$	*P2₁/c*	$^1_\infty[P_{16}S]$	14
$(CuI)_8(P_{14}Q)$; Q = S,Se	*modulated*	$^1_\infty[P_{14}Q]$	14

$(CuI)(P_4Se_4)$	*cmce*	$^1_\infty[P_4Se_4]$	86
$(CuX)_2(P_8Se_3)$; X = I,Br	*Pbcm*	P_8Se_3	87,88
$(CuI)(P_4Se_3)_2$	$P\bar{1}$	P_4Se_3	57
$(CuBr)(P_4S_3)$	*Cmce*	P_4S_3	40,57,89
$(CuI)(P_4Q_3)$; Q= S,Se	*Cmce*	P_4Q_3	90
$(CuCl)(P_4Se_3)$	$P2_1/c$	P_4Se_3	41,57
$(CuBr)_2(P_4S_3)_2$	$P\bar{1}$	P_4S_3	43,57
$(CuI)_3(P_4Q_3)$; Q= S,Se	*Pnma*	P_4Q_3	57,89,91
$(CuBr)_3(P_4S_3)$	*Pnma*	P_4S_3	90
$(CuI)_3(P_4Se_3)_2$	*Pnma*	P_4Se_3	41,57
$(CuBr)_7(P_4S_3)_3$; X = Br,Cl	$P6_3mc$	P_4S_3	39,40
$(CuX)_7(P_4Q_3)_3$; X = Br,Cl Q = S, Se	*Pnma*	P_4Q_3	40,41,57,91
α –(CuBr) (P_4Se_4)	*Cmce*	$^1_\infty[P_4Se_4]$	15
β –(CuBr) (P_4Se_4)	$P2_1/c$	$^1_\infty[P_4Se_4]$	15
Arsenic chalcogenide layers			
$(CuI)(As_2S_3)_2$	*C2/m*	$^2_\infty[As_2S_3]$	15
$(CuI)(As_2Se_3)_2$	*Cmce*	$^2_\infty[As_2Se_3]$	15
Arsenic chalcogenides			
$(CuI)(As_4S_3)$	*C2/c*	As_4S_3	58
$(CuBr)(As_4S_3)$	*Cmca*	As_4S_3	58
$(CuCl)(As_4S_3)$	*Pbcm*	As_4S_3	38
$(CuX)_2(As_4S_3)$; X = Br, Cl	$P2_1/m$	As_4S_3	38,58
$(CuI)(PAs_3S_3)$	$P2_13$	PAs_3S_3	58
$(CuI)_2(PAs_3S_3)_4{\cdot}CS_2$	$P\bar{1}$	PAs_3S_3	58
$[(Cu2I)(PAs_3S_3)_3]I$	$P2_1/c$	PAs_3S_3	58
$[Cu(PAs_3S_3)_4]X$; X = Br,Cl	$P3_1c$	PAs_3S_3	58
$(CuX)(PAs_3S_3)(As_4S_4)$; X= Br,Cl	$P2_1/c$	PAs_3S_3/ As_4S_4	58
$(CuI)_3(As_4Q_4)$; Q = S, Se	*C2/c*	As_4Q_4	15
$(CuBr)(As_4S_4)$	$P2_1/n$	As_4S_4	15
$(CuBr)(As_4Se_4)$	$P2_1/c$	As_4Se_4	15
$(CuBr)_3(As_4Se_4)$	*C2/c*	As_4Se_4	15

$(CuCl)(As_4S_4)$	$P2_1/c$	As_4S_4	[18]
$(CuCl)(As_4Se_4)$	$P2_1/c$	As_4Se_4	[92]
$(CuCl)(As_4Se_3)$	*Pbcm*	As_4Se_3	[92]
$(CuX)(As_4Se_3)$; X = Br,I	*Cmce*	As_4Se_3	[92]
$(CuI)_3(As_4S_4)$	$P2_1/c$	As_4S_4	This work
$(CuBr)_2(As_4S_4)$	$P2_1/n$	As_4S_4	This work
$(CuBr)_2(As_4Se_3)$	$P\bar{1}$	As_4Se_3	This work

Hoppe[93] and Blachnik[94] were able to synthesise and characterise adduct compounds from the other end of the periodic table, viz, adduct compounds with halides of niobium and tantalum (hard Lewis acids). The most common pnicogen chalcogenides that were to form adduct compounds with transition metal halides were he sulphur-containing cages with phosphorus and arsenic. As the minerals containing arsenic and sulphur cages have been a subject of active research for many years and also a major part of this work, it would not be out of place to have an overview of the known and characterised cage molecules.

Table 3.2.2: Overview of the known cage molecules consisting of arsenic and sulphur with their common names.

Mineral	Cage molecule	Common name
Dimorphite[95–97]	As_4S_3	Dimorphite I
Dimorphite[95–97]	As_4S_3	Dimorphite II
α – Realgar[98–100]	α- As_4S_4	Realgar
β - Realgar [98–100]	α- As_4S_4	Bonazzite
γ – Realgar[101]	β - As_4S_4	Pararealgar
Uzonite[102,103]	β -As_4S_5	Uzonite
Alacranite[104]	Cocrystal of α- As_4S_4 and β -As_4S_5	Alacranite

In the case of silver iodide, not many adduct compounds were known. Nigles *et.al* first published $(AgI)_2Ag_3SbS_3$[105] which was analogous to its copper counterpart[106]. Deiseroth *et.al* showed that cyclic Se_6 and Te_6 molecules were stabilized by a "AgI" solid solvent[107]. Recently,

Weis and Krossing[108,109] were able to demonstrate the coordination of silver iodide with undistorted As_4S_4 cages albeit the reaction were done in solvents. In the present dissertation we present the coordination of silver halides with arseno-chalcogenide cages synthesized via solid state synthesis, thus an attempt to bridge the gap and complete the row of coinage metals with respect to their reactivity towards (As_4Q_n); Q = S, Se; n=3/4.

3.2 Adduct compounds of Ag*X* with As_4Q_4 (X = Cl,Br,I; Q = S,Se)

3.2.1 The Adduct $(AgI)_2 \cdot (As_4S_4)$

3.2.1.1 Synthesis

Solvothermal Synthesis

As_4S_4 (0.238 g, 1 equiv) and AgI(0.261 g, 2 equiv) were transferred to a duran ampoule (7 cm) followed by addition of 1mL of toluene and ACN respectively. The reaction mixture was cooled under liquid nitrogen and subsequently evacuated and reacted in a stainless-steel autoclave under solvothermal conditions at 160 °C for 5 days. The oven was cooled down at 80 °C over a time period of 5 h and maintained at this temperature for another 2 days followed by slow cooling down (over 6 h) to RT. After cooling a few air stable yellow coloured block-like crystals of $(AgI)_2 \cdot (As_4S_4)$ were obtained.

Solid State Synthesis

In the aforementioned solvothermal approach, along with the desired product (which crystalises as distinct yellow blocks) many other side products and unreacted realgar was observed. A phase pure synthesis of $(AgI)_2 \cdot (As_4S_4)$ was achieved by reacting silver iodide (0.152 g, 2 equiv) and realgar (0.341 g, 1 equiv) at 220 °C for 2 weeks. The educts were weighed, transferred in a quartz ampoule, evacuated, sealed and then rested in oven. The heating rate was 1.5 °C/min, while the cooling rate was 0.5 °C/min. The resulting product was fine yellow powder (See Figure 1). This was used for further analysis. For finding the correct temperature

for reaction, each time a reaction was performed, every time with an increase of 10 °C, starting from 180 °C. Each time the reactions were monitored by X-ray powder diffraction.

Figure 3.2.1.1: Phase pure yellow $(AgI)_2 \cdot (As_4S_4)$ synthesized via solid state route.

3.2.1.2 Single Crystal Analysis

Table 3.2.1.1 gives an overview of the crystallographic data and measurement parameters of $(AgI)_2 \cdot (As_4S_4)$.

Table 3.2.1.1: Crystallographic data and measurement data for $(AgI)_2 \cdot (As_4S_4)$.

Empirical Formula	$Ag_2As_4I_2S_4$
Formula weight	897.46
Crystal colour and shape	Yellow block
Crystal system	triclinic
Space group	P-1
a/Å	8.64(2)
b/ Å	8.69(3)
c/ Å	9.72(3)
α/°	89.97(3)
β/°	65.43(3)
γ/°	73.22(3)
V/Å^3, *Z*	628.31(4), 2
Absorption coefficient(μ)/ mm^{-1}	19.10
ρ_{calc}/g/cm^3	4.744
Diffractometer	Rigaku Super Nova
Radiation, temperature	Mo Kα (λ = 0.71073 Å), 123 K
Θ-range/°	6.102 – 60.644
hkl-range/°	-12 ≤ h ≤ 12
	-12 ≤ k ≤ 12
	-13 ≤ l ≤ 13

Absorption correction	numerical (gaussian, Scale3 Abspack)
Number of reflexes	19356
Independent reflections	3513
R_σ, R_{int}	0.0473, 0.0344
Completeness	100%
Structure solution	SHELXT
Structure refinement	SHELXT - 2014
Data/Restraints/Parameters	3513/0/109
GooF	1.074
R_1, wR_2 [I>2σ(I)]	0.0288, 0.0682
R_1, wR_2 [all reflexes]	0.0317, 0.0699
Largest diff. peak/hole/e Å^{-3}	2.21/-1.94

$(AgI)_2{\cdot}(As_4S_4)$ crystallises in the space group P-1 with a = 8.794 Å, b = 8.826 Å, c = 9.854 Å, α = 89.95 ° β = 65.37 °, γ = 73.89 ° , V = 662.30 Å3 and Z =2 (T = 123 K). The refinement of all data converged at a GooF of 1.074, with R_1 = 3.17 % and wR_2 = 6.99 %. The positions and isotropic displacement parameters can be found in Appendix in **Table A.1**. The anisotropic displacement parameters are listed in **Table A.2**. The bond lengths and bond angles can be found in **Table A.3** and **Table A.4**. The complete structure can be subdivided into two sub-structures, viz. the neutral α - As_4S_4 cages and the one-dimensional AgI layers. The two substructures are connected through η1 Se and η^1 As coordination to Ag atoms. Here it must be noted that the measurement was carried out at 123 K and compared to literature values at 298 K.

α - As_4S_4 substructure

The cage molecule in the adduct compound $(AgI)_2{\cdot}(As_4S_4)$ is similar to the binary cage molecules of pure As_4S_4 (**Figure 3.2.1.2**)

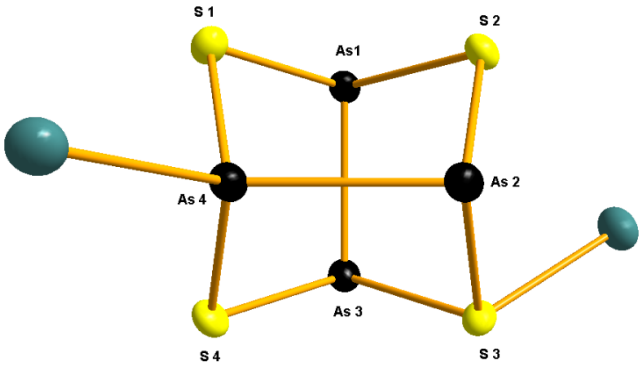

Figure 3.2.1.2: Isolated As_4S_4 cage molecule with coordinating silver atoms. The coordination takes place through both sulphur and arsenic atoms. Iodine atoms are not shown for the sake of simplicity. All ellipsoids are shown with 90% probability.

The coordination of silver iodide to the cage molecule has some effect on the bond lengths and bond angles which are discussed in the following section. As seen in Fig silver atom is coordinated to the As_4S_4 through η^1 (S) and η^1 (As). Further the sulphur and arsenic coordinated to the silver atom are not the immediate neighbours rather lie on the opposite side of each other. Here in Figure 2 it is noted the silver atom coordinated to As4 projects out of the plane of the paper while the silver atom coordinated to S3 is behind the plane of the paper.

Table 3.2.1.2: Selected interatomic distances (in Å) for (As_4S_4) in $(AgI)_2 \cdot (As_4S_4)$. Rows marked in orange represent contraction while in blue represent elongation upon coordination with AgI. Maximum deviation is observed at the sites of sulphur and arsenic coordination.

Bond/Distance	$(AgI)_2 \cdot (As_4S_4)$	As_4S_4	Difference
As1 – As3	2.564	2.563	0.001
As2 – As4	2.536	2.569	0.033
As1 – S1	2.244	2.246	0.002
As1 – S2	2.264	2.238	0.026
S2 – As2	2.239	2.229	0.01
As2 – S3	2.280	2.234	0.046
S3 – As3	2.272	2.237	0.035
As3 - S4	2.241	2.243	0.002

S4 – As4	2.236	2.241	0.005
As4 – S1	2.222	2.231	0.009

.

The bond lengths for As2-As4, S4-As4, As4-S1, S3-As2 and S3-As3 are expected to deviate from the free uncoordinated As4S4 after coordination with silver atom. As expected d(As2- S3) is slightly elongated where sulphur atom coordinates to silver atom. For the compound under consideration, d(As2- S3) shows the maximum deviation of 0.046 Å when compared to free As_4S_4 . d(As3- S3) also sees an elongation of 0.035 Å when compared to "free" realgar (See Table 2). In contradiction, no significant changes (neither elongation or contraction) are seen at sites where coordination of As takes place. d(As1- S2) is elongated by 0.026 Å, although it is not coordinated to sulphur or arsenic. d(As2- As3) is almost unchanged when compared to free realgar. On the other had As2-As4 bond is shortened by 0.033 Å, which in turn indicated the strengthening of the bond. It must be noted that this the only bond which sees a contraction when coordinated to AgI.

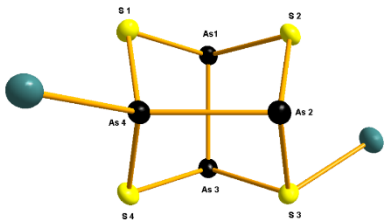

Figure 3.2.1.2: Isolated As_4S_4 cage molecule with coordinating silver atoms. The coordination takes place through both sulphur and arsenic atoms. Iodine atoms are not shown for the sake of simplicity. All ellipsoids are shown with 90% probability.

As with bond lengths, bond angles are also affected once coordinated to the silver atom (See Table 3). The highest deviation is seen in the angle ∠(S3-As2-S2). This angle sees a decrease of 3.25 ° when compared to free realgar. This is followed by ∠(S1-As4-As2), in which an increase of 3.2 ° is observed. In both the cases the deviation can be accounted by the respective coordination of As and S atoms to silver. Next, ∠(S4-As4-As2) is increased by 2.37 ° which can again be attributed to its coordination to silver atom. ∠(As1-S2-As2) also expands by 2.35 ° when compared to free uncoordinated realgar although the sulphur atom here is not coordinated with silver. The possible explanation here can be the lengthening of d(As1-S2) bond (bond length is increased by 1.16 % when compared to free realgar) which eventually is also manifested in an expanded bond angle

Table 3.2.1.3: Selected bond angles (in Å) for (As_4S_4) in $(AgI)_2$·(As_4S_4). Rows marked in orange represent contraction while in blue represent elongation upon coordination with AgI as a consequence of altered bond distances. Maximum deviation is observed at the sites sulphur and arsenic coordination.

Bond	$(AgI)_2$· (As_4S_4)	As_4S_4	Difference
As1-S2-As2	103.24	100.91	+2.33
As1-S1-As4	99.89	101.29	-1.40
As4-S4-As3	100.16	101.29	-1.13
As2-S3-As3	102.25	100.84	+1.41
S1-As4-As2	101.89	98.69	+3.20
S1-As1-As3	99.80	99.57	+0.23
S2-As1-S1	94.79	94.47	+0.32
S2-As2-As4	98.23	99.82	-1.59
S2-As1-As3	97.95	99.19	-1.24
S4-As3-As1	99.63	99.17	+0.46
S4-As4-As2	101.54	99.17	+2.37
S4-As4-S1	96.34	94.86	+1.48
S3-As3-S4	93.03	94.56	-1.53
S3-As2-S2	91.62	94.87	-3.25
S3-As3-As1	99.15	99.42	-0.27

The coordination sphere of silver

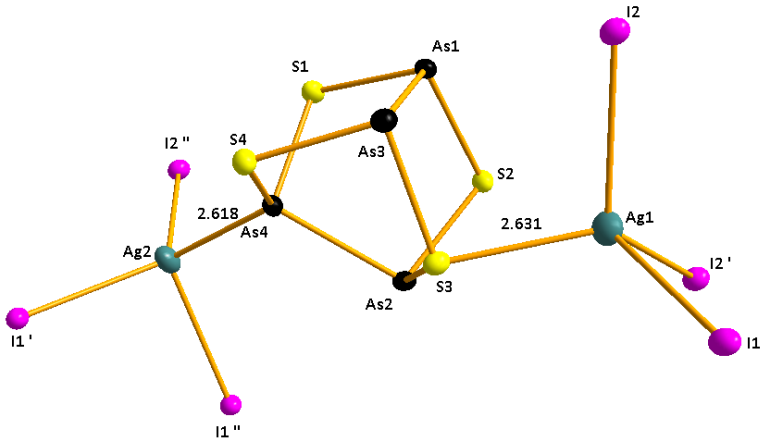

Figure 3.2.1.4: A section of the adduct compound $(AgI)_2(As_4S_4)$ showing the coordination of silver atom. Both silver atoms find themselves in a distorted tetrahedral environment. All ellipsoids are shown with 90% probability.

Both silver atoms show a distorted (3+1) tetrahedral coordination, coordinating to three iodine and one sulphur or arsenic atom respectively. See Figure 3 $(AgI)_2 \cdot (As_4S_4)$ represents one of the rarest examples of η^1 (As) coordination. The η1 (As) Ag-As bond length of 2.631 Å is comparable to recently published compound by Krossing et.al of 2.561 Å. As also in the case of $(AgI)_2 \cdot (As_4Se_4)$, Ag coordinates to S and As which are facing each other opposite rather than direct neighbours. Table 4 shows selected bond angles.

Table 3.1.1.4: Selected bond angles relevant for the silver coordination in the $(AgI)_2 \cdot (As_4S_4)$ adduct compound

Atoms	Angle / °	Atoms	Angle / °
S3-Ag1-I2	100.51	As4-Ag2-I2''	104.74
I2-Ag1-I2'	116.51	I2''-Ag2-I1'	117.51
I2'-Ag1-I1	96.94	I1'-Ag2-I1''	94.24
S3-Ag1-I1	105.09	As4-Ag2-I1''	100.74

It is seen that there is deviation from the ideal value of 109.4 ° for a tetrahedral geometry. It can be argued that the reason behind this distortion can be, how eventually the adduct molecule is packed in 3-D which will be discussed later.

AgI layers

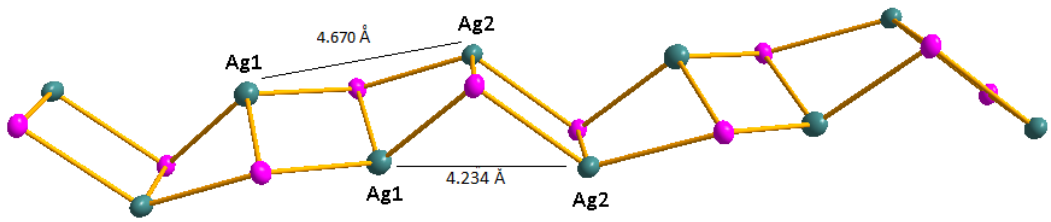

Figure 3.2.1.5: The visualisation of the AgI layers in the $(AgI)_2 \cdot (As_4S_4)$ adduct compound. Since there are two crystallographically distinct silver positions, two separate screw lengths could be visualised. All ellipsoids are shown with 90% probability.

The adduct $(AgI)_2 \cdot (As_4S_4)$ can be visualised as been flanked by two layers of AgI in which the As_4S_4 cages are embedded. These chains have two crystallographically distinct silver atoms with *d*(Ag2-Ag1) being 4.670 Å. and *d*(Ag2-Ag1) being 4.234 Å. (**Figure 3.2.1.5**) Since there are two different silver positions, two different screw lengths can be imagined depending on the viewing angle. As seen, these two distances differ by a small amount. This can also be the possible reason as to why the adjacent As_4S_4 cages are slightly shifted relative to one another in the complete structure.

Complete crystal structure

$(AgI)_2 \cdot (As_4S_4)$ consists of As_4S_4 cage molecules connected via AgI layers. The cage molecules are flanked from both sides by infinite silver iodide layers (See **Figure 3.2.1.6**). As seen in the figure when we consider an individual As_4S_4 cage molecule, both sulphur and arsenic atoms are coordinated to silver but on the other side of the cage molecule thus resulting in η^1(S) and η^1(As) coordination mode. Now, when we move on to the next adjacent As_4S_4 cage molecule, we see the exact same coordination modes but the As_4S_4 cage is flipped by 180 ° and this pattern goes on repeating itself. In the figure it can be seen that the AgI layers run parallel to the plane of the paper along the b axis and in between two of these layers, As_4S_4 cages are packed. Thus, it can be visualised that two of these cages (highlighted by a rectangle) make a general subunit and the pattern repeats itself. It must also be noted here that all the realgar cages are not in the same plane relative to each other, rather shifted either to the front or to the back of the plane of the paper relative to each other. Figure shows a part of the complete structure representing three adjacent repeating As_4S_4 cage molecules. It is seen that the first and the third As_4S_4 molecules go behind the plane while the one in the middle comes out of the plane of the paper. Thus, the first and the third As_4S_4 molecules have the same relative position and would coincide completely if there were superimposed om one another. This would be same for the second and the fourth As_4S_4 molecule. This “push pull effect” (See **Figure 3.2.1.6**) can be explained by taking into consideration that d(Ag-S) and d(Ag-As) differ by small amount [d(Ag-S) being 2.631 Å and d(Ag-As) being 2.618 Å respectively].

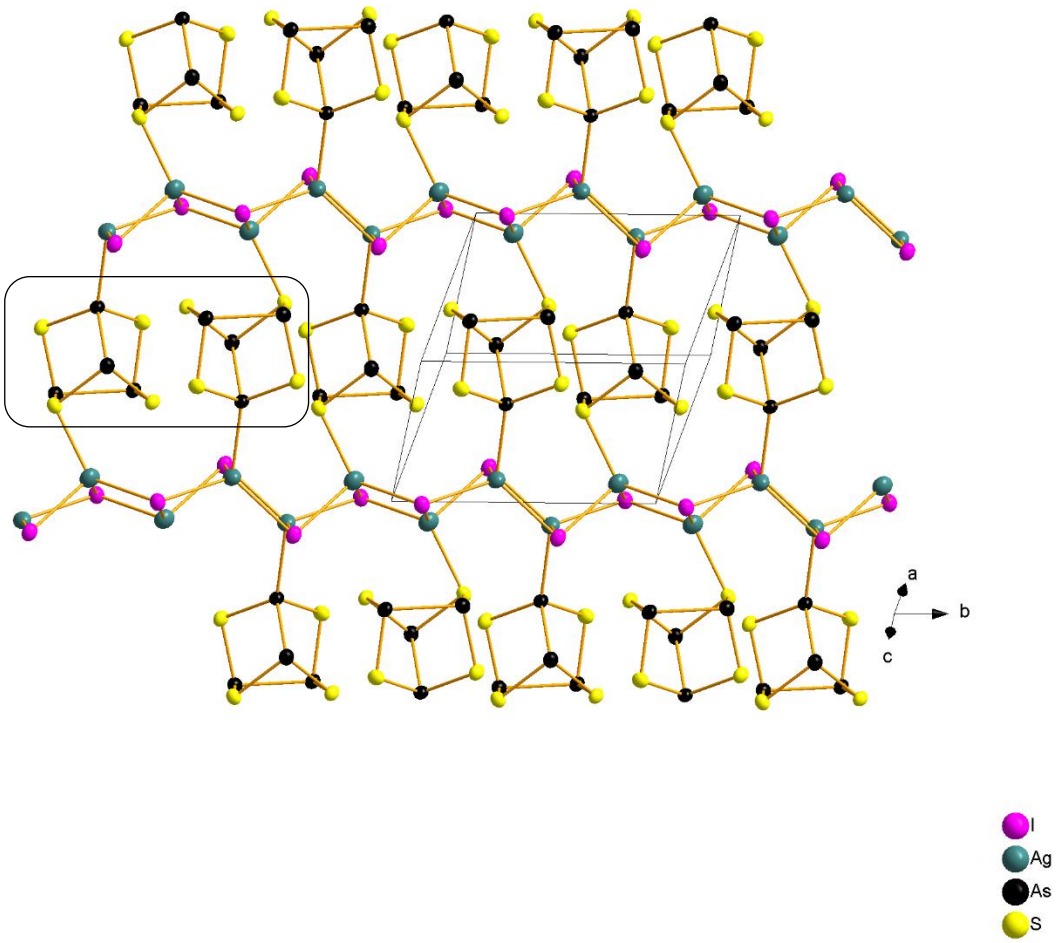

Figure 3.2.1.6: Complete crystal structure: As_4S_4 cages are flanked between two AgI cages. Sulphur and arsenic coordinate to silver atom through η^1 coordination mode. Two of the cage molecules (highlighted in rectangle) can be viewed as a subunit. All ellipsoids are shown with 90% probability.

The shortest distances between any two adjacent cage molecules are d(S2·····As2') – 3.244 Å, *d*(S2·····As4') – 3.461 Å and *d*(S2·····S2') – 3.578 Å respectively (See **Figure 3.2.1.8**). All these distances are shorter than the sum of their respective Van der Waals radii with *d*(S·····As) being 3.65 Å and *d*(S·····S) being 3.60 Å respectively. Thus, it can be assumed that a shorter screw length leads eventually to a better packing of the cages molecules which leads to stronger Van der Waals interaction between the cage molecules.

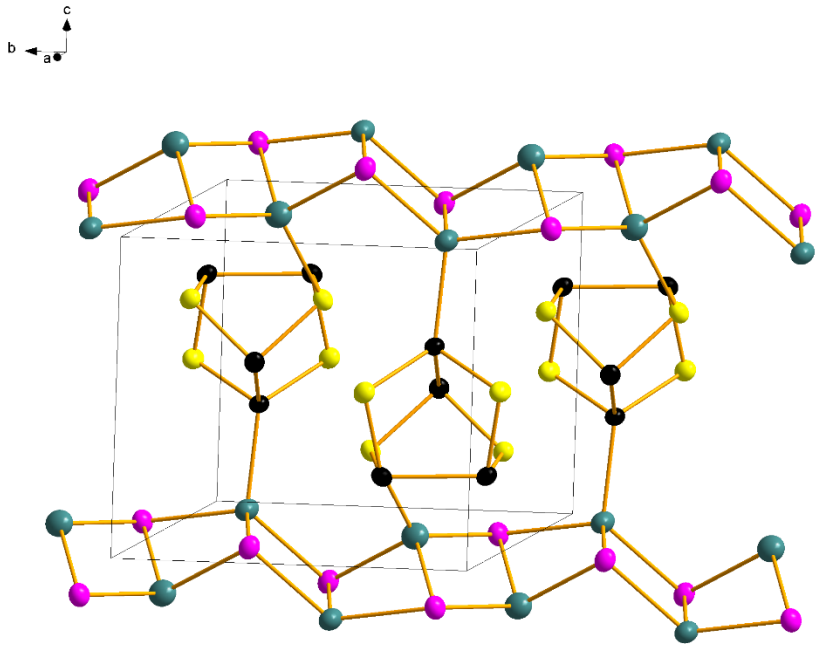

Figure 3.2.1.7: The realgar cages are not exactly in the same line. They are shifted relative to one another. This gives rise to a so called “push-pull” structure. All ellipsoids are shown with 90% probability.

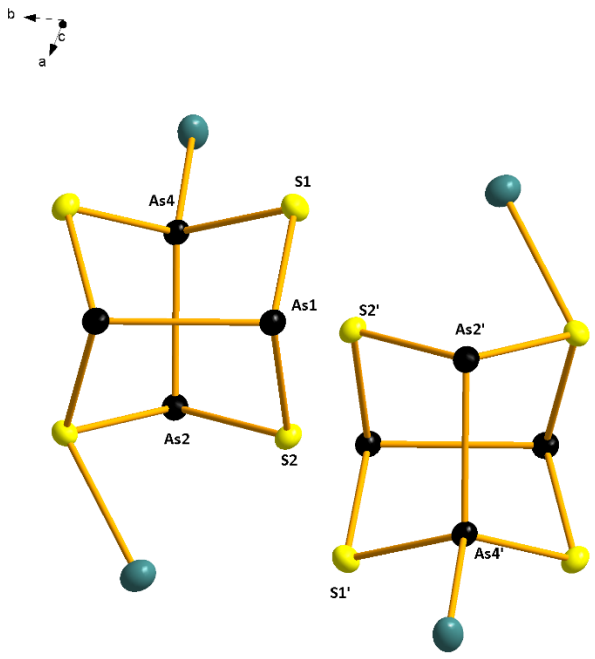

Figure 3.2.1.8: The shortest distances between any two adjacent cage molecules are *d*(S2·····As2’), *d*(S2·····As4’) and *d*(S2·····S2’) are shorter than the sum of their respective Van der Waals radii.

3.2.1.3 Powder X ray Diffraction

The yellow powder obtained from the solid-state synthesis was employed for recording the powder X-ray diffraction pattern of the adduct $(AgI)_2 \cdot (As_4S_4)$. The compound was homogenised by grinding it thoroughly in a mortar, packed between two mylar foils using minimum amount of grease and eventually loaded in a flat- bed sample holder. The comparison of the recorded and the simulated (from single crystal measurement) is depicted in the **Figure 3.2.1.9**. The positive intensity corresponds to the measured pattern while the negative intensity corresponds to the simulated pattern.

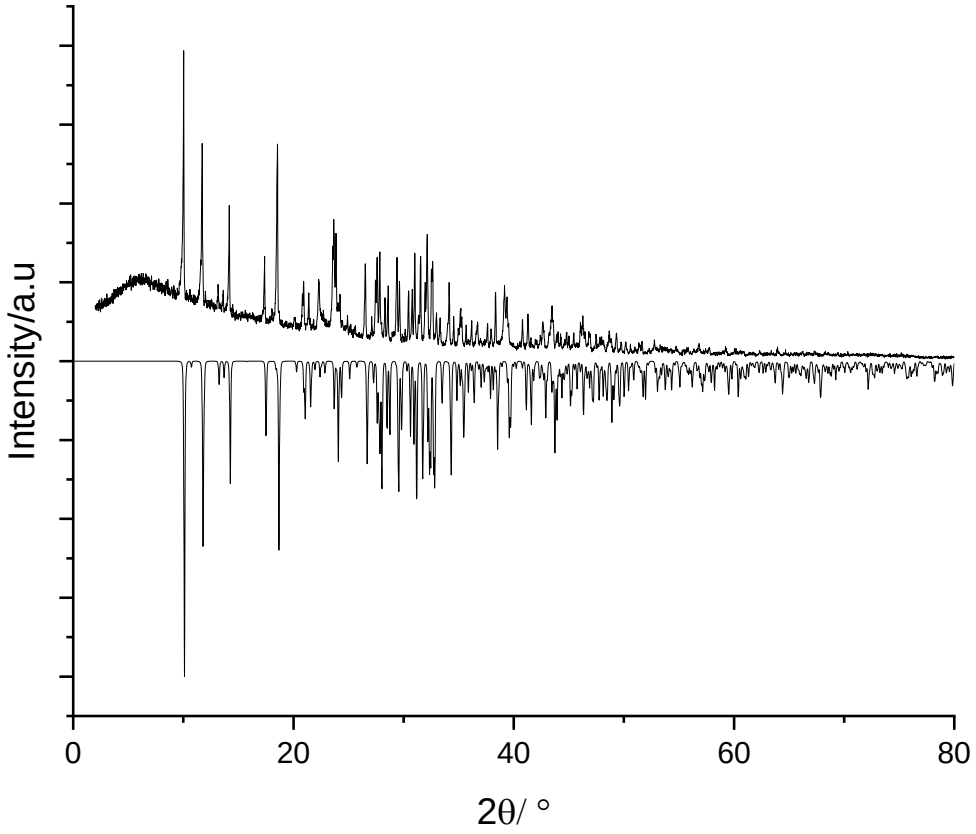

Figure 3.2.1.9: Measured powder pattern of $(AgI)_2 \cdot (As_4S_4)$ (positive intensity) in comparison to the theoretical powder pattern (negative intensity) derived from SC -XRD data.

Pattern Fitting and Refinement using JANA

As seen in the Figure, the measured and the simulated powder patterns are in good agreement with each other. The indexation and refinement of the measured was done with JANA 2006. For Jana 2006 refinement and pattern fitting were done with the Le Bail refinement algorithm.

Gaussian peak shape function with a cut-off of 12*FWHM was employed. Further a Legendre Polynomial correction was added. Lastly the background correction was done. This resulted in a difference plot. Still the peaks at the low angles show some asymmetry. For correcting this the "correction by divergence" correction was applied which resulted in better results. The final results after refinement converged to a GooF = 1.68, Rp = 9.45 and wRp = 12.92. **Figure 3.2.1.10** below shows the overlapping of the simulated(black) and the measured(yellow) powder pattern. **Table 3.2.1.5** shows the comparison of the lattice parameters. It should be noted that the single crystal X – ray diffraction experiment was performed at 123 K while powder pattern was recorded at room temperature.

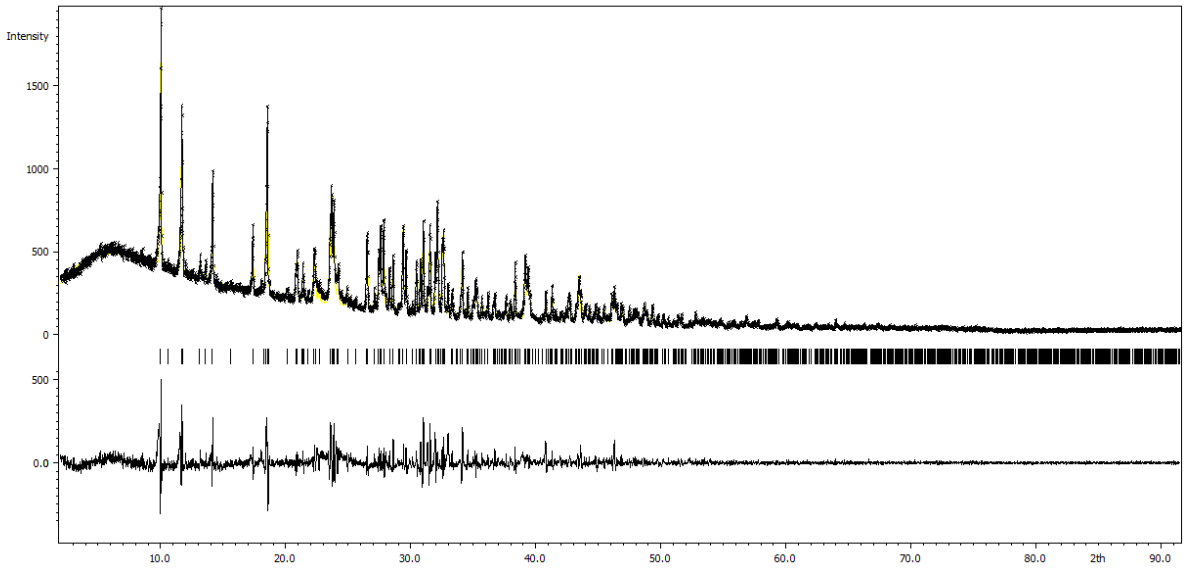

Figure 3.2.1.10: Refinement and pattern fitting using JANA2006. The figure displays the overlapping of the simulated powder pattern (black) and the measured powder pattern (yellow) with a difference plot.

Table 3.2.1.5: Comparison of the results of indexation and refinement done with JANA2006 (at room temperature) with the values obtained from single crystal diffraction experiment (T =123 K).

Method	a	b	c	α	β	γ	V
Single Crystal	8.633	8.685	9.714	89.97	65.43	73.22	628.31
Powder	8.680	8.727	9.750	89.97	65.42	73.23	637.10

3.2.1.4 SEM and EDX Analysis

For the scanning electron microscopic investigations and the EDX analysis, one of the shiny yellow blocks contained in the batch was separated under the light microscope and glued to the carbon-coated carrier. It must be noted here that only few crystals of the desired product were found in each reaction batch. **Figure 3.2.1.11** shows a scanning electron microscopic image of a $(AgI)_2 \cdot (As_4S_4)$ at a cathode voltage of 25 kV.

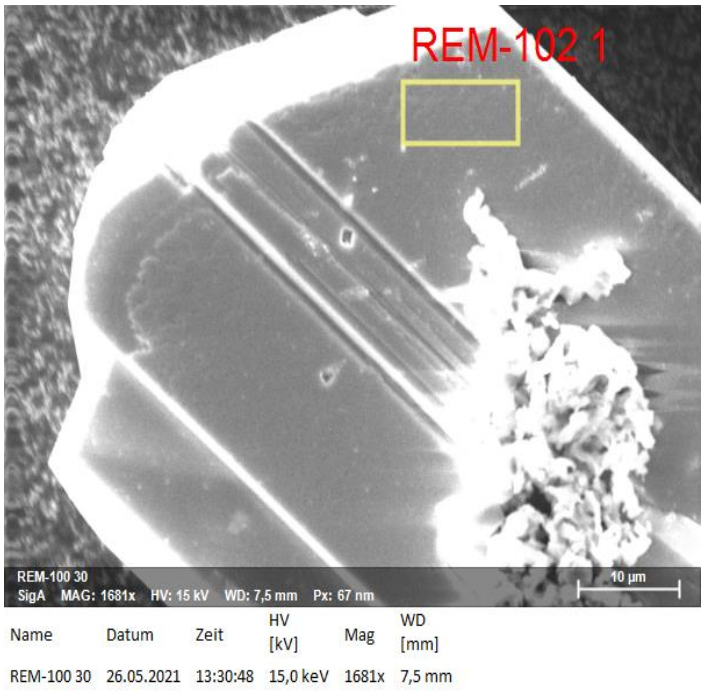

Figure 3.2.1.11: Electron microscopic image of a crystal of the adduct $(AgI)_2(As_4S_4)$ with an excitation voltage of 25kV.

Table 3.2.1.6: Result of energy dispersive X-ray spectroscopy and calculated proportions of silver, iodine, arsenic, and sulphur in the $(AgI)_2 \cdot (As_4S_4)$ adduct compound

Element	Ag	I	As	S
Abs. Error/ %	2.50	2.51	5.11	1.61
Rel. Error/ %	9.91	9.92	16.07	11.38
EDX results/Atom%	17.82	16.21	32.37	33.60
Calculated Results/Atom %	16.66	16.66	33.33	33.33

3.2.1.5 Raman Spectroscopy

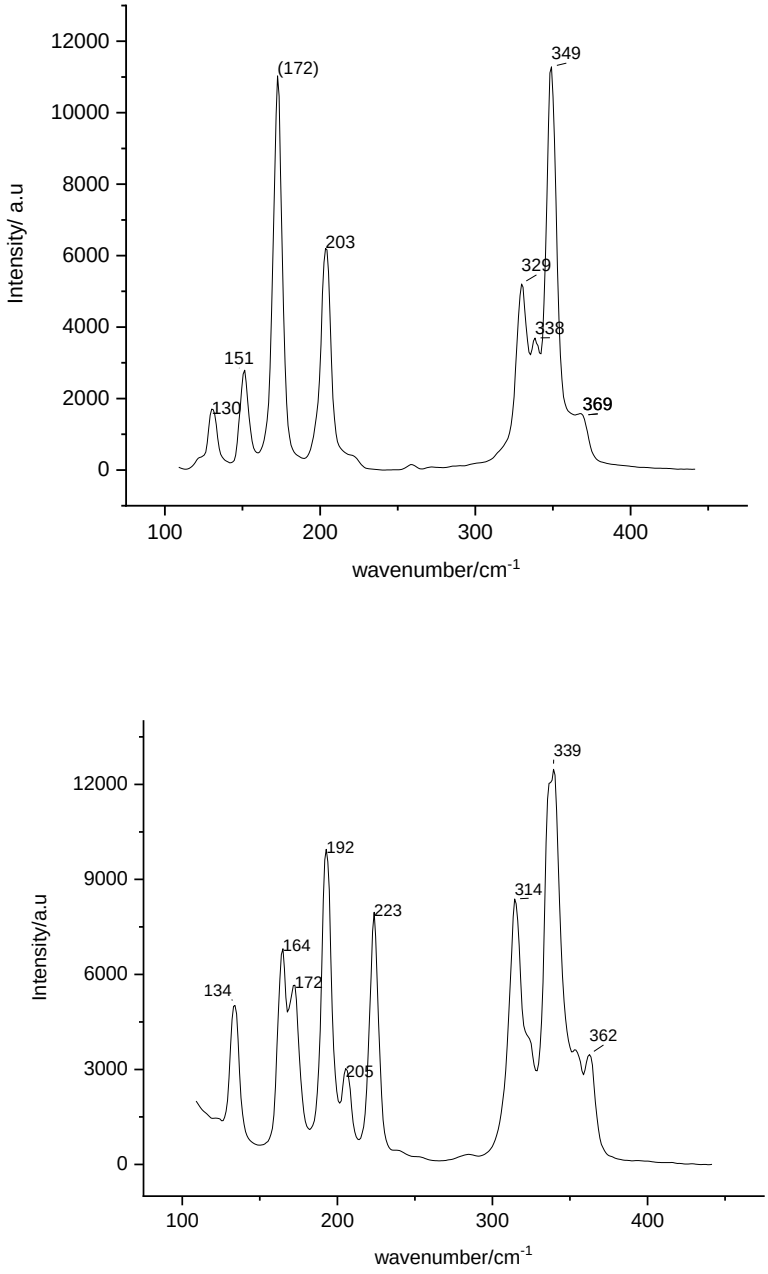

Figure 3.2.1.12: Raman spectra of As_4S_4(Realgar)(above) and $(AgI)_2{\cdot}(As_4S_4)$ (below).

Along with single crystal X ray measurement, the compound was investigated using Raman spectroscopy for a better understanding into the structural dynamics and bonding situation. The recorded Raman spectrum (See **Figure 3.2.1.12**) is seen to be divided into two distinct parts. First, the region between 300 cm^{-1} to 370 cm^{-1} which is the As-S stretching vibration

range and secondly, the deformation range from 140 cm^{-1} to 230 cm^{-1}. The measured frequencies and their comparison with α-As_4S_4 (Realgar) are listed in Table 7. Major changes are seen in the deformation range corresponding to As-S stretches. A red shift towards lower frequencies is seen. This fact can be readily corroborated from the single crystal analysis, where As-S bonds are up to 2.1 % longer in the adduct when compared to free As_4S_4. By analogy, the two bands at 203 cm^{-1} and 172 cm^{-1} can be assigned to As-As stretching vibrations, with 203 cm^{-1} being the symmetrical and 172 cm^{-1} the unsymmetrical stretching. When compared with "free" As_4S_4, these bands are seen to be blueshifted to higher frequencies by 20 cm^{-1}. Again, this is justified by the single crystal analysis where the As-As bonds are up to 1.2 % shorter than in the uncoordinated realgar. Thus, the coordination of AgI strengthens the As-As bonds at the same time weakening the As-S bonds. These results seem to be surprising when we consider the earlier attempts to incorporate undistorted As_4S_4 in a matrix which to cleavage of As-As bond eventually breaking up the cage molecule. But, in this case exact opposite scenario is observed. On coordination, the As-As bonds become stronger and hence more stable than in the free molecule.

Table 3.2.1.7: Raman frequencies in cm^{-1} for As_4S_4 and $(AgI)_2 \cdot (As_4S_4)$

Assignment	As_4S_4	$(AgI)_2 \cdot (As_4S_4)$	Intensity
ν(As-S)	130	134	strong
δ(As-S-As)	-	164	strong
δ(As-S-As)	151	-	weak
-	-	172	medium
δ(As-S-As)	172	192	very strong
-	-	205	weak
ν_{sym}(As-As)	203	223	strong
ν(As-As)	329	314	strong
ν(As-As)	338	-	very strong
ν(As-As)	349	339	very strong
ν(As-As)	369	362	weak shoulder

3.2.1.6 UV-Visible Spectroscopy

The yellow powder of $(AgI)_2 \cdot (As_4S_4)$ was homogenized with $BaSO_4$, filled in the sample container and measured with $BaSO_4$ as reference material. The **Figure 3.2.1.13** shows the solid – state absorption spectrum and the evaluation after Kubelka-Munk transformation.

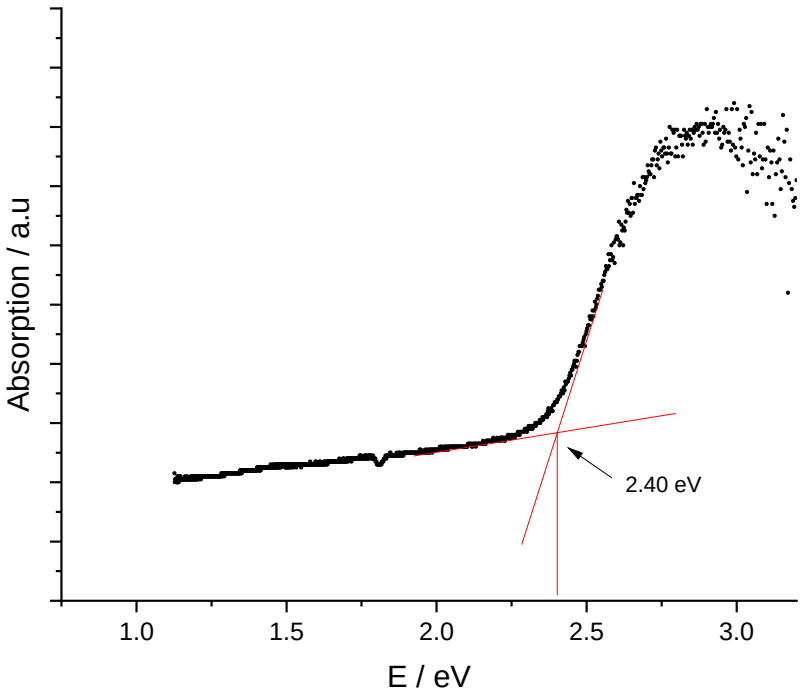

Figure 3.2.1.13: Solid-state UV / VIS absorption spectrum of $(AgI)_2 \cdot (As_4S_4)$. The absorption edge is 2.40 eV (517 nm).

For $(AgI)_2 \cdot (As_4S_4)$ the band gap was found to be 2.40 eV which corresponds to an absorption edge of 517 nm. The band gap so determined coincides well with the colour of the adduct compound. A photo of the compound can be found in Section **3.2.1.1**. The band gap of 2.40 eV renders the compound to be an optical semiconductor comparable to the (In/Ga) N system.

3.2.1.7 Thermal Analysis

A DTA measurement (heating rate 10 °C/min) of the yellow powder of the adduct the $(AgI)_2 \cdot (As_4S_4)$ was carried out to investigate the thermal behaviour which is depicted in the **Figure 3.2.1.14**. The compound decomposes at a temperature of 309 °C. This generated β -

realgar, which subsequently recrystallises at a temperature of 271 °C which can be seen in both cooling cycles. In order to verify β-realgar as the decomposition product, a powder diffractogram was recorded after the DTA measurement which proves the existence of β - realgar.

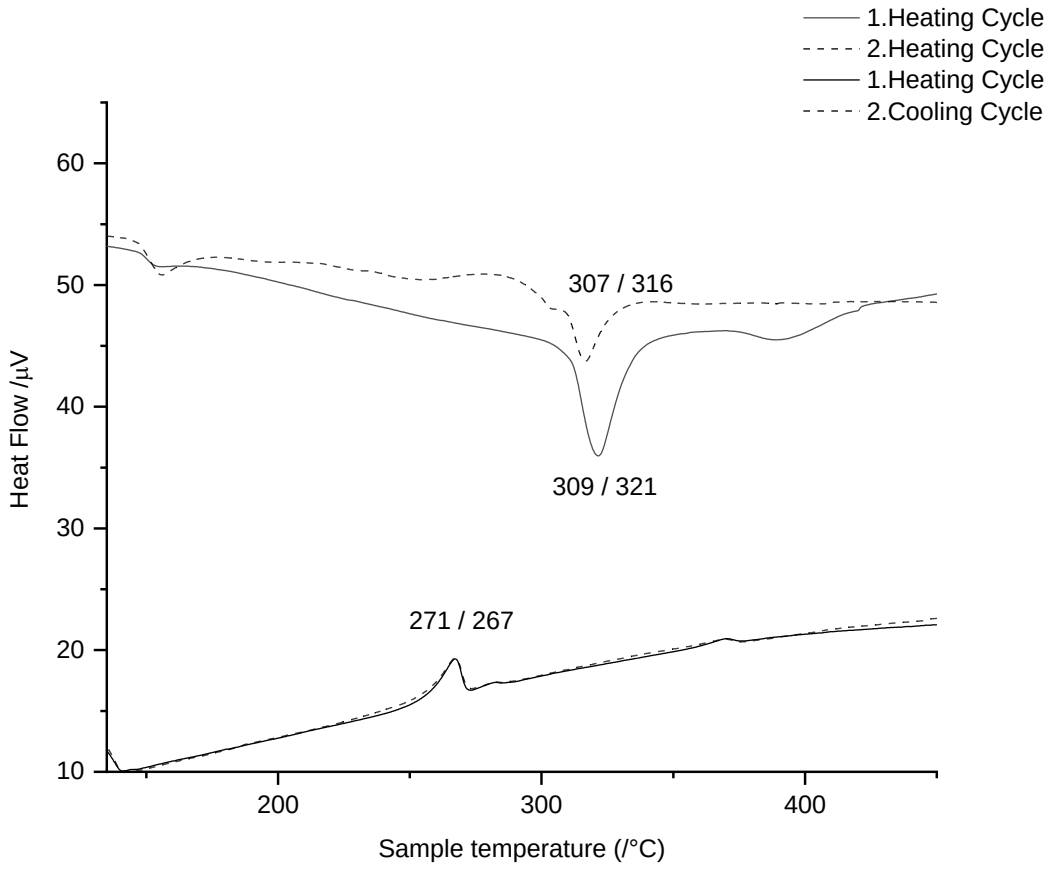

Figure 3.2.1.14: Excerpt from the DTA measurement of a sample of $(AgI)_2 \cdot (As_4S_4)$ showing Onset/Peak temperatures. The compound decomposes on heating to a temperature of 309 ° C.

.

3.2.1.8 Impedance Spectroscopy

In order to record the impedance spectrum, a sample of $(AgI)_2 \cdot (As_4S_4)$ was ground to a fine powder in a glove box under an argon atmosphere and pressed into a tablet using a hydraulic press at a pressure of six tons. The holding time during the pressing process was approximately ten minutes. The tablet obtained in this way had a density factor of 0.84. Temperature-

dependent spectra in the temperature range of 50-200 ° C were recorded, consisting of two cycles, each consisting of heating and subsequent cooling. The excitation voltage for the conductivity measurements for $(AgI)_2 \cdot (As_4S_4)$ was set at 50 mV. Spectra were recorded in the frequency range of 1 Hz ≤ ω ≤ 100 kHz. The first heating cycle was used to evaluate the data.

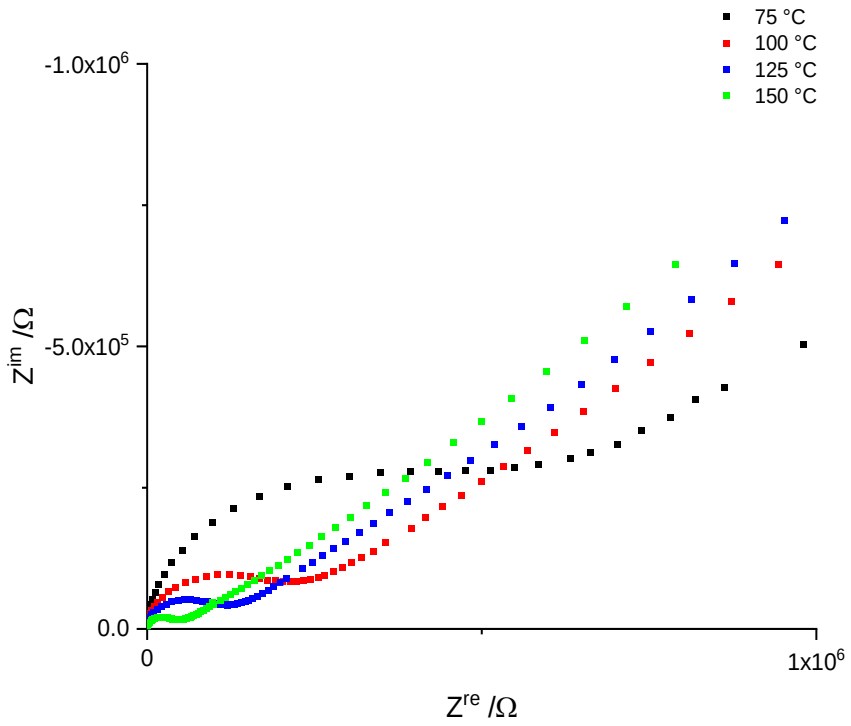

Figure 3.2.1.15: Nyquist plots of $(AgI)_2 \cdot (As_4S_4)$ at different temperatures.

The Nyquist plot in the **Figure 3.2.1.15** displays distinct semicircles, which corresponds to a characteristic plot for a semiconductor. For the specific conductivity of $(AgI)_2 \cdot (As_4S_4)$, a value of σ_{spec} = 2.25 * 10^{-7} Scm^{-1} was determined at 75 °C and a value of σ_{spec} = 1.44 * 10^{-5} Scm^{-1} at 175 °C. From the determined specific conductivities, an activation energy of E_A = 0.362 eV was calculated using Arrhenius plot (See **Figure 3.2.1.16)**. The activation energy was comparable to other similar compounds like $(AgI)_2 \cdot (Ag_3SbS_3)$ with E_A = 0.290 eV and $(AgI)_{0.5}(AgPO_3)_{0.5}$ = 0.308 eV.

Table 3.2.1.8: Specific conductivities of $(AgI)_2 \cdot (As_4S_4)$ at different temperatures

Temperature / °C	Specific conductivity /Scm^{-1}
75	$2.25*10^{-7}$
100	$7.93*10^{-7}$
125	$1.39*10^{-6}$
150	$3.36*10^{-6}$

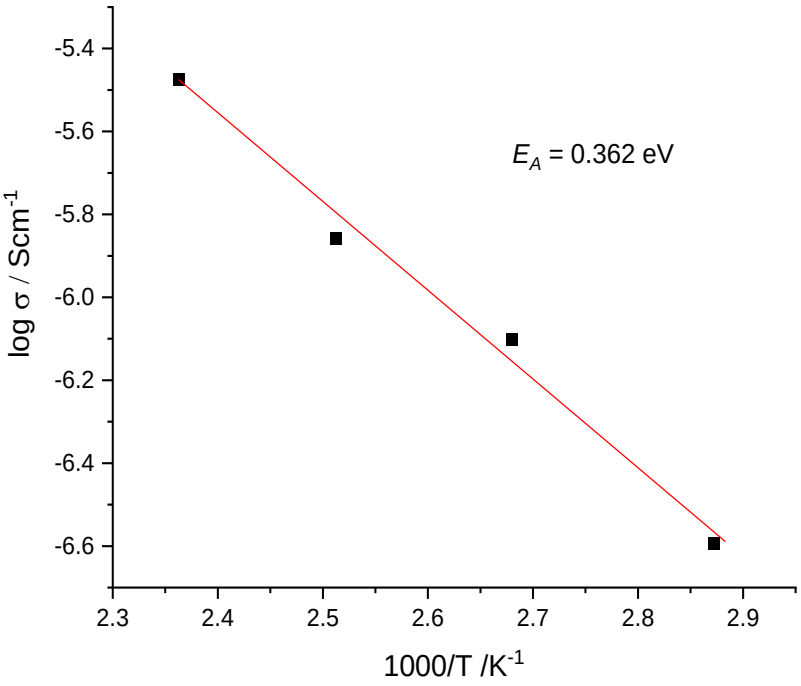

Figure 3.2.1.16: Arrhenius plot of the conductivities of $(AgI)_2 \cdot (As_4S_4)$.

2.1.9 Structural aspects and reactivity of As_4S_4 as a neutral ligand

The coordination chemistry of nortricyclane cages like P_4S_3, P_4Se_3, As_4S_3, α-P_4S_4 and β-P_4S_4 is well studied. In comparison, the mineral realgar was conceived to be an extremely weak ligand and hence was assumed to offer no coordination chemistry. When As_4S_4 cage molecule is reacted with a transition metal, fragmentation reactions are observed, and the cage is opened. An example in this direction is the compound $Co(Cp^*)CO(As_4S_4)$ ($Cp^* = C_5EtMe_4$). Here the cobalt atom inserts into the As-As bond which eventually leads to As1-As2 non-bonding distance of 3.71 Å as compared to 2.57 Å in free realgar. Also, a cage degradation can occur when the realgar cage is exposed to oxidising conditions. It was in 2006 when *Pfitzner et.al* successfully synthesised the adduct $(HgI_2)\cdot(As_4S_4)$ via a solid state approach that the common notion that the undistorted realgar displays no coordination chemistry was disproved. Subsequently *T.Rödl* was able to extend the concept further with copper(I) halides. In all the cases mentioned above the coordination took place exclusively through the sulphur atoms of the realgar. For example, in $(HgI_2)\cdot(As_4S_4)$, coordination of Hg atoms with As_4S_4 takes place through a η^2(S,S) coordination mode. Prior to the adduct $(AgI)_2\cdot(As_4S_4)$, *Krossing et. al* showed that, in the compound $Ag_3(As_4S_4)_4(o\text{-}dfb)[Al(ORF)_4]_3$, [RF = $C(CF_3)_3$, o-dbf = ortho diflurobenzene] along with S, coordination through As is also possible. Based on DFT calculation done in gas phase, they were able to demonstrate that this η^1(As) coordination mode was energetically closer to the cage degradation. Further they argued that with electronegativity arguments as well population analysis, it is shown that sulphur always bears a partial negative charge while arsenic bears a partial positive charge. In this scenario, if the reactions were only to be charge controlled, η^1(As) coordination would not have been possible. However the HOMO and HOMO-1 of realgar are separated by only 0.07 eV making a frontier orbital controlled reaction feasible which can proceed through either η^2(S,S) or η^1(As) coordination mode. This is exactly the case which is observed in the aforementioned compound and also in the adduct $(AgI)_2\cdot(As_4S_4)$. Here it must be noted that the calculations performed by *Krossing et. al* were in gas phase. Performing the population analysis in solid state would probably shed more light on the partial charges and eventually on the way we understand the bonding situation in realgar.

3.2.2 The Adduct $(AgI)_2 \cdot (As_4Se_4)$

3.2.2.1 Synthesis

As_4Se_4 (0.341 g, 1 equiv) and AgI(0.152 g, 2 equiv) were transferred to a duran ampoule (7 cm) followed by addition of 1mL of toluene and ACN respectively. The reaction mixture was cooled under liquid nitrogen and subsequently evacuated and reacted in a stainless-steel autoclave under solvothermal conditions at 160 °C for 5 days. The oven was cooled down at 80 °C over a time period of 5 h and maintained at this temperature for another 2 days followed by slow cooling down (over 6 h) to RT. After cooling a few dark red coloured crystals of $(AgI)_2 \cdot (As_4Se_4)$ were obtained.

3.2.2.2 Single Crystal Structure Analysis

$(AgI)_2 \cdot (As_4Se_4)$ crystallises in primitive monoclinic space group and exhibits a non- merohedral twining and therefore the initial data set showed only 39.9 % indexation corresponding to a batch scale factor of 0.399. The two components were related to each other by the following twin law:

$$M = \begin{bmatrix} 1 & 0 & 0 \\ 0.556 & -1 & 0 \\ 0 & 0 & -1 \end{bmatrix}$$

The **Figure 3.2.2.0-1** shows the diffraction pattern along (hk0) in the reciprocal space. The non-merohedral twinning is characterised by partially overlapping diffraction patterns which we can observe in the unwrapped precision diagram. We observe reflections which are not overlapped and belong to two different components as two spots which are close neighbours. The partially overlapped reflections can be identified with a relative increase in the intensity in comparison to the immediate neighbour.

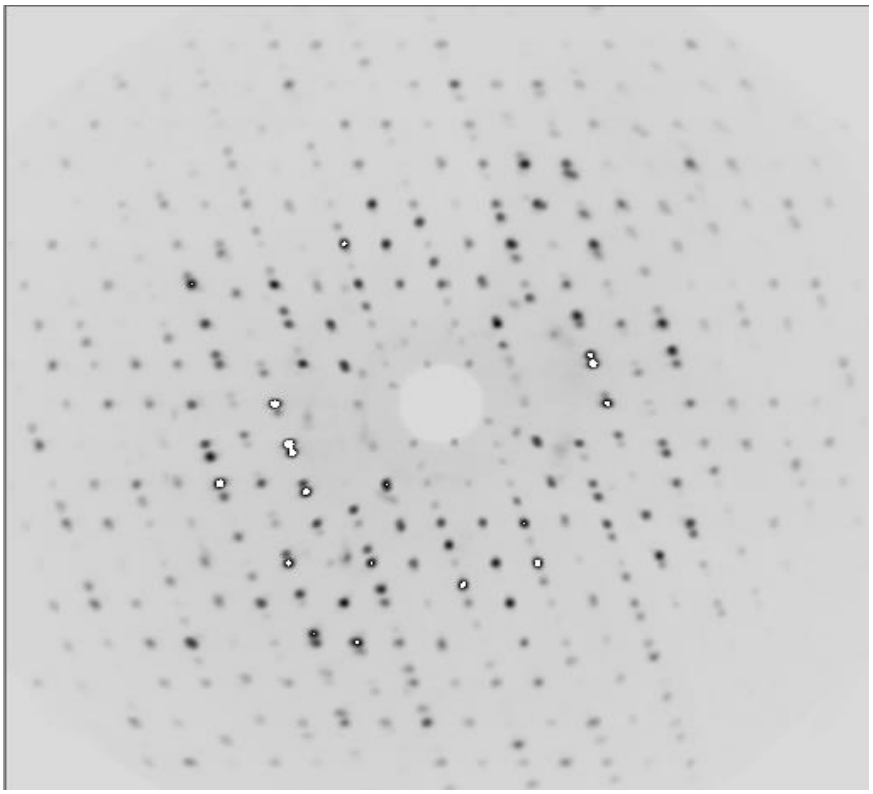

Figure 3.2.2.1: Diffraction pattern in the reciprocal space along (hk0) showing both partially overlapped intensities and also diffraction intensities from the two different components.

For structure solution a normal integration was performed considering the reflections from both the components. Next, the reciprocal space was investigated and using the automated twin finder in CrysalisPro the second component was found out. This procedure now gave the amount of each component (39.9% indexed reflections for component 1 and 29. 9% indexed reflections for component 2, in this case, thus leaving 30% reflections unindexed). Normal data reduction and finalisation was performed and .hklf4 and .hklf5 files were procured. The .hklf4 file is the merged file and contains reflections from both of the components while .hklf5 file contains the reflections only from sone component. Further, twin finalisation was performed, and the integration mask size was set to a lower value of 0.75 assuming it would result in better separation of the peaks. The .hklf4 file so obtained was used for structure solution. The input folder of the .hklf4 file was modified and hklf5 function and a BASF value of 0.5 (to start with, which was eventually corrected after the complete refinement was completed) was added. The final solution converged to R_σ to 0.045 and GooF of 1.153. The rest electron density also decreased a bit. This structure was solved and refined in Olex2 with SHELXT and SHELXL-2004.

Table 3.2.2.2 : Crystallographic data and measurement data for $(AgI)_2 \cdot (As_4Se_4)$. The table also shows the values when twinning is considered.

Empirical Formula	$Ag_2As_4I_2Se_4$	
Formula weight	1085.06	
Crystal colour and shape	Red block	
Crystal system	triclinic	
Space group	P-1	
a/Å	8.794	
b/ Å	8.826	
c/ Å	9.854	
α/°	89.95	
β/°	65.37	
γ/°	73.89	
V/Å^3, *Z*	662.30, 2	
Absorption coefficient(μ)/ mm^{-1}	28.47	
ρ_{calc}/g/cm^3	5.441	
Diffractometer	Rigaku Super Nova	
Radiation, temperature	Mo Kα (λ = 0.71073 Å) 123 K	
Θ-range/°	6.102 – 60.644	
hkl-range/°	-12 ≤ h ≤ 12 -12 ≤ k ≤ 12 -13 ≤ l ≤ 13	
Absorption correction	numerical (gaussian, Scale3 Abspack)	
Twinning considered	no(.hklf4)	yes(.hklf5)
Number of reflections	18173	8231
Independent reflections	3751	8231
BASF	-	0.595
R_σ, R_{int}	0.1065, 0.1535	0.045,-
Completeness	91%	100%
Structure solution	SHELXT	SHELXT
Structure refinement	SHELXT - 2014	SHELXT - 2014
Data/Restraints/Parameters	3751/0/109	8231/0/111
GooF	1.092	1.153
R_1, wR_2 *[I>2σ(I)]*	0.0554, 0.1655	0.0517, 0.1894
R_1, wR_2 *[all reflexes]*	0.0972, 0.2363	0.0866, 0.2473
Largest diff. peak/hole/e Å^{-3}	6.27/-7.18	5.30/-2.68

$(AgI)_2 \cdot (As_4Se_4)$ crystallises in the space group P-1 with a = 8.794 Å, b = 8.826 Å , c = 9.854 Å, α = 89.95 ° β = 65.37 ° , γ = 73.89 ° , V = 662.30 Å3 and Z =2. The positions and isotropic displacement parameters can be found in Appendix in **Table A.5**. The anisotropic displacement parameters are listed in **Table A.6**. The bond lengths and bond angles can be

found in **Table A.7** and **Table A.8**. The complete structure can be subdivided into two sub-structures, viz. the neutral α - As_4Se_4 cage and the one-dimensional AgI layers. The two substructures are connected through η^1 Se and η^1 As coordination to Ag atoms. Here must be noted that the measurement was carried out at 123 K and compared to literature values at 298 K.

α - As_4Se_4 substructure

The cage molecule in the adduct compound $(AgI)_2 \cdot (As_4Se_4)$ is similar to the binary cage molecules of pure As_4Se_4.

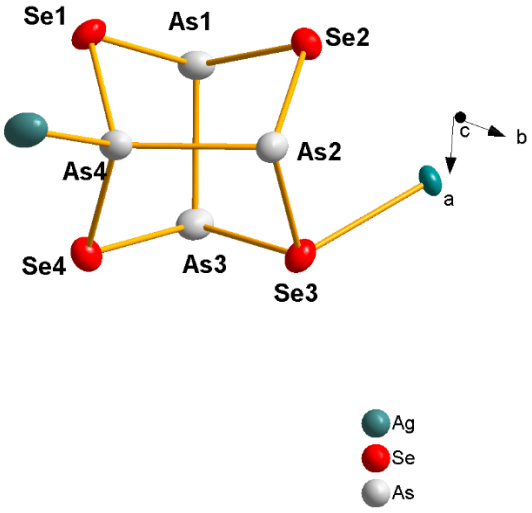

Figure 3.2.2.2: Isolated As_4Se_4 cage molecule with silver atoms. The coordination takes place through both sulphur and arsenic atoms. Iodine atoms are not shown for the sake of simplicity. All ellipsoids are shown with 90% probability.

The coordination of silver iodide to the cage molecule has some effect on the bond lengths and bond angles which are discussed in the following section. As seen in **Figure 3.2.2.2** silver atom is coordinated to the As_4Se_4 through η^1 (Se) and η^1 (As). Further the selenium and arsenic coordinated to the silver atom are not the immediate neighbours rather lie on the opposite side of each other. Here in **Figure 3.2.2.2**, it is noted that the silver atom coordinated to As4 projects out of the plane of the paper while the silver atom coordinated to Se3 is behind the plane of the paper.

Table 3.2.2.2: Selected interatomic distances (in Å) for (As_4S_4) in $(AgI)_2 \cdot (As_4Se_4)$. Rows marked in orange represent contraction while in blue represent elongation upon coordination with AgI. Maximum deviation is observed at the sites of selenium and arsenic coordination.

Bond/Distance	$(AgI)_2 \cdot (As_4Se_4)$	As_4Se_4	Difference
As1 – As3	2.569	2.560	+0.009
As2 – As4	2.532	2.571	-0.039
As1 – Se1	2.386	2.384	+0.002
As1 – Se2	2.409	2.289	+0.020
Se2 – As2	2.405	2.393	+0.012
As2 – Se3	2.439	2.381	+0.058
Se3 – As3	2.415	2.387	+0.028
As3 - Se4	2.388	2.386	+0.002
Se4 – As4	2.393	2.378	+0.015
As4 – Se1	2.376	2.376	0.00

The bond lengths for As2-As4, Se4-As4, As4-Se1, Se3-As2 and Se3-As3 are expected to deviate from the free uncoordinated As_4Se_4 after coordination with silver atom. As expected, d(As2-Se3) shows the maximum deviation, an elongation of 0.058 Å when compared to free uncoordinated As_4Se_4 upon coordination. d(Se4-As4) also shows an elongation of 0.015 Å. Interestingly enough d(As4-Se1) did not show any change at all although As4 is coordinated to silver atom. It is noteworthy here that d(Se4-As4) shows deviation and d(As4-Se1) does not deviate at all although they have the atom As4 in common. Thus, the coordination of silver atom affected the bond length d(Se4-As4) while leaving d(As4-Se1) unchanged. The only bond that was curtailed was d(As2- As4) which was shortened by 0.039 Å when compared to free As_4Se_4 cage molecule. d (As1- Se2) and d(Se2-As2) show slight lengthening which runs against the common assumption that coordination of silver atom is the reason for lengthening of the bonds in the cage molecule of the adduct compound.

As with bond lengths, bond angles of As_4Se_4 cages are affected once coordinated to silver atom. (See **Table 3.2.2.3**). The highest deviation is seen in the angle ∠(As2-Se3-As3) which is a good 4.82 ° greater than in the uncoordinated free As4Se4 cage. This can be attributed to the fact that Se3 is coordinated to silver atom. It should be noted here that d(As2-Se3) and d(Se3-As3) were also lengthened upon coordination. An increase of 3.23 ° from 100.2 ° to 103.43 ° was

Table 3.2.2.3: Selected bond angles (in Å) for (As_4Se_4) in $(AgI)_2{\cdot}(As_4Se_4)$. Rows marked in orange represent contraction while in blue represent elongation upon coordination with AgI as a consequence of altered bond distances. Maximum deviation is observed at the sites selenium and arsenic coordination.

Bond	$(AgI)_2{\cdot}$ (As_4Se_4)	As_4Se_4	Difference
As1-Se2-As2	100.32	97.8	+2.5
As1-Se1-As4	96.91	98.4	-1.49
As4-Se4-As3	96.90	98.2	-1.30
As2-Se3-As3	99.52	94.7	+4.82
Se1-As4-As2	103.63	101.2	+2.43
Se1-As1-As3	102.13	100.7	+1.43
Se2-As1-Se1	94.47	94.70	-0.23
Se2-As2-As4	100.07	101.6	-1.53
Se2-As1-As3	99.15	97.9	+1.25
Se4-As3-As1	101.72	101.90	-0.18
Se4-As4-As2	103.43	100.2	+3.23
Se4-As4-Se1	96.44	94.2	+2.24
Se3-As3-Se4	92.22	94.0	-1.78
Se3-As2-Se2	90.10	93.9	-3.80
Se3-As3-As1	101.33	100.9	+0.43

seen in ∠(Se4-As4-As2). This can be attributed to the shortening of the d(As2-As4). The combined effect of shortening of d(As2- As4) and lengthening of d(Se2-As2) and d(As2-Se2) results in reduction of ∠(Se3-As2-Se2) to 90.10 ° in the adduct from 93.9 ° in the uncoordinated As_4Se_4 cage.

The coordination sphere of silver

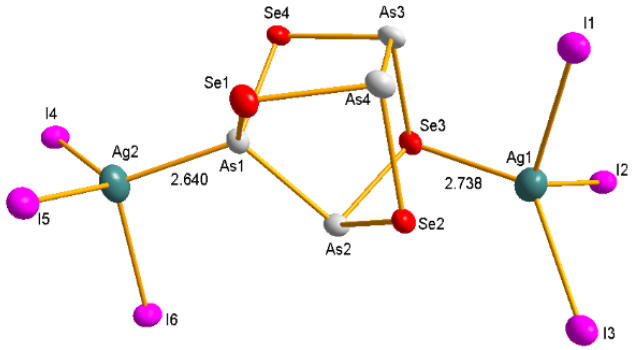

Figure 3.2.2.3: A section of the adduct compound $(AgI)_2(As_4Se_4)$ showing the coordination of silver atom. Both silver atoms find themselves in a distorted tetrahedral environment. All ellipsoids are shown with 90% probability.

Both silver atoms show a distorted (3+1) tetrahedral coordination, coordinating to three iodine and one selenium or arsenic atom respectively. $(AgI)_2 \cdot (As_4Se_4)$ represents one of the rarest examples of η^1 (As) coordination. The η^1 (As) Ag-As bond length of 2.640 Å is comparable to recently published compound by Krossing et.al of 2.561 Å. As also in the case of $(AgI)_2 \cdot (As_4S_4)$, Ag coordinates to Se and As which are facing each other opposite rather than direct neighbours. The **Table 3.2.3.4** shows selected bond angles.

Table 3.2.4.4: Selected bond angles relevant for the silver coordination in the (AgI)2·(As4S4) adduct compound.

Se3-Ag1-I1	99.37	As1-Ag2-I4	125.93
I1-Ag1-I2	108.67	As1-Ag2-I5	117.62
I2-Ag1-I3	96.94	I5-Ag2-I6	111.24
Se3-Ag1-I3	130.95	As1-Ag2-I6	101.67

It is seen that there is deviation from the ideal value of 109.4 ° for a tetrahedral geometry. It can be argued that the reason behind this distortion can be, how eventually the adduct molecules are packed in 3-D which will be discussed later.

AgI Layers

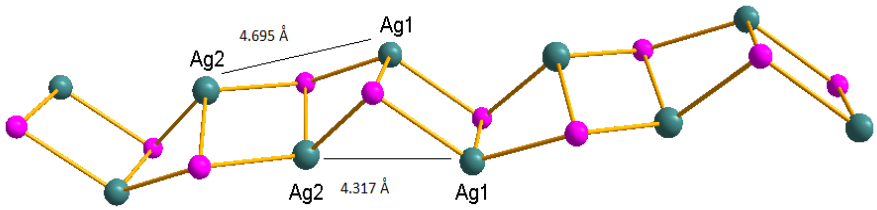

Figure 3.2.2.4: The visualisation of the AgI layers in the $(AgI)_2 \cdot (As_4Se_4)$ adduct compound. Since there are two crystallographically distinct silver positions, two separate screw lengths could be visualised. All ellipsoids are shown with 90% probability.

The adduct $(AgI)_2 \cdot (As_4Se_4)$ can be visualised as been flanked by two layers of AgI in which the As_4Se_4 cages are embedded. These chains have two crystallographically distinct silver atoms with d(Ag2-Ag1) being 4.695 Å. and d(Ag2-Ag1) being 4.317 Å. Since there are two different silver positions, two different screw lengths can be imagined depending on the viewing angle. As seen, these two distances differ by a small amount. This can also be the possible reason as to why the adjacent As_4Se_4 cages are slightly shifted relative to one another in the complete structure.

Complete Crystal structure

$(AgI)_2 \cdot (As_4Se_4)$ consists of As_4Se_4 cage molecules connected via AgI layers. The cage molecules are flanked from both sides by infinite silver iodide layers (See **Figure 3.2.2.5**)

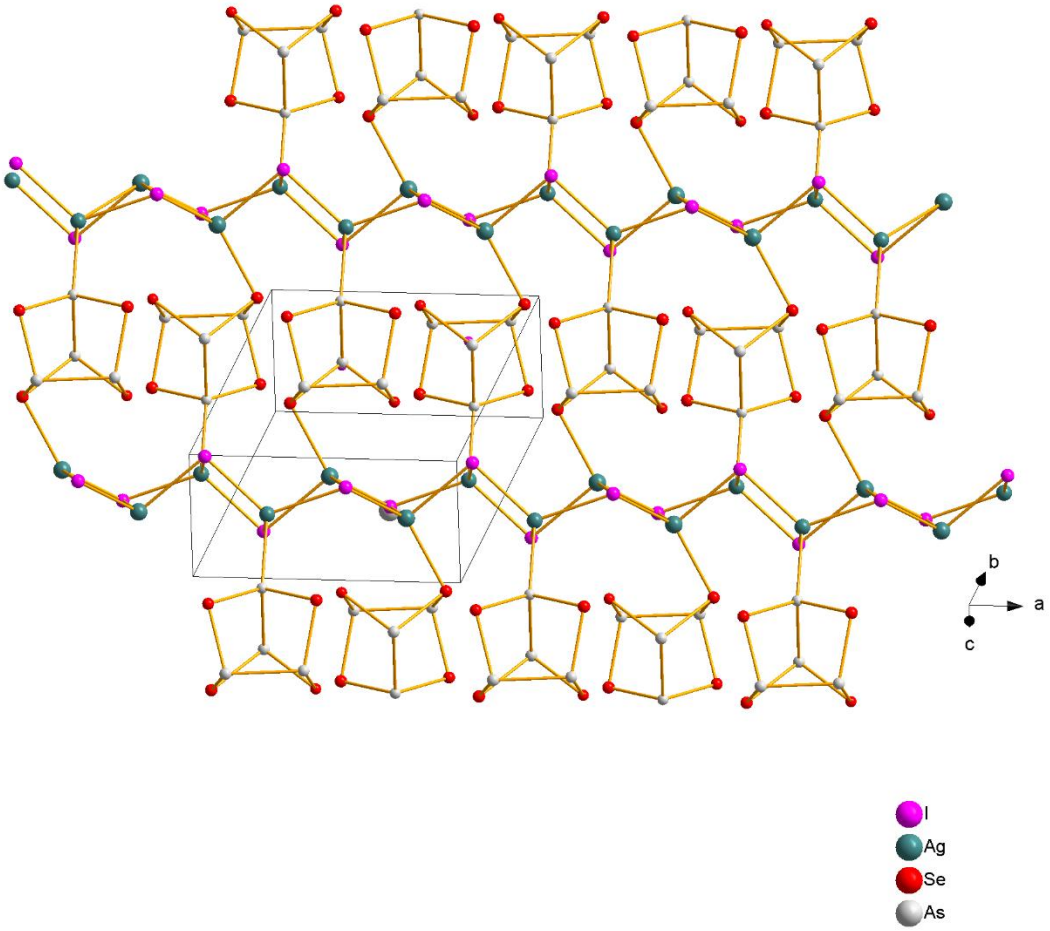

Figure 3.2.2.5: Complete crystal structure: As_4Se_4 cages are flanked between two AgI cages. Selenium and arsenic coordinate to silver atom through η1 coordination mode. The AgI layers run parallel to the *a* axis. All ellipsoids are shown with 90% probability.

It can be seen that the AgI layers propagate along the *a* axis, parallel to the plane of the paper. Between two such layers, the As_4Se_4 cages lie almost perpendicular to the plane of the silver iodide layers. Further it is observed that As and Se coordinate alternatingly to silver atom, making it a kind of push-pull substructure. As also already mentioned in the earlier sub section, the distances d(Ag-Se) and d(Ag-As) differ by small amount [d(Ag-Se) being 2.738 Å and d(Ag-As) being 2.640 Å respectively] which explains the partially skewed substructure.

The shortest distances between any two adjacent cage molecules are d(Se4…As2) – 3.394 Å, d(Se4…Se1) – 3.698 Å and d(Se2…Se3) – 3.785 Å respectively (See **Figure 3.2.2.6**).

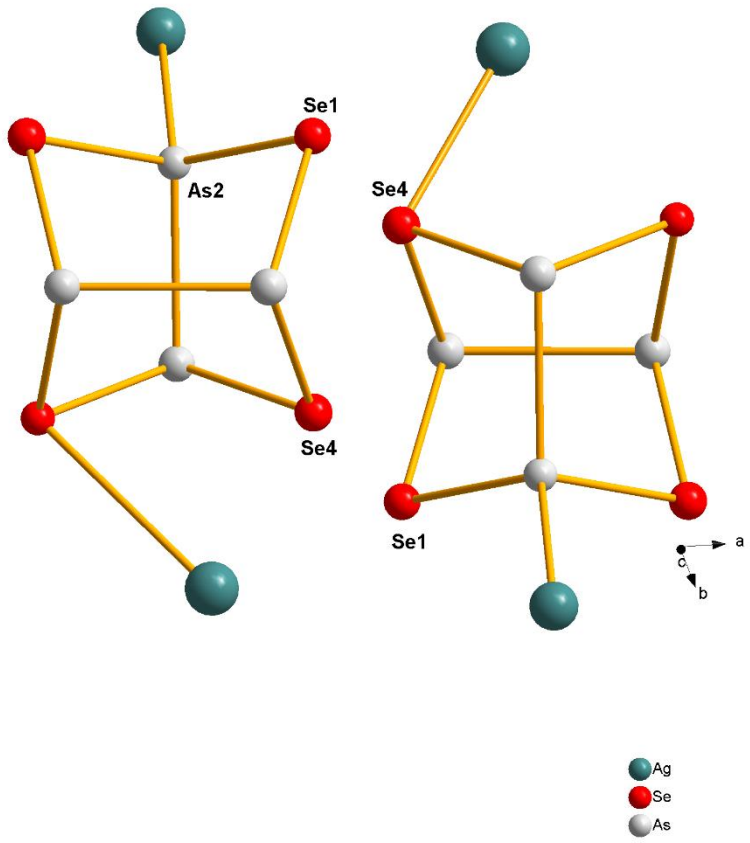

Figure 3.2.2.6: The shortest distances between any two adjacent cage molecules are d(Se4·····As2), d(Se4·····Se1) and d(Se2·····Se3) are shorter than the sum of their respective Van der Waals radii.

All these distances are shorter than the sum of their respective Van der Waals radii with d(Se…As) being 3.75 Å and d(Se…Se) being 3.80 Å respectively. Thus, it can be assumed that a shorter screw length leads eventually to a better packing of the cages molecules which leads to stronger Van der Waals interaction between the cage molecules.

3.2.2.3 SEM and EDX Analysis

For the scanning electron microscopic investigations and the EDX analysis, one of the shiny red blocks contained in the batch was separated under the light microscope and glued to the carbon-coated carrier. It must be noted here that only few crystals of the desired product were found in each reaction batch. **Figure 3.2.2.6** shows a scanning electron microscopic image of a $(AgI)_2 \cdot (As_4Se_4)$ at a cathode voltage of 25 kV.

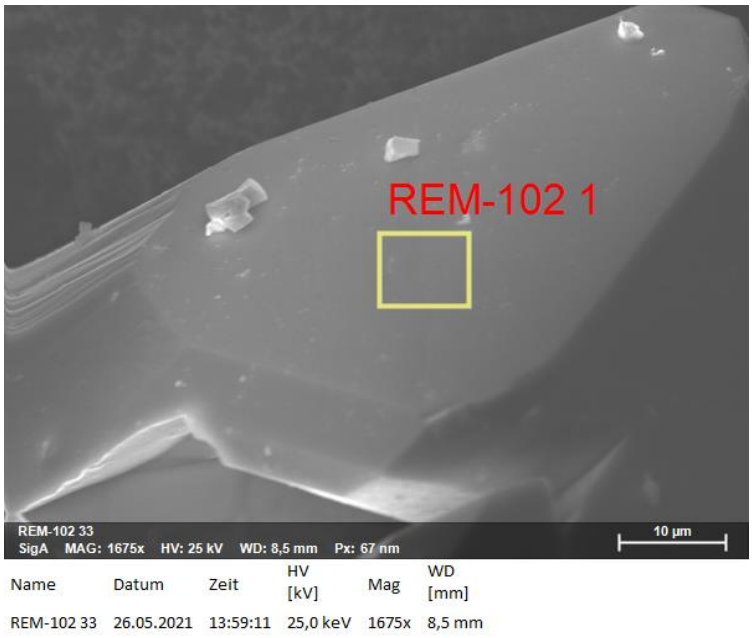

Figure 3.2.2.6: Electron microscopic image of a crystal of the adduct $(AgI)_2(As_4Se_4)$ with an excitation voltage of 25kV.

To verify the chemical constitution of $(AgI)_2 \cdot (As_4Se_4)$ an EDX analysis was performed and compared with the calculated values from single crystal X-ray experiment. These results are shown in **Table 3.2.5.5**

Table 3.2.6.5: Result of energy dispersive X-ray spectroscopy and calculated proportions of silver, iodine, arsenic, and sulphur in the $(AgI)_2 \cdot (As_4Se_4)$ adduct compound

Element	Ag	I	As	Se
Abs. Error/ %	1.58	1.79	1.98	2.26
Rel. Error/ %	10.23	9.11	8.57	8.73
EDX results/Atom%	15.30	16.55	33.03	35.12
Calculated Results/Atom %	16.66	16.66	33.33	33.33

3.2.3 The Adduct $(AgBr)\cdot(As_4S_4)$

3.2.3.1 Synthesis

Solvothermal Synthesis

As_4S_4 (0.347 g, 1 equiv) and AgBr(0.152 g, 1 equiv) were transferred to a duran ampoule (7 cm) followed by addition of 1mL of toluene and ACN respectively. The reaction mixture was cooled under liquid nitrogen and subsequently evacuated and reacted in a stainless-steel autoclave under solvothermal conditions at 160 °C for 5 days. The oven was cooled down at 80 °C over a time period of 5 h and maintained at this temperature for another 2 days followed by slow cooling down (over 6 h) to RT. After cooling a few air stable yellow coloured block-like crystals of $(AgBr)\cdot(As_4S_4)$ were obtained.

Solid State Synthesis

In the aforementioned solvothermal approach, along with the desired product (which crystalises as distinct yellow blocks) many other side products and unreacted realgar was observed. A phase pure synthesis of $(AgBr)\cdot(As_4S_4)$ was tried by reacting silver bromide (0.152 g, 1 equiv) and realgar (0.347 g, 1 equiv) at 210 °C for 2 weeks. The educts were weighed, transferred in a quartz ampoule, evacuated, sealed and then rested in oven. The heating rate was 1.5 °C/min, while the cooling rate was 0.5 °C/min. The resulting product was fine yellow powder. This was used for further analysis. For finding the correct temperature for reaction, each time a reaction was performed, every time with an increase of 10 °C, starting from 180 °C. Each time the reactions were monitored by X-ray powder diffraction. With this approach the desired product was obtained but every time reminiscent of silver bromide was observed as monitored from X ray powder diffraction analysis.

3.2.3.2 Single Crystal Analysis-

Table 3.2.3.1: Table gives an overview of the crystallographic data and measurement parameters of $(AgBr)\cdot(As_4S_4)$.

Empirical Formula	$AgAs_4BrS_4$
Formula weight	615.70
Crystal colour and shape	Yellow block
Crystal system	monoclinic
Space group	$P2_1/n$ (Nr. 14)
a/Å	7.2706(3)
b/ Å	12.3640(5)
c/ Å	11.2160(5)
α/°	90
β/°	98.506(4)
γ/°	90
V/Å^3, *Z*	997.14, 4
Absorption coefficient(μ)/ mm^{-1}	19.964
ρ_{calc}/g/cm^3	4.101
Diffractometer	Rigaku Super Nova
Radiation, temperature	Mo Kα (λ = 0.71073 Å), 298 K
Θ-range/°	6.28 – 6.338
hkl-range/°	-10 ≤ h ≤ 10
	-17 ≤ k ≤ 17
	-15 ≤ l ≤ 15
Absorption correction	numerical (gaussian, Scale3 Abspack)
Number of reflexes	11661
Independent reflections	2831
R_σ, R_{int}	0.0272, 0.0284
Completeness	100%
Structure solution	SHELXT
Structure refinement	SHELXT - 2014
Data/Restraints/Parameters	2831/0/91
GooF	1.073
R_1, wR_2 *[I>2σ(I)]*	0.0348, 0.0794
R_1, wR_2 *[all reflexes]*	0.0442, 0.0837
Largest diff. peak/hole/e Å^{-3}	1.82/-2.35

$(AgBr)\cdot(As_4S_4)$ crystallises in the space group $P2_1/n$ (Nr. 14) with a = 7.270 Å, b = 12.364 Å , c = 11.215 Å, α = 90.00 ° β = 98.50 ° , γ = 90.00 ° , V = 997.14 $Å^3$ and Z =4 (T = 298 K). The refinement of all data converged at a GooF of 1.073, with R_1 = 3.48 % and wR_2 = 7.94 %. The positions and isotropic displacement parameters can be found in Appendix in **Table A.9**. The anisotropic displacement parameters are listed in **Table A.10**. The bond lengths and bond angles can be found in **Table A.11** and **Table A.12**. The complete structure can be subdivided into two sub- structures, viz. the neutral α - As_4S_4 cages and the one-dimensional AgBr layers which connect the As_4S_4 cages. The two adjacent As_4S_4 cages are connected to each other through a silver atom via a η^1(S) coordination mode.

α - As_4S_4 substructure

The cage molecule in the adduct compound $(AgBr)\cdot(As_4S_4)$ is similar to the binary cage molecules of pure As_4S_4 which explained in the following tables.

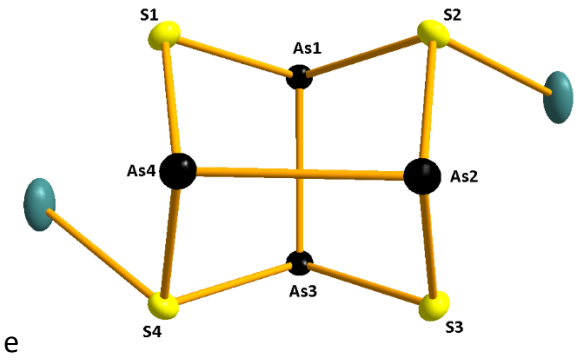

e

Figure 3.2.3.1: Isolated As_4S_4 cage molecule with silver atoms. The coordination takes place exclusively through sulphur and atoms. Bromine atoms are not shown for the sake of simplicity. All ellipsoids are shown with 90% probability.

The coordination of silver bromide to the cage molecule has some effect on the bond lengths and bond angles which are discussed in the following section. As seen in the **Figure 3.2.3.1** the coordination of silver atom takes place exclusively through the sulphur atoms in contrast to the adduct $(AgI)_2\cdot(As_4S_4)$ and $(AgI)_2\cdot(As_4Se_4)$ where coordination takes place both via sulphur and arsenic. Furthermore, here the silver atom is shared between two molecules of As_4S_4,

making the overall stoichiometry of the adduct 1:1 in contrast to 2:1 in $(AgI)_2 \cdot (As_4S_4)$ and $(AgI)_2 \cdot (As_4Se_4)$.

Table 3.2.3.2: Selected interatomic distances (in Å) for (As_4S_4) in $(AgBr) \cdot (As_4S_4)$. Rows marked in blue represent elongation upon coordination with AgI. Maximum deviation is observed at the sites of sulphur and arsenic coordination.

Bond/Distance	$(AgBr) \cdot (As_4S_4)$	As_4S_4	Difference
As1 – As3	2.559	2.563	-0.004
As2 – As4	2.560	2.569	-0.009
As1 – S1	2.256	2.246	+0.010
As1 – S2	2.261	2.238	+0.023
S2 – As2	2.279	2.229	+0.050
As2 – S3	2.228	2.234	-0.006
S3 – As3	2.245	2.237	+0.008
As3 - S4	2.265	2.243	+0.022
S4 – As4	2.257	2.241	+0.016
As4 – S1	2.235	2.231	+0.004

As expected, maximum deviation is seen at the sites of silver coordination. Thus, the bond lengths – As1-S2, S2-As2, As3-S4 and S4-As4 are expected to alter. For the compound under consideration the highest digression is seen for *d*(S2-As2). The S2-As2 bond is elongated by 0.050 Å when compared to the free uncoordinated As_4S_4 cage molecule. This is followed by *d*(As1-S2) and *d*(As3-S4) which are elongated by 0.023 Å and 0.022 Å respectively in comparison to free realgar. The least deviation of 0.016 Å is observed for *d*(S4-As4). Thus, in all the above-mentioned cases, the coordination of silver atoms results in elongation of the bonds in the cage molecule. As mentioned in the earlier chapter coordination of transition metals to the realgar molecule usually either destroys the cage molecule resulting in fragmentation or leads to ligand recombination reactions. Here it is worth noting that after

silver bromide coordination, the As-As bonds see almost no change (rather are strengthened by a tiny margin).

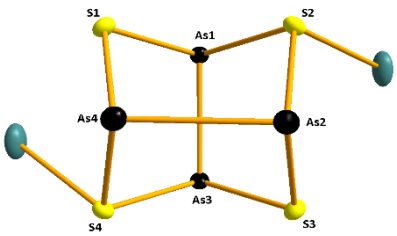

Figure 3.2.3.2: Isolated As_4S_4 cage molecule with silver atoms. The coordination takes place exclusively through sulphur and atoms. Bromine atoms are not shown for the sake of simplicity. All ellipsoids are shown with 90% probability.

As with bond lengths, bond angles are also affected once coordinated to the silver atom. (See Table). The highest deviation is seen for ∠ (S2-As2-As4). This bond is contracted by 2.47 ° when compared to "free" realgar cage molecule. This can be attributed to lengthening of d(As2-S2) which in turn reflects the effect of the silver coordination. ∠(S2-As1-S1) sees a decrease of 2.27 ° which can also be attributed to the lengthening of *d*(As1-S2) and the subsequent coordination of the silver atom with S2 which is also the case for ∠(As1-S2-As2) which increases by 1.3 °. The ∠(As2-S3-As3) and ∠(S1-As4-As2) both see an increase by 2.16 ° and 1.67 ° respectively as compared to free realgar although in this case there is no direct coordination of silver atom to sulphur.

Table 3.2.3.3: Selected bond angles (in Å) for (As_4S_4) in (AgBr)·(As_4S_4). Rows marked in orange represent contraction while in blue represent elongation upon coordination with AgI as a consequence of altered bond distances. Maximum deviation is observed at the sites of sulphur and arsenic coordination.

Bond	(AgBr)·(As_4S_4)	As_4S_4	Difference
As1-S2-As2	102.21	100.91	+1.3
As1-S1-As4	102.39	101.29	+1.1
As4-S4-As3	101.81	101.29	+0.52
As2-S3-As3	103.00	100.84	+2.16
S1-As4-As2	100.36	98.69	+1.67
S1-As1-As3	99.18	99.57	-0.39
S2-As1-S1	92.20	94.47	-2.27
S2-As2-As4	97.35	99.82	-2.47
S2-As1-As3	99.52	99.19	+0.33
S4-As3-As1	98.92	99.17	-0.25
S4-As4-As2	98.89	99.17	-0.28
S4-As4-S1	93.46	94.86	-1.4
S3-As3-S4	93.60	94.56	-0.96
S3-As2-S2	93.93	94.87	-0.94
S3-As3-As1	99.25	99.42	-0.17

The coordination sphere of silver

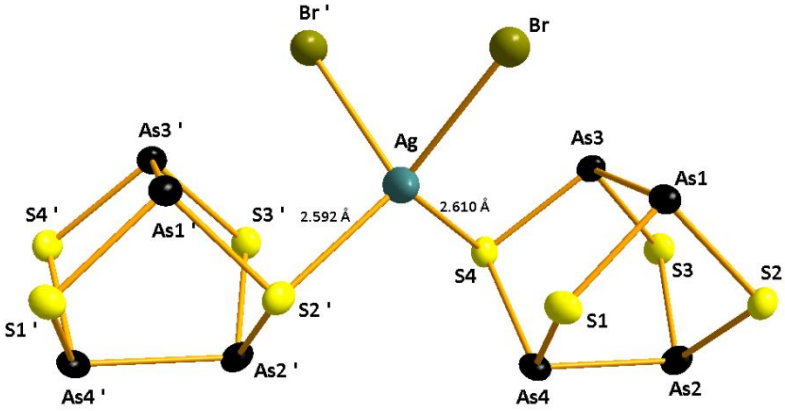

Figure 3.2.3.3: Silver atom displaying a (2+2) distorted tetrahedral coordination. One silver atom is shared between two realgar cage molecules.

The silver atom shows a distorted (2 + 2) tetrahedral coordination, coordinating to two sulphur atoms and two bromine atoms. One silver atom is shared between two sulphur atoms of the adjacent realgar molecules and two bromine atoms making the overall stoichiometry of the adduct 1:1. More details on the overall crystal structure are discussed later in the following Section. As mentioned earlier, in this adduct compound, coordination takes place exclusively through sulphur atoms. The bond lengths d(Ag - S4) and d(Ag – S2') which sum up to 2.610 Å and 2.592 Å are in consonance with the Ag-S bond length of 2.47 Å. Following table shows the concerned bond angles

Table 3.2.2.4: Selected bond angles relevant for the silver coordination in the $(AgBr)\cdot(As_4S_4)$ adduct compound.

Angle	Bond angle/ °
Br'-Ag-Br	81.89
Br'-Ag-S2	103.85
S2-Ag-S4'	109.88
S4-Ag-Br	108.17
Br'-Ag-S4	115.24
Br-Ag-S2'	133.96

Complete crystal structure

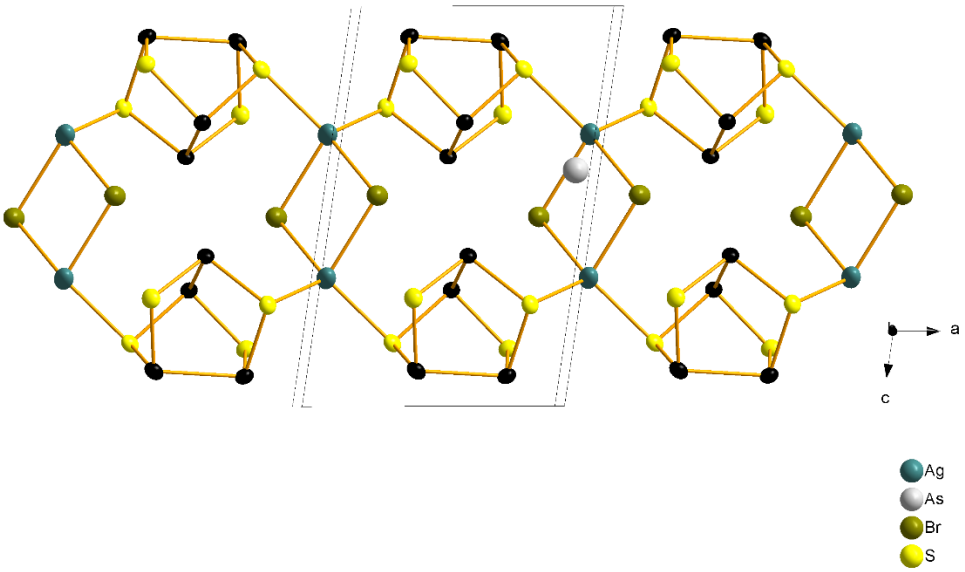

Figure 3.2.3.4: Neutral As_4S_4 layers being connected by silver bromide. Bonding takes place only through sulphur atoms.

In $(AgBr)\cdot(As_4S_4)$ the As_4S_4 cage molecules are bridged by silver bromide with two molecules of As_4S_4 sharing one silver atom through a $\eta^1(S)$ coordination. This silver atom is bonded to two bromine atoms which in turn are bonded to a silver atom which subsequently connects the second layer of the next layer. The AgBr bridges run parallel to the *a* axis (See **Figure 3.2.3.4**). Thus, we have two realgar molecules facing each other while being bridged by AgBr layers.

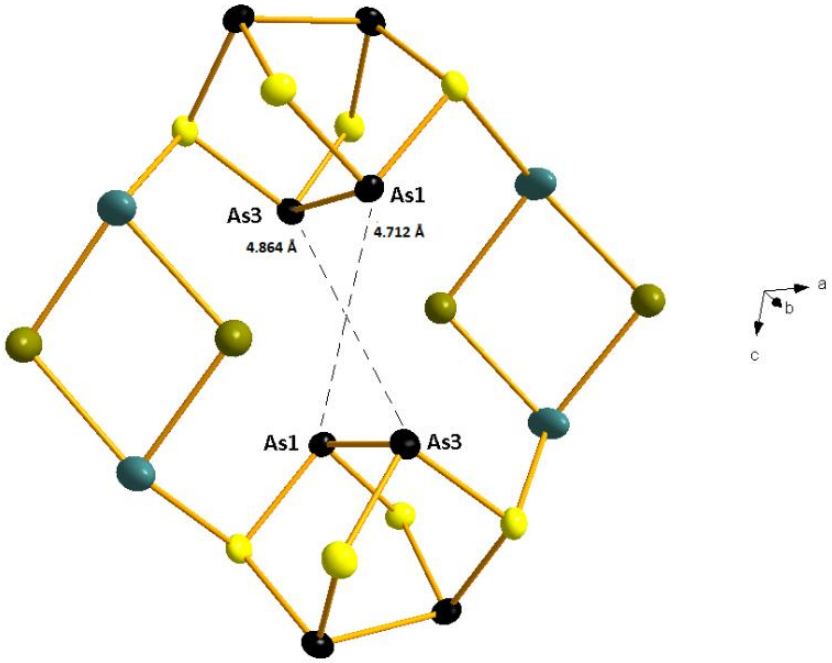

Figure 3.2.3.5: The two arsenic atoms in the two respective layers are resp. 4.712 Å; *d*(As1····As1) and 4.864 Å; *d*(As3····As3) apart.

The distance *d*(As1····As1) of the opposite facing As_4S_4 is 4.712 Å while that of d(As3····As3) is 4.864 Å. When the structure is grown along the b axis, a one-dimensional infinite chain like structure is observed.

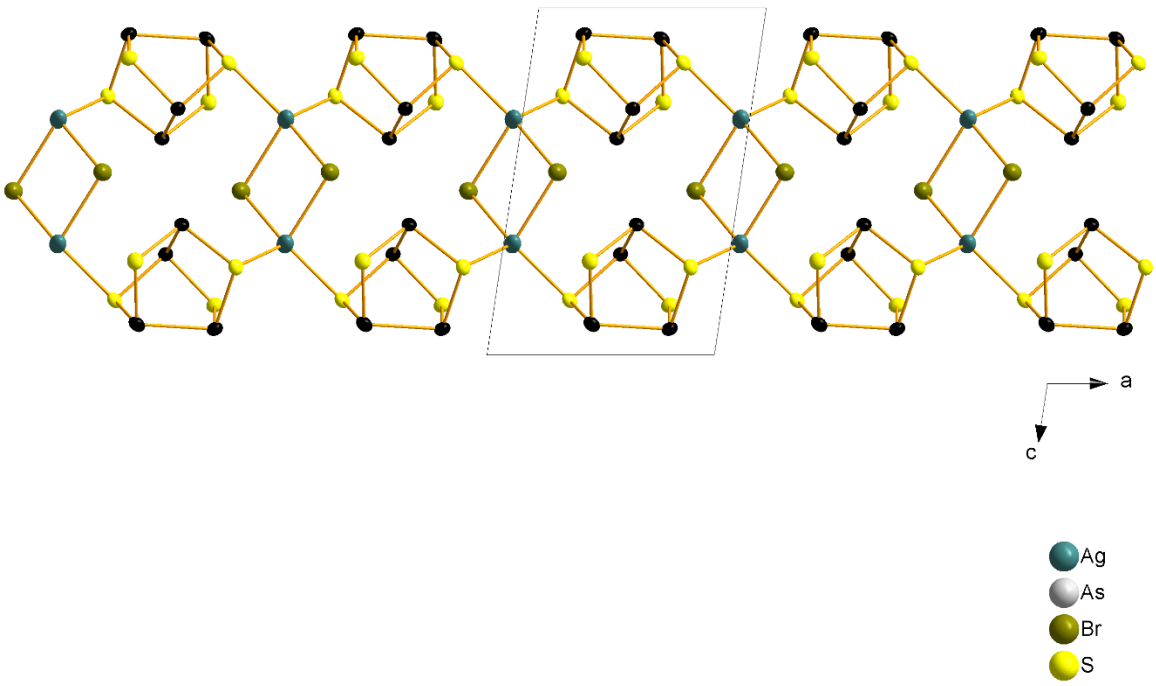

Figure 3.2.3.6: When grown along b axis, we get a one-dimensional infinite chain-like structure.

The adduct molecule is isostructural to the α- As_4S_4 cage molecule. The $\bar{4}2m$ (D_{2d}) molecular symmetry of the 'free' As_4S_4 cage is preserved in the adduct compound and is not altered by the space group symmetry. As seen earlier in **Table 3.2.3.2** the Arsenic-Arsenic distances *d*(As1-As3) = 2.559 Å and *d*(As2-As4) Å are more or less similar to the As-As distances in realgar with $d(\text{As-As})_{avg}$ = 2.566 Å. In contrast, the As-S bonds see an expansion when the As_4S_4 molecule is coordinated to the silver halide matrix. The maximum elongation of 2.24% is observed for *d*(S2-As2) (See **Table 3.2.3.2**).

The silver(I) bromide substructure in (AgBr)·(As_4S_4) consists of almost square [Ag_2Br_2]-units. Therein the distance between the two silver atoms in each [Ag_2Br_2] unit, d(Ag- Ag') = 4.157 Å, is large enough so the attractive argentophilic interactions between the d^{10} ions can be excluded. The [Ag_2Br_2]-units connect the As_4S_4 molecules with an 1D infinite double strand (See **Figure 3.2.3.7**). Therein every [Ag_2Br_2]-unit is connected with four As_4S_4 molecules and vice versa each As_4S_4 molecule is bound to two [Ag_2Br_2]-units. As stated in earlier section, here the coordination takes place exclusively through sulphur atoms. The double strands in (AgBr)·(As_4S_4) run in [100] direction eventually building a distorted hexagonal packing (See **Figure 3.2.3.7**). Here each double strand has four immediate neighbours and two neighbours which are situated little further away. The shortest distances between the strands are d(As···Br) with 3.418 Å, d(S···S) with 3.469 Å and d(As···S) with 3.473 Å. Thereby all the distances are smaller than the sum of the corresponding van der Waals radii. A complete list of bond distances and bond angles for (AgBr)·(As_4S_4) is found in **Table A.11** and **Table A.12** in the appendix.

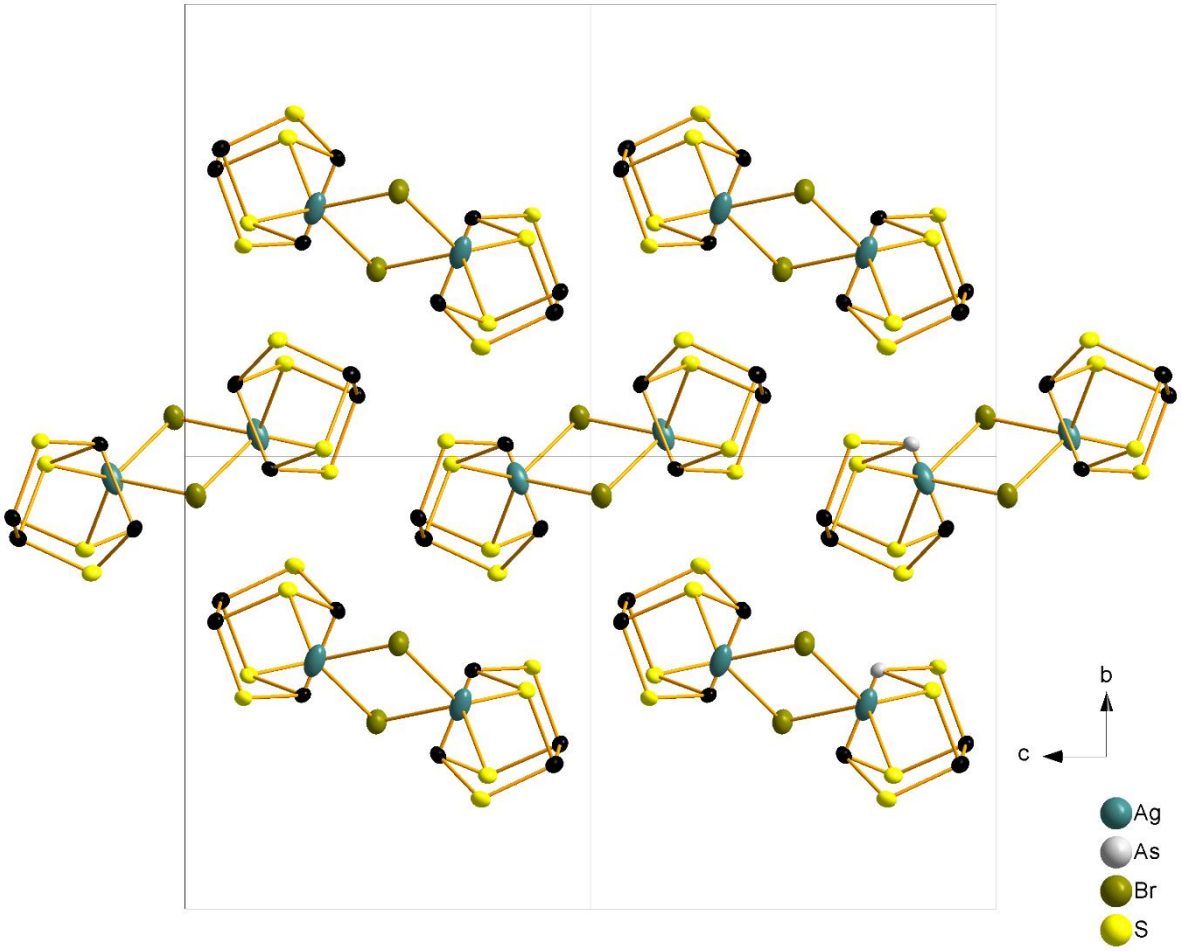

Figure 3.2.3.7: A section of the crystal structure of (AgBr)·(As_4S_4) along the a axis. The double strands seen in **Figure 3.2.3.6** are arranged in hexagonal close pack motif with only the Van der Waals forces acting in between them.

Similar isostructural compound was synthesized by Thomas Rödl, where instead of AgBr, CuBr was employed. Hence a comparison between these two is not out of place. The following table shows the selected bond distances while representing the comparison between the free uncoordinated realgar, (CuBr)·(As_4S_4) and (AgBr)·(As_4S_4).

Table 3.2.3.5: Comparison of selected bond lengths for the adduct compounds $(CuBr)\cdot(As_4S_4)$ and $(AgBr)\cdot(As_4S_4)$ and comparison with As_4S_4. The areas marked in blue indicate maximum deviation in comparison to As_4S_4.

Bond Distance/Angle	As_4S_4	$(CuBr)\cdot(As_4S_4)$/ Å	$(AgBr)\cdot(As_4S_4)$/ Å
Cu-Br/Ag-Br	-	2.544	2.742
Cu-Br'/Ag-Br'	-	2.568	2.763
Cu-S2/ Ag-S2	-	2.313	2.592
As1-As3	2.563	2.551	2.560
As2-As4	2.569	2.577	2.560
S2-As2	2.229	2.279	2.279
As2-S3	2.234	2.240	2.228
As4-S1	2.231	2.223	2.235
S4-As4	2.241	2.287	2.257
As1-S2	2.238	2.248	2.261
As1-S1	2.246	2.238	2.256
S3-As3	2.237	2.238	2.245
As3-S4	2.234	2.255	2.265

As seen in the **Table 3.2.3.5**, very little distortion is seen in As-As bonds in both adduct compounds. As opposed to that, elongation of As-S bonds is observed in both adduct compounds, particularly at the site of the coordination of silver atom.

3.2.3.3 Powder X ray Diffraction

The yellow powder obtained from the solid-state synthesis was employed for recording the powder X-ray diffraction pattern of the adduct $(AgBr)\cdot(As_4S_4)$. The compound was homogenised by grinding it thoroughly in a mortar, packed between two mylar foils using minimum amount of grease and eventually loaded in a flat- bed sample holder. The comparison of the recorded and the simulated (from single crystal measurement) is depicted in the **Figure 3.2.3.8**. The positive intensity corresponds to the measured pattern while the negative intensity corresponds to the simulated pattern (from SC-XRD). A total of 6 unindexed

lines were observed (See **Figure 3.2.3.8** marked with asterisk). By comparing the powder pattern with literature data, the presence of both realgar and silver bromide is excluded. Refinement, indexation, and pattern fitting was done using WinXPOW. Detailed information and the corresponding tables are found in the Appendix in **Table A.13**. Here it must be noted that with solvothermal synthesis also a few yellow block shaped crystals were obtained.

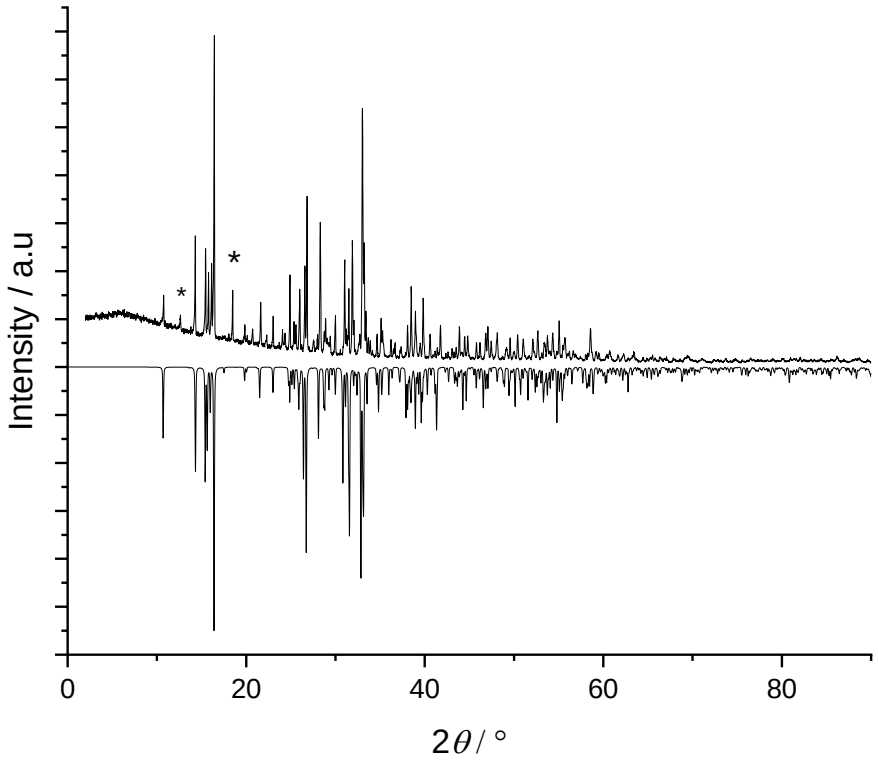

Figure 3.2.3.8: Measured powder pattern of (AgBr)·(As4S4) (positive intensity) in comparison to the theoretical powder pattern (negative intensity) derived from SC -XRD data. A total of six unindexed lines were observed. Two of them are shown marked with asterisk. The remaining four have too low intensity to be shown in the above figure. By comparing the powder pattern with literature data, the presence of both realgar and silver bromide is excluded.

3.2.3.4 UV-Visible Spectroscopy

The yellow powder of $(AgBr)\cdot(As_4S_4)$ was homogenized with $BaSO_4$, filled in the sample container and measured with $BaSO_4$ as reference material. The **Figure 3.2.3.9** shows the solid – state absorption spectrum and the evaluation after Kubelka-Munk transformation.

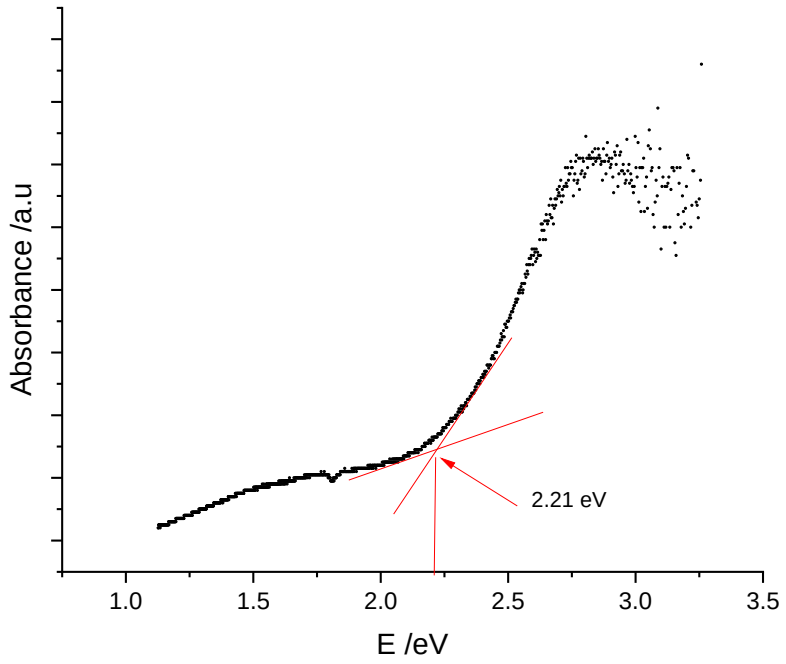

Figure 3.2.3.9: Solid-state UV / VIS absorption spectrum of $(AgBr)\cdot(As_4S_4)$. The absorption edge is at 2.21 eV (561 nm).

For $(AgBr)\cdot(As_4S_4)$ the band gap was found to be 2.21 eV which corresponds to an absorption edge of 561 nm. The band gap so determined coincides well with the colour of the adduct compound. The band gap of 2.21 eV renders the compound to be an optical semiconductor.

3.2.3.5 Thermal Analysis

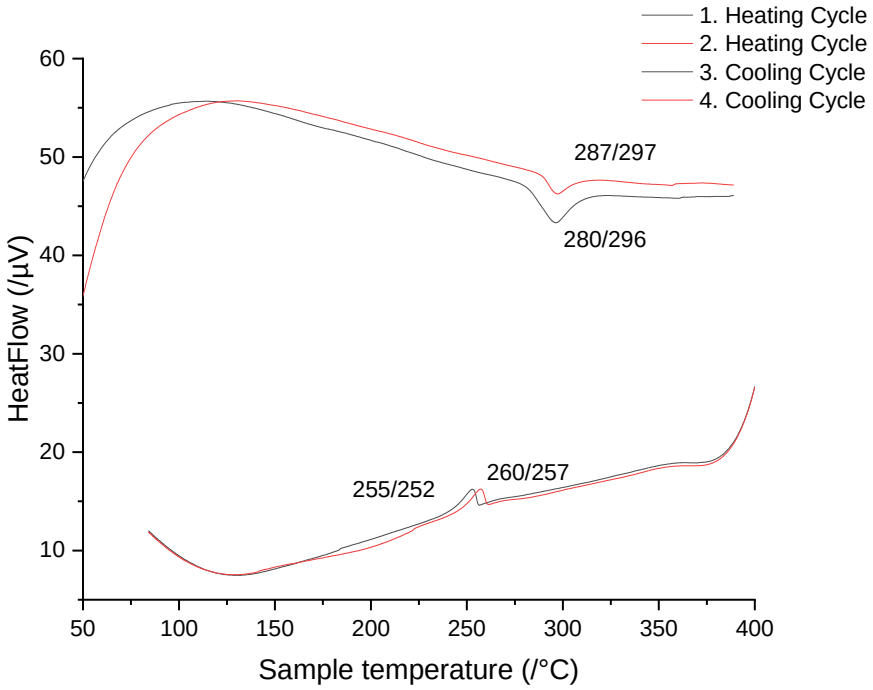

Figure 3.2.3.10: Excerpt from the DTA measurement of a sample of $(AgBr)\cdot(As_4S_4)$ showing Onset/Peak temperatures. The compound decomposes on heating from a temperature of 280 ° C.

A DTA measurement (heating rate 10 °C/min) of the yellow powder of the adduct the $(AgBr)\cdot(As_4S_4)$ was carried out to investigate the thermal behaviour which is depicted in the **Figure 3.2.3.10**. The compound decomposes at a temperature of 280 °C. This generated β - realgar, which subsequently recrystallises at a temperature of 251 °C which can be seen in both the cooling cycles. In order to verify β-realgar as the decomposition product, a powder diffractogram was recorded after the DTA measurement which proves the existence of β - realgar.

3.2.4 The Adduct $(AgCl)\cdot(As_4S_4)$

3.2.4.1 Synthesis

Solvothermal Synthesis

As_4S_4 (0.374 g, 1 equiv) and AgCl (0.125 g, 1 equiv) were transferred to a duran ampoule (7 cm) followed by addition of 1mL of toluene and ACN respectively. The reaction mixture was cooled under liquid nitrogen and subsequently evacuated and reacted in a stainless-steel autoclave under solvothermal conditions at 160 °C for 5 days. The oven was cooled down at 80 °C over a time period of 5 h and maintained at this temperature for another 3 days followed by slow cooling down (over 6 h) to RT. After cooling a few air stable yellow coloured block-like crystals of $(AgCl)\cdot(As_4S_4)$ were obtained.

Solid State Synthesis

In the aforementioned solvothermal approach, along with the desired product (which crystalises as distinct yellow blocks) many other side products and unreacted realgar was observed. A phase pure synthesis of $(AgCl)\cdot(As_4S_4)$ was tried by reacting silver chloride (0.125 g, 1 equiv) and realgar (0.374 g, 1 equiv) at 220 °C for 2 weeks. The educts were weighed, transferred in a quartz ampoule, evacuated, sealed and then rested in oven. The heating rate was 1.5 °C/min, while the cooling rate was 0.5 °C/min. The resulting product was fine yellow powder. This was used for further analysis. For finding the correct temperature for reaction, each time a reaction was performed, every time with an increase of 10 °C, starting from 180 °C. Each time the reactions were monitored by X-ray powder diffraction. With this approach the desired product was obtained but every time reminiscent of silver chloride was observed as monitored from X ray powder diffraction analysis.

3.2.4.2 Single Crystal Analysis

Table 3.2.4.1: Table gives an overview of the crystallographic data and measurement parameters of $(AgCl)\cdot(As_4S_4)$.

Empirical Formula	$AgAs_4ClS_4$
Formula weight	571.24
Crystal colour and shape	Yellow block
Crystal system	monoclinic
Space group	$P2_1/n$ (Nr. 14)
a/Å	7.2012(3)
b/ Å	12.3428(5)
c/ Å	11.0396(5)
α/°	90
β/°	98.983(4)
γ/°	90
V/Å^3, Z	969.20, 4
Absorption coefficient(μ)/ mm^{-1}	19.693
ρ_{calc}/g/cm^3	3.915
Diffractometer	Rigaku Super Nova
Radiation, temperature	Mo Kα (λ = 0.71073 Å), 293 K
Θ-range/°	6.332 – 61.204
hkl-range/°	-10 ≤ h ≤ 9
	-17 ≤ k ≤ 16
	-15 ≤ l ≤ 14
Absorption correction	numerical (gaussian, Scale3 Abspack)
Number of reflexes	8213
Independent reflections	2685
R_σ, R_{int}	0.0463, 0.0439
Completeness	100%
Structure solution	SHELXT
Structure refinement	SHELXT - 2014
Data/Restraints/Parameters	2831/0/91
GooF	1.128
R_1, wR_2 *[I>2σ(I)]*	0.0277, 0.0686
R_1, wR_2 *[all reflexes]*	0.0478, 0.1157
Largest diff. peak/hole/e Å^{-3}	1.69/-2.47

$(AgCl)\cdot(As_4S_4)$ crystallises in the space group $P2_1/n$ (Nr. 14) with a = 7.2012 Å, b = 12.3428 Å , c = 11.0396 Å, α = 90.00 ° β = 98.983 ° , γ = 90.00 ° , V = 969.20 Å3 and Z =4 (T = 293 K). The refinement of all data converged at a GooF of 1.128, with R_1 = 2.77 % and wR_2 = 6.86 %. The positions and isotropic displacement parameters can be found in Appendix in **Table A.14**. The anisotropic displacement parameters are listed in **Table A.15**. The bond lengths and bond angles can be found in **Table A.16** and **Table A.17**. The complete structure can be subdivided into two sub- structures, viz. the neutral α - As_4S_4 cages and the one-dimensional AgCl layers which connect the As_4S_4 cages. The two adjacent As_4S_4 cages are connected to each other through a silver atom via a η^1(S) coordination mode.

α - As_4S_4 substructure

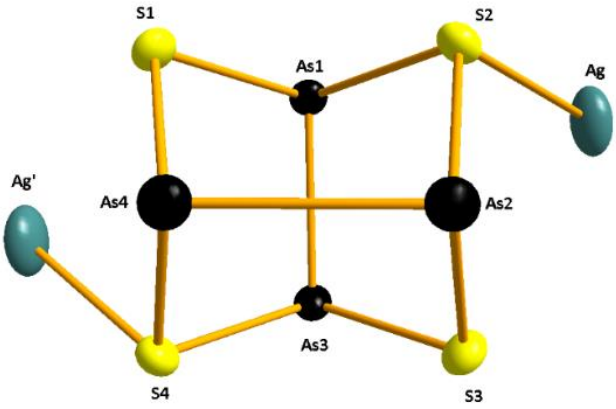

Figure 3.2.4.1: Isolated As_4S_4 cage molecule with silver atoms. The coordination takes place exclusively through sulphur and atoms. Bromine atoms are not shown for the sake of simplicity. All ellipsoids are shown with 90% probability.

The coordination of silver chloride to the cage molecule has some effect on the bond lengths and bond angles which are discussed in the following section. As seen in the **Figure 3.2.4.1**, the coordination of silver atom takes place exclusively through the sulphur atoms, similar to $(As_4S_4)\cdot(AgBr)$ in contrast to the adduct $(AgI)_2\cdot(As_4S_4)$ and $(AgI)_2\cdot(As_4Se_4)$ where coordination takes place both via sulphur and arsenic. Furthermore, here the silver atom is shared between two molecules of As_4S_4, making the overall stoichiometry of the adduct 1:1 in contrast to 2:1 in $(AgI)_2\cdot(As_4S_4)$ and $(AgI)_2\cdot(As_4Se_4)$.

Table 3.2.4.2: Selected interatomic distances (in Å) for (As_4S_4) in (AgCl)·(As_4S_4). Rows marked in blue represent elongation while marked in orange represent contraction upon coordination with AgI. Maximum deviation is observed at the sites of sulphur and arsenic coordination.

Bond/Distance	(AgCl)·(As_4S_4)	As_4S_4	Difference
As1 – As3	2.557	2.563	-0.006
As2 – As4	2.555	2.569	-0.014
As1 – S1	2.253	2.246	+0.007
As1 – S2	2.263	2.238	+0.025
S2 – As2	2.276	2.229	+0.047
As2 – S3	2.226	2.234	-0.008
S3 – As3	2.243	2.237	+0.006
As3 - S4	2.261	2.243	+0.018
S4 – As4	2.258	2.241	+0.017
As4 – S1	2.232	2.231	+0.001

When coordinated to AgCl, only small changes in the bond lengths of As-As are observed. While *d*(As2-As4) sees a contraction of 0.014 Å, *d*(As1-As3) is barely altered. Thus, the coordination of AgCl to the cage molecules has no significant effect on the As-As distances, left aside the slight contraction of *d*(As2-As4). On the contrary, coordination of AgCl to realgar has more effect on the As-S bonds. For the compound under consideration the highest digression is seen for *d*(S2-As2). The S2-As2 bond is elongated by 0.047 Å when compared to the free uncoordinated As_4S_4 cage molecule. This is followed by *d*(As1-S2), *d*(As3-S4) and *d*(As4-S4) which also shows an elongation of 0.025 Å, 0.018 Å and 0.017 Å respectively when coordinated with AgCl when compared with uncoordinated As_4S_4. Thus, maximum deviation is seen at the sites of silver coordination. Similar to the case of (AgBr)·(As_4S_4), so with (AgCl)·(As_4S_4), contrary to the earlier reports, showing that the coordination of transition metal halides with the chalcogenide cages results in cage degradation or ligand recombination, here the As_4S_4 cages are retained intact albeit become slightly stronger as seen from the contraction of As-As bond distances.

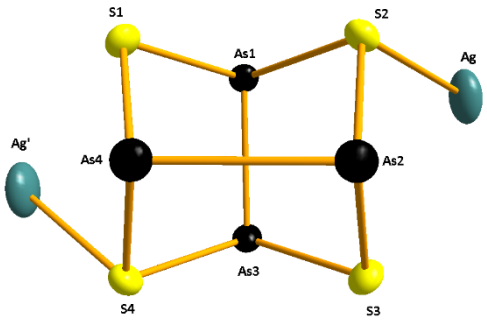

Figure 3.2.4.2: Isolated As_4S_4 cage molecule with silver atoms. The coordination takes place exclusively through sulphur and atoms. Bromine atoms are not shown for the sake of simplicity. All ellipsoids are shown with 90% probability.

As with bond lengths, bond angles are also affected once coordinated to the silver atom. (See **Table 3.2.4.3**). As observed in $(AgBr)\cdot(As_4S_4)$, in $(AgCl)\cdot(As_4S_4)$ also the highest deviation is observed for ∠ (S2-As2-As4). This bond is contracted by 2.411 ° when compared to "free" realgar cage molecule. This is followed by ∠ (As2-S3-As3) which sees an increase of 2.28 °. The next is ∠ (S2-As1-S1) which contracts by 2.23 ° when coordinated to AgCl. All other angles show a deviation of less than 2 ° when compared to the uncoordinated free realgar cage molecule.

Table 3.2.4.3: Selected bond angles (in Å) for (As_4S_4) in $(AgCl)\cdot(As_4S_4)$. Rows marked in orange represent contraction while in blue represent elongation upon coordination with AgI as a consequence of altered bond distances. Maximum deviation is observed at the sites of sulphur and arsenic coordination.

Bond angle	$(AgCl)\cdot(As_4S_4)$	As_4S_4	Difference
As1-S2-As2	102.32	100.91	+1.41
As1-S1-As4	102.32	101.29	+1.03
As4-S4-As3	101.76	101.29	+0.29
As2-S3-As3	103.12	100.8	+2.28
S1-As4-As2	100.48	98.69	+1.79
S1-As1-As3	99.38	99.57	-0.185
S2-As1-S1	92.23	94.47	-2.23
S2-As2-As4	97.40	99.82	-2.41
S2-As1-As3	99.17	99.19	-0.01
S4-As3-As1	98.75	99.17	-0.41
S4-As4-As2	99.06	99.17	-0.10
S4-As4-S1	93.46	94.86	-1.39
S3-As3-S4	93.48	94.56	-1.07
S3-As2-S2	93.81	94.87	-1.06
S3-As3-As1	99.49	99.42	+0.07

The coordination sphere of silver

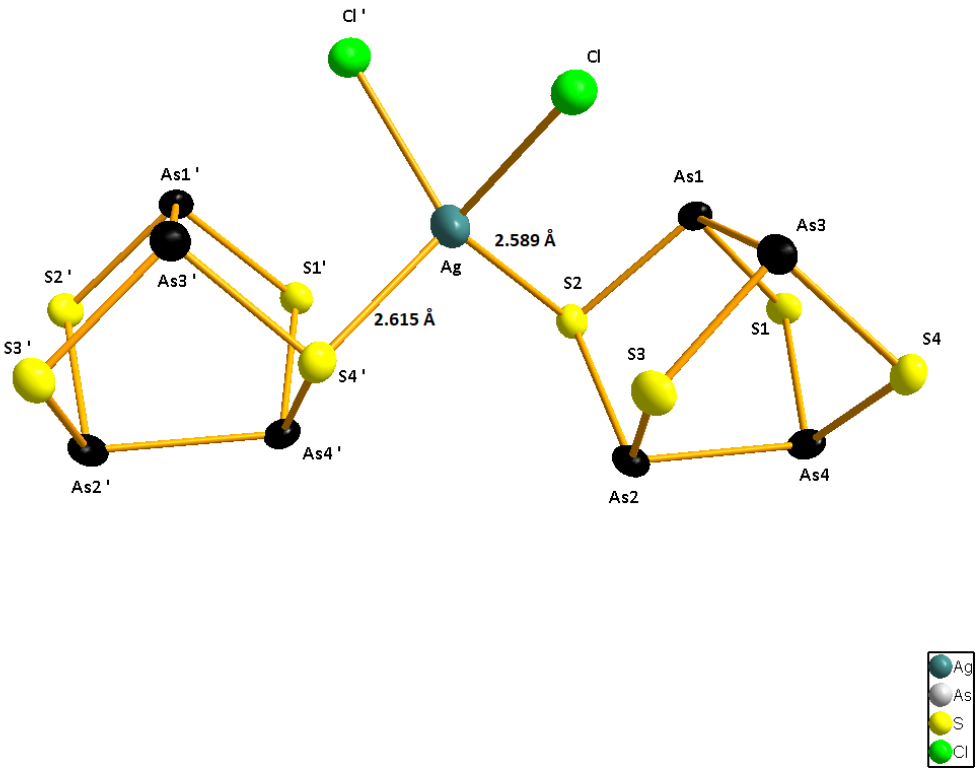

Figure 3.2.4.3: Silver atom displaying a (2+2) distorted tetrahedral coordination. One silver atom is shared between two realgar cage molecules.

The silver atom shows a distorted (2 + 2) tetrahedral coordination, coordinating to two sulphur atoms and two chlorine atoms. One silver atom is shared between two sulphur atoms of the adjacent realgar molecules and two chlorine atoms making the overall stoichiometry of the adduct 1:1. More details on the overall crystal structure are discussed in the following section. As mentioned earlier, in this adduct compound, coordination takes place exclusively through sulphur atoms. The bond lengths *d*(Ag – S2) and *d*(Ag – S4') which sum up to 2.589 Å and 2.615 Å are in consonance with the Ag-S bond length of 2.47 Å. Following table shows the concerned bond angles

Table 3.2.4.7: Selected bond angles relevant for the silver coordination in the $(AgCl)\cdot(As_4S_4)$ adduct compound.

Angle	Bond angle/ °
Cl'-Ag-Cl	83.78
Cl-Ag-S2	104.57
S2-Ag-S4'	109.44
S4'-Ag-Cl'	108.03
Cl'-Ag-S2	132.92
Cl-Ag-S4'	115.18

Complete crystal structure

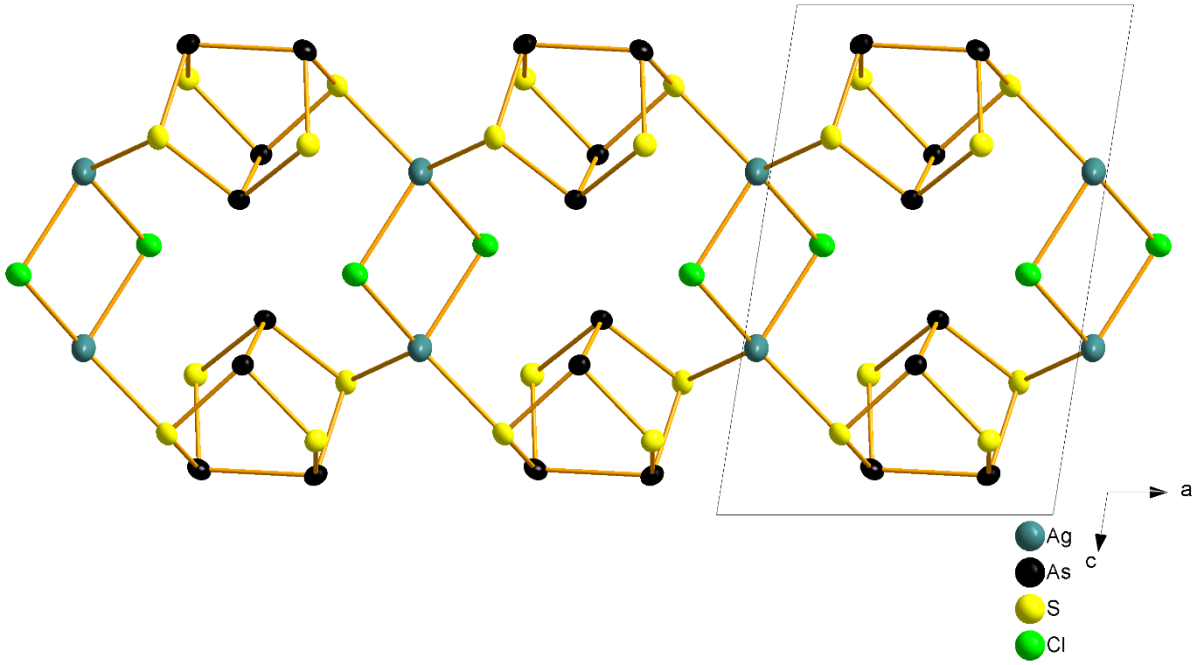

Figure 3.2.4.0-2: Neutral As_4S_4 layers being connected by silver bromide. Bonding takes place only through sulphur atoms.

In (AgCl)·(As_4S_4) the As_4S_4 cage molecules are bridged by silver chloride molecules, with two molecules of As_4S_4 sharing one silver atom through a η^1(S) coordination. This silver atom is bonded to two chlorine atoms which in turn are bonded to a silver atom which is subsequently connected to the sulphur atom of the next layer. The AgCl bridges run parallel to the *a* axis (See **Figure 3.2.4.4**). Thus, we have two realgar molecules facing each other while being bridged by AgCl layers (See **Figure 3.2.4.5**).

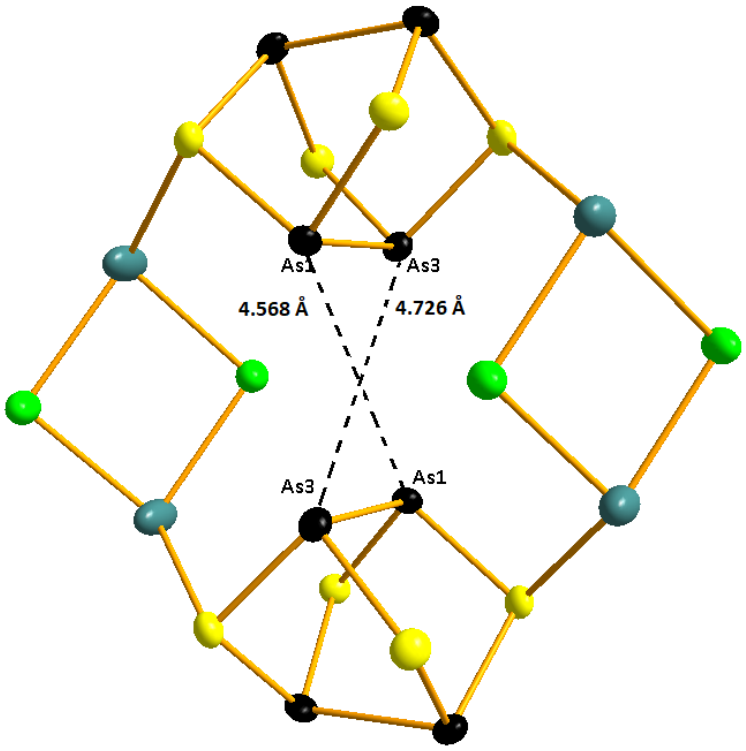

Figure 3.2.4.5 The two arsenic atoms in the two respective layers are resp. 4.568 Å; *d*(As1····As1) and 4.726 Å; *d*(As3····As3) apart.

The distance *d*(As1····As1) of the opposite facing As_4S_4 is 4.568 Å while that of d(As3····As3) is 4.726 Å. When the structure is grown along the b axis, a one-dimensional infinite chain like structure is observed.

The adduct molecule is isostructural to α- As_4S_4 cage molecule. The $\bar{4}2m$ (D_{2d}) molecular symmetry of the 'free' As_4S_4 cage is preserved in the adduct compound and is not altered by the space group symmetry. As seen earlier in **Table 3.2.4.2** the Arsenic-Arsenic distances, *d*(As1-As3) = 2.557 Å and *d*(As2-As4) = 2.555 Å are more or less similar to the As-As distances

in realgar with $d(\text{As-As})_{avg}$ = 2.566 Å. In contrast, the As-S bonds see an expansion when the As_4S_4 molecule is coordinated to the silver halide matrix. The maximum elongation of 2.10 % is observed for *d*(S2-As2).

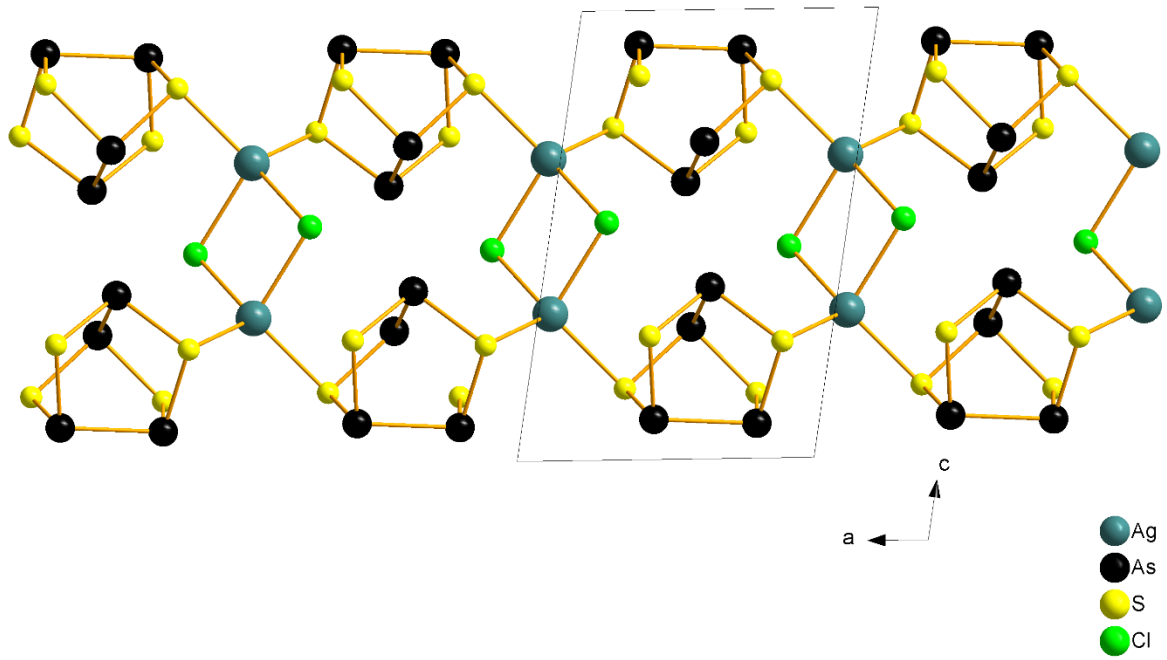

Figure 3.2.4.6: A section of the crystal structure of $(AgCl)\cdot(As_4S_4)$. Rhombic $[Ag_2Cl_2]$- units connect the As_4S_4 molecules to form a 1-D infinite double strand along *a* axis.

The silver(I) chloride substructure in $(AgCl)\cdot(As_4S_4)$ consists of almost square $[Ag_2Cl_2]$-units. Therein the distance between the two silver atoms in each $[Ag_2Cl_2]$, d(Ag- Ag') = 3.544 Å, is large enough so the attractive argentophilic interactions between the d^{10} ions can be excluded. The $[Ag_2Cl_2]$-units connect the As_4S_4 molecules with an 1D infinite double strand (See **Figure 3.2.4.6**). Therein every $[Ag_2Cl_2]$-unit is connected with four As_4S_4 molecules and vice versa each As_4S_4 molecule is bound to two $[Ag_2Cl_2]$-units. As stated in Section, here the coordination takes place exclusively through sulphur atoms. The double strands in $(AgCl)\cdot(As_4S_4)$ run in [100] direction eventually building a distorted hexagonal packing (See **Figure 3.2.4.7**). Here each double strand has four immediate neighbours and two neighbours which are situated little further away. The shortest distances between the strands are

d(As···Cl) with 3.406 Å, *d*(S···S) with 3.441 Å and *d*(As···S) with 3.451 Å. Thereby all the distances are smaller than the sum of the corresponding van der Waals radii. A complete list of bond distances and bond angles for (AgCl)·(As_4S_4) is found in Table in the appendix.

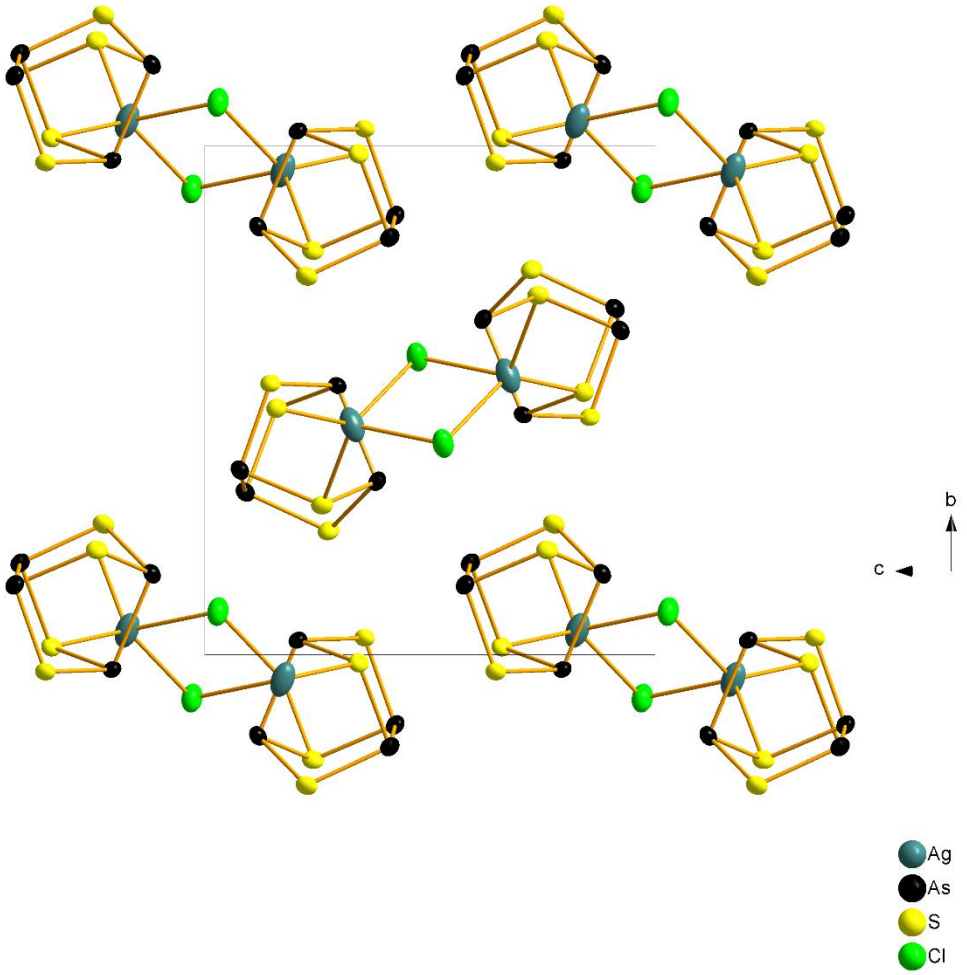

Figure 3.2.4.7: A section of crystal structure of (AgCl)·(As_4S_4) along the *a* axis. The double strands seen in **Figure 3.2.4.6** are arranged in hexagonal close pack motif with only the Van der Waals forces acting in between them.

Similar isostructural compound was synthesized by *Vitzthumecker*, where instead of AgCl, CuCl was employed. Hence a comparison between these two is not out of place. The following table shows the selected bond distances while representing the comparison between the free uncoordinated realgar, (CuCl)·(As_4S_4) and (AgCl)·(As_4S_4).

Table 3.2.4.8: Comparison of selected bond lengths for the adduct compounds $(CuCl)\cdot(As_4S_4)$ and $(AgCl)\cdot(As_4S_4)$ and comparison with As_4S_4. The areas marked in blue indicate maximum deviation in comparison to As_4S_4.

Bond Distance	As_4S_4	$(CuCl)\cdot(As_4S_4)$/ Å	$(AgCl)\cdot(As_4S_4)$/ Å
Cu-Br/Ag-Br	-	2.544	2.742
Cu-Br'/Ag-Br'	-	2.568	2.763
Cu-S2/Ag-S2	-	2.313	2.592
As1-As3	2.563	2.563	2.560
As2-As4	2.569	2.551	2.560
S2-As2	2.229	2.228	2.279
As2-S3	2.234	2.278	2.228
As4-S1	2.231	2.222	2.235
S4-As4	2.241	2.273	2.257
As1-S2	2.238	2.307	2.261
As1-S1	2.246	2.256	2.256
S3-As3	2.237	2.263	2.245
As3-S4	2.234	2.260	2.265

As seen in the Table, very little distortion is seen in As-As bonds in the adduct compound $(CuCl)\cdot(As_4S_4)$ when compared to $(AgCl)\cdot(As_4S_4)$. As opposed to that, elongation of As-S bonds is observed in both adduct compounds, particularly at the site of the coordination of silver atom.

3.2.5 The Adduct $(CuI)_3 \cdot (As_4S_4)$

3.2.5.1 Synthesis

Solvothermal Synthesis

As_4S_4 (0.214 g, 1 equiv)) and CuI (0.386 g, 3 equiv) were transferred to a duran ampoule (7 cm) followed by addition of 1mL of toluene and ACN respectively. The reaction mixture was cooled under liquid nitrogen and subsequently evacuated and reacted in a stainless-steel autoclave under solvothermal conditions at 160 °C for 5 days. The oven was cooled down at 80 °C over a time period of 5 h and maintained at this temperature for another 2 days followed by slow cooling down (over 6 h) to RT. After cooling a few air stable red coloured block-like crystals of $(CuI)_3 \cdot (As_4S_4)$ were obtained.

Solid State Synthesis

In the aforementioned solvothermal approach, along with the desired product (which crystalises as distinct red blocks) many other side products and unreacted realgar was observed. An attempt of phase pure synthesis of $(CuI)_3 \cdot (As_4S_4)$ was achieved by reacting copper iodide (0.285 g, 3 equiv) and realgar (0.214 g, 1 equiv) at 170 °C for 2 weeks. The educts were weighed, transferred in a quartz ampoule, evacuated, sealed, and then rested in oven. The heating rate was 1.5 °C/min, while the cooling rate was 0.5 °C/min. The resulting product was fine red-orange powder. Powder X ray diffraction studies showed the presence of unreacted realgar and some more phase which are not identified.

3.2.5.2 Single Crystal Analysis

Table 3.2.5.1: Table gives an overview of the crystallographic data and measurement parameters of $(CuI)_3 \cdot (As_4S_4)$.

Empirical Formula	$Cu_3As_4I_3S_4$
Formula weight	999.24
Crystal colour and shape	red block
Crystal system	monoclinic
Space group	$P2_1/c$
a/Å	20.009(3)
b/ Å	10.945(1)
c/ Å	13.563(2)
β/°	105.30(1)
V/Å^3, Z	2865.16, 8
Absorption coefficient(μ)/ mm^{-1}	20.589
ρ_{calc}/g/cm^3	4.633
Diffractometer	Rigaku Super Nova
Radiation, temperature	Mo Kα (λ = 0.71073 Å), 123 K
Θ-range/°	5.868 - 65.026
hkl-range/°	-29 ≤ h ≤ 29
	-16 ≤ k ≤ 16
	-19 ≤ l ≤ 20
Absorption correction	numerical (gaussian, Scale3 Abspack)
Number of reflexes	37235
Independent reflections	9669
R_σ, R_{int}	0.0363, 0.0408
Completeness	100%
Structure solution	SHELXT
Structure refinement	SHELXT - 2014
Data/Restraints/Parameters	9669/0/253
GooF	1.166
R_1, wR_2 *[I>2σ(I)]*	0.0304, 0.0595
R_1, wR_2 *[all reflexes]*	0.0358, 0.0611
Largest diff. peak/hole/e Å^{-3}	2.06/-1.20

$(CuI)_3 \cdot (As_4S_4)$ crystallises in the space group $P2_1/c$ with a = 20.009 Å, b = 10.945 Å , c = 13.562 Å, β = 105.30° , V = 2865.16 $Å^3$ and Z = 8 (T = 123 K). The refinement of all data converged at a GooF of 1.166, with R_1 = 3.58 % and wR_2 = 6.11 %. The positions and isotropic displacement parameters can be found in Appendix in **Table A.18**. The anisotropic displacement parameters are listed in **Table A.19**. The bond lengths and bond angles can be found in **Table A.20** and **Table A.21**. The complete structure can be subdivided into two sub- structures, the neutral α - As_4S_4 cages and wave like CuI layers which are connected by the As_4S_4 cages. One of the copper atoms is connected to the As_4S_4 cage via two sulphur atoms while the other two sulphur atoms are connected to two different copper atoms respectively.

α - As_4S_4 substructure

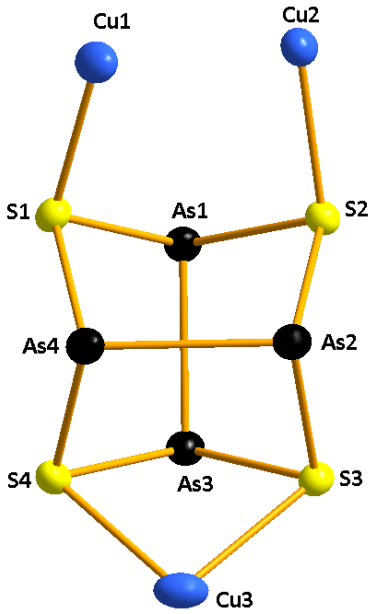

Figure 3.2.5.1: Isolated As_4S_4 cage molecule with silver atoms. The coordination takes place exclusively through sulphur and atoms. Bromine atoms are not shown for the sake of simplicity. All ellipsoids are shown with 90% probability.

The coordination of copper iodide to the cage molecule has some effect on the bond lengths and bond angles which are discussed in the following section. As seen in the **Figure 3.2.5.1**, the coordination of copper atom takes place exclusively through the sulphur atoms. Cu3 is shared between two sulphur atoms, while, on the opposite side of the As_4S_4 cage, each Cu

atom is connected to a separate copper atom making the overall stoichiometry of the compound 1:3.

Table 3.2.5.2: Selected interatomic distances (in Å) for (As_4S_4) in $(CuI)_3 \cdot (As_4S_4)$. Rows marked in blue represent elongation while marked in orange represent contraction upon coordination with CuI. Maximum deviation is observed at the sites of sulphur and arsenic coordination.

Bond/Distance	$(CuI)_3 \cdot (As_4S_4)$	As_4S_4	Difference
As1 – As3	2.534	2.563	-0.029
As2 – As4	2.568	2.569	-0.001
As1 – S1	2.289	2.246	+0.043
As1 – S2	2.262	2.238	+0.024
S2 – As2	2.267	2.229	+0.038
As2 – S3	2.240	2.234	+0.006
S3 – As3	2.293	2.237	+0.056
As3 - S4	2.277	2.243	+0.034
S4 – As4	2.249	2.241	+0.008
As4 – S1	2.243	2.231	+0.012

When coordinated to CuI, only small changes in the bond lengths of As-As are observed. While *d*(As1-As3) sees a contraction of 0.029 Å (deviation of 1.13 %), *d*(As2-As4) is barely altered. Thus, the coordination of CuI to the cage molecules has no significant effect on the As-As distances, left aside the slight contraction of *d*(As1-As3). On the contrary, coordination of CuI to realgar has more effect on the As-S bond lengths. For the compound under consideration the highest digression is seen for *d*(S3-As3). The S3-As3 bond is elongated by 0.056 Å (2.50 %) when compared to the free uncoordinated As_4S_4 cage molecule. This is followed by *d*(As1-S1), *d*(As2-S2) and *d*(As3-S4) which also shows an elongation of 0.043 Å, 0.038 Å and 0.034 Å respectively when coordinated with CuI when compared with uncoordinated As_4S_4. Thus, as expected, maximum deviation is seen at the sites of copper coordination. Similar to the case of the silver analogues and contrary to the established belief that the coordination of transition metal halides to the chalcogenide cages results in cage degradation or ligand recombination, here the As_4S_4 cages are retained intact, albeit become slightly stronger as

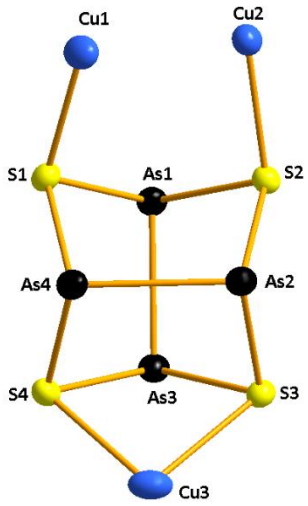

Figure 3.2.5.2: Isolated As_4S_4 cage molecule with silver atoms. The coordination takes place exclusively through sulphur and atoms. Bromine atoms are not shown for the sake of simplicity. All ellipsoids are shown with 90% probability.

seen from the contraction of As-As bond distances. As with bond lengths, bond angles are also affected once coordinated to the copper atoms. (See **Table 3.2.5.3**).

The highest deviation is observed for ∠ (S3-As3-S4). This bond is contracted by 3.51 ° (3.72 %) when compared to "free" realgar cage molecule. This was rather expected because a single copper atom is shared between S3 and S4. The angles on the opposite end of the cage where S1 and S2 are respectively coordinated to copper atom each, on the other hand, show no change with ∠ (S2-As1-S1) being just 0.21 ° greater when compared to uncoordinated realgar. This is followed by ∠ (S3-As2-S2) which is contracted by 2.36 ° when compared to uncoordinated realgar molecule. Interestingly enough the analogous bond on the other side of the cage, viz. ∠ (S4-As4-S1) sees a contraction of only 1.48 °. Both the angles ∠ (As1-S2-As2) and ∠ (As1-S1-As4) see an expansion of 1.66 ° and 1.22 ° respectively when compared to uncoordinated realgar. This can be a consequence of the copper coordination to the sulphur atoms. The ∠ (S4-Cu-S3) amounts to 86.33 °. The other angles which show deviation are listed in **Table 3.2.5.3**.

Table 3.2.5.3: Selected bond angles (in Å) for (As_4S_4) in $(CuI)_3{\cdot}(As_4S_4)$. Rows marked in orange represent contraction while in blue represent elongation upon coordination with CuI as a consequence of altered bond distances. Maximum deviation is observed at the sites of sulphur and arsenic coordination.

Bond angle	$(CuI)_3{\cdot}(As_4S_4)$	As_4S_4	Difference
As1-S2-As2	102.57	100.91	+1.66
As1-S1-As4	102.51	101.29	+1.22
As4-S4-As3	101.95	101.29	+0.66
As2-S3-As3	102.28	100.84	+1.44
S1-As4-As2	98.67	98.69	-0.02
S1-As1-As3	99.25	99.57	-0.31
S2-As1-S1	94.68	94.47	+0.21
S2-As2-As4	101.11	99.82	+1.29
S2-As1-As3	97.31	99.19	-1.87
S4-As3-As1	99.25	99.17	+0.08
S4-As4-As2	100.33	99.17	+1.16
S4-As4-S1	93.37	94.86	-1.48

S3-As3-S4	91.04	94.56	-3.51
S3-As2-S2	92.50	94.87	-2.36
S3-As3-As1	100.75	99.42	+1.33

The coordination sphere of copper

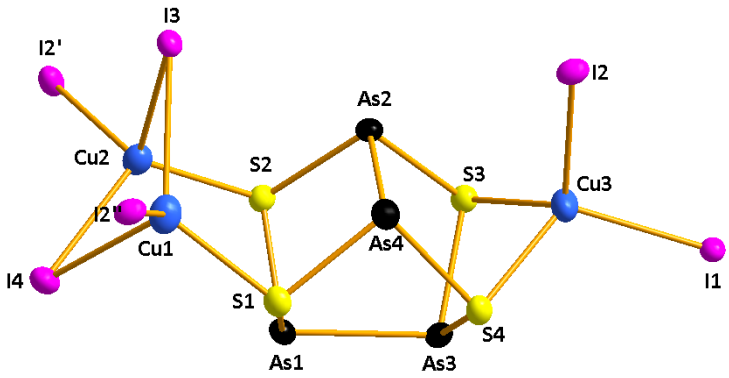

Figure 3.2.5.3: All three copper atoms in $(CuI)_3 \cdot (As_4S_4)$ display a distorted tetrahedral coordination.

The copper atom shows a distorted (2 + 2) and (3 + 1) tetrahedral coordination as shown in **Figure 3.2.5.3**, coordinating to two sulphur atoms (S3 and S4) and two iodine atoms (I1 and I2) for Cu3 and one sulphur and three iodine for Cu1 and Cu2. Cu1 and Cu2 are connected to each other via edge sharing of their tetrahedra, thus sharing I3 and I4. In contrast to $(CuBr)_2 \cdot (As_4S_4)$, copper atoms are not shared by two cages, making the overall stoichiometry of the adduct 3:1. As mentioned before, in this adduct compound, coordination of the cages takes place exclusively through sulphur atoms. The bond lengths *d*(Cu3 – S4), *d*(Cu3 – S3), *d*(Cu1 – S1) and *d*(Cu2 – S2) which sum up to 2.364 Å, 2.401 Å, 2.319 Å and 2.299 Å are in consonance with the Cu-S bond length of 2.47 Å. The following tables shows the bond length and bond angles at the copper atoms.

Table 3.2.5.4: Selected bond lengths and bond angles relevant for the silver coordination in the $(CuI)_3 \cdot (As_4S_4)$ adduct compound.

Bond	Bond length/ Å
Cu3-I2	2.586

Cu3-I1	2.534
Cu3-S4	2.364
Cu3-S3	2.401
Cu1-I2''	2.580
Cu1-I3	2.787
Cu1-I4	2.619
Cu1-S1	2.319
Cu3-I3	2.672
Cu2-I4	2.635
Cu2-I2'	2.581
Cu2-S2	2.299

Angle	Bond Angle /°
I2-Cu3-I1	107.39
I2-Cu3-S3	114.36
I2-Cu3-S4	113.29
S4-Cu3-I4	115.25
I3-Cu2-I2'	104.23
I3-Cu2-S2	107.63
I3-Cu2-I4	111.13
I2'-Cu2-I4	108.24
I4-Cu1-I2"	111.67
I2"-Cu1-S1	111.17
I2"-Cu1-I3	100.33
I4-Cu1-I3	108.15

Complete crystal structure

As mentioned in earlier section, in the given compound, we see that on the one side of the cage molecule copper atom is shared between two sulphur atoms (Cu3, refer **Figure 3.2.5.3**) while on the other side each sulphur atom is coordinated to separate copper atoms (Cu1 and Cu2. **Figure 3.2.5.4** depicts a part of the extended structure. It is observed that the below

marked motif repeats itself. Each motif contains a realgar cage, which on one side is bound to one copper atom and two on another. Two such realgar subunits are bridged by an iodine atom. Further each strand is connected to a strand in the adjacent layer in the direction of c axis again through an iodine atom.

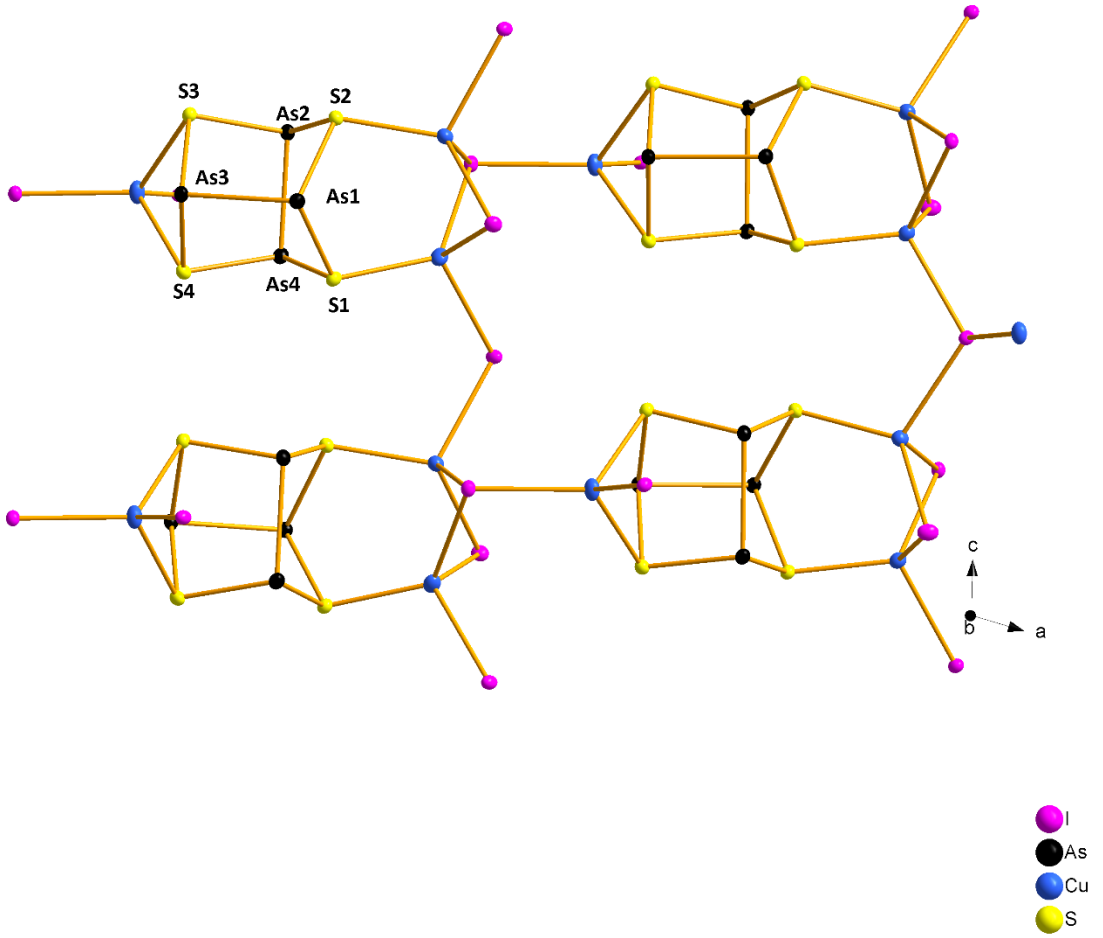

Figure 3.2.5.4: A part of the crystal structure of $(CuI)_3 \cdot (As_4S_4)$ showing the arrangement of realgar cages in the CuI matrix.

The shortest distances (See **Figure 3.2.5.5**) between the two strands are d(S1·····S2) and d(S4·····S3) amounting to 3.64 Å und 3.68 Å respectively. The distances are almost equal to the sum of van der Wall radii for sulphur (S-S = 3.6 Å).

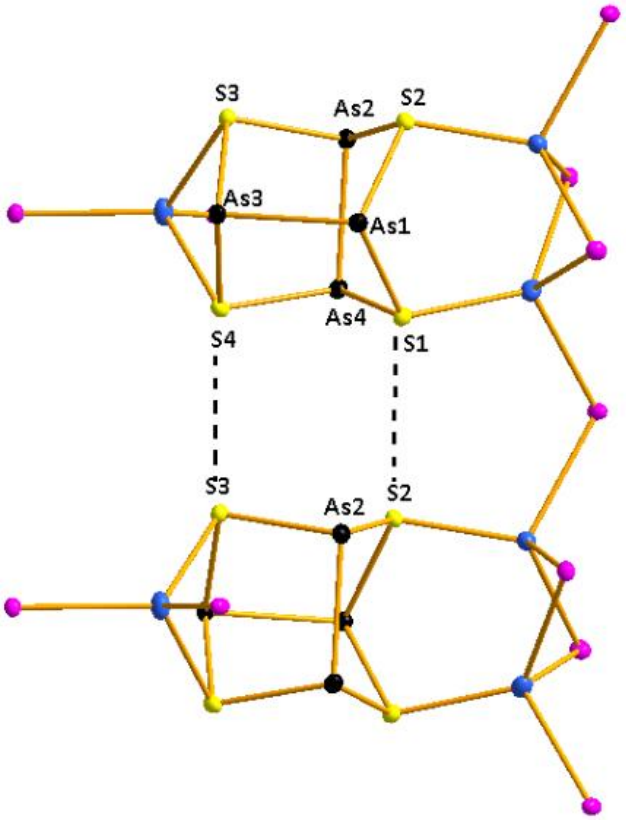

Figure 3.2.5.5: A part of the crystal structure of $(CuI)_3 \cdot (As_4S_4)$ depicting the shortest distance between two strands of As_4S_4.

CuI layers

In addition to As_4S_4 cages, the adduct compound $(CuI)_3 \cdot (As_4S_4)$ consists of a very complex copper(I)iodide substructure. This consists if $^{1}_{\infty}[CuI]$ zigzag chains, two of which are connected to each other through [CuI] dumbbells to form a puckered ladder type structure See **Figure 3.2.5.6**.

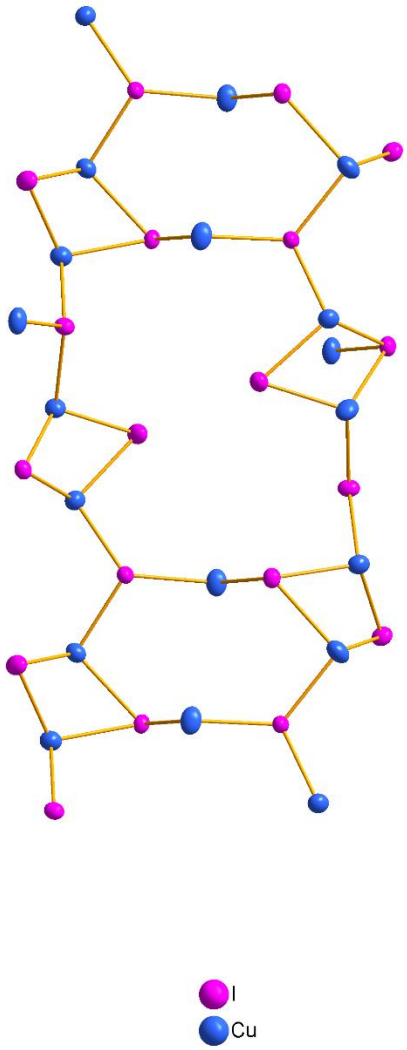

Figure 3.2.5.6: Copper(I) iodide sub structure in $(CuI)_3 \cdot (As_4S_4)$. Every alternating $^1_\infty[CuI]$ chain is connected with [CuI] dumbbell resulting in a ladder like structure.

3.2.5.3 Powder X - ray Diffraction

The orange-red powder obtained from the solid-state synthesis was employed for recording the powder X-ray diffraction pattern of the adduct $(CuI)_3 \cdot (As_4S_4)$. The compound was homogenised by grinding it thoroughly in a mortar, packed between two mylar foils using minimum amount of grease and eventually loaded in a flat- bed sample holder. The recorded diffraction pattern revealed the presence of unidentified phase(s) and realgar (See **Figure 3.2.5.7**). Attempt to record a powder diffraction pattern from the product from solvothermal synthesis also revealed some unidentified phases although the reaction mixture was washed

three times with toluene and acetonitrile. Here it is to be noted that very few crystals were obtained by solvothermal synthesis.

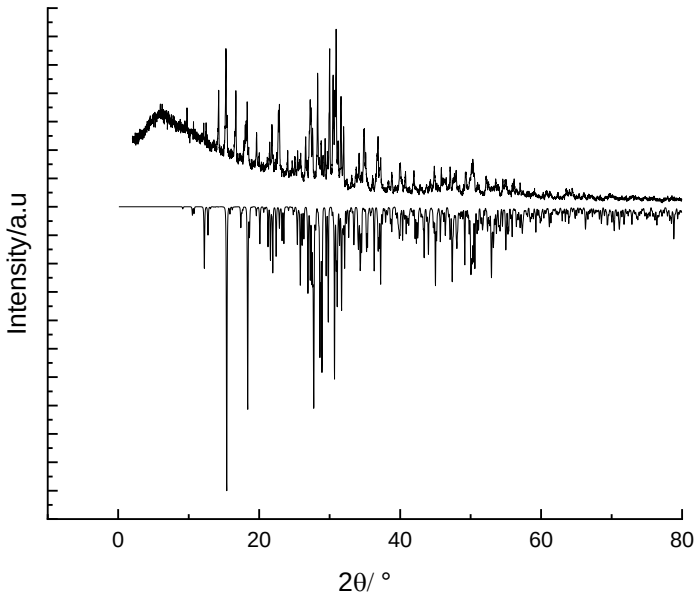

Figure 3.2.5.7: Measured powder pattern of $(CuI)_3 \cdot (As_4S_4)$ (positive intensity) in comparison to the theoretical powder pattern (negative intensity) derived from SC -XRD data. As seen the measured intensity does not match with the theoretical pattern indicating the presence of still unidentified phase(s).

3.2.5.4 SEM and EDX Analysis

For the scanning electron microscopic investigations and the EDX analysis, one of the shiny red blocks contained in the batch was separated under the light microscope and glued to the carbon-coated carrier. It must be noted here that only few crystals of the desired product were found in each reaction batch **Figure 3.2.5.8** shows a scanning electron microscopic image of a $(CuI)_3 \cdot (As_4S_4)$ at a cathode voltage of 25 kV and **Table 3.2.5.5** shows the results.

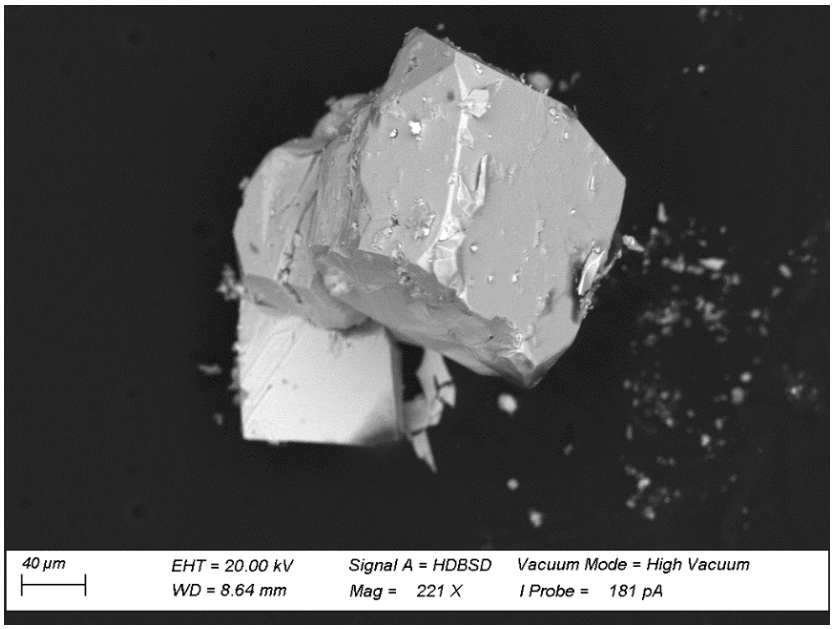

Figure 3.2.5.8: Electron microscopic image of a crystal of the adduct $(CuI)_3 \cdot (As_4S_4)$ with an excitation voltage of 25kV.

Table 3.2.5.5: Result of energy dispersive X-ray spectroscopy and calculated proportions of silver, iodine, arsenic, and sulphur in the $(CuI)_3 \cdot (As_4S_4)$ adduct compound.

Element	Cu	I	As	S
Abs. Error/ %	1.52	2.98	2.36	1.33
Rel. Error/ %	8.72	8.74	9.30	11.48
EDX results/Atom%	22.10	21.58	27.30	29.02
Calculated Results/Atom %	21.42	21.42	28.57	28.57

3.2.6 The Adduct $(CuBr)_2 \cdot (As_4S_4)$

3.2.6.1 Synthesis

Solvothermal Synthesis

As_4S_4 (0.3 g, 1 equiv) and CuBr(0.2 g, 2 equiv) were transferred to a duran ampoule (7 cm) followed by addition of 1mL of toluene and ACN respectively. The reaction mixture was cooled under liquid nitrogen and subsequently evacuated and reacted in a stainless-steel autoclave under solvothermal conditions at 160 °C for 5 days. The oven was cooled down at 80 °C over a time period of 5 h and maintained at this temperature for another 2 days followed by slow cooling down (over 6 h) to RT. After cooling a few air stable red coloured block-like crystals of $(CuBr)_2 \cdot (As_4S_4)$ were obtained.

3.2.6.2 Single Crystal Analysis

Table 3.2.9.1: Table gives an overview of the crystallographic data and measurement parameters of $(CuBr)_2 \cdot (As_4S_4)$.

Empirical Formula	$As_4Br_2Cu_2S_4$
Formula weight	714.82
Crystal colour and shape	Red block
Crystal system	monoclinic
Space group	$P2_1$ (Nr. 4)
a/Å	7.5100(3)
b/ Å	7.5881(3)
c/ Å	10.2898(4)
β/°	102.369(4)
V/Å^3, *Z*	572.77(4),2
Absorption coefficient(μ)/ mm^{-1}	22.825
ρ_{calc}/g/cm^3	4.145
Diffractometer	Rigaku Super Nova
Radiation, temperature	Mo Kα (λ = 0.71073 Å), 123 K
Θ-range/°	5.55 – 61.424
hkl-range/°	-10 ≤ h ≤ 10
	-10 ≤ k ≤ 10
	-14 ≤ l ≤ 14

Absorption correction	numerical (gaussian, Scale3 Abspack)
Number of reflexes	7970
Independent reflections	3606
R_σ, R_{int}	0.0328, 0.0425
Completeness	100%
Structure solution	SHELXT
Structure refinement	SHELXT - 2014
Data/Restraints/Parameters	5156//109
GooF	1.050
R_1, wR_2 [I>2σ(I)]	0.0312, 0.0653
R_1, wR_2 [all reflexes]	0.0342, 0.0665
Largest diff. peak/hole/e Å^{-3}	0.79/-0.78

$(CuBr)_2 \cdot (As_4S_4)$ crystallises in the space group $P2_1$ (Nr. 4) with a = 7.51 Å, b = 7.588 Å , c = 10.289 Å, β = 102.37 °, V = 572.77 Å^3 and Z = 2 (T = 123 K). The refinement of all data converged at a GooF of 1.034, with R_1 = 3.12 % and wR_2 = 6.53 %. The positions and isotropic displacement parameters can be found in Appendix in **Table A.22**. The anisotropic displacement parameters are listed in **Table A.23**. The bond lengths and bond angles can be found in **Table A.24** and **Table A.25**. The complete structure can be subdivided into two sub- structures, viz. the neutral α - As_4S_4 cages and the one-dimensional $^1_\infty[CuBr]$ wave- like chains which connect the As_4S_4 cages.

α - As_4S_4 substructure

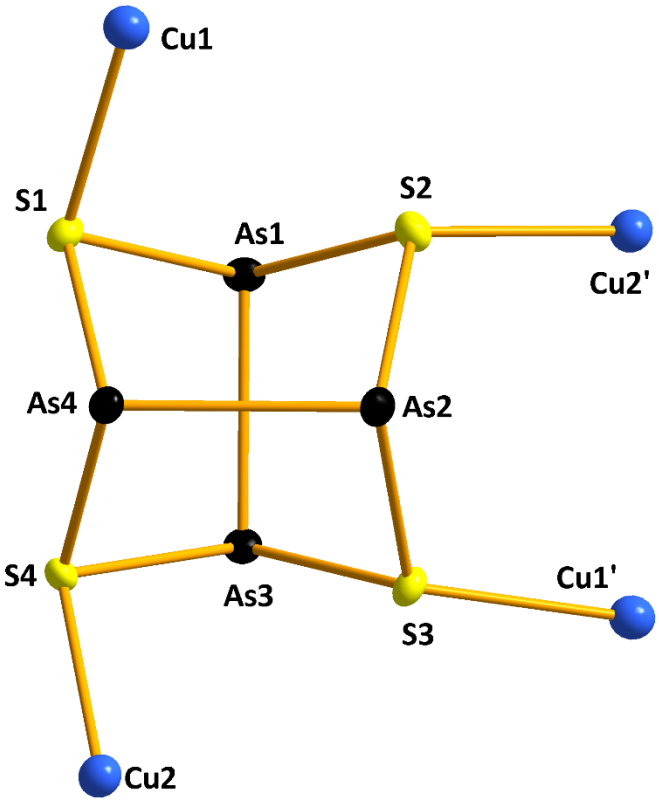

Figure 3.2.6.1: Isolated As_4S_4 cage molecule with copper atoms. The coordination takes place only through sulphur atoms. Bromine atoms are not shown for the sake of simplicity. All ellipsoids are shown with 70% probability.

The coordination of copper bromide to the cage molecule has some effect on the bond lengths and bond angles which are discussed in the following section. As seen in the **Figure 3.2.6.1**, the coordination of copper atom takes place exclusively through the sulphur atoms in contrast to the adduct $(AgI)_2 \cdot (As_4S_4)$ and $(AgI)_2 \cdot (As_4Se_4)$ where coordination takes place both via sulphur and arsenic. Here the copper atoms are shared between two cage molecules, making the overall stoichiometry 1:2.

Table 3.2.6.2: Selected interatomic distances (in Å) for (As_4S_4) in $(CuBr)_2 \cdot (As_4S_4)$. Rows marked in blue represent elongation while marked in orange represent contraction upon coordination with CuBr. Maximum deviation is observed at the sites of sulphur and arsenic coordination.

Bond/Distance	$(CuBr)_2 \cdot (As_4S_4)$	As_4S_4	Difference
As1 – As3	2.550	2.563	-0.013
As2 – As4	2.548	2.569	-0.021
As1 – S1	2.268	2.246	+0.022
As1 – S2	2.243	2.238	+0.005
S2 – As2	2.274	2.229	+0.045
As2 – S3	2.269	2.234	+0.035
S3 – As3	2.249	2.237	+0.012
As3 - S4	2.270	2.243	+0.027
S4 – As4	2.268	2.241	+0.027
As4 – S1	2.282	2.231	+0.051

As expected, maximum deviation is seen at the sites of copper coordination. For the compound under consideration the highest digression is seen for *d*(As4-S1). The As4-S1 bond is elongated by 0.051 Å when compared to the free uncoordinated As_4S_4 cage molecule which amounts to an increase of 2.23%. This is followed by *d*(S2-As2) and *d*(As2-S3) which are elongated by 0.045 Å and 0.035 Å respectively in comparison to free realgar. *d*(As3-S4) also sees an expansion of 0.027 Å. Thus, in all the above-mentioned cases (See **Table 3.2.6.2**), the coordination of copper atoms results in elongation of the bonds in the cage molecule. Both *d*(As1-As3) and *d*(As2-As4) are seen to be contracted by 0.013 Å and 0.021 Å respectively. As mentioned in the earlier chapter coordination of transition metals to the realgar molecule usually either destroys the cage molecule resulting in fragmentation or leads to ligand recombination reactions. Here it is worth noting that after coordination As-As bonds are intact albeit a bit stronger as indicated by shortening of their bond lengths.

Table 3.2.6.3: Selected bond angles (in Å) for (As_4S_4) in $(CuBr)_2 \cdot (As_4S_4)$. Rows marked in orange represent contraction while in blue represent elongation upon coordination with CuBr as a consequence of altered bond distances. Maximum deviation is observed at the sites of sulphur and arsenic coordination.

Bond angle	$(CuBr)_2 \cdot (As_4S_4)$/ °	As_4S_4/°	Difference/°
As1-S2-As2	102.95	100.91	2.04
As1-S1-As4	101.59	101.29	0.30
As4-S4-As3	102.79	101.29	1.50
As2-S3-As3	103.71	100.84	2.87
S1-As4-As2	100.30	98.69	1.61
S1-As1-As3	99.39	99.57	0.18
S2-As1-S1	92.85	94.47	1.62
S2-As2-As4	97.86	99.82	1.96
S2-As1-As3	100.72	99.19	1.53
S4-As3-As1	97.22	99.17	0.05
S4-As4-As2	100.86	99.17	1.69
S4-As4-S1	89.57	94.86	5.29
S3-As3-S4	92.93	94.56	1.63
S3-As2-S2	94.61	94.87	0.26
S3-As3-As1	99.70	99.42	0.28

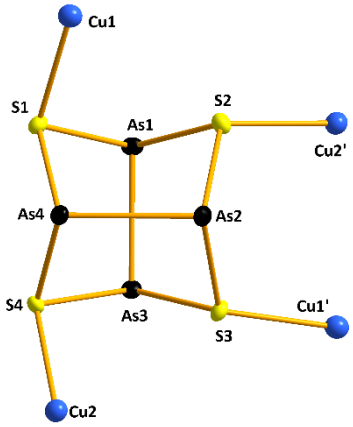

Figure 3.2.6.2: Isolated As_4S_4 cage molecule with copper atoms. The coordination takes place only through sulphur atoms. Bromine atoms are not shown for the sake of simplicity. All ellipsoids are shown with 70% probability

As with bond lengths, bond angles are also affected once coordinated to the copper atoms which are summarized in **Table 3.2.6.3**. The highest deviation is seen for ∠(S4-As4-S1), which sees an expansion of 5.29 ° as compared to free uncoordinated realgar. This was expected since both *d*(As4-S4) and *d*(S1-As4) see an elongation, which is turn is the manifestation of copper coordination. Next, ∠ (S2-As2-As4) also sees a contraction of 1.96 °. This can be attributed to the shortening of *d*(As2-As4). ∠(As2-S3-As3) sees the largest expansion amounting to 2.87 ° which again is a result of copper coordination. The rest of the bond angles which see deviation upon coordination are summarized in **Table 3.2.6.3.**

The coordination sphere of copper

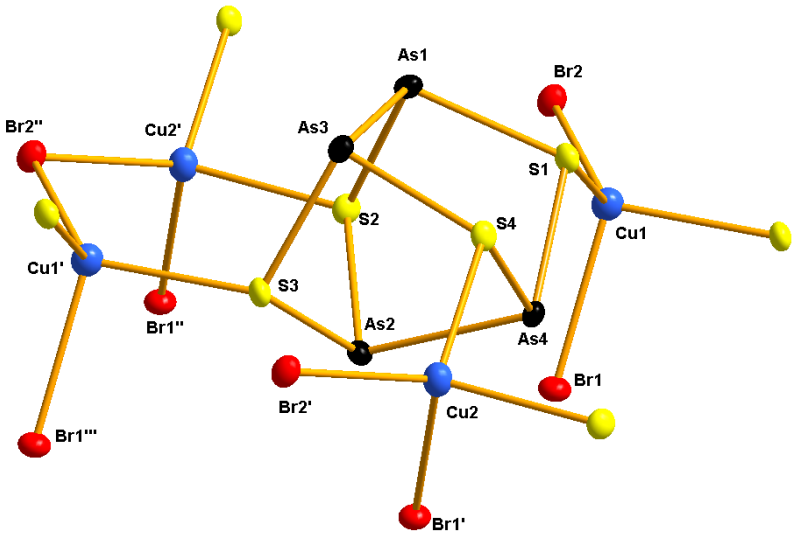

Figure 3.2.6.3: All the copper atoms display a distorted (2+2) tetrahedral coordination mode.

In the adduct $(CuBr)_2 \cdot (As_4S_4)$ all the copper atoms show a distorted tetrahedral coordination mode. It must be noted that there are two crystallographically distinct copper atoms (named Cu1 and Cu2 for the sake of convenience). Cu1 and Cu2 show a (2+2) distorted tetrahedral coordination with two bromine and two sulphur atoms respectively. On the other hand, Cu1' and Cu2' also display a (2+2) distorted tetrahedral coordination although here a bromine atom is shared between the two copper atoms (See **Figure 3.2.6.3**). Following table demonstrates the bond angles for all the copper atoms. A deviation from the ideal value of 109.5 ° is seen because of coordination to the cage molecule.

Table 3.2.6.4: All copper atoms show a distorted tetrahedral coordination. Table below demonstrates the respective bond angles for all copper atoms.

Angle	Bond Angle /°
Br2-Cu1-S	122.13
Br2-Cu1-S1	120.59
S1-Cu1-Br1	101.73

Br1-Cu1-S	95.37
Br2'-Cu2-S4	118.30
S4-Cu2-S	96.59
S-Cu2-Br1'	97.26
Br1'-Cu2-Br2'	108.85
S-Cu2'-S2	96.59
S2-Cu2'-Br1''	97.26
Br1''-Cu2'- Br2''	108.85
Br2''-Cu2'-S	118.30
S3-Cu1'-Br1''	95.37
Br1''-Cu1'-S	101.73
S-Cu1'-Br2''	120.59
Br2''-Cu1'-S3	122.13

The Cu-S distances viz. *d*(S1-Cu2) = 2.34 Å, *d*(S4-Cu2) = 2.32(1) Å, *d*(S2-Cu2') = 2.29(3) Å, and *d*(S3-Cu1')= 2.32 Å are all the normal *d*(Cu-S) range.

Complete crystal structure

As stated in the earlier sub-section, in the adduct compound $(CuBr)_2 \cdot (As_4S_4)$, the coordination of copper(I) bromide takes place only through the sulphur atoms of the neutral As_4S_4 cage molecule. Along with the cage molecules, $(CuBr)_2 \cdot (As_4S_4)$ consists of a one-dimensional $^1_\infty[CuBr]$ wave- like chains. The shortest distance between two copper atoms, *d*(Cu1-Cu2), amounts to 5.55 Å (See **Figure 3.2.6.4**).

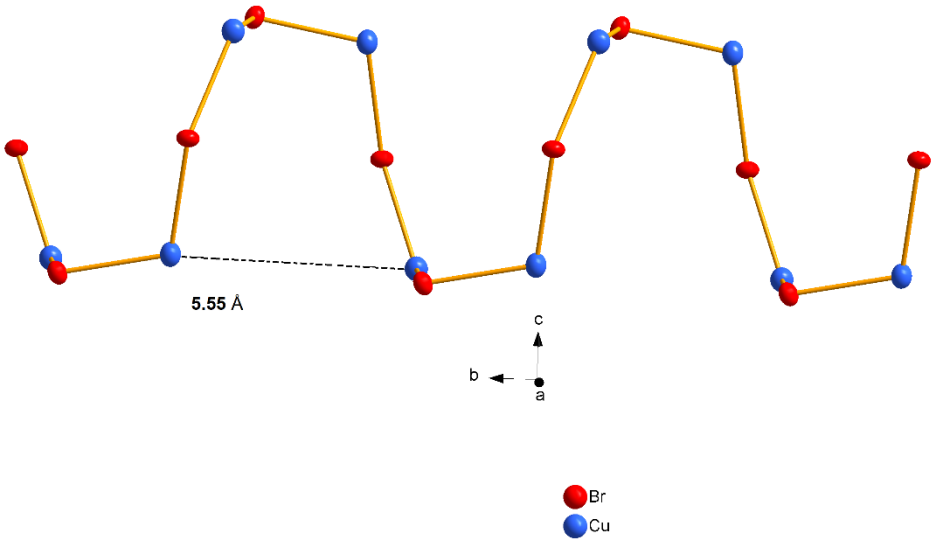

Figure 3.2.6.4: CuBr is arranged as a one dimensional $^{1}_{\infty}[CuBr]$ wave- like chains. All ellipsoids are shown with 70% probability.

Figure 3.2.6.5 shows the representation of the adduct $(CuBr)_2 \cdot (As_4S_4)$ along the b axis. As seen the individual As_4S_4 units are embedded in the $^{1}_{\infty}[CuBr]$ network. The coordination takes place only through the sulphur atoms. The shortest distance between any to cage molecules along the a axis is *d*(As4-S2) = 4.15 Å and *d*(S2-As2) amounting to 5.47 Å along the b axis. Along the a axis (See **Figure 3.2.6.6**) it can be seen that the As_4S_4 form a layer-like substructure and are connected by copper(I) bromide chains.

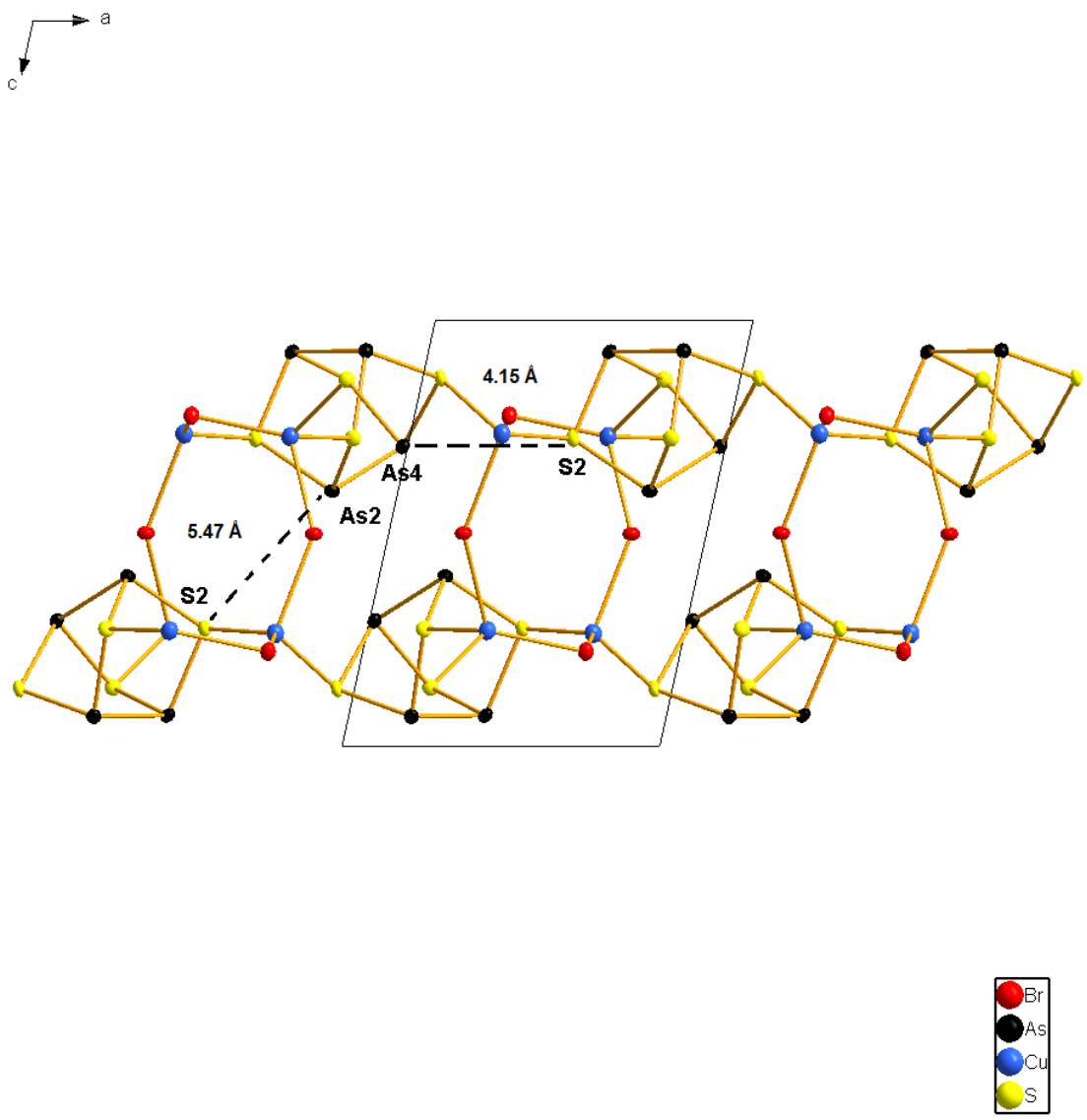

Figure 3.2.6.5: As_4S_4 cages intertwined in $^{1}_{\infty}[CuBr]$ one dimensional chains in the $(CuBr)_2 \cdot (As_4S_4)$ adduct molecule. The above representation is along the b axis. All ellipsoids are shown with 70% probability.

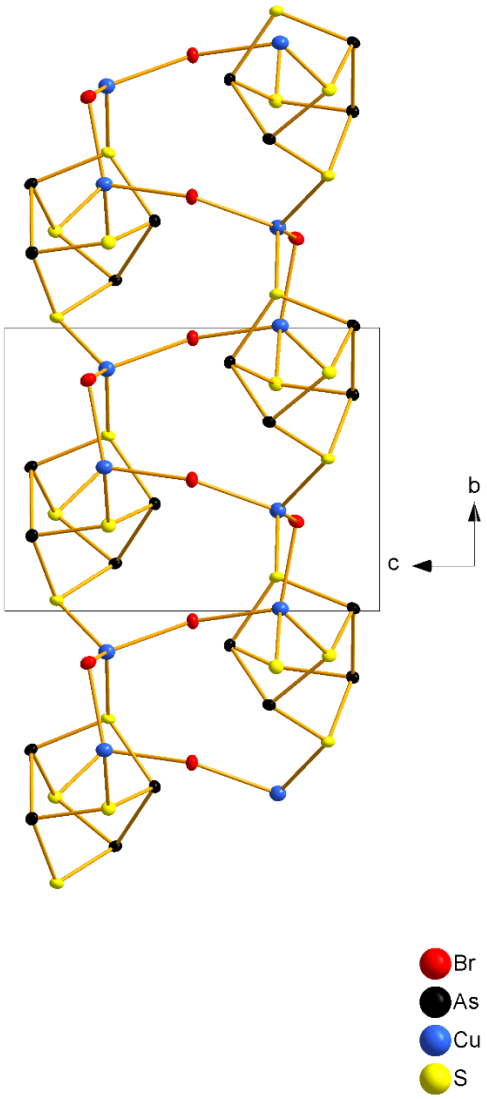

Figure 3.2.6.6: The adduct $(CuBr)_2 \cdot (As_4S_4)$ as seen along a axis. Layers of As_4S_4 are seen flanked in between the copper(I) bromide network. All ellipsoids are shown with 70% probability.

3.2.6.3 SEM and EDX Analysis

For the scanning electron microscopic investigations and the EDX analysis, one of the shiny red blocks contained in the batch was separated under the light microscope and glued to the carbon-coated carrier. It must be noted here that only few crystals of the desired product were found in each reaction batch **Figure 3.2.6.6** shows a scanning electron microscopic image of a $(CuI)_3 \cdot (As_4S_4)$ at a cathode voltage of 25 kV and **Table 3.2.6.4** shows the results.

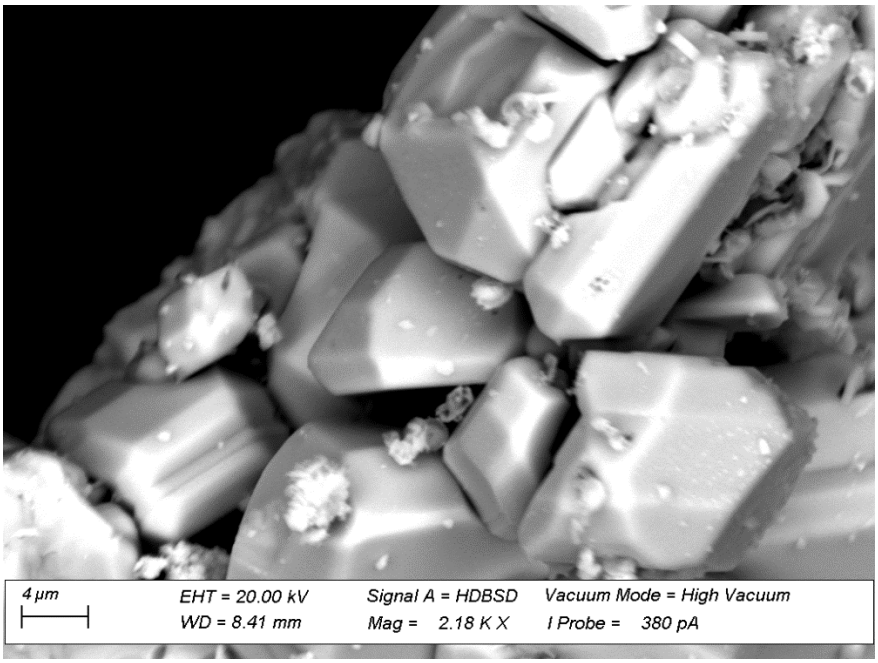

Figure 3.2.6.6: Electron microscopic image of a crystal of the adduct $(CuBr)_2 \cdot (As_4S_4)$ with an excitation voltage of 25kV.

Table 3.2.6.4: Result of energy dispersive X-ray spectroscopy and calculated proportions of silver, iodine, arsenic, and sulphur in the $(CuBr)_2 \cdot (As_4S_4)$ adduct compound.

Element	Cu	Br	As	S
Abs. Error/ %	1.50	2.17	3.07	1.75
Rel. Error/ %	8.67	10.39	9.04	11.28
EDX results/Atom%	18.52	17.81	30.80	32.87
Calculated Results/Atom %	16.66	16.66	33.33	33.33

3.2.7 The Adduct $(CuBr)_2 \cdot (As_4Se_3)$

3.2.7.1 Synthesis

As_4Se_3 (0.325 g, 1 equiv) and CuBr(0.174 g, 2 equiv) were transferred to a duran ampoule (7 cm) followed by addition of 1mL of toluene and ACN respectively. The reaction mixture was cooled under liquid nitrogen and subsequently evacuated and reacted in a stainless-steel autoclave under solvothermal conditions at 160 °C for 5 days. The oven was cooled down at 80 °C over a time period of 5 h and maintained at this temperature for another 2 days followed by slow cooling down (over 6 h) to RT. After cooling a few dark red coloured crystals of $(CuBr)_2 \cdot (As_4Se_3)$ were obtained.

3.2.7.2 Single Crystal Analysis

$(CuBr)_2 \cdot (As_4Se_3)$ crystallises in primitive triclinic space group and exhibits a non- merohedral twining and therefore the initial data set showed only 77.8 % indexation corresponding to a batch scale factor of 0.18. The two components were related to each other by the following twin law:

$$M = \begin{bmatrix} -1 & 0 & 0 \\ 0 & 1 & 0 \\ 0 & 0 & -1 \end{bmatrix}$$

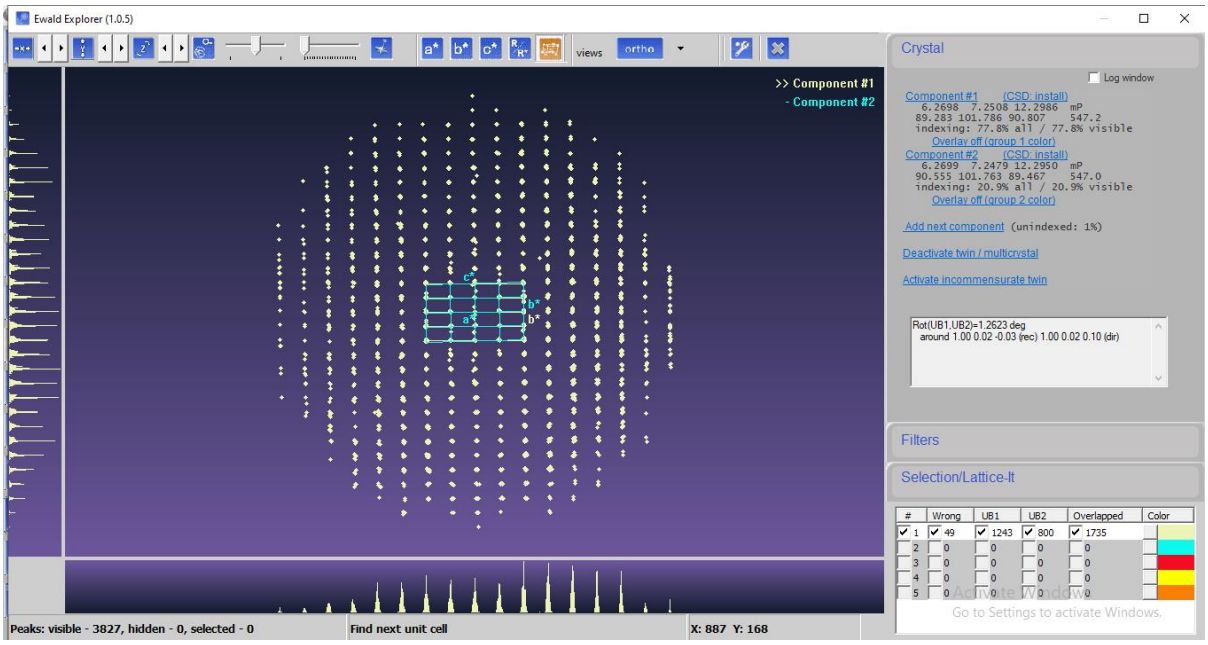

Figure 3.2.7.1: Ewald sphere along a* showing both components of the twinned crystal. Component 1 accounting for 77.8 % indexed reflections is shown in grey, while the second component accounting for 20.9 % is shown in turquoise.

The data reduction and finalization and the subsequent treatment for twinning was done in the same way as stated in the **Section 3.2.2.2**. **Figure 3.2.7.1** depicts the Ewald sphere where the first component is shown in grey while the second in turquoise. The first component accounts for 77.8 % of the indexed reflections while the second accounting for 20.9 %, leaving 1 % unindexed reflections.

Table 3.2.7.1: Table gives an overview of the crystallographic data and measurement parameters of $(CuBr)_2 \cdot (As_4Se_3)$.

Empirical Formula	$As_4Br_2Cu_2Se_3$	
Formula weight	823.46	
Crystal colour and shape	Red block	
Crystal system	triclinic	
Space group	P-1	
a/Å	6.259	
b/ Å	7.241	
c/ Å	12.297	
α/°	89.19	
β/°	78.26	
γ/°	89.15	
V/Å^3, *Z*	545.64, 2	
Absorption coefficient(μ)/ mm^{-1}	37.82	
ρ_{calc}/g/cm^3	5.021	
Diffractometer	Rigaku Super Nova	
Radiation, temperature	Cu Kα (λ = 1.541 Å) 293 K	
Θ-range/°	12.22 – 144.72	
hkl-range/°	-7 ≤ h ≤ 7 -8 ≤ k ≤ 8 -15 ≤ l ≤ 15	
Absorption correction	numerical (gaussian, Scale3 Abspack)	
Twinning considered	no(.hklf4)	yes(.hklf5)
Number of reflections	4615	3642
Independent reflections	1747	3642
BASF	-	0.18
R_σ, R_{int}	0.0696, 0.0842	0.0375,-
Completeness	94 %	100%
Structure solution	SHELXT	SHELXT
Structure refinement	SHELXT - 2014	SHELXT - 2014
Data/Restraints/Parameters	1747/0/100	3642/0/102
GooF	1.150	1.101
R_1, wR_2 *[I>2σ(I)]*	0.0658, 0.1946	0.0457, 0.1342
R_1, wR_2 *[all reflexes]*	0.0924, 0.2512	0.0544, 0.1393
Largest diff. peak/hole/e Å^{-3}	3.61/-4.29	1.52/-1.45

$(CuBr)_2 \cdot (As_4Se_3)$ crystallises in the space group P-1 with a = 6.259Å, b = 7.241 Å, c = 12.297 Å, α = 89.19° β = 78.26°, γ = 89.15°, V = 545.64 $Å^3$ and Z = 2. The positions and isotropic displacement parameters can be found in Appendix in **Table A.26**. The anisotropic displacement parameters are listed in **Table A.27**. The bond lengths and bond angles can be found in **Table A.28** and **Table A.29**. The complete structure can be subdivided into two sub-structures, viz. the neutral As_4Se_3 cages and the one dimensional $[Cu_2Br_2]$ dimers.

As_4Se_3 sub- structure

Like As_3Se_4 cage molecule, also in the adduct $(CuBr)_2 \cdot (As_4Se_3)$, the four arsenic atoms are situation in pyramidal position while selenium bridges along the apical bridges (See **Figure 3.2.7.2**).

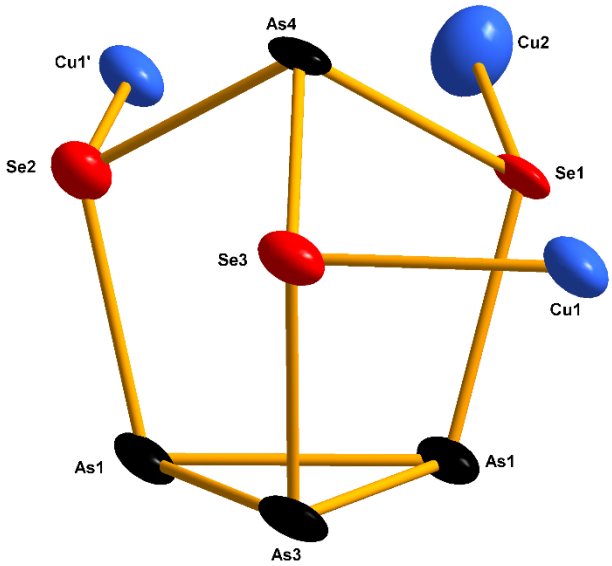

Figure 3.2.7.2: Isolated As_4Se_3 cage molecule with copper atoms. The coordination takes place only through selenium atoms. Bromine atoms are not shown for the sake of simplicity. All ellipsoids are shown with 80% probability.

The coordination of copper bromide to the cage molecule has some effect on the bond lengths and bond angles which are discussed in the following section. As seen in the **Figure 3.2.7.2**, the coordination of copper atom takes place exclusively through the selenium atoms. Here

the copper atoms are shared between two cage molecules (on one side of the cage), making the overall stoichiometry 1:2. As expected a elongation of bonds is seen the site of copper coordination. The highest digression is seen for *d*(As2-Se1) amounting to 0.184 Å. Contraction

Table3.2.7.2: Selected interatomic distances (in Å) for (As_4S_4) in $(CuBr)_2{\cdot}(As_4Se_3)$. Rows marked in blue represent elongation while marked in orange represent contraction upon coordination with CuBr.

Bond/Distance	$(CuBr)_2{\cdot}(As_4Se_3)$/ Å	As_4Se_3/ Å	Difference/ Å
As1-As2	2.463	2.420	+0.023
As1-As3	2.249	2.498	-0.249
As1-Se1	2.402	2.271	+0.138
As3-Se2	2.401	2.279	+0.122
As2-Se1	2.423	2.239	+0.184
As2-Se2	2.392	2.292	+0.1

is seen only for *d*(As1-As3) amounting to 0.249 Å, which is 2.13 % when compared to uncoordinated As_4Se_3 cage molecule. It is also worth noting that d(As1-As1) is barely altered. The altered bond angles do also have an effect on the respective bond angles which are summarized in **Table 3.2.7.3**.

Table 3.2.7.3: Selected bond angles (in Å) for (As_4S_4) in $(CuBr)_2{\cdot}(As_4Se_3)$. Rows marked in orange represent contraction while in blue represent elongation upon coordination with CuBr as a consequence of altered bond distances.

Bond Angle	$(CuBr)_2{\cdot}(As_4Se_3)$ / °	As_4Se_3 / °[110]	Difference
As1-Se1-As2	106.51	104.81	+1.7
Se1-As2-Se1	95.78	96.43	-0.65
As2-Se2-As3	106.81	105.36	+1.45
Se1-As1-As3	102.58	103.72	-1.14
As1-As3-As2	57.95	59.52	-1.57
Se1-Se2-As1	101.45	104.21	-2.76
As1-As2-As3	61.02	60.90	+0.12

Coordination sphere of copper

All the three copper atoms in the adduct $(CuBr)_2 \cdot (As_4Se_3)$ show a (2+2) distorted tetrahedral coordination coordinating to selenium and bromine. Here it must be noted that there are two crystallographically distinct copper atoms which are named Cu1 and Cu2 for the sake of

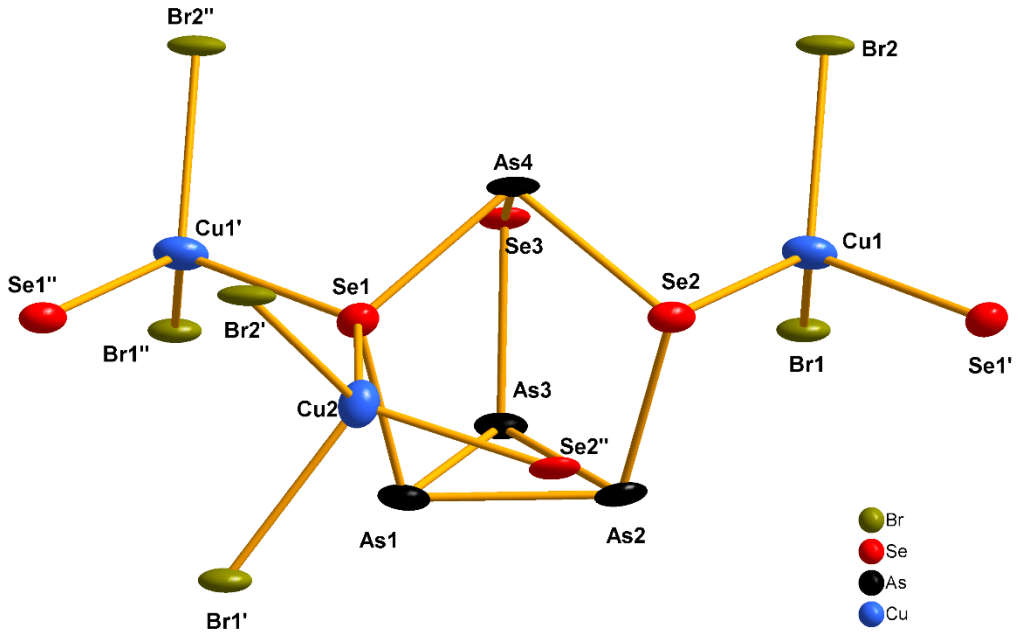

Figure 3.2.7.3: All the copper atoms display a distorted (2+2) tetrahedral coordination mode. All ellipsoids are shown with 50% probability.

convenience. All the three copper atoms are coordinated to two selenium atoms and two bromine atoms to complete the tetrahedral coordination environment (See **Figure 3.2.7.3**). Following table demonstrates the bond angles for all the copper atoms. A deviation from the ideal value of 109.5 ° is seen because of coordination to the cage molecule.

Table 3.2.7.4: All copper atoms show a distorted tetrahedral coordination. Table below demonstrates the respective bond angles for all copper atoms

Angle	Bond Angle /°
Br2-Cu1-Se1’	109.47
Se1’-Cu1-Br1	111.72
Br1-Cu1-Se1	121.02
Se1-Cu1-Br2	118.70
Se1-Cu2-Br2’	114.35
Br2’-Cu2-Br1’	98.96
Br1’-Cu2-Se2’’	109.75
Se2’’-Cu2-Se1	105.51
Br2’’-Cu1’-Se1	109.47
Se1-Cu1’-Br1’’	117.2
Br1’’-Cu1’-Se1’’	121.02
Se1’’-Cu1’-Br2’’	118.70

Complete Crystal Structure

As discussed in the earlier section, the adduct $(CuBr)_2 \cdot (As_4Se_3)$ consist of neutral As_4Se_3 cages which are connected to each other by $[Cu_2Br_2]$ dimers. As seen in **Figure 3.2.7.4** we see the strands of neutral As_4Se_3 cages are embedded in a copper(I) bromide network. Each $[Cu_2Br_2]$

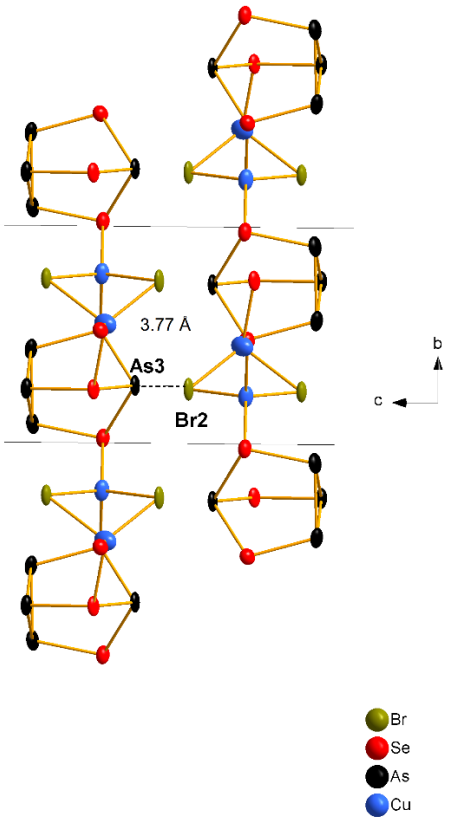

Figure 3.2.7.4: A section of the crystal structure of $(CuBr)_2 \cdot (As_4Se_3)$ shown along the a axis.

unit is connected to two As_4Se_3 cages and vice versa a single $[Cu_2Br_2]$ is shared between two As_4Se_3 cages. The cages run parallel the [010] direction. The shortest distances between the strands is *d*(As3···Br2) with 3.772 Å (See **Figure 3.2.7.4**) which is almost equal to the sum of the corresponding van der Waals radii ($r_{Se} + r_{Br}$ = 3.75 Å). The Cu-Cu distance in the $[Cu_2Br_2]$ unit amounts to 2.79 Å. This distance is almost equal to the sum of the Van der Waal radii (2.80 Å) but shorter than the sum of the metal ion radii (2.556 Å) which suggest no or very weak attractive metallophilic d^{10}-d^{10} interaction between the two copper centres. A complete list of bond distances and bond angles for $(CuBr)_2 \cdot (As_4Se_3)$ is found in **Table A.28** and **Table A.29** in the Appendix.

3.2.7.3. SEM and EDX Analysis

For the scanning electron microscopic investigations and the EDX analysis, one of the shiny red blocks contained in the batch was separated under the light microscope and glued to the carbon-coated carrier. It must be noted here that only few crystals of the desired product

were found in each reaction batch **Figure 3.2.7.5** shows a scanning electron microscopic image of a $(CuI)_3 \cdot (As_4S_4)$ at a cathode voltage of 25 kV and **Table 3.2.7.5** shows the results.

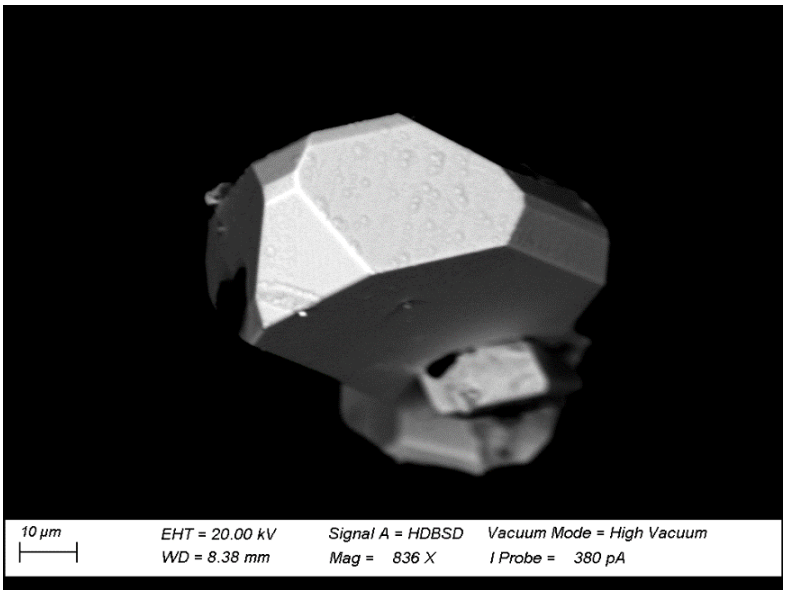

Figure 3.2.7.5: Electron microscopic image of a crystal of the adduct $(CuBr)_2 \cdot (As_4Se_3)$ with an excitation voltage of 25kV.

Table 3.2.7.5: Result of energy dispersive X-ray spectroscopy and calculated proportions of silver, iodine, arsenic, and sulphur in the $(CuBr)_2 \cdot (As_4Se_3)$ adduct compound.

Element	Cu	Br	As	Se
Abs. Error/ %	1.12	1.83	2.83	2.44
Rel. Error/ %	8.72	10.31	8.98	9.45
EDX results/Atom%	18.53	18.62	35.39	27.46
Calculated Results/Atom %	18.18	18.18	36.36	27.27

4. Host/Guest Compounds

4.1 Introduction

Inclusion compounds are long known area of research and form an important part of solid-state chemistry. An practical example are the Zeolites which are produced in million tons annually and find applications ranging from waste water treatment, catalysis to nuclear waste management[111,112]. To this class also belong the sodalite and iodoindates[113,114]. Next, inclusion compounds in which the Pn_4Q_x cages (Pn = P, As; Q = S, Se) are positioned in the matrices of transition metal halides are also known. For instance, the inclusion compounds like $(CdI_2)_6(CdS)(As_4S_x)$[14] and $(ZnI_2)_6(ZnS)(P_4S_x)$[115]. Yet another type are the clathrate compounds in which again a guest compound is embedded or trapped in the host[116,117]. Yet another is the boracite type compounds. Boracite ($Mg_3B_7O_{13}Cl$) is a naturally occurring mineral in which the host is a metal-borate framework[118–121]. Previous works by Jung and Bräu demonstrated that the compounds of the type $(ZnI_2)_6(ZnS)(P_4S_x)$ and $(CdI_2)_6(CdS)(As_4S_x)$ with a network consisting of zinc/cadmium halides showed host-guest type interactions with the pnictogen chalcogenide cages embedded in the 3-D network was similar to boracite. Next, Vitzthumecker[18] was able to synthesis new series of similar compounds involving copper(I) halides and mercury(II) halides,viz, $(CuI)_7(HgI_2)_3(Pn_4S_x)$ where Pn_4 = P, As.

4.2 The Adduct $(CuI)_7(HgI_2)_3(As_4Se_3)$

4.2.1 Synthesis

CuI (0.302 g , 7 equiv), HgI_2 (0.302 g, 3 equiv) and As_4Se_3(0.055g, 1 equiv) were weighed, transferred in a quartz ampoule, evacuated, sealed, and then rested in oven at 500 °C for 14 days. The heating rate was 0.5 °C/min, while the cooling rate was 1.5 °C/min. This resulted in a very few block-like red crystals of the adduct $(CuI)_7(HgI_2)_3(As_4Se_3)$. These were isolated manually under nitrogen and used for further analysis (See **Figure 4.2.1**).

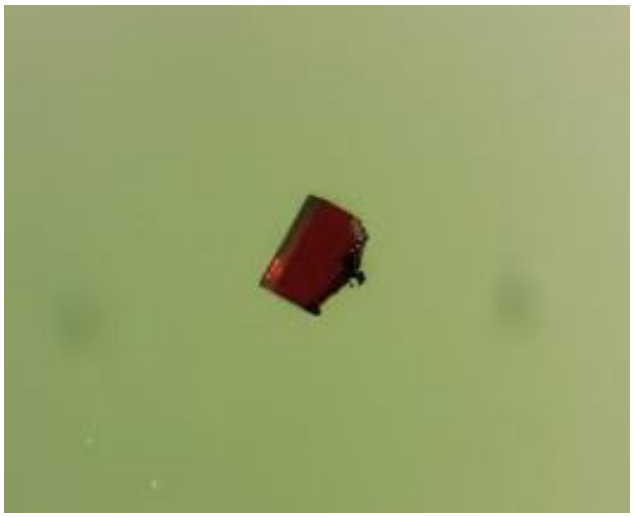

Figure 4.2.1: Isolated crystal of the adduct $(CuI)_7(HgI_2)_3(As_4Se_3)$ isolated for single crystal X ray diffraction experiment under oil (size of the crystal - 0.08 mm * 0.08mm * 0.11mm).

In similar manner adduct compounds $(CuI)_7(ZnI_2)_3(As_4Se_3)$ and $(CuI)_7(CdI_2)_3(As_4Se_3)$ were synthesised. The summary of the weights and equivalents is presented in **Table 4.2.1**.

Table 4.2.1: Summary of the weights and equivalents during the synthesis of adduct compounds $(CuI)_7(ZnI_2)_3(As_4Se_3)$ and $(CuI)_7(CdI_2)_3(As_4Se_3)$.

Educts	Equivalents	Weight/g
CuI	7	0.2245/0.2357
ZnI_2/CdI_2	3	0.1693/0.185
As_4Se_3	1	0.094/0.0903

As all the three compounds are isostructural, a detail structural analysis of only one, viz. $(CuI)_7(HgI_2)_3(As_4Se_3)$ is presented in the following section.

4.2.2 Single Crystal Analysis

Table 4.2.2: Table gives an overview of the crystallographic data and measurement parameters of the adduct compound $(CuI)_7(HgI_2)_3(As_4Se_3)$, $(CuI)_7(ZnI_2)_3(As_4Se_3)$ and $(CuI)_7(CdI_2)_3(As_4Se_3)$.

Empirical Formula	$As_4Cu_7Zn_3I_{13}Se_3$	$As_4Cu_7Cd_3I_{13}Se_3$	$As_4Cu_7Hg_3I_{13}Se_3$
Formula weight	2827.3	2968.39	3232.98
Crystal colour and shape		Red block	
Crystal system		cubic	
Space group		*F*-43c (219)	
a/Å	19.4080(8)	19.679(1)	19.7475(6)
V/Å^3, *Z*	7310.4(5),8	7621.7(8), 8	7703.1(1), 8
Absorption coefficient(μ)/ mm^{-1}	22.47	222.313	32.357
ρ_{calc}/g/cm^3	5.3177	5.1757	5.5753
Diffractometer		Rigaku Super Nova	
Radiation, temperature		Mo Kα (λ = 0.71073 Å), 123 K	
Θ-range/°	2.97 – 37.23	2.93 – 32.62	3.57- 44.99
hkl-range/°	-23 ≤ *h* ≤31	-28 ≤ *h* ≤ 29	-27 ≤ *h* ≤ 38
	-32 ≤ *k* ≤ 24	-19 ≤ *k* ≤ 26	-38 ≤ *k* ≤ 14
	-26 ≤ *l* ≤ 32	-27 ≤ *l* ≤ 15	-18 ≤ *l* ≤ 36
Absorption correction		numerical (gaussian, Scale3 Abspack)	
Number of reflexes	5768	9096	8085
Independent reflections	404	234	788
R_{int}	0.0539	0.0857	0.0269
Completeness	99 %	99.8 %	99 %
Twin Matrix		$\begin{matrix}-1 & 0 & 0\\ 0 & -1 & 0\\ 0 & 0 & -1\end{matrix}$	
Twin Fraction	0.48	0.506	0.502
Structure solution		*JANA2006*	
Structure refinement		Charge Flipping,Superflip	
Parameters	34	27	31
GooF	1.61	1.55	2.34
R_1, wR_2 *[I>2σ(I)]*	0.0524, 0.0796	0.0371, 0.0269	0.0799, 0.1054
R_1, wR_2 [all reflexes]	0.0580, 0.0819	0.0539, 0.0286	0.2174, 0.1125
Largest diff. peak/hole/e Å^{-3}	6.85/-4.16	5.46/-4.79	7.33/-3.96

The adduct $(CuI)_7(HgI_2)_3(As_4Se_3)$ crystallises in the cubic $F\bar{4}3c$ space group with the lattice parameter, a = 19.749 Å. The refinement of all the data converges to a GooF of 2.34 with *R1*= 7.99 % and wR_2 = 10.54 %. For $(CuI)_7(ZnI_2)_3(As_4Se_3)$ the refinement data converges to a GooF of 1.61 with *R1*= 5.24 % and wR_2 = 7.96 %. Lastly, the refinement data for $(CuI)_7(CdI_2)_3(As_4Se_3)$ converges to a GooF of 1.55 with *R1*= 3.71 % and wR_2 = 2.69 %. The positions and isotropic displacement parameters for $(CuI)_7(ZnI_2)_3(As_4Se_3)$ can be found in Appendix in **Table A.30**. The anisotropic displacement parameters are listed in **Table A.31**. The bond lengths and bond angles can be found in **Table A.32** and **Table A.33**. The positions and isotropic displacement parameters for $(CuI)_7(CdI_2)_3(As_4Se_3)$ can be found in Appendix in **Table A.34**. The anisotropic displacement parameters are listed in **Table A.35**. The bond lengths and bond angles can be found in **Table A.36** and **Table A.37**. The positions and isotropic displacement parameters for $(CuI)_7(HgI_2)_3(As_4Se_3)$ can be found in Appendix in **Table A.38**. The anisotropic displacement parameters are listed in **Table A.39**. The bond lengths and bond angles can be found in **Table A.40** and **Table A.41**.

Table 4.2.2 gives an overview of the crystallographic data and measured measurement parameters for $(CuI)_7(HgI_2)_3(As_4Se_3)$. It must be noted that the values given in the Appendix correspond to the refinement in the $F\bar{4}3c$ space group. For the correct assignment of the electron density for the As_4Se_3 cages, arsenic and selenium atoms were added according to their symmetry requirements. The apical As atom is assigned to the rest electron density with 3 fold symmetry while the rest electron density with site symmetry 1 is assigned to the basal As atoms and Se atoms respectively.

The data reduction, finalisation, and refinement for the compound $(CuI)_7(HgI_2)_3(As_4Se_3)$ can be carried out in both the space groups, viz - $Fm\bar{3}c$ or in the lower symmetric $F\bar{4}3c$ as an inversion twin. In the space group $Fm\bar{3}c$, five symmetry independent positions with the following Wyckoff positions were obtained.

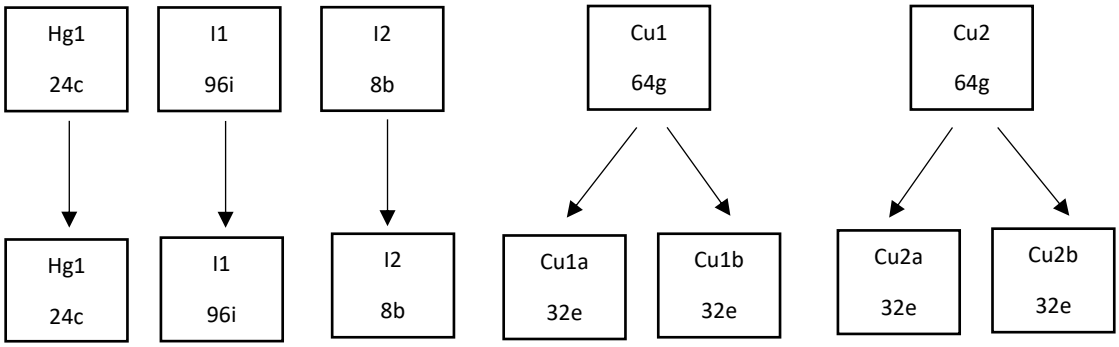

Figure 4.2.2: A Bärnighausen Diagram showing the Wyckoff positions descending from a higher symmetric F$m\bar{3}c$ space group to $F\bar{4}3c$.

When refinement was done with $Fm\bar{3}c$ although a high residual electron density was observed, locating a new atom corresponding to that electron density was not possible. When a descend from $Fm\bar{3}c$ to $F\bar{4}3c$ was performed, a total of seven symmetry independent positions were identified. Here it must be noted that the positions of arsenic and selenium atoms were not considered and secondly, the occupation factors of copper, arsenic and selenium were refined independently. An overview of the resultant positions is shown in the **Figure 4.2.2**, thus resulting in a total of nine symmetry independent positions when arsenic and selenium are included. A significantly better R values, GooF are seen when refined in $F\bar{4}3c$. Also, a decrease in the rest electron density was seen.

After the refinement of the occupation factors of copper atoms, the number of copper atoms were set to a reasonable number of seven per formula unit and a further refinement was excluded. Since all other compounds in the following chapter are isostructural to $(CuI)_7(HgI_2)_3(As_4Se_3)$, it is worthwhile to discuss the structure of the matrix comprising of copper, mercury and iodine which is done in the following section.

The basic structural unit of these type of inclusion compounds is the disordered ICu_4 tetrahedron. This disordered tetrahedron is in turn surrounded by an icosahedron of iodine atoms. The capped copper atoms are located in between this I_{12} icosahedron. The eight of the twelve tetrahedral voids in the I_{12} icosahedral are filled with the partially occupied copper atoms. The rest twelve triangular faces each share a common edge. Via these common edges they form a HgI_4 tetrahedra. Thus, the icosahedra are linked to each other in 3-D and form a network having a central iodine atom as a "core". Thereby, each icosahedron is linked to six other icosahedra through a HgI_4 tetrahedra (See **Figure 4.2.3**).

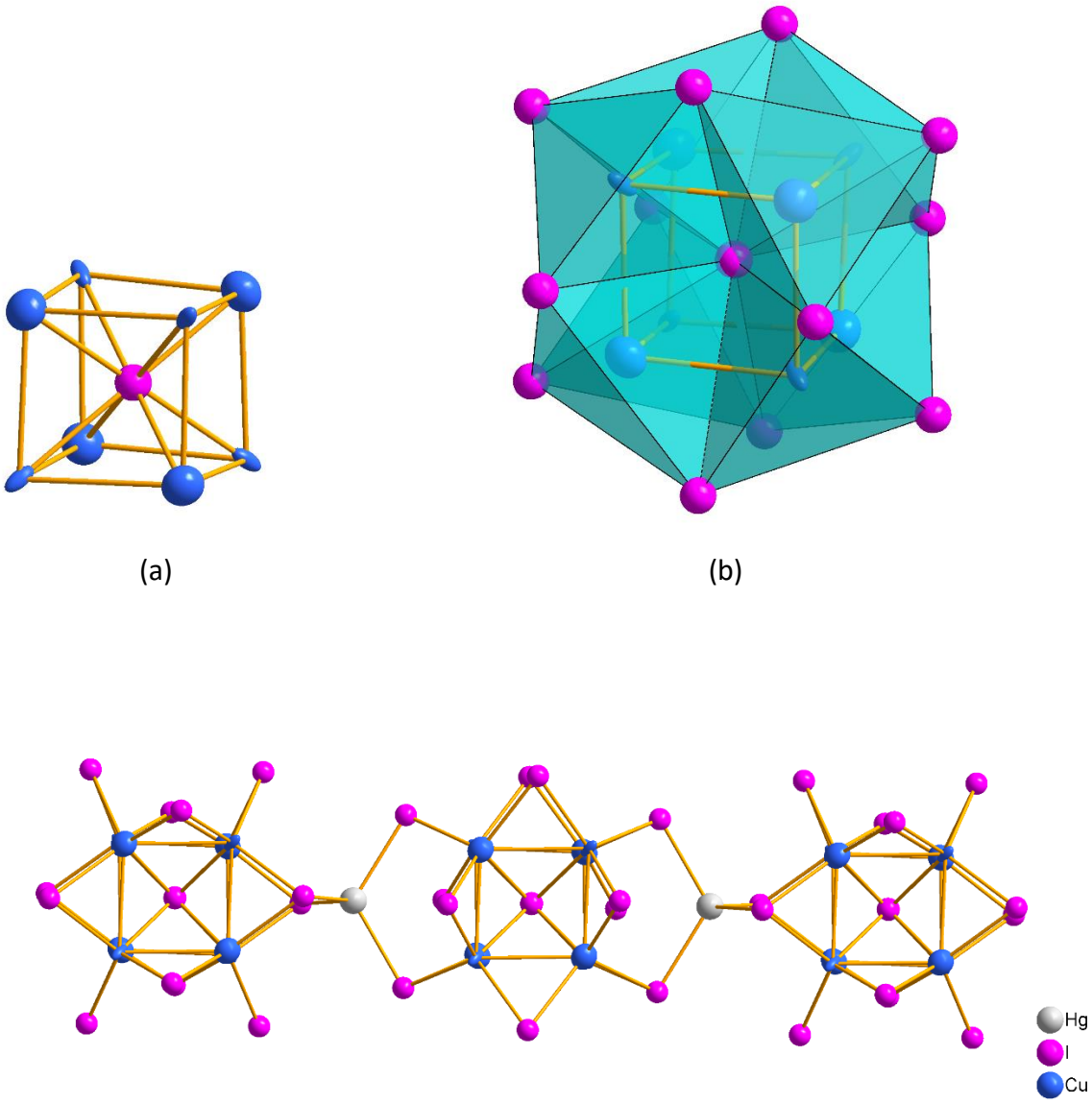

Figure 4.2.3: The basic building block – the distorted ICu_4 tetrahedron (a). This distorted ICu_4 tetrahedron is surrounded by iodine atoms forming an icosahedron with the partially occupied copper atoms occupy eight out of the twelve tetrahedral voids (b). The rest twelve tetrahedral voids each share a common edge are connected via HgI_4 tetrahedra (c).

Table 4.2.3: Selected bond distances in $(CuI)_7(HgI_2)_3(As_4Se_3)$. For better visualisation the I_{12} icosahedron is also shown.

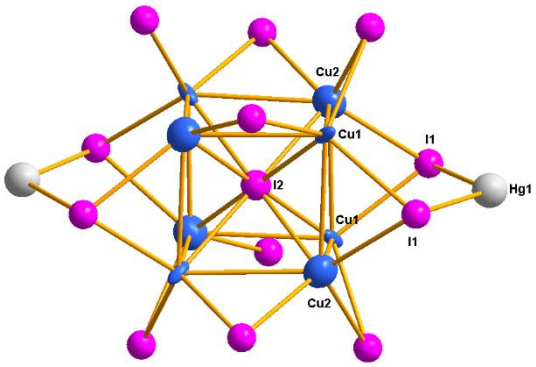

Bond	Bond length / Å
d(I2-Cu2)	2.523
d(I2-Cu1)	2.666
d(I2-Cu1)	2.666
d(I2-Cu2)	2.523
d(I1-Hg1)	2.728
d(I1-Cu1)	2.598
d(I1-Cu2)	2.737

A similar compound, $(DabcoH_x)_4(Cu_yI_{16})$, where DabcoH stands for 1-Azonium-4-azabicyclo [2.2.2] octane), was reported earlier. In this compound,14 of the 20 possible tetrahedral voids in an iodine centered I_{12} icosahedron were filled by partially occupied copper sites[122]. The copper atom distances *d*(Cu-I) in this compound were in the range of 2.76 Å - 5.51 Å which matches well with the compound under study (See **Table 4.2.3**). The *d*(I1-Hg1) amounting to 2.728 Å is also comparable to the literature known value of *d*(I-Hg) amounting to 2.79 Å in the red mercury iodide (HgI_2)[123]. In red HgI_2, as in $(CuI)_7(HgI_2)_3(As_4Se_3)$, the mercury atoms are bound to iodine atoms in a tetrahedral fashion giving rise to a HgI_4 tetrahedron.

Thus, a rigid framework of cubic symmetry containing an icosahedron of copper and iodine atoms is obtained. These icosahedra are further connected to each other via mercury atoms eventually resulting in a 3-D network with large empty spaces or channels between them. The arseno-chalcogenide cages, in this case, As_4Se_3, are located in these empty channels (See **Figure 4.2.4**). To locate the positions of the atoms in the cage molecule has not been necessarily easy as seen the previous works[14,18,115]. In cubic symmetry there are four orthogonal triple axes of rotation. As_4Se_3 belongs to C_{3v} point group and thus is not the best candidate to fill the cavity of the network. This results in a high disorder of the As_4Se_3 cage molecules owing to the mismatch between the molecular symmetry and the cell symmetry. But As_4Se_3, with its C_{3v} symmetry also has three-fold rotational axis and As_4Se_3 can be oriented in opposite directions along this axis, meaning that the As_4Se_3 molecule can orient itself in 8

different ways in the cavity. This fact was taken to advantage during refining the structure using *JANA2006* to get a reasonably good structural model. For the ease of visualisation only

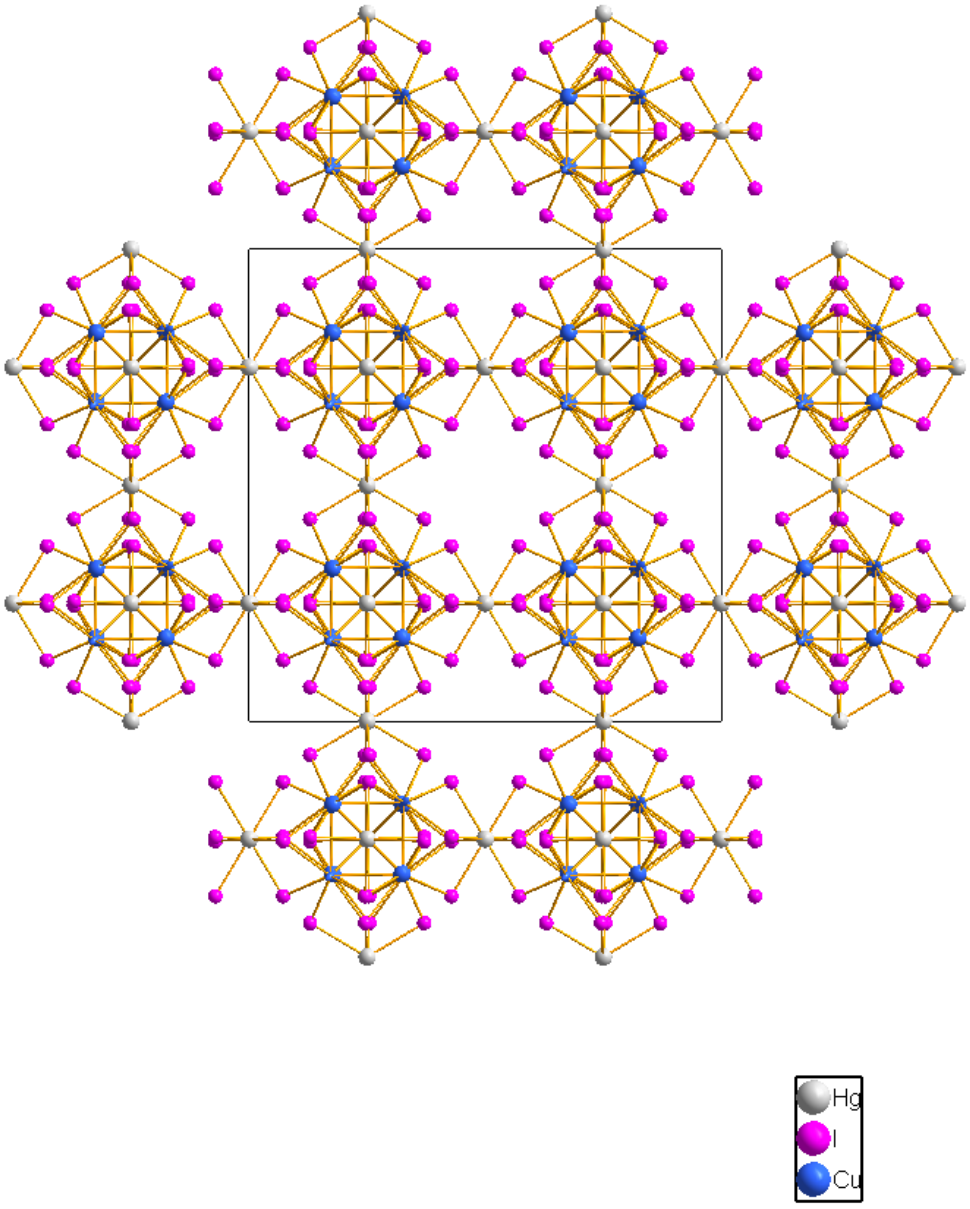

Figure 4.2.4: 3-D matrix comprising of I_{12} icosahedra, the eight of the twelve tetrahedral voids are filled with partially occupied copper atoms. These icosahedra are further connected to each other via tetrahedrally coordinated mercury atoms resulting in a structure with open voids/channels.

4 different orientations were considered while refining. Thus, although the following case represents a discrepancy between the molecular and cell symmetry, it was possible to have a structural model where the cage molecule is embedded in the empty channels of the Cu-I-Hg

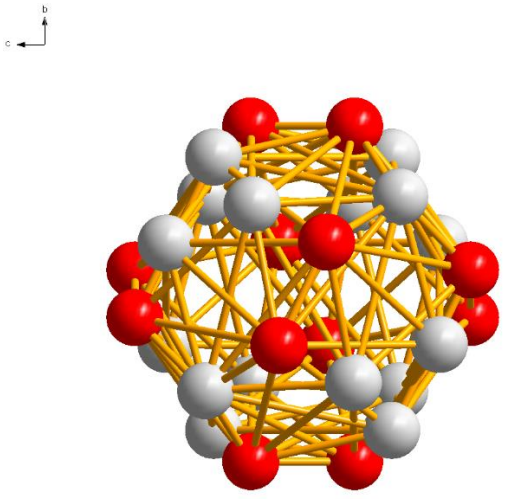

Figure 4.2.5: As_4Se_3 cage molecule (As atoms are depicted in grey while Se atoms are depicted in red) embedded in the Cu-I-Hg matrix. A total of four orientations are feasible which are depicted in the figure. A total of 28 atoms are seen which correspond to the four orientations of the cage molecule.

matrix. After having a reasonable refinement of the matrix, arsenic and selenium atoms were added according to symmetry requirements as dictated by the C_{3v} symmetry of the cage molecule. The rest electron density with 3-fold symmetry was allocated to apical arsenic atom while the basal arsenic and selenium atoms were assigned to the rest electron density with site symmetry 1. This results into four different cage molecules in four different orientations in the cavity. **Fig 4.2.5** depicts such a cage molecule. As seen in the Figure, we find a total of 28 atoms (16 arsenic and 12 selenium) corresponding to four different orientations. Third order anharmonic oscillation tensor was not applied during refinement. Thus, there are four different As_4Se_3 molecules embedded in the cavity which is physically not possible but represents that the cage is rotating inside the Cu-I-Hg matrix. **Figure 4.2.6** depicts the As_4Se_3 cages intercalated in the Cu-I-Hg matrix. It must be however noted that the refinement of the cage molecule posed a problem owing to the very meagre electron density difference between arsenic and selenium atoms. The shortest possible diagonal distance in between the cavities, viz *d*(Cu-Cu) sums to 9.72 Å. The diameter of the cage molecule was calculated as the farthest possible distance between arsenic atoms, *d*(As-As) which amounts to 4.1 Å. Here, it must be noted that the distance between the pnictogen is only approximate since the exact localisation of the cage is not possible. This discrepancy between the diameters of the cage molecules and the diameter of the cavity can explain the free movement of the cage molecule inside the cavity. Further NMR studies are needed to corroborate that fact that there is no or minimal interaction between the cage molecule and the 3-D Cu-I-Hg matrix. Furthermore, a transformation of the cage molecule in another modification cannot be ruled out. It is also possible that there exist cage molecules with different compositions, for instance, a combination of As_4Se_3 and As_4Se_4.

To rationalise the arrangement of the cage molecule in the matrix, two possible scenarios could be arguable. Firstly, it can be visualised that the intercalated cage molecule does not have any preferred orientation and can, up to a certain degree, rotate freely within the voids. Secondly, it can be thought that each cage molecule is coordinated in a distorted tetrahedral manner with the partially occupied copper positions. Furthermore, it is conceivable that each cage molecule could be drifted in the direction of one of the coordinating copper atoms which was to be the observed case. In all the three compounds, the Cu – As distance vary depending on whether the arsenic in question is apical or basal. It is observed in all cases that the Cu - As_{apical} is shorter than Cu- As_{basal}. The diameter of the embedded cage molecule, the diameter of the cavity and the Cu -As distances are summarised in **Table 4.2.4**

Table 4.2.4: Cu-As distances, cage diameter and cavity diameter for $(CuI)_7(HgI_2)_3(As_4Se_3)$, $(CuI)_7(ZnI_2)_3(As_4Se_3)$ and $(CuI)_7(CdI_2)_3(As_4Se_3)$.

Entry	$(CuI)_7(ZnI_2)_3(As_4Se_3)$	$(CuI)_7(CdI_2)_3(As_4Se_3)$	$(CuI)_7(HgI_2)_3(As_4Se_3)$	Literature
Cu -As_{apical}	1.987 Å	1.795 Å	2.180 Å	2.410 Å[124]
Cu- As_{basal}	2.787 Å	2.872 Å	2.940 Å	2.410 Å[124]
Cu- Se	2.890 Å	2.659 Å	2.966 Å	2.506 Å[124]
cage diameter	4.38 Å	4.18 Å	4.23 Å	-
cavity diameter	7.272 Å	7.608 Å	9.721 Å	-

Thus, the exact structure of the intercalated cage molecule could not be completely elucidated with X-Ray diffraction methods. As stated earlier other spectroscopic methods, especially solid-state NMR would shed more light.

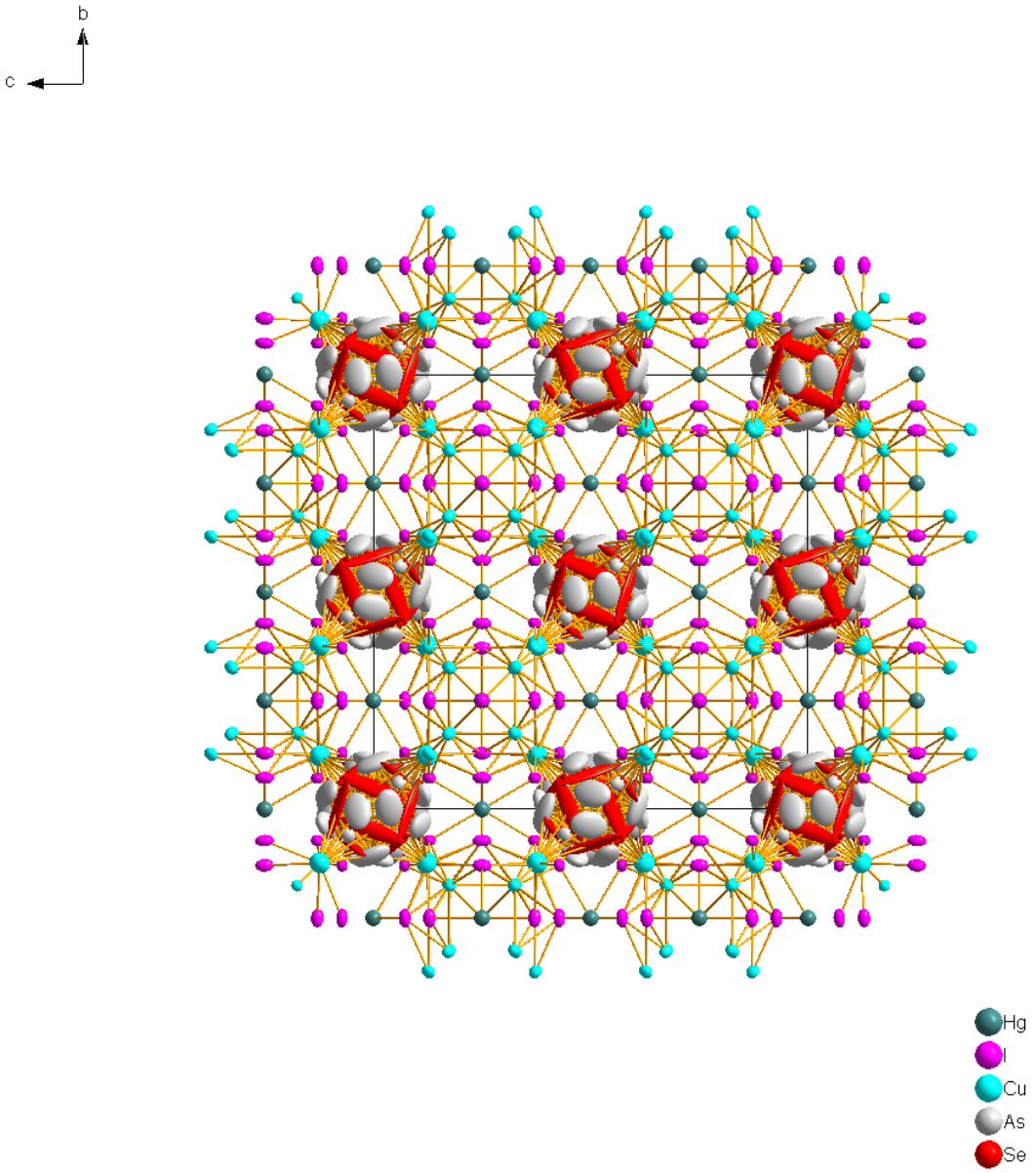

Figure 4.2.6: Disordered As_4Se_3 cages embedded in the Cu-I-Hg matrix shown in the unit cell.

4.2.3 SEM and EDX Analysis

Electron microscopic images were taken of all the crystals. Red, shiny crystals with proper habitus were carefully chosen and were separated under the light microscope under nitrogen atmosphere and glued to the carbon-coated carrier though EDX analysis was not successful for

all the three compounds. **Figure 4.2.7** shows a scanning electron microscopic image of a $(CuI)_7(CdI_2)_3(As_4Se_3)$ at a cathode voltage of 20 kV and **Table 4.2.5** shows the results.

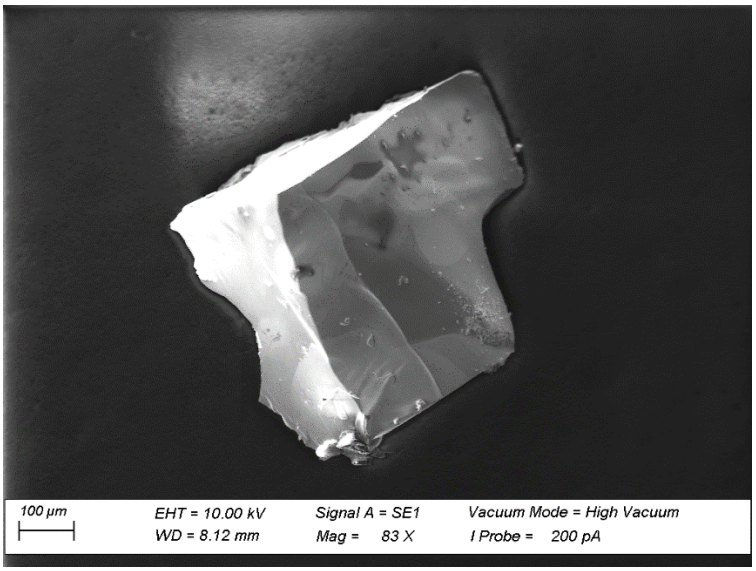

Figure 4.2.7: Electron microscopic image of a crystal of the adduct $(CuI)_7(CdI_2)_3(As_4Se_3)$ with an excitation voltage of 20kV.

Table 4.2.5: Result of energy dispersive X-ray spectroscopy and calculated proportions of arsenic, cadmium selenium, copper and iodine in the compound $(CuI)_7(CdI_2)_3(As_4Se_3)$.

Element	Cu	I	Cd	As	Se
Abs. Error/ %	1.6	4.01	0.90	0.90	0.85
Rel. Error/ %	8.68	8.62	10.04	9.74	10.30
EDX results/Atom%	23.73	41.45	9.04	13.99	11.79
Calculated Results/Atom %	23.33	43.33	10.00	13.33	10.00

Chapter 5

5.1 The compound $[(Hg_2I_6)\ (HgI_2)][Cu(MeCN)_4]_2$

5.1.1 Introduction

Since the breakthrough discovery of its use in opto-electronics in 1957, HgI_2 has been studied extensively[125]. It is quiet fascinating from a standpoint of crystallographic interest that HgI_2 displays such a plethora of different crystal structures. Until now at least seven different phases are known[126–128]. Out of these, three of them can be crystallized at room temperature from organic solvents. Normally Hg(II) in its corresponding halides takes on coordination number of either 2 or 4. This fact leads eventually HgI_2 having totally different crystal structures – a tetrahedral environment or molecular structures. The red (α) and orange form have HgI_4 tetrahedra corner linked into layers. Then we have the metastable yellow phase which is linear under ambient conditions and also the variation with bent I-Hg-I with shorter Hg-I contacts which is observed at high temperatures[127,129,130] [5-6]. Herein we report the title compound which contains both the red (α) and the metastable linear yellow form in the framework of a Cu – acetonitrile complex.

5.1.2 Synthesis

$[(Hg_2I_6)\ (HgI_2)][Cu(MeCN)_4]$was obtained by reacting α-HgI_2(0.264 g, 1 equiv) and CuI (0.235 g, 2 equiv) under solvothermal conditions. Toluene and acetonitrile (in 1:1 ratio; 1 mL each) were used as solvents. The educts and solvents were transferred in a Duran ampoule, evacuated, and heated under isothermal conditions for 5 days in a drying cabinet at 180 °C. The system was cooled to room temperature over 48 h. The ampoule was opened under nitrogen atmosphere. The contents were transferred to a Schlenk tube and stirred for two days ensuring enough solvent is present. Later the Schlenk tube was kept undisturbed for 4 months to get a few colourless crystals of $[(Hg_2I_6)\ (HgI_2)][Cu(MeCN)_4]$ which immediately turn red when separated from the solvent. Due to the sensitive nature of the compound only single crystal X ray diffraction experiment could be successfully carried out. Powder ray diffraction

experiment and electron microscopy were not successful as the compound readily decomposed.

5.1.3 Single Crystal Analysis

Table 5.1.1: Table gives an overview of the crystallographic data and measurement parameters of [(Hg_2I_6)(HgI_2)][$Cu(MeCN)_4$]$_2$.

Empirical Formula	$C_{16}H_{24}Cu_2Hg_3I_8N_8$
Formula weight	2072.48
Crystal colour and shape	Orange block
Crystal system	orthorhombic
Space group	*Fddd* (Nr. 70)
a/Å	11.003(5)
b/ Å	27.34(9)
c/ Å	27.68(9)
V/Å^3, *Z*	8330.1(5),8
Absorption coefficient(μ)/ mm^{-1}	9.706
ρ_{calc}/g/cm^3	3.305
Diffractometer	Rigaku Super Nova
Radiation, temperature	Ag Kα (λ = 0.0.560 Å), 100 K
Θ-range/°	4.724 – 71.596
hkl-range/°	-22 ≤ h ≤ 13
	-54 ≤ k ≤ 44
	-57 ≤ l ≤ 34
Absorption correction	numerical (gaussian, Scale3 Abspack)
Number of reflexes	48700
Independent reflections	9369
R_σ, R_{int}	0.0431, 0.0558
Completeness	100%
Structure solution	SHELXT
Structure refinement	SHELXT - 2014
Data/Restraints/Parameters	9369/0/89
GooF	1.130
R_1, wR_2 [$I>2\sigma(I)$]	0.0718, 0.1537
R_1, wR_2 [all reflexes]	0.125, 0.1802
Largest diff. peak/hole/e Å^{-3}	3.76/-2.71

$[(Hg_2I_6)\ (HgI_2)][Cu(MeCN)_4]_2$ crystallises in the space group *Fddd* (Nr. 70) with a = 11.003(5) Å, b = 27.34(9) Å, c = 27.68(9) Å, α = 90.00 ° β = 90 ° , γ = 90.00 ° , V = 8330.1(5) $Å^3$ and Z =8 (T = 100 K). The refinement of all data converged at a GooF of 1.130, with R_1 = 7.18 % and wR_2 = 15.37 %. The positions and isotropic displacement parameters can be found in Appendix in **Table A.42**. The anisotropic displacement parameters are listed in **Table A.43**. The bond lengths and bond angles can be found in **Table A.44** and **Table A.45**.

The structure consists of the two polymorphs residing together as neighbours separated by 3.64 Å. According to Hostettler et.al. the observed rate of crystallization of the different polymorphs of HgI_2 is a strongly a kinetic effect. Rapid crystallization of the solvent is imperative for the formation of the metastable yellow form. Thus, evaporation of the solvent in a closed vessel served to deliver only a sparing amount of metastable yellow form[127]. In view of this observation, it is quite surprising to see how both the forms crystallize together. Thus, this compound presents a rare example of tetrahedrally coordinated and the molecular species of HgI_2 coexisting in a single motif.

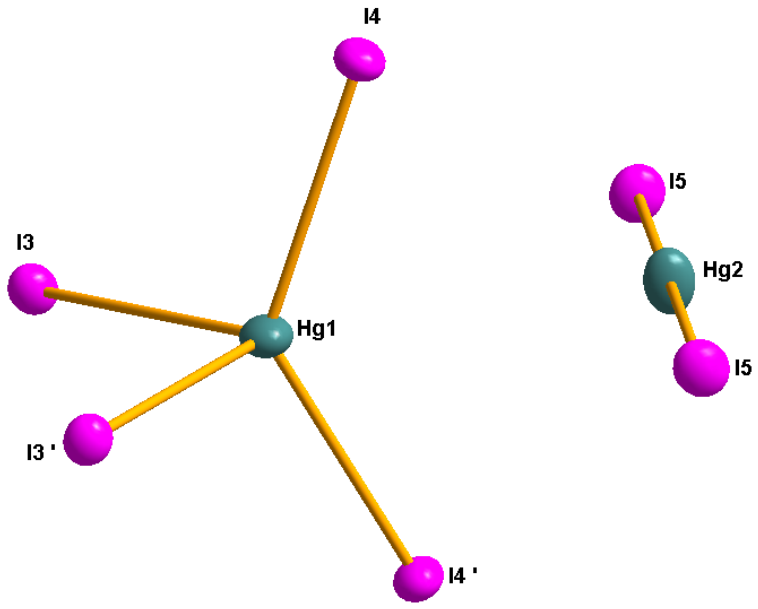

Figure 5.1.0-1: A section from the complete structure showing the two polymorphs separated by 3.64 Å. Mercury atoms are shown in turquoise while iodine atoms are depicted in pink. All atoms are shown with 50% ellipsoid probability.

This special coordination influences the bond lengths and bond angles when compared to α – HgI_2. The title compound has two crystallographically distinct iodine positions in the HgI_4 tetrahedron. Two iodine atoms (I4 and I4') (Refer **Figure 5.1.1**) are "terminal" while the other two (I3 and I3') are "bridging". Thus, two adjacent HgI_4 share two iodine atoms, completing the coordination sphere of the Hg atom. Further in α – HgI_2 all four Hg-I distances are 2.783 Å [6]. In the case of the title compound, we have distortion from this value and two sets of bond lengths corresponding to bridging or terminal iodine atoms are seen. *d*(Hg1-I4) and *d*(Hg1-I4') are 2.695 Å while *d*(Hg1-I3) and *d*(Hg1-I3') are 2.91 Å. The bond angles also see a deviation. All four tetrahedral bonds in HgI_4 tetrahedron sum up to 112.54 °. In the title compound all four angles are different. ∠(I3-Hg1-I4) = 105.18, ∠(I3'-Hg1-I4') = 105.30, ∠(I4-Hg1-I4') = 131.34 and ∠(I3-Hg1-I3') = 100.62. The crystal structure of the metastable yellow HgI_2 yielded by sublimation was determined by Jefrey and Vlasse[123]. The average Hg-I distance is 2.617 Å while the molecule is almost linear with I-Hg-I angle being 179.3(3) °. The present compound is completely linear with I-Hg-I angle being 179.99 °. The average Hg-I distance is 2.59 Å, slightly less than the yellow HgI_2.

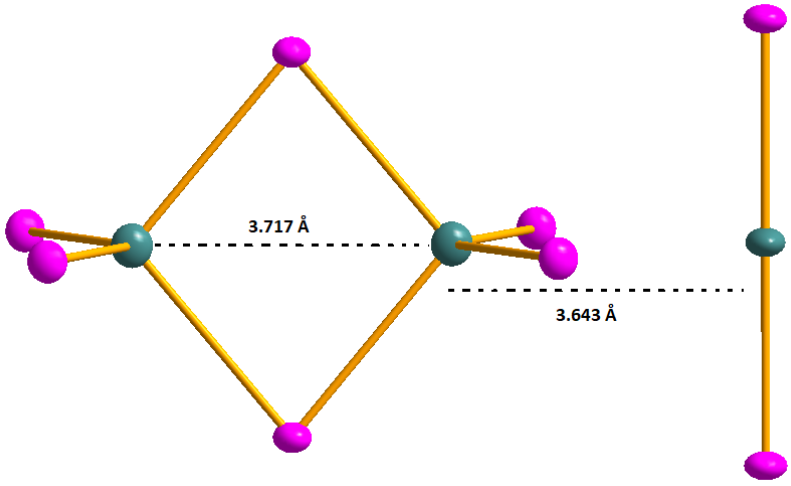

Figure 5.1.2: Hg_2I_6 and HgI_2 subunits as a part of the total crystal structure. Mercury atoms are shown in turquoise while iodine atoms are depicted in pink. All atoms are shown with 50% ellipsoid probability.

Figure 5.1.2 depicts the completely grown Hg_2I_6 unit with the bridging iodine atoms and the linear HgI_2 as a sub- unit of the complete crystal structure. The Hg-Hg distance bridged by the iodine atoms is 3.717 Å which is longer than the *d* (Hg1⋯Hg2) (Refer **Figure 5.1.2**:) which sums

up to 3.643 Å. It is noteworthy to observe that the mercury atoms from the red and the yellow polymorph are closer to each other than the mercury atoms in the red polymorph itself. The I-I distance is larger in the linear form when compared to the tetrahedral one with I3-I3' being 4.47 Å and I5-I5' being 5.19 Å. It is also noticeable that both Hg atoms lie in the same plane.

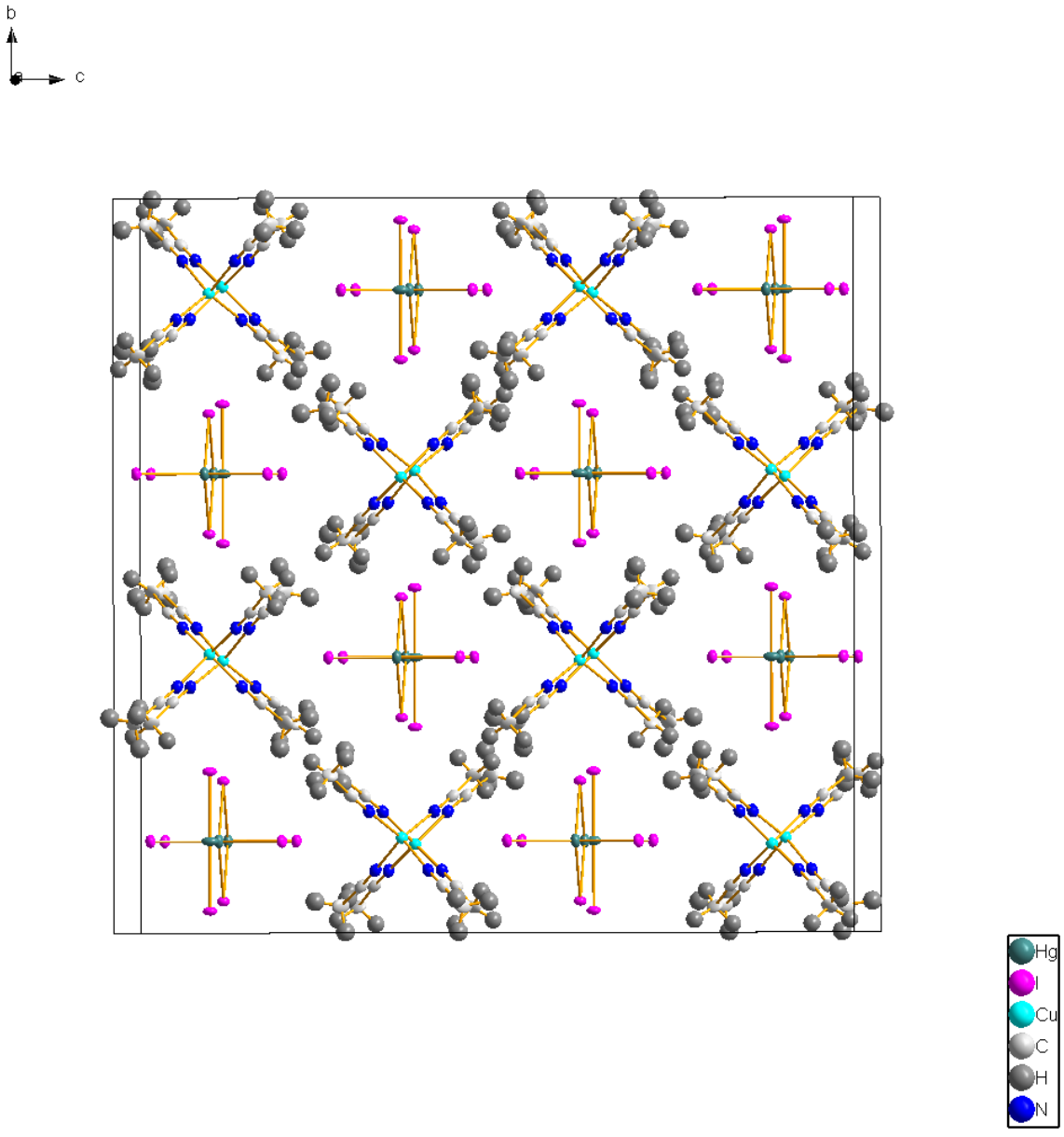

Figure 5.1.2: 3-D packing results in discrete mercuric iodide subunits flanked by Cu-MeCN network. All atoms are shown with 50% ellipsoid probability.

When the molecule is packed in 3 dimensions, one can see that the Hg_2I_6 and HgI_2 sub units are enclaved in the pockets created by the $Cu(MeCN)_4$ network (Refer **Figure 5.1.3**). Each

(Hg_2I_6) (HgI_2) moiety is discrete and is flanked by four $Cu(MeCN)_4$ sub units creating a pseudo host – guest type structure. It is a well-established fact that complexes of the type $[Cu(CH_3CN)_4]X$, X = BF_4−, PF_6−, ClO_4− serve as precursor in non-aqueous syntheses of Cu(I) complexes as the coordinated acetonitrile ligands are easily displaced in other solvents[131–134]. In the title compound we have tetrahedral Cu(I) coordinated to four acetonitrile ligands, much in the same fashion as the traditional compounds. Hg_2I_6 provides the necessary negative charges, making the overall complex neutral. Thus, the title compound serves to extend the scope of the $[Cu(CH_3CN)_4]X$ type compounds.

5.2 The compound Cu_2AsS_2I

As mentioned in Introduction and Chapter 1, the coordination of transition metal halides to arseno-chalcogenide cage molecules often leads to cage degradation or further fragmentation. All adduct compounds synthesised and characterised in the present work all contain an intact arseno-chalcogenide cage. Solvothermal method was the favoured synthesis route for having good quality crystals suitable for single crystal X-ray diffraction experiment, albeit only few crystals were harvested each time. In order to get a phase pure product in reasonable quantity, synthesis of all reactions was also tried using the conventional solid-state route. The major challenge at this junction was the optimisation of temperature. Reactions were carried out with a temperature increase of 10 °C and monitored by powder X-ray diffraction experiment and thermal analysis (DTA) to check the purity so as to know exactly at what temperature a phase pure product will be obtained. This approach was successful for the adduct compound $(AgI)_2{\cdot}(As_4S_4)$ and $(AgBr){\cdot}(As_4S_4)$ for which the temperatures were found to be 220 °C and 210 °C respectively. In a similar attempt for the phase pure synthesis of $(CuI)_3{\cdot}(As_4S_4)$ when the educts were tempered at 170 °C, instead of the desired product, an unexpected compound Cu_2AsS_2I was isolated which is the result of the cage decomposition.

5.2.1 Synthesis

CuI (0.285 g, 3 equiv) and As_4S_4 (0.214 g, 1 equiv) at 170 °C for 2 weeks. The educts were weighed, transferred in a quartz ampoule, evacuated, sealed, and then rested in oven. The heating rate was 1.5 °C/min, while the cooling rate was 0.5 °C/min. The resulting product was fine red powder with block type red crystals which were air stable for few weeks. Further, these crystals were analysed using single crystal X-ray diffraction experiment and REM/EDX.

5.2.2 Single Crystal X-ray Diffraction

Table 5.2.1: Table gives an overview of the crystallographic data and measurement parameters of Cu_2AsS_2I.

Empirical Formula	Cu_2AsS_2I
Formula weight	786.04
Crystal colour and shape	Red block
Crystal system	monoclinic
Space group	$P2_1$ (Nr. 4)
a/Å	7.23(8)
b/ Å	4.68(6)
c/ Å	8.15(2)
α/°	90
β/°	103.27
γ/°	90
V/Å^3, *Z*	269.07, 2
Absorption coefficient(μ)/ mm^{-1}	20.34
ρ_{calc}/g/cm^3	4.85
Diffractometer	Rigaku Super Nova
Radiation, temperature	Mo Kα (λ = 0.71073 Å), 123 K
Θ-range/°	5.78 – 75.05
hkl-range/°	-12 ≤ h ≤ 12
	-4 ≤ k ≤ 7
	-13 ≤ l ≤ 13
Absorption correction	numerical (gaussian, Scale3 Abspack)
Number of reflexes	7170
Independent reflections	2308
R_σ, R_{int}	0.0354, 0.0326
Completeness	96 %
Structure solution	SHELXT

Structure refinement	SHELXT - 2014
Data/Restraints/Parameters	2308/1/55
GooF	1.050
R_1, wR_2 *[I>2σ(I)]*	0.0290, 0.0663
R_1, wR_2 *[all reflexes]*	0.0304, 0.0675
Largest diff. peak/hole/e Å^{-3}	2.32/-2.53

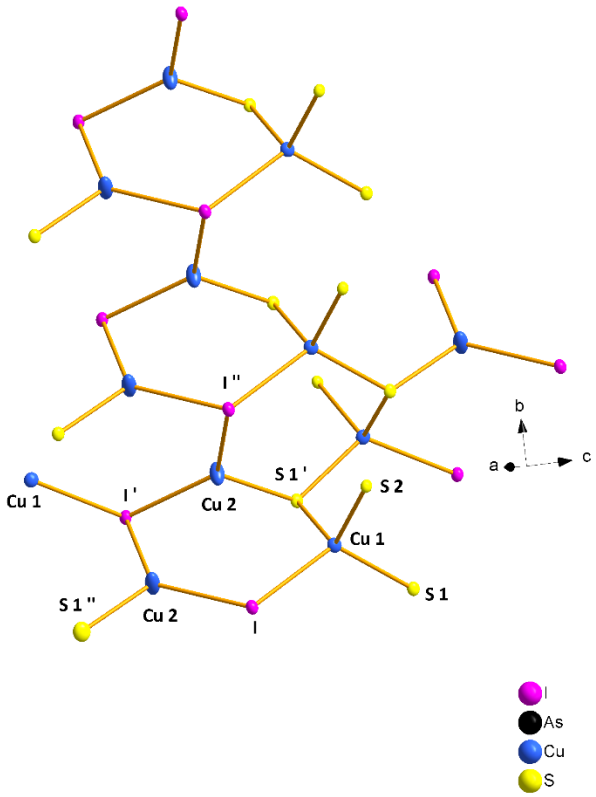

Figure 5.2.1: A section of the complete crystal structure of the compound Cu_2AsS_2I. Arsenic atoms are not shown for the sake of simplicity. All atoms are shown with 60% ellipsoid probability.

The positions and isotropic displacement parameters can be found in Appendix in **Table A.46**. The anisotropic displacement parameters are listed in **Table A.47**. The bond lengths and bond angles can be found in **Table A.48** and **Table A.49**. **Figure 5.2.1** depicts a part of the complete crystal structure of the compound Cu_2AsS_2I. The structure can be best described as chair- like half step wherein CuI serves as a linker between an infinite one-dimensional chain consisting

of sulphur, arsenic and copper. The structure consists of two types of neighbouring six membered rings, viz- Ring 1 consisting of Cu_3I_2S and Ring 2 consisting of Cu_3IS_2 (See **Figure 5.2.1**). Ring 1 creates a stacking sequence in the (010) direction whilst Ring 2 is stacked in between two such rings sharing a common face. As mentioned in **Section 3.1**, copper(I) halides are known for their flexibility and can take on a range of different coordination. In the compound under consideration, Cu1 shows a tetrahedral coordination with four neighbours while Cu2 with three neighbours, adopts a trigonal coordination.

Table 5.2.2: Bond angles for Cu1(tetrahedral coordination) and Cu2(trigonal coordination).

Bond	Bond Angle/ °
S2-Cu1-S1	107.05
S1-Cu1-I	120.35
S1'-Cu1-I	107.22
S2-Cu1-S1'	115.77
I'-Cu2-I	127.97
S1'-Cu2-I	114.51
S1''-Cu2-I'	117.39

Table 5.2.3: Selected bond lengths for the compound Cu_2AsS_2I.

Bond	Bond length / Å
Cu1-S2	2.299
Cu1-S1	2.309
Cu1-I	2.661
Cu1-S1'	2.281
Cu2-S1'	2.251
Cu2-I'	2.556
Cu2-I''	2.536

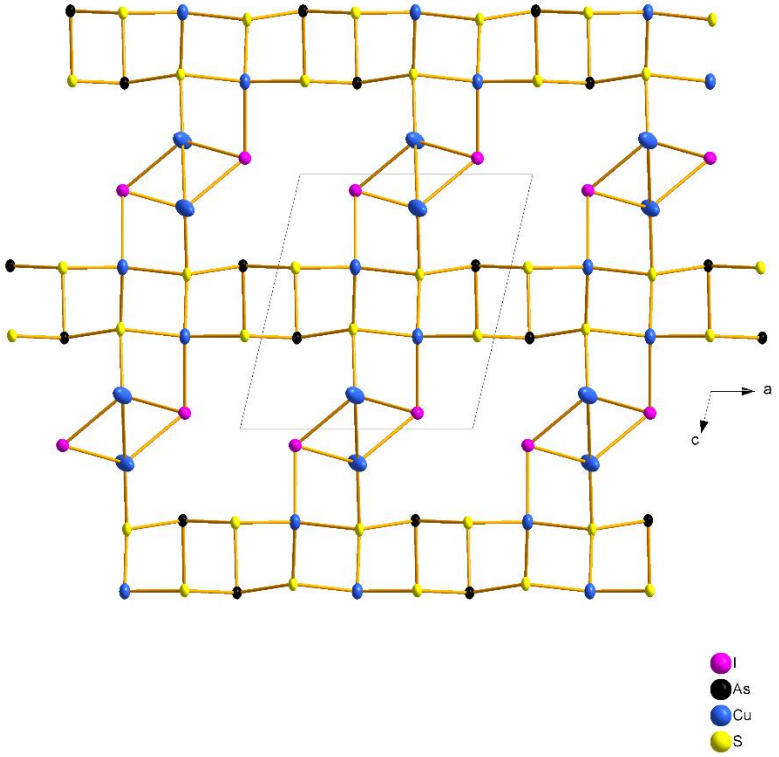

Figure 5.2.2: A section of the crystal structure Cu_2AsS_2I as seen along the b axis. Infinite 1-D As-S-Cu 'rods' run along the a axis which are connected to each other by $[Cu_2I_2]$ dimers.

Figure 5.2.2 depicts a part of the crystal structure of Cu_2AsS_2I along b axis. It is seen that an infinite 1-D chain/rods of As-S-Cu which run parallel to the a axis are connected to each other through $[Cu_2I_2]$ dimers. The distance between the copper atoms in these dimers *d*(Cu2-Cu2) amounts to 3.149 Å. This is large enough distance and any d^{10}- d^{10} cuprophilic interactions can be excluded. $[Cu_2I_2]$ dimers are separated from each other by 4.28 Å[135,136].The shortest possible distance between any two As-S-Cu layers is *d*(S-S) amounting to 6.279 Å.

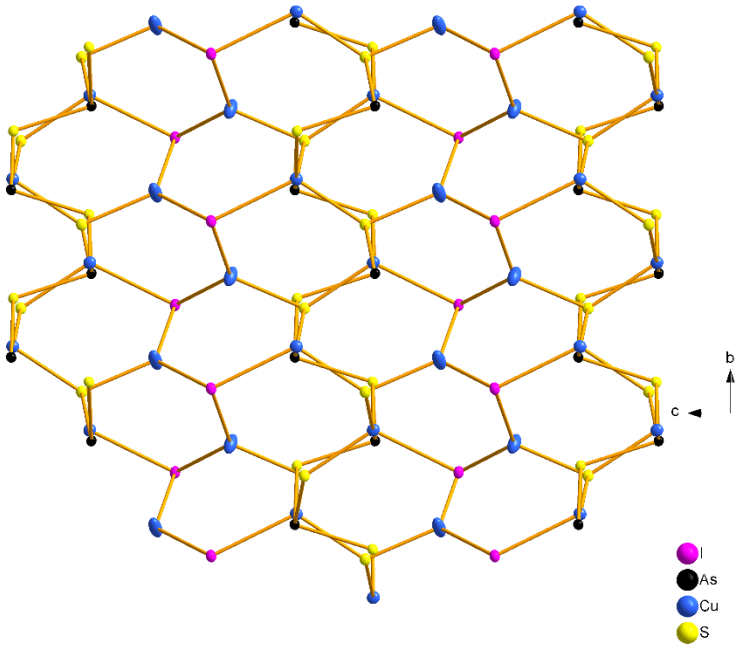

Figure 5.2.3: A section of the crystal structure of Cu_2AsS_2I as seen along the a axis. The six membered rings are seen to overlap giving rise to a beehive like motif.

5.2.3 SEM and EDX Analysis

For the scanning electron microscopic investigations and the EDX analysis, one of the shiny red blocks contained in the batch was separated under the light microscope and glued to the carbon-coated carrier. It must be noted here that only few crystals of the desired product were found in each reaction batch. **Figure 5.2.4** shows a scanning electron microscopic image of a Cu_2AsS_2I at a cathode voltage of 20 kV and **Table 5.2.4** shows the results.

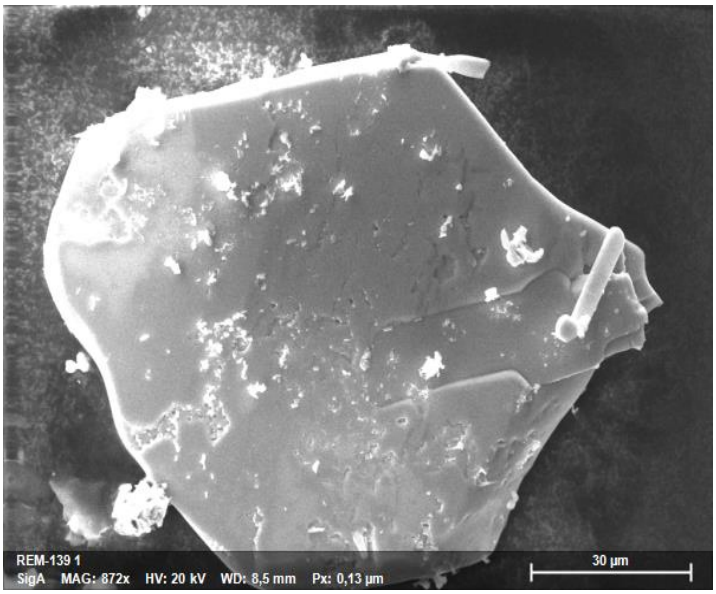

Figure 5.2.4: Electron microscopic image of a crystal of the adduct Cu_2AsS_2I with an excitation voltage of 20kV.

Table 5.2.4: Result of energy dispersive X-ray spectroscopy and calculated proportions of arsenic, sulphur, copper and iodine in the compound Cu_2AsS_2I.

Element	As	S	Cu	I
Abs. Error/ %	1.49	1.71	2.45	2.65
Rel. Error/ %	9.93	11.25	8.33	8.73
EDX results/Atom%	15.98	34.15	33.29	17.21
Calculated Results/Atom %	16.66	33.33	33.33	16.66

6. Summary and Outlook

In the present work we were able to synthesise adduct compounds of late transition metal halides with arseno - chalcogenide cages (As_4Q_n, *Q* = S / Se ; n = 3/4) taking this chemistry one step further. In contrast to the common observation of the degradation or decomposition of the cage compounds once bound to the metal halide matrix, here in all the compounds, the As_4Q_n cages remained intact. Further for the first time adduct compounds of silver halides with arseno - chalcogenide cages were successfully synthesised and characterised. Albeit phase pure synthesis for all the compounds still remains a synthetic challenge. With hydrothermal synthesis it was possible to produce crystals of suitable quality for single crystal X-ray diffraction analysis. Phase pure synthesis via high temperature solid state route was employed resulting in optimisation of reaction temperature for the adduct compounds $(AgI)_2{\cdot}(As_4S_4)$ and $(AgBr){\cdot}(As_4S_4)$. The aforementioned adduct compounds present a rare case of Ag-As coordination, indicating the fact that silver necessarily does not have any preference towards sulphur/selenium and arsenic. Exploration in this direction gave a further impetus to study As_4S_4 as neutral ligand. The major challenge remains the phase pure synthesis of the adduct compounds. Again, light needs to shed on as to why $(AgI)_2{\cdot}(As_4S_4)$ has a stoichiometry 1:2, while $(AgBr){\cdot}(As_4S_4)$ and $(AgCl){\cdot}(As_4S_4)$ have 1:1. Further, population analysis would prove fruitful in investigating the strengthening of As-As bond in the cages, albeit very meagre. A logical step forward would be the synthesis of analogous Au(I) compounds. Herein one has to be careful as Au(I)*X* are highly susceptible to oxidation or decomposition. It would also be interesting in the future to evaluate the reactivity of As_4Se_x with AgBr and AgCl.

In the next part of the work, new inclusion compounds were synthesised. In these compounds the highly disordered pnictogen chalcogenide cages ($As_4Se_3/_4$) are embedded in a $(ICu_4)@I_{12}$ matrix which is connected through HgI_4 tetrahedra. Together with other very similar compounds - $(CuI)_7(HgI_2)_3(Pn_4S_x)$ (*Pn* = P, As) and $Cd_7I_{12}S{\cdot}(As_4S_x)$ it was possible to develop a reasonable formula and a structural model which also fits in the general scheme of the nature of these compounds. The formula must be verified in further works in order to get a general notation. In view of this, it is reasonable to synthesise mixed halide inclusion compounds in the future, for example $(CuBr)_7(MI_2)_3(As_4Q_n)$, where M = Zn/Cd/Hg, *Q* = S/Se, n = 3/4. Due to the very similar electron density of arsenic and selenium, these atoms could not be

determined by X - ray diffraction. Further NMR studies would be instrumental in more detailed structural elucidation.

According to the literature survey, it is observed that we have adduct compounds with metals on the left-hand side of the periodic table, for example, with Ti, W, Ta and also with that on the right, for example, with Cu, Ag and Hg. It would be highly interesting to see whether we can develop adduct compounds of metals which lie in the middle, for example, Fe, Ni or Co.

7. References

(1) Rao, C. N. R.; Gopalakrishnan, J. *New Directions in Solid State Chemistry*, 2nd ed.; Cambridge University Press, **1997**.

(2) M. Jansen, *Angew. Chem. Int. Ed.* **2002**, *41 (20)*, 3746–3766.

(3) M. Jansen, *Angew. Chem*. **2002**, *114 (20)*, 3896–3917, German Edition.

(4) A. Rabenau, Angew. Chem. Int. Ed. **1985**, *24 (12)*, 1026–1040.

(5) H. Schäfer, *Chemical Transport Reactions*; Elsevier, **2016**.

(6) J.B.Wiley, R.B.Kaner, *Science* **1992**, *255 (5048)*, 1093–1097.

(7) W. Milius, A. Rabenau, *Mat. Res. Bull.***1987**, *22 (11)*, 1493–1497.

(8) M.H.Möller, W. Jeitschko, *J.Solid State Chem.* **1986**, *65 (2)*, 178–189.

(9) A. Pfitzner, E. Freudenthaler, *Angew. Chem. Int. Ed.* **1995**, *34 (15)*, 1647–1649.

(10) A.Pfitzner, E. Freudenthaler, *Z. Naturforsch. B* **1997**, *52 (2)*, 199–202.

(11) A. Pfitzner, S. Reiser, *Inorg. Chem.* **1999**, *38 (10)*, 2451–2454.

(12) A. Pfitzner, S. Reiser, T. Nilges, *Angew. Chem. Int. Ed.* **2000**, *39 (22)*, 4160–4162.

(13) S. Nilges, T. Nilges, H. Haeuseler, A. Pfitzner, *J. Mol. Struct.* **2004**, *706 (1-3)*, 89–94.

(14) M. Bräu, *Dissertation,* Universität Regensburg, **2008**.

(15) T. Rödl, *Dissertation*, Universität Regensburg, **2013**.

(16) R. G. Pearson, *J. Am. Chem. Soc.* **1963**, *85 (22)*, 3533–3539.

(17) J. J. O'Connor, A.F. Armington, *Mat. Res. Bull.* **1971**, *6 (8)*, 765–769.

(18) C. Vitzthumecker, *Dissertation,* Universität Regensburg, **2019**.

(19) STOE -WinXPOW, *Vol.Version 3.0.2.5*, STOE & Cie GmbH, Darmstadt, **2011**.

(20) Crysalis-Pro, *Vol.Version 1.171.40.14a,* Rigaku Oxford Diffraction, **2018**.

(21) O. V. Dolomanov, L. J. Bourhis, R. J.Gildea, J. A. K . Howard, H. Puschmann, *J. Appl. Cryst.* **2009**, *42 (2)*, 339–341.

(22) G. M. Sheldrick, *Acta Crystallogr. A*, **2015**, *71 (Pt 1)*, 3–8.

(23) G. M. Sheldrick, *Acta Crystallogr. A*, **2008**, *64 (Pt 1)*, 112-122.

(24) V. Petricek, M. Dusek, L. Palatinus, *Z. Kristallogr.* **2014**, *229*, 345.

(25) A. L. Spek, *J Appl Cryst*, **2003**, *36 (1)*, 7–13.

(26) V. Diamond, *Crystal Impact GbR*, Bonn, **2017**.

(27) OMNIC™ Specta Software, *V.OMNIC 9*, Thermo Fisher Scientific, Waltham, **2012**.

(28) V. OMEGA, Bruins Instruments, Puchheim, **2004**.

(29) P. Kubelka, F. Munk, *Z. Techn. Phys.***1931**, *12*, 593 -601.

(30) ZEISS - Smart SEM, Ver. 6.05, Ed **2018**.

(31) BRUKER - Quantax - Esprit, Ver. 2.1.1.17832, Ed **2018**.

(32) Zahner Meßtechnik GmbH & Co, Ver. Z.3.03, Thales Flink, Kronach, **2015**.

(33) S. Huber, *Dissertation*, Universität Regensburg, **2017**.

(34) C. De-Giorgi, *Dissertation*, Universität Regensburg, **2021**.

(35) A. Pfitzner, *Chem. Eur. J.* **2000**, *6 (11)*, 1891–1898.

(36) A. Pfitzner, *Habilitationsschrift*, Universität Siegen, 2000

(37) J. Wachter, *Coord. Chem. Rev.* **2010**, *254 (17-18),* 2078–2085.

(38) P. Schwarz, J. Wachter, M. Zabel, *Eur. J. Inorg. Chem*. **2008**, *35*, 5460–5463.

(39) A. Biegerl, C. Gröger, H. R. Kalbitzer, J.Wachter, M. Zabel, *Zeit. Anorganische und Allg. Chemie*, **2010**, *636 (5)*, 770–774.

(40) A. Biegerl, E. Brunner, C. Gröger, M. Scheer, J. Wachter, M. Zabel, *Chem. Eur. J*. **2007**, 1*3 (33)*, 9270–9276.

(41) A. Biegerl, C. Gröger, H. R. Kalbitzer, A. Pfitzner, J. Wachter, R. Weihrich, M. Zabel, *Jour. Solid State Chem.* **2011**, *184 (7)*, 1719–1725.

(42) A. Pfitzner, S. Reiser, H-J. Deiseroth, *Zeit. Anorg und allg. Chemie*, **1999,** *625 (12)*, 2196–2201.

(43) A. Biegerl, D. Piryazev, M. Scheer, J. Wachter, A. Virovets, M. Zabel, *Eur. J. Inorg. Chem.* **2011**, *27*, 4248–4255.

(44) S. Reiser, T. Nilges, A. Pfitzner, *Zeit. Anorg und allg. Chemie,* **2003**, *629 (3)*, 563–568.

(45) S. Reiser, G. Brunklaus, J.H. Hong, J. C. C Chan, H. Eckert, A. Pfitzner, *Chem. Eur. J*. **2002**, *8 (18)*, 4228–4233.

(46) A. Pfitzner, S. Reiser, *Inorg. Chem.* **1999**, *38 (10)*, 2451–2454.

(47) A. Pfitzner; S. Reiser, H-J. Deiseroth, *Zeit. Anorg und allg. Chemie,* **1999**, *625 (12)*, 2196–2201.

(48) J. Wachter, *Angew. Chem. Int. Ed.* **1998**, *37 (6)*, 750–768.

(49) T. Bernert, Z. Kristallogr. – *Cryst. Mater*. *5398 (1)*, 20–26.

(50) S. Weinbaum. Z. Kristallogr. – *Cryst. Mater*. **1934**, *(1-6)*, 48–53.

(51) D. C . Craig, N. C. Stephenson, *Acta Cryst.* **1965**, *19 (4)*, 543–547.

(52) A.Müller, R. Blachnik, *Z. anorg. allg. Chem,* **2003**, *629 (10)*, 1833–1838.

(53) A. Pfitzner. Z. Kristallogr. – *Cryst. Mater*. *9142* (2-3), 281–294.

(54) W. F Kuhs, R. Nitsche, K. Scheunemann, *Mat. Res. Bull*. **1979**, *14 (2)*, 241–248.

(55) M. F. Bräu, A. Pfitzner, *Angew. Chem.International ed*. **2006**, *45 (27)*, 4464–4467.

(56) M. F. Bräu, A. Pfitzner, *Z. anorg. allg. Chem,* **2007,** *633 (7)*, 935–937.

(57) A. Biegerl, *Dissertation*, Universität Regensburg, **2011**.

(58) P. Schwarz, *Dissertation*, Universität Regensburg, **2011**.

(59) T.Rödl, A. Pfitzner, *Z. anorg. allg. Chem.* **2010**, *636 (11*), 2052.

(60) E. Freundenthaler, Solid State Ion. **1997**, *101-103*, 1053–1059.

(61) A. Pfitzner, E. Freundenthaler, *Z. Kristallogr. – Cryst. Mater.* **1995**, *210 (1)*, 59.

(62) A. Pfitzner, E. Freundenthaler, *Z. Kristallogr. – Cryst. Mater.* **1997**, *212 (2)*, 103–109.

(63) W. Milius, *Z. anorg. allg. Chem.* **1990**, *586 (1)*, 175–184.

(64) U.v.Alpen, J. Fenner,A. Rabenau, B. Predel, G. Schluckebier, *Z. Anorg. Allg. Chem* **1978**, *438* , 5-14.

(65) J. Fenner, A. Rabenau, *Z. Anorg. Allg. Chem* **1976**, *426 (1)*, 7–14.

(66) J. Fenner, H. Schulz, *Acta Crystallogr B Struct Crystallogr Cryst Chem* **1979**, *35 (2)*, 307–311.

(67) R. Bachmann, K. D. Kreuer, A. Rabenau, H. Schulz, *Acta Cryst B* **1982**, *38 (9)*, 2361–2364.

(68) T. Sakuma, T. Kaneko, H. Takahashi, K.T. Honma, *J. Phys. Soc. Jpn.* **1991**, *60 (3)*, 1136–1137.

(69) T. Sakuma, T. Kaneko, *J. Phys. Soc. Jpn.* **1991**, *60 (9)*, 3188–3189.

(70) W. Milius; A. Rabenau. *Z. Naturforsch. B, 219 (2)*, 243–244.

(71) A. Pfitzner, T. Nilges, H.-J Deiseroth, *Z. Anorg. Allg. Chem* **1999**, *625 (2)*, 201–206.

(72) W. Milius. *Z. Naturforsch. B, 822 (8)*, 990–992.

(73) J. Fenner, *Acta Cryst B*, **1976**, *32 (11)*, 3084–3086.

(74) A. Pfitzner, S. Zimmerer, Z. *Anorg. Allg. Chem* **1996**, *622 (5)*, 853–857.

(75) A. Pfitzner, S. Zimmerer, Z. *Anorg. Allg. Chem* **1995**, *621 (6)*, 969–974.

(76) H. M Haendler, P. M. Carkner, *J. Solid State Chem.* **1979**, *29 (1)*, 35–39.

(77) T. Sakuma, T. Kaneko, T. Kurita, H. Takahashi, *J. Phys. Soc. Jpn.* **1991**, *60 (5)*, 1608–1611.

(78) A. Pfitzner, S. Zimmerer, *Z. Kristallogr. – Cryst. Mater.***1997**, *212 (3)*, 203–207.

(79) A. Pfitzner, S. Zimmerer, *Angew. Chem. Int. Ed.* **1997**, *36 (9)*, 982–984.

(80) A. Pfitzner, *Chem. Eur. J.* **1997**, *3 (12)*, 2032–2038.

(81) A. Pfitzner, *Inorg. Chem.* **1998**, *37 (20)*, 5164–5167.

(82) A. Pfitzner; F. Baumann, W.Kaim, *Angew. Chem. Int. Ed*. **1998**, *37 (13-14)*, 1955–1957.

(83) A. Pfitzner, S. Reiser, *Inorg.Chem*. **1999**, *38(10)*, 2451-2454.

(84) S. Reiser, G. Brunklaus, J. H Hong, J. C. C Chan, H. Eckert, A. Pfitzner *Chem. Eur. J.* **2002**, *8 (18)*, 4228–4233.

(85) S. Reiser, T. Nilges, A. Pfitzner, Z. *Anorg. Allg. Chem,* **2003**, *629*, 563-568.

(86) A. Pfitzner; S. Reiser, H.-J Deiseroth Z. *Anorg. Allg. Chem* ,**1999**, *625 (12)*, 2196–2201.

(87) A. Pfitzner; S. Reiser, T. Nilges. *Angew. Chem. Int. Ed*. **2000**, *39 (22)*, 4160–4162.

(88) S. Nilges, T. Nilges, H. Haeuseler, A. Pfitzner *J. Mol. Structure*. **2004**, *706 (1-3)*, 89–94.

(89) A. Biegerl, C. Gröger, H. R. Kalbitzer, A. Pfitzner, J. Wachter, R. Weihrich, M. Zabel, *J.Solid State Chem.* **2011**, *184 (7)*, 1719–1725.

(90) A. Biegerl, C. Gröger, H. R. Kalbitzer, J. Wachter, M. Zabel, *Z. Anorg. Allg. Chem*. **2010**, *636 (5)*, 770–774.

(91) A. Biegerl.; E. Brunner, C. Gröger, M. Scheer, J. Wachter, M. Zabel. *Chem. Eur. J*. **2007**, *13 (33),* 9270–9276.

(92) M.Sehr, *Masterarbeit*, Universität Regensburg, **2017**.

(93) D. Hoppe, *Dissertation*, Universität Regensburg, **2009**.

(94) H. Nowottnick, K. Stumpf, R. Blachnik, H. Reuter, Z. *Anorg. Allg. Chem* **1999,** *625 (4)*, 693–697.

(95) H. J . Whitfield J. *Chem. Soc.*, A. **1970**,1800 -1803.

(96) H. J. Whitfield. *J. Chem. Soc., Dalton Trans.* **1973**, *17*, 1737–1738.

(97) A. Gavezzotti, F. Demartin,C. Castellano,I. Campostrini. *Phys Chem Minerals*. **2013**, *40 (2)*, 175–182.

(98) T. Ito, N. Morimoto, R. Sadanaga *Acta Cryst.* **1952**, *5 (6)*, 775–782.

(99) E.J.Porter,G.M. Sheldrick. *J. Chem. Soc., Dalton Trans.* **1972**, *13*, 1347-1349

(100) Kyono, *Am Min*. **2005**, *90 (10)*, 1563–1570.

(101) P. Bonazzi, S. Menchetti, G. Pratesi. *Am Min*. **1995**, *80 (3-4)*, 400–403.

(102) H. J Whitfield. *J. Chem. Soc., Dalton Trans.* **1973**, *17*, 1740.

(103) L. Bindi, V. Popova, P. Bonazzi. *The Canad. Minerl.* **2003**, *41 (6)*, 1463–1468.

(104) P. Bonazzi.; L. Bindi.; V. Popova.; G. Pratesi, S. Menchetti. *Am Min*. **2003**, *88 (11-12)*, 1796–1800.

(105) T. Nilges.; S. Reiser, J. H Hong, E.Gaudin, A. Pfitzner, *Phys. Chem. Chem. Phys.* **2002**, *4 (23)*, 5888–5894.

(106) A. Pfitzner, *Chem. Eur. J.* **1997**, *3 (12)*, 2032–2038.

(107) H.-J. Deiseroth, M. Wagener, E. Neumann, E. *Eur. J. Inorg. Chem.* **2004,** *2004 (24)*, 4755–4758.

(108) P. Weis, D. Kratzert, I. Krossing, *Eur. J. Inorg. Chem.* **2018**, *27*, 3203–3212.

(109) P. Weis, *Dissertation*, Universität Freiburg, **2019.**

(110) T. J Bastow, H. J .Whitfield, J. *Chem. Soc., Dalton Trans*. **1977,** *10,* 959.

(111) A. F.Holleman,E. Wiberg, *Lehrbuch der Anorganischen Chemie*, 91.–100. Aufl. Reprint 2019; De Gruyter, **1985**.

(112) B.Bogdanov, B. Georgiev, K. Angelova, K. Yaneva, *Natural & Mathematical Science*,International Science Conference,Stara Zagora, Bulgaria, **2009**.

(113) K. L Moran, T. E Gier, W. T. A Harrison, G. D. Stucky, H Eckert, K. Eichele, R. E Wasylishen. *J. Am. Chem. Soc*. **1993**, *115 (23)*, 10553–10558.

(114) R. Burnus, G. Meyer, *Z. Anorg. Allg. Chem.* **1991**, *602 (1)*, 31–37.

(115) J. H. Hong, *Dissertation*, Universität Regensburg, **2004**

(116) I. Chatti, A.Delahaye,L. Fournaison, J.-P. B Petitet. *Energy Convers. Manag.* **2005**, *46 (9-10)*, 1333–1343.

(117) L. Mandelcorn, *Clathrates. Chem. Rev.* **1959,** *59 (5)*, 827–839.

(118) F.Kubel, *Ferroelectrics*. **1994**, *160*, 61-65.

(119) G. Berset, W.Depmeier,R. Boutellier, H. Schmid, *Acta Cryst* **1985,** *C41* 1694-1696.

(120) R. J Nelmes, F. R Thornley, *J. Phys. C: Solid State Phys.* **1974**, *7 (21)*, 3855–3874.

(121) O. Crottaz, F. Kubel, H.Schmid, J.Solid State Chem. **1995**, *120 (1)*, 60–63.

(122) S. Maderlehner, *Dissertation*, Universität Regensburg, **2015.**

(123) G. A. Jeffrey, M. Vlasse, *Inorg. Chem.* **1967**, *6 (2)*, 396–399.

(124) M.Oliveria, *Solid State Ion.* **1988**, *28-30*, 1332–1337.

(125) R. H Bube, *Phys. Rev.* **1957**, *106 (4)*, 703–717.

(126) G. A. Jeffrey, M. Vlasse, *Inorg. Chem.* **1967**, *6 (2)*, 396–399.

(127) M Hostettler, H. Birkedal, *Chimia*, **2001**, *55 (6)*, 541 -545.

(128) M. Hostettler, H. Birkedal, D. Schwarzenbach, *Acta crystallogr. Sec B, Struct Sci* **2002**, *58 (6)*, 903–913. (129)

(130) M. Hostettler, H. Birkedal, D. Schwarzenbach, *Helv.Chim.Acta ,* **2003**, *86 (5)*, 1410–1422

(131) J. R Black, W. Levason, M. Webster, *Acta Cryst C,* **1995**, *51 (4)*, 623–625.

(132) H. H. Morgan, *J. Chem. Soc., Trans.* **1923**, *123*, 2901–2907.

(133) E. J Parish, H.Qin, B. H. Lipshutz, C.T .Lee, *Encyclopedia of reagents for organic synthesis*; Paquette, L. A., Ed.; Wiley, **1995**

(134) H.-G. Huang, W. Li, D. Zhong, H.-C. Wang, J. Zhao, W.-B. Liu, *Chemical Science*, **2021**, *12 (9)*, 3210–3215.

(135) N. V. S. Harisomayajula,S. Makovetskyi, Y.-C Tsai, *Chem. Eur. J.* **2019**, *25 (38)*, 8936–8954.

(136) S. Sculfort, P. Braunstein, *Chem. Soc. Rev*. **2011**, *40 (5)*, 2741–2760.

8. Appendix

Photos of mounted crystals for single crystal diffraction experiment

$(AgI)_2 \cdot (As_4S_4)$

$(AgI)_2 \cdot (As_4Se_4)$

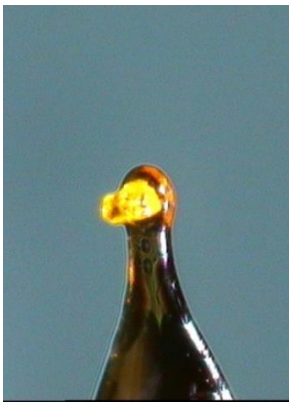

$(AgBr) \cdot (As_4S_4)$

$(AgCl) \cdot (As_4S_4)$

$(CuI)_3 \cdot (As_4S_4)$

$(CuBr)_2 \cdot (As_4S_4)$

$(CuBr)_2 \cdot (As_4Se_3)$

$(CuI)_7(ZnI_2)_3(As_4Se_3)$

$(CuI)_7(CdI_2)_3(As_4Se_3)$

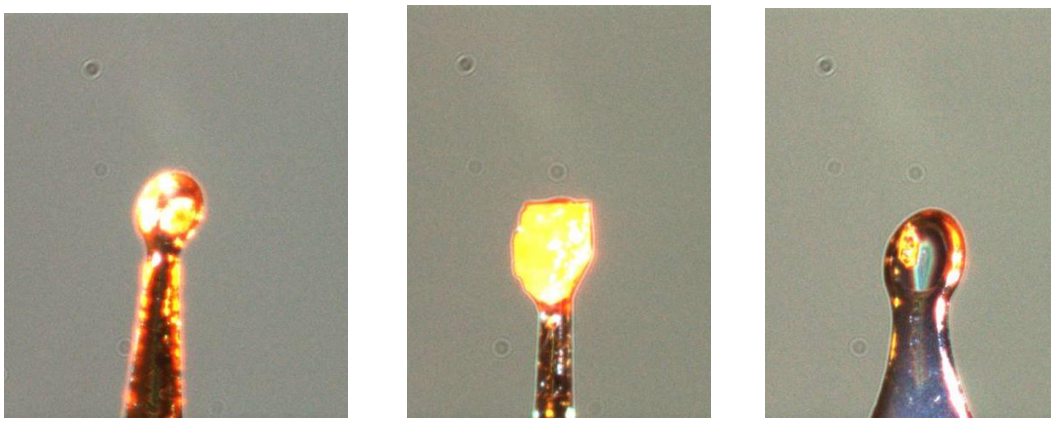

$(CuI)_7(HgI_2)_3(As_4Se_3)$ $[(Hg_2I_6)\ (HgI_2)][Cu(MeCN)_4]$ $As_2Cu_2I_2S_4$

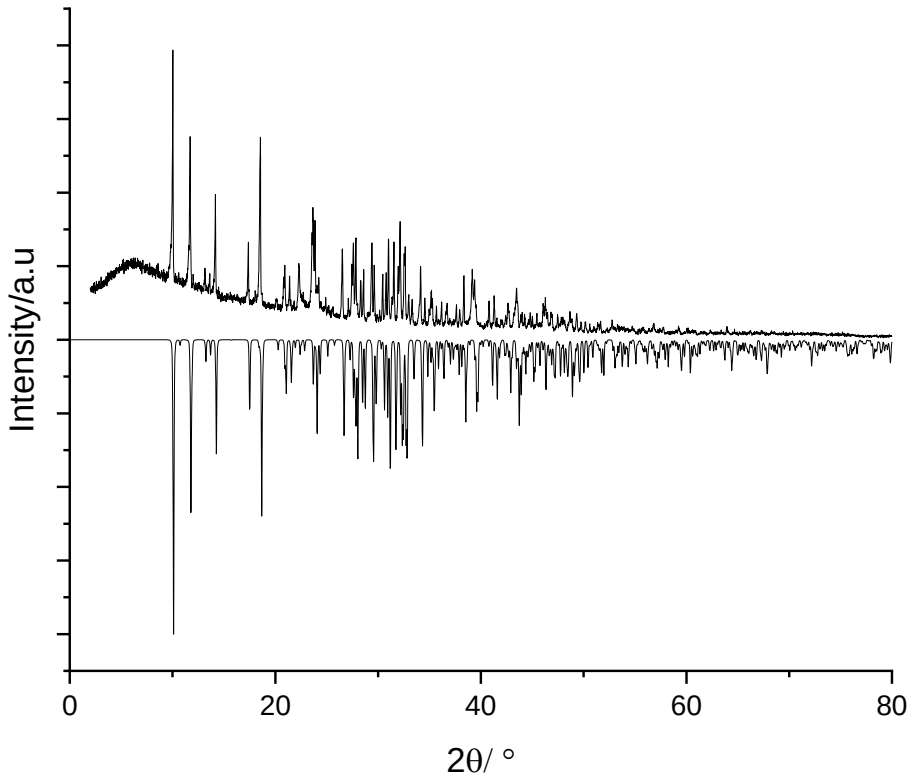

***Figure A.1**: Measured powder pattern of $(AgI)_2{\cdot}(As_4S_4)$ (positive intensity) in comparison to the theoretical powder pattern (negative intensity) derived from SC -XRD data.*

***Table A.1**: Fractional Atomic Coordinates (* 10^4) and equivalent Isotropic Displacement Parameters ($Å^2$* 10^3) for $(AgI)_2 \cdot (As_4S_4)$ at 123 K*

Atom	*Wyckoff*	*x*	*y*	*z*	*U(eq)*
I1	2i	-2279.4(4)	6791.7(4)	10056.7(3)	11.40(8)
I2	2i	-1615.8(4)	1327.1(4)	8517.1(3)	11.77(8)
Ag2	2i	-58.2(5)	3792.3(5)	8331.6(4)	15.59(9)
Ag1	2i	9530.1(5)	1616.5(5)	939.0(4)	17.41(1)
As4	2i	2341.5(6)	3341.5(6)	5486.4(5)	9.23(1)
As3	2i	4770.3(6)	3999.2(6)	1839.2(5)	9.74(1)
As2	2i	5659.9(6)	2203.7(6)	4823.5(5)	9.62(1)
As1	2i	4547.1(6)	1117.1(6)	1934.0(5)	9.52(1)
S2	2i	6390.4(1)	133.0(1)	3061.2(3)	9.9(2)
S4	2i	2311.9(1)	5279.8(1)	3973.4(3)	10.9(2)
S3	2i	6630.9(1)	3788.8(1)	2988.9(3)	9.9(2)
S1	2i	2006.4(2)	1552.2(1)	4086.8(3)	11.4(2)

***Table A.2**: Anisotropic Displacement Parameters ($Å^2$* 10^3) for for $(AgI)_2 \cdot (As_4S_4)$ at 123 K.*

Atom	U_{11}	U_{22}	U_{33}	U_{23}	U_{13}	U_{12}
I1	11.79(1)	9.91(1)	13.61(6)	0.87(2)	-7.46(1)	-2.04(1)
I2	12.24(2)	11.28(2)	13.65(1)	2.65(2)	-6.87(1)	-4.46(1)
Ag2	16.78(7)	14.2(2)	13.03(2)	-0.91(1)	-3.74(1)	-5.18(1)
Ag1	15.77(7)	16.1(2)	18.1(2)	1.95(1)	-7.17(1)	-2.08(4)
As4	9.5(2)	9.3(2)	8.0(2)	0.60(17)	-3.44(17)	-2.11(2)
As3	11.1(2)	10.6(2	8.8(2)	3.29(18)	-5.54(2)	-3.31(2)
As2	11.2(2)	9.9(2)	9.8(2)	1.98(18)	-6.63(2)	-3.05(1)
As1	10.4(2)	9.6(2)	8.8(2)	0.04(18)	-4.99(2)	-2.31(1)
S4	11.5(5)	9.3(6)	11.1(5)	1.3(4)	-5.6(4)	-0.9(4)
S3	10.3(5)	10.7(6)	10.9(5)	3.3(4)	-5.9(4)	-4.4(4)
S1	10.9(5)	12.5(6)	11.1(6)	0.7(4)	-4.3(4)	-4.9(4)

***Table A.3**: Selected bond lengths for $(AgI)_2 \cdot (As_4S_4)$ at 123 K*

Atom	Atom	Length/ Å	Atom	Atom	Length/ Å
I1’	Ag2	2.7785(5)	As4	S4	2.2359(14)
I1”	Ag2	2.9694(5)	As4	S1	2.2216(1)
I	Ag1	2.9095(5)	As3	As1	2.5643(7)
I2”	Ag2	2.8082(5)	As3	S4	2.2407(12)
I2	Ag1	2.9422(5)	As3	S3	2.2767(12)
I2’	Ag1	2.8619(5)	As2	S2	2.2390(12)
Ag2	As4	2.6185(6)	As2	S3	2.2796(13)
Ag1	S3	2.6311(1)	As1	S2	2.2638(12)
As4	As2	2.5360(6)	As1	S1	2.2441(12)

***Table A.4:** Selected bond angles for $(AgI)_2 \cdot (As_4S_4)$ at 123 K*

Atom	Atom	Atom	Angle/°	Atom	Atom	Atom	Angle/°
As1	S2	As2	103.24	S3	Ag1	I2	100.51
As1	S1	As4	99.89	I2	Ag1	I2’	116.50
As4	S4	As3	100.16	I2’	Ag1	I1	96.94
As2	S3	As3	102.25	S3	Ag1	I1	105.09
S1	As4	As2	101.89	As4	Ag2	I2’’	104.74
S1	As1	As3	99.80	I2’’	Ag2	I1’	117.51
S2	As1	S1	94.79	I1’	Ag2	I1’’	94.24
S2	As2	As4	98.23	As4	Ag2	I1’’	100.74
S2	As1	As3	97.95				
S4	As3	As1	99.63				
S4	As4	As2	101.54				
S4	As4	S1	96.34				
S3	As3	S4	93.03				
S3	As2	S2	91.62				
S3	As3	As1	99.15				

Table A.5: *Fractional Atomic Coordinates (* 10^4) and equivalent Isotropic Displacement Parameters ($Å^2$* 10^3) for $(AgI)_2 \cdot (As_4Se_4)$ at 123 K*

Atom	*Wyckoff*	*x*	*y*	*z*	*U(eq)*
I1	2i	1346.4(13)	-1602.7(14)	8549.4(12)	11.9(2)
I2	2i	6776.2(12)	-2189.6(14)	10011.1(12)	11.8(2)

Ag2	2i	3800.3(16)	-38.9(18)	8342.7(15)	16.3(3)
Ag1	2i	1569.2(17)	9506.7(19)	973.0(16)	18.3(3)
As1	2i	3312(2)	2326(2)	5517.0(18)	8.8(3)
As2	2i	2254(2)	5538(2)	4908.9(19)	9.4(3)
As3	2i	3976(2)	4762(2)	1747.4(19)	9.7(3)
As4	2i	1125(2)	4537(2)	1848.0(19)	9.7(3)
Se1	2i	1438(2)	1917(2)	4088.1(19)	10.9(3)
Se2	2i	73.8(19)	6454(2)	3011.9(18)	9.6(3)
Se3	2i	3890.6(19)	6646(2)	2958.9(19)	9.6(3)
Se4	2i	5365.5(19)	2215(2)	3949.3(18)	10.2(3)

Table A.6: *Anisotropic Displacement Parameters ($Å^2 * 10^3$) for for $(AgI)_2 \cdot (As_4Se_4)$ at 123 K*

Atom	***U_{11}***	***U_{22}***	***U_{33}***	***U_{23}***	***U_{13}***	***U_{12}***
I1	10.5(5)	12.3(5)	13.9(5)	-6.1(4)	2.5(4)	-4.3(4)
I2	9.0(5)	12.3(5)	14.2(5)	-7.1(4)	0.7(4)	-1.5(4)
Ag2	13.3(6)	17.5(6)	14.3(6)	-3.1(5)	-0.9(5)	-5.0(5)
Ag1	15.0(6)	16.2(6)	19.4(7)	-6.4(5)	1.0(5)	-0.3(5)
As1	8.5(7)	8.6(7)	8.7(7)	-3.3(6)	1.1(6)	-2.3(6)
As2	8.5(7)	10.0(8)	10.6(7)	-5.8(6)	1.7(6)	-2.0(6)
As3	9.4(7)	10.8(8)	9.8(7)	-5.3(6)	3.8(6)	-3.0(6)
As4	8.2(7)	10.9(8)	9.4(7)	-4.4(6)	0.6(6)	-2.3(6)
Se1	9.8(7)	10.9(8)	11.6(8)	-4.0(6)	0.6(6)	-4.0(6)
Se2	6.6(7)	9.5(7)	10.2(7)	-3.5(6)	1.1(6)	0.1(6)
Se3	8.2(7)	10.6(7)	10.7(7)	-4.8(6)	2.2(6)	-3.9(6)
Se4	7.5(7)	9.8(7)	11.4(7)	-4.8(6)	1.8(6)	0.4(6)

Table A.7*: Selected bond lengths for $(AgI)_2 \cdot (As_4Se_4)$ at 123 K*

Atom	Atom	Length/ Å	Atom	Atom	Length/ Å
I1	Ag2	2.8322(18)	As1	Se1	2.364(2)
I1	Ag1	2.8830(17)	As1	As2	2.527(2)
I1	Ag1	2.9595(18)	Se2	As4	2.404(2)
I2	Ag2	2.9772(18)	Se2	As2	2.390(2)
I2	Ag2	2.7938(17)	Se3	As3	2.405(2)
I2	Ag1	2.9430(18)	Se3	As2	2.435(2)

Ag2	As1	2.637(2)	Se4	As3	2.381(2)
Ag1	Se3	2.720(2)	Se1	As4	2.386(2)
As1	Se4	2.384(2)	As3	As4	2.568(2)

Table A.8*: Selected bond angles for $(AgI)_2 \cdot (As_4Se_4)$ at 123 K*

Atom	Atom	Atom	Angle/°	Atom	Atom	Atom	Angle/°
As1	Se2	As2	100.32	Se3	Ag1	I1	99.37
As1	Se1	As4	96.91	I1	Ag1	I2	108.67
As4	Se4	As3	96.90	I2	Ag1	I1’	96.94
As2	Se3	As3	99.52	Se3	Ag1	I1’	130.95
Se1	As4	As2	103.63	As1	Ag2	I2’	125.93
Se1	As1	As3	102.13	As1	Ag2	I1’’	117.62
Se2	As1	Se1	94.47	I1’’	Ag2	I2’’	111.24
Se2	As2	As4	100.07	As1	Ag2	I2’’	101.67
Se2	As1	As3	99.15				
Se4	As3	As1	101.72				
Se4	As4	As2	103.43				
Se4	As4	Se1	96.44				
Se3	As3	Se4	92.22				
Se3	As2	Se2	90.10				
Se3	As3	As1	101.33				

Click or tap here to enter text.

Table A.9*: Fractional Atomic Coordinates (* 10^4) and equivalent Isotropic Displacement Parameters ($Å^2$* 10^3) for $(AgBr) \cdot (As_4S_4)$ at 123 K*

Atom	Wyckoff	*x*	*y*	*z*	*U(eq)*
Ag	4e	397.1(8)	5484.1(6)	6794.8(6)	52.45(19))
As1	4e	5207.1(8)	4724.3(5)	7094.4(5)	21.92(13)
As3	4e	5721.0(8)	6601.6(5)	6240.4(5)	23.34(13)
As4	4e	7860.9(8	6358.9(5)	9245.8(5)	24.78(14)
As5	4e	4399.2(9)	6808.6(5)	9109.4(6)	26.45(14)
Br	4e	1895.1(10)	5863.5(7)	4729.6(6)	41.17(18)
S4	4e	8375(2)	7052.6(12)	7462.8(14)	25.0(3)

S2	4e	3272(2)	5168.2(12)	8420.2(13)	25.0(3)
S1	4e	7691(2)	4659.1(11)	8560.0(13)	24.9(3)
S3	4e	3910(2)	7576.8(12)	7293.1(14)	27.9(3)

***Table A.10**: Anisotropic Displacement Parameters ($Å^2 * 10^3$) for $(AgBr)\cdot(As_4S_4)$ at 123 K*

Atom	U_{11}	U_{22}	U_{33}	U_{23}	U_{13}	U_{12}
Ag	31.9(3)	84.9(5)	40.1(3)	-19.4(3)	4.1(2)	9.1(3)
As1	24.4(3)	18.7(3)	22.4(3)	-3.2(2)	2.7(2)	-1.3(2)
As3	25.4(3)	24.6(3)	20.2(3)	4.7(2)	3.9(2)	0.7(2)
As4	27.4(3)	24.2(3)	21.4(3)	-3.0(2)	-0.8(2)	-1.2(2)
As5	31.3(3)	23.9(3)	26.2(3)	-3.5(2)	10.9(2)	0.6(2)
Br	38.5(4)	50.7(4)	34.7(4)	-2.8(3)	6.7(3)	-7.8(3)
S4	24.0(7)	21.9(7)	30.0(7)	0.4(5)	5.9(6)	-4.0(5)
S2	26.5(7)	23.4(7)	26.5(7)	0.5(5)	8.6(5)	-5.1(5)
S1	28.7(7)	19.7(6)	25.2(7)	1.2(5)	0.5(5)	4.7(5)
S3	28.7(7)	22.2(7)	33.0(8)	2.8(6)	5.0(6)	6.0(6)

***Table A.11**: Selected bond lengths for $(AgBr)\cdot(As_4S_4)$ at 123 K*

Atom	Atom	Length/ Å	Atom	Atom	Length/ Å
Ag	Br^1	2.7630(10)	As3	S4	2.2652(16)
Ag	Br	2.7418(10)	As3	S3	2.2452(16)
Ag	$S4^2$	2.6095(16)	As4	As2	2.5599(9)
Ag	S2	2.5918(17)	As4	S4	2.2573(16)
As1	As3	2.5595(8)	As4	S1	2.2351(15)
As1	S2	2.2607(16)	As2	S2	2.2795(16)
As1	S1	2.2563(16)	As2	S3	2.2280(17)

[1]-x,1-y,1-z; [2]-1+x, +y, + z

***Table A.12**: Selected bond angles for (AgBr)·(As_4S_4) at 123 K.*

Atom	Atom	Atom	Angle/°	Atom	Atom	Atom	Angle/°
As1	S2	As2	102.21	Br’	Ag	Br	81.89
As1	S1	As4	102.39	Br	Ag	S2	103.85
As4	S4	As3	101.81	S2	Ag	S4’	109.88
As2	S3	As3	103.00	S4	Ag	Br	108.17
S2	As1	As3	99.52				
S4	As3	As1	99.92				
S4	As4	As2	98.89				
S4	As4	S1	93.46				
S3	As3	S4	93.60				
S3	As2	S2	93.93				
S3	As3	As1	99.25				

***Table A.13**: Refinement parameters of powder diffractogram for (AgBr)·(As_4S_4) at room temperature.*

Wavelength : 1.540598

Number of accepted peaks: 99

2Theta window: 0.050

2Theta zeropoint: 0.0000 (refinable)

Symmetry: Monoclinic P

Initial cell parameters:

Cell_A: 11.1070

Cell_B: 12.3550

Cell_C: 7.2264

Cell_Beta: 98.833

Refined cell parameters:

Cell_A: 11.1028(18)

Cell_B: 12.360(4)

Cell_C: 7.2228(11)

Cell_Beta: 98.800(12)

Cell_Volume: 979.5(5)

Number of single indexed lines: 35

Number of unindexed lines: 6

2Theta zeropoint: -0.028(7)

Final 2Theta window: 0.0500

N	2Th[obs]	H	K	L	2Th[calc]	obs-calc	Int.	d[obs]	d[calc]
1	10.772	1	1	0	10.773	-0.0018	10.0	8.2068	8.2054
2	14.316	0	1	1	14.318	-0.0013	33.4	6.1817	6.1811
		0	2	0	14.321	-0.0042		6.1799	
3	15.473	-1	1	1	15.481	-0.0086	29.6	5.7222	5.7191
4	15.802	1	0	1	15.801	0.0006	21.3	5.6039	5.6041
5	16.148	2	0	0	16.143	0.0049	23.4	5.4844	5.4860
6	16.444	1	2	0	16.450	-0.0054	100.0	5.3863	5.3845
7	18.505	--- not indexed ---					17.5	4.7908	
8	19.874	-1	2	1	19.879	-0.0054	5.4	4.4639	4.4627
9	21.650	2	2	0	21.644	0.0060	15.2	4.1016	4.1027
10	23.043	2	1	1	23.039	0.0035	11.4	3.8566	3.8572
		1	3	0	23.041	0.0022		3.8570	

11	23.726	-2	2	1	23.727	-0.0007	1.6	3.7471	3.7470
12	24.926	0	0	2	24.929	-0.0030	26.0	3.5693	3.5689
		0	3	1	24.934	-0.0080		3.5682	
13	25.386	3	1	0	25.376	0.0094	9.5	3.5058	3.5070
14	26.015	-1	1	2	26.042	-0.0263	20.9	3.4223	3.4189
15	26.599	-3	1	1	26.603	-0.0041	30.5	3.3485	3.3480
16	26.836	1	3	1	26.837	-0.0002	56.9	3.3195	3.3194
17	27.575	--- not indexed ---					3.8	3.2322	
18	28.322	3	2	0	28.332	-0.0101	47.5	3.1486	3.1475
		1	1	2	28.366	-0.0437			3.1438
19	28.762	-2	3	1	28.761	0.0014	4.6	3.1014	3.1015
20	28.952	-1	2	2	28.935	0.0173	6.9	3.0815	3.0833
21	29.434	-3	2	1	29.445	-0.0116	5.5	3.0322	3.0310
22	30.008	3	1	1	29.967	0.0404	13.6	2.9755	2.9794
		1	4	0	30.020	-0.0126			2.9743
23	31.059	1	2	2	31.060	-0.0008	32.2	2.8771	2.8770
24	31.518	0	4	1	31.525	-0.0066	21.6	2.8362	2.8356
25	31.921	2	0	2	31.913	0.0086	39.4	2.8013	2.8020
26	32.699	3	3	0	32.715	-0.0159	3.4	2.7364	2.7351
		2	1	2	32.745	-0.0458			2.7327
27	33.072	-3	1	2	33.054	0.0183	73.2	2.7064	2.7079
		1	4	1	33.079	-0.0070			2.7059
		-4	0	1	33.120	-0.0477			2.7027
28	34.682	-2	4	1	34.689	-0.0068	7.9	2.5844	2.5839
29	35.216	--- not indexed ---					9.0	2.5464	
30	36.246	-4	2	1	36.249	-0.0022	6.4	2.4764	2.4762
31	37.887	--- not indexed ---					1.1	2.3728	
32	38.102	3	4	0	38.095	0.0067	11.2	2.3599	2.3603
		-1	1	3	38.127	-0.0249			2.3585
33	38.511	0	1	3	38.501	0.0100	24.0	2.3358	2.3364

		0	4	2	38.507	0.0043		2.3360
		3	1	2	38.508	0.0032		2.3360
		0	5	1	38.510	0.0009		2.3358
		-1	4	2	38.560	-0.0494		2.3329
34	39.000	-3	4	1	38.958	0.0416	13.5 2.3076	2.3100
		-1	5	1	38.988	0.0118		2.3083
35	39.851	1	5	1	39.825	0.0258	20.6 2.2603	2.2617
		-4	3	1	39.860	-0.0090		2.2598
36	40.626	0	2	3	40.598	0.0282	8.7 2.2189	2.2204
		3	2	2	40.605	0.0218		2.2201
		1	1	3	40.639	-0.0124		2.2183
37	41.180	-2	5	1	41.206	-0.0259	2.0 2.1903	2.1890
38	41.443	3	4	1	41.428	0.0148	3.5 2.1771	2.1778
39	41.784	5	1	0	41.773	0.0116	12.1 2.1601	2.1606
		-5	1	1	41.782	0.0021		2.1602
40	42.643	-3	1	3	42.641	0.0015	2.1 2.1185	2.1186
		1	2	3	42.648	-0.0054		2.1183
41	43.087	4	3	1	43.070	0.0173	3.3 2.0977	2.0985
42	43.543	2	4	2	43.568	-0.0244	3.5 2.0768	2.0757
		-1	3	3	43.573	-0.0292		2.0755
43	43.910	0	3	3	43.908	0.0014	11.3 2.0603	2.0604
		3	3	2	43.914	-0.0047		2.0601
		0	6	0	43.917	-0.0077		2.0600
44	44.501	-4	4	1	44.501	-0.0004	7.6 2.0343	2.0343
45	44.844	-2	3	3	44.859	-0.0150	8.0 2.0195	2.0189
46	45.821	0	6	1	45.809	0.0112	5.9 1.9787	1.9792
		1	3	3	45.838	-0.0179		1.9780
47	46.216	2	2	3	46.208	0.0082	6.0 1.9627	1.9630
		-1	6	1	46.225	-0.0091		1.9624
		-2	5	2	46.232	-0.0162		1.9621

48	46.856	5	3	0	46.871	-0.0148	9.1	1.9374	1.9368
		-5	3	1	46.880	-0.0235			1.9365
49	47.097	4	2	2	47.083	0.0149	11.7	1.9280	1.9286
		2	6	0	47.085	0.0123			1.9285
		-4	1	3	47.116	-0.0188			1.9273
50	47.475	4	4	1	47.457	0.0187	5.7	1.9135	1.9143
		5	2	1	47.467	0.0082			1.9139
		-5	2	2	47.493	-0.0176			1.9129
51	48.127	-2	6	1	48.173	-0.0451	9.1	1.8891	1.8875
52	49.180	2	3	3	49.217	-0.0368	4.0	1.8511	1.8498
53	49.587	2	6	1	49.583	0.0039	8.0	1.8369	1.8370
		4	5	0	49.604	-0.0167			1.8363
54	50.025	1	4	3	50.036	-0.0115	2.5	1.8218	1.8215
		4	3	2	50.051	-0.0267			1.8209
		-6	1	1	50.068	-0.0429			1.8204
55	50.436	6	1	0	50.405	0.0311	9.0	1.8079	1.8090
		5	3	1	50.419	0.0172			1.8085
		-5	3	2	50.444	-0.0075			1.8077
56	51.069	3	2	3	51.035	0.0337	7.1	1.7870	1.7881
		-1	1	4	51.080	-0.0112			1.7867
57	52.151	6	2	0	52.117	0.0339	6.7	1.7525	1.7535
		5	0	2	52.119	0.0318			1.7535
		-5	0	3	52.159	-0.0083			1.7522
58	52.690	-2	6	2	52.679	0.0114	10.2	1.7358	1.7361
		5	1	2	52.681	0.0094			1.7361
		4	5	1	52.682	0.0076			1.7360
		-5	1	3	52.720	-0.0304			1.7349
59	53.138	-1	5	3	53.115	0.0227	1.8	1.7222	1.7229
		-6	1	2	53.143	-0.0047			1.7221
60	53.448	0	2	4	53.399	0.0491	5.8	1.7129	1.7144

		0	5	3	53.405	0.0430		1.7142
		3	5	2	53.410	0.0377		1.7141
		0	7	1	53.412	0.0360		1.7140
61	53.788	1	1	4	53.762	0.0259	7.3 1.7029	1.7037
		-1	7	1	53.784	0.0041		1.7030
62	54.363	5	2	2	54.342	0.0218	8.8 1.6862	1.6869
		5	4	1	54.353	0.0106		1.6865
		-5	4	2	54.376	-0.0128		1.6859
		-5	2	3	54.381	-0.0172		1.6858
63	54.832	-6	2	2	54.794	0.0384	1.9 1.6729	1.6740
64	55.081	1	5	3	55.083	-0.0023	13.6 1.6660	1.6659
65	55.683	-4	4	3	55.668	0.0152	6.5 1.6494	1.6498
		-3	2	4	55.725	-0.0421		1.6482
66	56.190	--- not indexed ---					2.3 1.6357	
67	56.708	-3	5	3	56.690	0.0180	2.3 1.6220	1.6224
68	57.460	-6	3	2	57.474	-0.0143	0.9 1.6025	1.6021
69	58.073	1	3	4	58.062	0.0104	1.9 1.5871	1.5873
		2	5	3	58.068	0.0043		1.5872
70	58.597	-3	7	1	58.584	0.0130	10.6 1.5741	1.5744
		6	4	0	58.612	-0.0149		1.5737
		4	6	1	58.615	-0.0185		1.5736
71	59.221	-1	4	4	59.222	-0.0009	3.0 1.5590	1.5590
		-6	1	3	59.258	-0.0364		1.5581
72	59.538	4	3	3	59.530	0.0084	2.4 1.5514	1.5516
		1	7	2	59.532	0.0056		1.5516
		-4	6	2	59.566	-0.0283		1.5508
73	60.419	-4	5	3	60.391	0.0274	1.8 1.5309	1.5315
		3	7	1	60.434	-0.0148		1.5306
		1	8	0	60.464	-0.0453		1.5299
74	60.762	-5	4	3	60.713	0.0483	3.2 1.5231	1.5242

		-7	0	2	60.744	0.0180		1.5235
		6	1	2	60.755	0.0071		1.5233
		-6	2	3	60.799	-0.0373		1.5223
75	61.678	3	1	4	61.628	0.0496	2.0 1.5027	1.5037
		1	4	4	61.665	0.0123		1.5029
		5	0	3	61.681	-0.0033		1.5026
		-1	8	1	61.685	-0.0077		1.5025
		5	6	0	61.712	-0.0345		1.5019
		-4	3	4	61.715	-0.0370		1.5018
		-5	6	1	61.719	-0.0417		1.5017
76	62.277	-5	1	4	62.236	0.0411	2.4 1.4896	1.4905
		3	5	3	62.244	0.0329		1.4903
		-3	7	2	62.272	0.0051		1.4897
		6	2	2	62.274	0.0028		1.4897
		1	8	1	62.287	-0.0105		1.4894
77	62.834	-4	7	1	62.814	0.0206	1.0 1.4777	1.4782
		-7	3	1	62.856	-0.0218		1.4773
78	63.423	7	3	0	63.445	-0.0218	2.5 1.4654	1.4650
79	64.489	-1	0	5	64.469	0.0201	1.2 1.4438	1.4442
		2	8	1	64.480	0.0090		1.4440
		-2	5	4	64.484	0.0051		1.4439
		7	2	1	64.522	-0.0338		1.4431
80	64.937	-1	1	5	64.961	-0.0239	1.0 1.434	1.4344
81	65.453	--- not indexed ---					1.3 1.4248	
82	65.827	0	1	5	65.801	0.0268	1.0 1.4176	1.4181
		0	7	3	65.813	0.0145		1.4179
		0	8	2	65.817	0.0106		1.4178
		3	7	2	65.818	0.0099		1.4178
		-1	8	2	65.854	-0.0261		1.4171
83	66.441	-3	5	4	66.420	0.0210	1.2 1.4060	1.4064

		-1	2	5	66.426	0.0152		1.4063
		6	5	1	66.434	0.0073		1.4061
84	67.964	-6	1	4	67.917	0.0467	0.8	1.3782	1.3790
		-8	1	1	67.967	-0.0030		1.3781
85	68.625	-7	4	2	68.628	-0.0030	0.8	1.3665	1.3664
		4	2	4	68.633	-0.0082		1.3663
86	69.457	2	8	2	69.410	0.0467	1.9	1.3521	1.3529
		7	1	2	69.444	0.0130		1.3524
		-8	0	2	69.505	-0.0483		1.3513
87	71.112	2	1	5	71.088	0.0245	1.0	1.3247	1.3251
88	73.180	-4	8	2	73.200	-0.0208	0.4	1.2923	1.2920
		7	3	2	73.203	-0.0233		1.2919
		3	5	4	73.217	-0.0371		1.2917
89	73.743	-7	4	3	73.715	0.0278	1.0	1.2838	1.2842
		5	1	4	73.717	0.0257		1.2842
		-8	3	2	73.727	0.0156		1.2840
		5	5	3	73.730	0.0132		1.2840
		-5	5	4	73.776	-0.0330		1.2833
		-5	1	5	73.777	-0.0337		1.2833
		3	7	3	73.783	-0.0405		1.2832
90	76.538	5	7	2	76.504	0.0340	0.9	1.2437	1.2442
		-5	7	3	76.537	0.0014		1.2437
91	80.997	-4	9	2	80.969	0.0282	1.0	1.1861	1.1865
		-3	0	6	81.014	-0.0162		1.1859
		-8	5	2	81.030	-0.0324		1.1857
92	81.452	-3	1	6	81.464	-0.0115	0.7	1.1806	1.1805
		-1	2	6	81.469	-0.0162		1.1804
		6	8	0	81.492	-0.0391		1.1802
93	82.077	-6	7	3	82.051	0.0268	1.1	1.1732	1.1735
		0	6	5	82.067	0.0107		1.1733

		2	5	5	82.086	-0.0092		1.1731
		1	9	3	82.105	-0.0274		1.1729
		-8	1	4	82.124	-0.0468		1.1727
94	83.670	1	10	2	83.635	0.0349	0.6	1.1549	1.1553
		-6	8	2	83.660	0.0092		1.1550
		-1	3	6	83.713	-0.0434		1.1544
95	84.422	4	3	5	84.415	0.0068	0.6	1.1465	1.1466
		3	10	1	84.419	0.0027		1.1465
		-3	8	4	84.430	-0.0079		1.1464
		-7	0	5	84.437	-0.0152		1.1463
		6	8	1	84.443	-0.0205		1.1463
96	86.219	9	3	1	86.181	0.0382	1.7	1.1272	1.1276
		2	0	6	86.193	0.0264		1.1274
		-7	2	5	86.224	-0.0042		1.1271
		4	10	0	86.248	-0.0281		1.1269
		3	5	5	86.261	-0.0417		1.1267
97	86.943	-5	0	6	86.898	0.0455	0.7	1.1196	1.1201
		1	3	6	86.912	0.0314		1.1200
		2	8	4	86.926	0.0172		1.1198
		- 2	4	6	86.940	0.0030		1.1197
98	88.453	-7	3	5	88.452	0.0013	0.8	1.1044	1.1044
99	89.647	-1	9	4	89.612	0.0350	0.7	1.0927	1.0931
		7	1	4	89.616	0.0315		1.0930
		-2	11	1	89.623	0.0243		1.0930
		10	1	0	89.629	0.0181		1.0929
		-10	2	1	89.642	0.0047		1.0928
		-10	1	2	89.654	-0.0072		1.0927

Average delta(2Theta) = 0.010

Maximum delta(2Theta) = 0.045 (peak 51) = 4.5 * average

Figure of Merit F (30) = 45.8 (0.007, 98)

Durbin-Watson serial correlation = 2.106 (not significant)

Sqrt [sum(w * delta(q)^2) / (Nobs - Nvar)] = 0.00011232

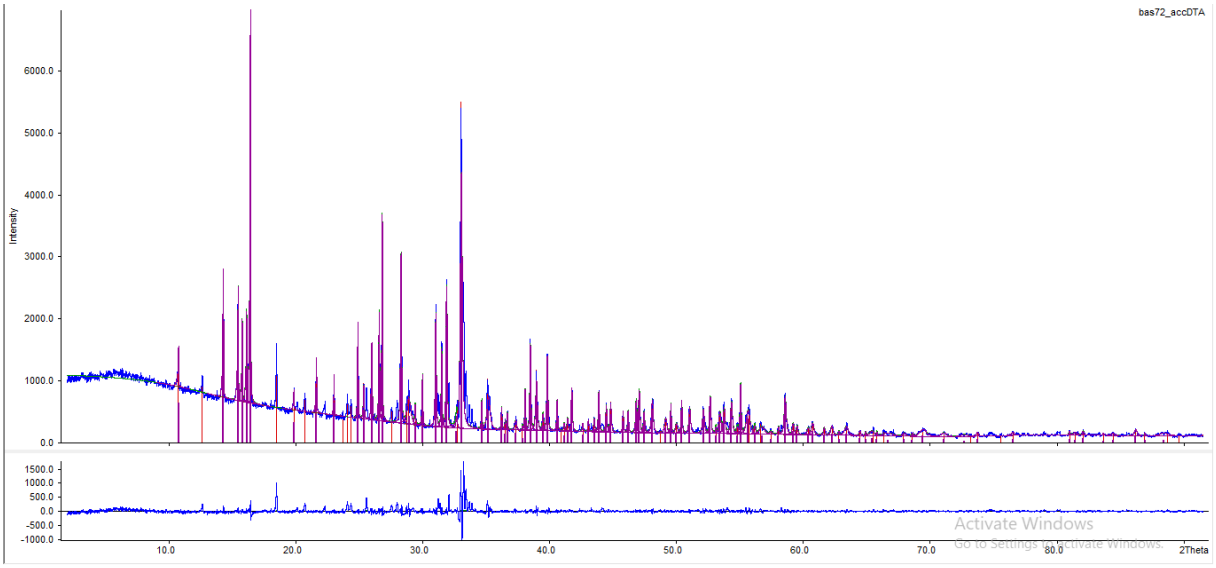

***Fig A.2**: Indexation of the powder diffractogram of (AgBr)·(As_4S_4) with difference plot.*

***Table A.14**: Fractional Atomic Coordinates (* 10^4) and equivalent Isotropic Displacement Parameters ($Å^2$* 10^3) for (AgCl)·(As_4S_4) at 123 K.*

Atom	Wyckoff	*x*	*y*	*z*	*U(eq)*
Ag	4e	9595.1(9)	5481.8(6)	3272.0(6)	48.1(2)
As4	4e	2096.6(10)	6373.8(5	775.0(6)	24.25(17)
As1	4e	4780.2(9	4712.2(5)	2938.7(6)	21.26(17)
As3	4e	4329.7(9)	6591.6(5)	3823.2(6)	22.65(17)
As2	4e	5591.0(10)	6803.7(5)	895.6(6)	25.00(18)

Cl	4e	8133(3)	5849.5(16)	5287.9(17)	37.9(4)
S2	4e	6719(2)	5157.0(12)	1588.5(16)	24.1(3)
S1	4e	2249(2)	4668.3(12)	1454.3(16)	23.7(3)
S4	4e	1632(2)	7060.1(12)	2599.7(16)	24.8(3)
S3	4e	6134(2)	7565.3(13)	2745.2(16)	26.7(4)

***Table A.15**: Anisotropic Displacement Parameters ($Å^2 * 10^3$) for $(AgCl)\cdot(As_4S_4)$ at 123 K*

Atom	U_{11}	U_{22}	U_{33}	U_{23}	U_{13}	U_{12}
Ag	29.6(3)	75.9(5)	38.9(4)	16.7(3)	5.3(3)	-4.8(3)
As4	25.6(4)	24.1(3)	21.4(4)	3.8(2)	-1.4(3)	1.9(3)
As1	23.8(3)	18.2(3	21.4(3)	2.9(2)	2.3(3)	1.2(2)
As3	24.8(4)	24.0(3)	19.5(3)	-4.2(2)	4.5(3)	-1.5(2)
As2	29.8(4)	23.3(3)	23.6(4)	4.0(2)	9.6(3)	-0.7(3)
Cl	34.0(10)	51.8(11)	28.6(10)	4.4(8)	6.5(8)	10.3(8)
S2	24.2(8)	23.6(7)	25.9(9)	-1.2(6)	8.2(7)	3.7(6)
S1	25.3(8)	19.4(7)	25.9(9)	-0.9(6)	1.9(7)	-4.0(6)
S4	22.6(8)	21.8(7)	30.2(9)	-0.6(6)	4.9(7)	4.3(6)
S3	27.8(9)	22.5(7)	29.6(9)	-3.1(6)	4.0(7)	-6.5(6)

***Table A.16**: Selected bond lengths for $(AgCl)\cdot(As_4S_4)$ at 123 K.*

Atom	Atom	Length/ Å	Atom	Atom	Length/ Å
Ag	S2	2.5886(19)	As1	As3	2.5570(9)
Ag	S41	2.6148(17)	As1	S2	2.2635(18)
Ag	Cl2	2.663(2)	As1	As1	2.2533(18)
Ag	Cl	2.6459(19)	As3	S4	2.2613(18)
As4	As2	2.5547(10)	As3	S3	2.2430(18)

As4	S1	2.2315(16)	As2	S2	2.2764(17)
As4	S4	2.2579(18)	As2	S3	2.2263(19)

1-1+x,+y,+z; 2-2-x, 1-y, 1- z

***Table A.17**: Selected bond angles for $(AgCl)\cdot(As_4S_4)$ at 123 K.*

Atom	Atom	Atom	Angle/°	Atom	Atom	Atom	Angle/°
S2	Ag	S4	109.45(6)	S3	As3	S4	93.49(7)
S2	Ag	Cl	104.57(6)	S2	As2	As4	97.42(5)
S2	Ag	Cl2	132.93(6)	S3	As2	As4	99.55(5)
S4	Ag	Cl	115.19(6)	S3	As2	S2	93.81(7)
S4	Ag	Cl2	108.03(6)	As1	S2	Ag	94.10(6)
Cl	Ag	Cl2	83.80(6)	As1	S2	As2	102.31(6)
S1	As4	As2	100.48(5)	As2	S2	Ag	107.85(7)
S1	As4	S4	93.47(6)	As4	S1	As1	102.33(6)
S4	As4	As2	99.06(5)	As4	S4	Ag3	98.14(6)
S2	As1	As3	99.18(5)	As4	S4	As3	101.76(7)
S1	As1	As3	99.39(5)	As3	S4	Ag3	96.18(6)
S1	As1	S2	92.24(7)	As2	S3	As3	103.13(7)
S4	As3	As1	98.76(5)	Ag	Cl	Ag2	96.21(6)
S3	As3	As1	99.50(5)				

***Table A.18**: Fractional Atomic Coordinates (* 10^4) and equivalent Isotropic Displacement Parameters ($Å^2$* 10^3) for $(CuI)_3\cdot(As_4S_4)$ at 123 K.*

Atom	Wyckoff	*x*	*y*	*z*	*U(eq)*
I1	4e	1509.2(2)	9470.3(2)	4778.5(2)	9.95(6)
I2	4e	6688.2(2)	6497.0(2)	9463.5(2)	11.46(6)
I3	4e	6402.6(2)	9264.4(2)	7303.0(2)	10.69(6)

I4	4e	6600.8(2)	5456.3(2)	6430.2(2)	12.59(6)
As1	4e	4491.0(2)	5764.0(4)	5892.6(4)	10.71(9)
As2	4e	4413.5(2)	8702.1(4)	6938.2(4)	10.75(9)
As3	4e	3254.6(2)	6539.4(4)	5484.2(4)	11.22(9)
As4	4e	4372.8(2)	8825.4(4)	5032.1(4)	11.64(9)
S1	4e	4923.7(5)	7072.9(10)	4897.6(9)	11.7(2)
S2	4e	4903.5(5)	6840.2(9)	7351.4(9)	10.5(2)
S3	4e	3342.9(5)	7967.3(9)	6749.1(9)	10.8(2)
S4	4e	3319.1(5)	8022.6(10)	4335.9(9)	12.0(2)
Cu1	4e	6061.9(3)	7563.3(5)	5719.6(5)	16.05(12)
Cu2	4e	6081.4(3)	6939.3(5)	7568.8(5)	13.44(11)
Cu3	4e	2818.1(3)	9300.1(5)	5352.8(5)	16.78(12)

***Table A.19**: Anisotropic Displacement Parameters ($Å^2 * 10^3$) for for $(CuI)_3 \cdot (As_4S_4)$ at 123 K*

Atom	U_{11}	U_{22}	U_{33}	U_{23}	U_{13}	U_{12}
I1	8.93(12)	8.99(11)	11.77(14)	-1.11(10)	2.44(10)	-0.60(9)
I2	12.47(12)	12.29(12)	9.90(14)	0.73(10)	3.46(10)	3.63(9)
I3	9.88(12)	9.04(11)	13.00(14)	0.23(10)	2.77(10)	0.52(9)
I4	14.59(13)	10.87(12)	12.26(14)	-1.38(10)	3.45(10)	1.47(9)
As1	11.7(2)	8.59(18)	11.8(2)	-0.44(16)	3.08(17)	1.18(15)
As2	10.21(19)	9.34(18)	12.4(2)	-2.15(16)	2.40(17)	-1.27(1)
As3	9.47(19)	11.56(19)	12.2(2)	-1.91(17)	2.08(16)	-1.49(1)
As4	11.9(2)	10.27(19)	13.3(2)	2.37(17)	4.34(17)	0.03(15)
S1	11.2(5)	13.1(5)	12.0(5)	0.4(4)	5.0(4)	1.0(4)
S2	10.1(4)	10.9(4)	10.0(5)	0.3(4)	1.9(4)	0.1(3)
S3	9.7(4)	11.8(4)	11.2(5)	-0.6(4)	3.5(4)	-0.2(4)
S4	11.1(5)	14.1(5)	10.3(5)	-0.2(4)	1.7(4)	2.4(4)
Cu1	14.4(3)	18.0(3)	16.5(3)	5.0(2)	5.4(2)	-0.3(2)
Cu2	12.7(2)	15.7(2)	11.4(3)	-0.2(2)	2.3(2)	0.5(2)
Cu3	11.5(3)	13.3(2)	24.2(3)	-1.1(2)	2.4(2)	1.5(2)

***Table A.20**: Selected bond lengths for $(CuI)_3 \cdot (As_4S_4)$ at 123 K.*

Atom	Atom	Length/ Å	Atom	Atom	Length/ Å
As1	As3	2.534	I3	Cu2	2.6724
As2	As4	2.568	I3	Cu1	2.7876
As1	S1	2.289	I2	Cu3[4]	2.5866
As1	S2	2.262	I2	Cu1[5]	2.5802
S2	As2	2.267	I4	Cu2	2.6357
As2	S3	2.240	I4	Cu1	2.6196
S3	As[3]	2.293	Cu2	S2	2.2994
As3	S4	2.277	Cu3	S3	2.4015
S4	As4	2.249	Cu3	S4	2.3648
As4	S1	2.243	Cu1	S1	2.319
I1	Cu3	2.5347			

[4] 1-x,-1/2+y,[3]/2-z; [5] +x,3/2-y,1/2+z

***Table A.21**: Selected bond angles for $(CuI)_3 \cdot (As_4S_4)$ at 123 K.*

Atom	Atom	Atom	Angle/°	Atom	Atom	Atom	Angle/°
As1	S2	As2	102.57	I2	Cu3	Cu3	107.39
As1	S1	As4	102.51	I2	Cu3	S3	114.36
As4	S4	As3	101.95	I2	Cu3	S4	113.29
As2	S3	As3	102.28	S4	Cu3	I4	115.25
S1	As4	As2	98.67	I3	Cu2	I2’	104.23
S1	As1	As3	99.25	I3	Cu2	S2	107.63
S2	As1	S1	94.68	I3	Cu2	I4	111.13
S2	As2	As4	101.11	I2’	Cu2	I4	108.24
S2	As1	As3	97.31	I4	Cu1	I2’’	111.67
S4	As3	As1	99.25	I2’’	Cu1	S1	111.17
S4	As4	As2	100.33	I2’’	Cu1	I3	100.33
S4	As4	S1	93.37	I4	Cu1	I3	108.15
S3	As3	S4	91.04				
S3	As2	S2	92.50				
S3	As3	As1	100.75				

***Table A.22**: Fractional Atomic Coordinates (* 10^4) and equivalent Isotropic Displacement Parameters (Å^2* 10^3) for $(CuBr)_2 \cdot (As_4S_4)$ at 123 K.*

Atom	*Wyckoff*	*x*	*y*	*z*	*U(eq)*
Br1	2a	2354.9(12)	9630.5(12)	4989.8(9)	10.79(19)
As4	2a	158.5(12)	1672.8(13)	7050.0(9)	7.86(19)
Br2	2a	7018.7(12)	8157.9(12)	7773.9(9)	10.63(19)
As3	2a	1976.5(12)	5089.4(13)	9296.6(9)	8.31(19)
As2	2a	2080.3(13)	3783.4(13)	5997.7(9)	8.38(19)
As1	2a	4305.7(12)	2650.1(13)	9274.7(9)	8.51(19)
Cu1	2a	3771.6(16)	8542.6(16)	7282.2(12)	12.7(2)
Cu2	2a	7126.4(16)	5072.1(17)	7344.0(12)	12.3(2)
S4	2a	-562(3)	3413(3)	8653(2)	8.5(4)
S3	2a	1777(3)	6190(3)	7241(2)	9.2(4)
S2	2a	4859(3)	3017(3)	7234(2)	9.7(4)
S1	2a	2377(3)	364(3)	8616(2)	9.2(4)

***Table A.23**: Anisotropic Displacement Parameters (Å^2* 10^3) for $(CuBr)_2 \cdot (As_4S_4)$ at 123 K.*

Atom	U_{11}	U_{22}	U_{33}	U_{23}	U_{13}	U_{12}
Br1	12.0(4)	12.8(5)	7.3(4)	0.4(3)	1.4(3)	0.4(4)
As4	7.3(4)	6.7(4)	9.2(4)	-0.7(3)	0.8(3)	-1.3(4)
Br2	9.5(4)	9.3(4)	13.1(4)	-2.0(3)	2.4(3)	0.2(3)
As3	8.8(4)	7.0(4)	9.1(4)	-1.9(4)	1.8(3)	-0.2(4)
As2	9.8(4)	8.4(4)	7.0(4)	0.8(3)	2.0(3)	-0.5(4)
As1	7.3(4)	8.8(4)	8.5(4)	-0.6(4)	-0.3(3)	1.1(4)
Cu1	11.3(5)	12.5(6)	14.1(5)	0.0(5)	2.1(4)	0.1(5)
Cu2	11.9(5)	10.3(5)	14.7(6)	0.0(5)	3.3(4)	-0.4(5)
S4	6.6(9)	8.8(11)	11.0(10)	0.6(8)	3.8(7)	0.0(8)
S3	10.8(10)	6.2(10)	10.6(11)	1.2(8)	2.3(8)	-1.0(8)
S2	7.4(9)	10.7(11)	11.4(10)	-0.3(8)	3.1(8)	-0.6(9)
S1	10.9(10)	6.2(10)	10.7(10)	0.6(8)	2.5(8)	0.6(9)

***Table A.24**: Selected bond lengths for $(CuBr)_2 \cdot (As_4S_4)$ at 123 K.*

Atom	Atom	Length/ Å	Atom	Atom	Length/ Å
Br1	Cu1	2.5105(15)	As3	S3	2.249(3)
Br1	Cu2	2.5361(15)1	As2	S3	2.269(3)
As4	As2	2.5476(14)	As2	S2	2.275(2)
As4	S4	2.267(2)	As1	S2	2.244(3)
As4	S1	2.282(2)	As1	S1	2.268(2)
Br2	Cu1	2.3998(15)	Cu1	S3	2.325(3)
Br2	Cu2	2.3876(16)	Cu1	S1	2.347(3)
As3	As1	2.5501(14)	Cu2	S4[2]	2.326(2)
As3	S4	2.270(2)	Cu2	S2[3]	2.293(3)

[1]1-x,1/2+y,1-z; [2]+x,1+y,+z; [3]1+x,+y,+z

***Table A.25**: Selected bond angles for $(CuBr)_2 \cdot (As_4S_4)$ at 123 K.*

Atom	Atom	Atom	Angle/°	Atom	Atom	Atom	Angle/°
Cu1	Br1	Cu2	144.39(6)1	S12	Cu1	Br2	120.60(8)
S4	As4	As2	100.86(7)	Br2	Cu2	Br1[3]	108.86(6
S4	As4	S1	89.52(9)	S44	Cu2	Br1[3]	103.29(8)
S1	As4	As2	100.32(7)	S44	Cu2	Br2	118.31(8)
Cu2	Br1	Cu1	98.83(5)	S2	Cu2	Br1[3]	97.26(8)
S4	As3	As1	97.21(7)	S2	Cu2	Br2	128.43(8)
S3	As3	As1	99.72(7)	S2	Cu2	S44	96.58(9)
S3	As3	S4	92.93(9)	As4	S4	As3	102.83(9)
S3	As2	As4	97.57(7)	As4	S4	Cu2[5]	99.14(9)
S3	As2	S2	94.66(9)	As3	S4	Cu2[5]	109.98(10)
S2	As2	As4	97.88(7)	As3	S3	As2	103.72(10)
S2	As1	As3	100.55(7)	As3	S3	Cu1	110.80(10)
S2	As1	S1	92.85(9)	As2	S3	Cu1	119.08(11)
S1	As1	As2	99.34(7)	As2	S2	Cu2	115.88(11)
Br1	Cu1	Br1	116.43(6)	As1	S2	As2	102.91(10)
S3	Cu1	Br1	95.38(7	As1	S2	Cu2	108.82(10)
S3	Cu1	Br2	122.14(8)	As4	S1	Cu1[6]	101.13(9)
S3	Cu1	S1	95.53(9)2	As1	S1	As4	101.61(10)
S1	Cu1	Br1	101.74(7)	As1	S1	Cu1[6]	106.78(10)

[1]1-x,1/2+y,1-z; [2]+x,1+y,+z; [3]1-x,-1/2+y,1-z; [4]1+x,+y,+z; [5]-1+x,+y,+z; [6]+x,-1+y,+z

***Table A.26**: Fractional Atomic Coordinates (* 10^4) and equivalent Isotropic Displacement Parameters (Å^2* 10^3) for $(CuBr)_2 \cdot (As_4Se_3)$ at 123 K.*

Atom	*Wyckoff*	*x*	*y*	*z*	*U(eq)*
As1	2i	7435(4)	5700(3)	1025.3(19)	16.9(6)
As2	2i	7487(4)	9136(3)	1087.2(19)	17.7(6)
As3	2i	4651(4)	7329(3)	3924.2(18)	15.7(6)
As4	2i	4135(4)	7516(3)	907.0(18)	16.7(6)
Se1	2i	6751(4)	4799(3)	2951.2(17	15.2(6)
Se2	2i	6901(4)	9768(3)	3040.3(17)	16.7(6)
Se3	2i	2055(4)	7544(3)	2764.5(17)	15.5(6)
Cu1	2i	4214(5)	12176(4)	3005(3)	19.1(7)
Cu2	2i	587(6)	4507(4)	3096(3)	22.3(8)
Br1	2i	2165(4)	12428(3)	1453.7(17)	18.6(6)
Br2	2i	1232(4)	2510(3)	4590.9(17)	19.2(6)

***Table A.27**: Anisotropic Displacement Parameters (Å^2* 10^3) for $(CuBr)_2 \cdot (As_4Se_3)$ at 123 K.*

Atom	***U_{11}***	***U_{22}***	***U_{33}***	***U_{23}***	***U_{13}***	***U_{12}***
As1	16.6(13)	16.8(11)	16.6(11)	-2.4(7)	-1.4(9)	4.1(8)
As2	17.1(13)	16.3(11)	19.4(12)	2.4(8)	-2.9(10)	-1.8(9)
As3	16.6(13)	16.0(11)	14.6(11)	0.1(7)	-3.3(9)	1.3(8)
As4	16.5(13)	17.7(11)	16.3(11)	0.9(7)	-4.0(9)	0.8(8)
Se1	14.9(12)	12.9(9)	17.8(11)	1.0(7)	-3.3(9)	0.0(8)
Se2	16.7(13)	13.8(10)	20.3(11)	-1.1(7)	-5.3(9)	0.4(8)
Se3	13.8(12)	14.9(10)	17.7(11)	0.6(7)	-3.1(9)	0.9(8)
Cu1	16.0(17)	18.9(15)	21.0(16)	-0.5(11)	-0.8(13)	3.3(12)
Cu2	24(2)	18.4(15)	26.3(17)	3.4(11)	-9.1(15)	-0.9(13)
Br1	22.2(13)	17.7(10)	16.2(10)	-0.5(7)	-4.2(9)	1.7(8)
Br2	19.9(13)	23.3(11)	13.7(10)	1.9(7)	-1.8(9)	3.7(8)

***Table A.28**: Selected bond lengths for $(CuBr)_2 \cdot (As_4Se_3)$ at 123 K.*

Atom	Atom	Length/ Å	Atom	Atom	Length/ Å
Se1	As3	2.422(3)	Br2	$Cu1^1$	2.6724
Se1	As1	2.402(3)	Br2	Cu2	2.7876
Se1	$Cu1^1$	2.485(3)	Se1	As3	2.5866
Se1	$Cu2^2$	2.449(4)	Se1	As2	2.5802
Se3	As4	2.388(3)	Se1	Cu1	2.6357
Se3	As3	2.372(3)	As4	As1	2.6196
Se3	Cu2	2.393(3)	As4	As2	2.2994
Br1	Cu1	2.509(4)	As1	As2	2.4015
Br1	$Cu2^3$	2.560(4)	Cu1	$Cu2^3$	2.3648

^{1}+x,-1+y,+z; ^{2}1+x,+y,+z; ^{3}+x,1+y,+z

***Table A.29**: Selected bond angles for $(CuBr)_2 \cdot (As_4Se_3)$ at 123 K.*

Atom	Atom	Atom	Angle/°	Atom	Atom	Atom	Angle/°
As3	Se1	$Cu1^1$	106.94(12)	Se2	As2	As4	103.22(11)
As3	Se1	$Cu2^2$	117.31(11)	Se2	As2	As1	103.44(10)
As1	Se1	As3	105.11(10)	As4	As2	As1	59.49(9)
As1	Se1	$Cu1^1$	102.27(11)	Se1	Cu1	Br1	111.10(12)
As1	Se1	$Cu2^2$	96.27(12)	Se1	Cu1	$Cu2^3$	92.99(12)
Cu2	Se1	$Cu1^1$	125.01(13)	Br1	Cu1	$Cu2^3$	57.43(11)
As4	Se3	Cu2	105.43(12)	Br2	Cu1	$Se1^3$	109.13(13)
As3	Se3	As4	105.51(12)	Br2	Cu1	Br2	100.21(14)
As3	Se3	Cu2	98.06(11)	Br2	Cu1	$Cu2^3$	54.64(11)
Cu1	Br1	$Cu2^3$	66.88(12)	Se2	Cu1	Se1	96.17(13)
Cu2	Br2	$Cu1^1$	70.54(13)	Se2	Cu1	Br1	121.24(14)
As3	Se2	As2	105.13(10)	Se2	Cu1	Br2	118.89(14)
As3	Se2	Cu1	100.85(12)	Se2	Cu1	$Cu2^3$	170.35(15)
As2	Se2	Cu1	95.25(12)	Se1	Cu2	Br1	102.19(12)
Se3	As4	As1	104.57(11)	Se1	Cu2	$Cu1^1$	147.08(14)
Se3	As4	As2	102.43(11)	Se3	Cu2	$Se1^3$	105.69(13)
As1	As4	As2	60.70(9)	Se3	Cu2	$Br1^1$	109.85(15)
Se3	As3	Se1	96.19(10)	Se3	Cu2	Br^2	123.47(14)
Se3	As3	Se2	95.99(10)	Se3	Cu2	$Cu1^1$	105.01(15)
Se2	As3	Se1	97.19(11)	Br1	Cu2	$Cu1^1$	55.69(11)

Se1	As1	As4	102.13(12)	Br2	Cu2	Se1[4]	114.48(15)
Se1	As1	As2	103.34(11)	Br2	Cu2	Br1[1]	98.94(13)
As4	As1	As2	59.80(9)	Br2	Cu2	Cu1[1]	54.82(11)

[1]+x,-1+y,+z; [2]1+x,+y,+z; [3]+x,1+y,+z; [4]-1+x,+y,+z

***Table A.30**: Fractional Atomic Coordinates (* 10^4) and equivalent Isotropic Displacement Parameters (Å^2* 10^3) for $(CuI)_7(ZnI_2)_3(As_4Se_3)$ at 123 K.*

Atom	*Wyckoff*	*x*	*y*	*z*	*U(eq)*
I1	96h	0.17949(5)	0.11524(5)	0.00781(5)	0.0192(2)
I2	8a	0	0	0	0.0401(14)
Zn	24d	0.25	0	0	0.0121(7)
Cu1	32e	0.07290(9)	0.07290(9)	0.07290(9)	0.0140(8)
Cu2	32e	0.0829(6)	-0.0829(6)	0.0829(6)	0.071(7)
Cu3	32e	0.12596(16)	0.12596(16)	0.12596(16)	0.0370(10)
Cu4	32e	0.12413(15)	-0.12413(15)	0.12413(15)	0.0399(11)
As1	32e	0.3131(3)	0.1869(3)	-0.1869(3)	0.036(3)
As2	96h	0.3598(10)	0.2754(9)	-0.2513(19)	0.146(13)
Se1	96h	0.2517(2)	0.2953(2)	-0.1510(2)	0.0047(13)

***Table A.31**: Anisotropic Displacement Parameters (Å^2* 10^3) for for $(CuI)_7(ZnI_2)_3(As_4Se_3)$ at 123 K.*

Atom	U_{11}	U_{22}	U_{33}	U_{23}	U_{13}	U_{12}
I1	16.374	19.793	20.277	-1.883	0.142	-1.883
I2	44.664	44.664	44.664	0	0	0
Zn	9.232	13.02	13.02	0	0	0
Cu1	12.708	12.708	12.708	2.095	2.095	2.095

Cu2	89.954	89.954	89.954	-1.294	-1.294	-1.294
Cu3	34.843	34.843	34.843	-1.933	-1.933	-1.933
Cu4	40.948	40.948	40.948	-0.604	-0.604	-0.604
As1	32.746	32.746	32.746	-3.981	-3.981	-3.981
As2	305.062	167.535	130.569	-125.148	1.606	14.627
Se1	12.672	8.147	8.797	2.838	-3.134	2.567

***Table A.32**: Selected bond lengths for $(CuI)_7(ZnI_2)_3(As_4Se_3)$ at 123 K.*

Atom	Atom	Length/ Å	Atom	Atom	Length/ Å
Zn	I1	2.628	I1	Cu3	2.527
Cu1	I1	2.558	I1	Cu4	2.786
Cu2	I1	2.664	Cu4	Se	2.918
I2	Cu1	2.446	As2	Cu3	2.998
I2	Cu2	2.677	As1	Cu3	1.962
Cu1	Cu2	2.963	As2	As2	2.542
Cu1	Cu3	1.797	As1	As2	2.443

***Table A.33**: Selected bond angles for $(CuI)_7(ZnI_2)_3(As_4Se_3)$ at 123 K.*

Atom	Atom	Atom	Angle/°	Atom	Atom	Atom	Angle/°
Cu2	I2	Cu1	70.529(4)	Zn	I1	Cu1	100.164(1)
Cu1	I2	Cu1	109.47(1)	I1	Zn	I1	105.827(2)
Cu2	I2	Cu2	109.50(2)	I1	Zn	I1	117.034(2)
I1	Cu2	I1	116.063(1)				
I1	Cu2	Cu1	105.232(2)				
Cu1	Cu2	I1	53.746(2)				
Cu2	I1	Cu1	69.118(2)				
Cu2	I1	Cu4	32.109(1)				
Cu1	I1	Cu3	41.378(1)				
Cu1	I1	Zn	109.705(2)				
Cu4	I1	Zn	101.164(1)				

***Table A.34**: Fractional Atomic Coordinates (* 10^2) and equivalent Isotropic Displacement Parameters (Å^2* 10^2) for $(CuI)_7(CdI_2)_3(As_4Se_3)$ at 123 K.*

Atom	*Wyckoff*	*x*	*y*	*z*	*U(eq)*
I1	8b	25	25	25	2.7182
I2	96h	24.027	7.3461	13.1283	1.4511
Cd	24d	25	0	25	2.3884
Cu3	32e	17.8011	17.8011	17.8011	3.7836
Cu2	32e	11.879	11.879	11.879	6.852
Cu1	32e	31.8277	18.1723	18.1723	10.3925
As1	32e	6.2522	6.2522	6.2522	18.7762
As2	96h	-3.4782	2.6602	13.243	39.803
Se1	96h	2.1851	-12.9052	22.3161	102.5692

***Table A.35**: Anisotropic Displacement Parameters (Å^2* 10^3) for for $(CuI)_7(CdI_2)_3(As_4Se_3)$ at 123 K.*

Atom	U_{11}	U_{22}	U_{33}	U_{23}	U_{13}	U_{12}
I1	27.182	27.182	27.182	0	0	0
I2	140	140	140	0	0	0
Cd	23.642	23.642	23.642	0	0	0
Cu1	99.449	99.449	99.449	-14.916	-14.916	-14.916
Cu2	79.795	79.795	79.795	-14.883	-14.883	-14.883
Cu3	49.796	49.796	49.796	24.227	24.227	24.227
As1	226.03	226.03	226.03	-83.528	-83.528	-83.528
As2	259.635	824.242	199.344	256.003	168.279	187.774
Se1	25.06	390.679	2261.1	-700.90	-31.227	-700.9

***Table A.36**: Selected bond lengths for $(CuI)_7(CdI_2)_3(As_4Se_3)$ at 123 K.*

Atom	Atom	Length/ Å	Atom	Atom	Length/ Å
I1	Cu1	2.352	Cu2	I2	2.566
I1	Cu3	2.451	Cu2	As2	2.872
Cu1	Cu3	2.760	Cu2	As1	1.798
Cu3	Cu2	2.001	As2	As2	2.561
Cu1	I2	2.799	As1	As1	2.663
Cu3	I2	2.571	Cu2	Se	2.650
Cd	I2	2.759			

***Table A.37**: Selected bond angles for $(CuI)_7(CdI_2)_3(As_4Se_3)$ at 123 K.*

Atom	Atom	Atom	Angle/°	Atom	Atom	Atom	Angle/°
Cu1	I1	Cu1	109.47(2)	Cu1	Cu3	Cu2	127.400(2)
Cu3	I1	Cu3	109.47(2)	Cu3	Cu1	Cu2	92.980(2)
Cu1	Cu3	Cu1	86.94(1)	I2	Cu1	Cu3	110.538(2)
Cu2	Cu3	I2	66.953(2)	I2	Cu3	Cu1	111.610(3)
I2	Cu3	I2	105.670(2)	Cd	I2	Cu3	98.336(3)
Cu1	Cu3	Cu2	127.401(1)				
Cu3	I2	Cu1	61.67(1)				
I2	Cd	I2	106.00(2)				
I2	Cd	I2	116.661(1)				

***Table A.38**: Fractional Atomic Coordinates (* 10^2) and equivalent Isotropic Displacement Parameters ($Å^2$* 10^2) for $(CuI)_7(HgI_2)_3(As_4Se_3)$ at 123 K.*

Atom	*Wyckoff*	*x*	*y*	*z*	*U(eq)*
I1	8b	25.5666	12.9076	7.1874	3.8648

I2	96h	0.25	0.25	0.25	4.0636
Cd	24d	0.25	0.25	0	5.4702
Cu1	32e	17.2173	17.2173	17.2173	4.2157
Cu2	32e	32.2721	17.7279	17.7279	3.1534
Cu3	32e	12.6575	12.6575	12.6575	4.6904
As1	32e	6.0613	6.0613	6.0613	3.17504
As2	96h	-1.2427	11.0165	-3.1286	3.7995
Se1	96h	-1.9025	-3.1949	11.3087	3.7995

***Table A.39**: Anisotropic Displacement Parameters ($Å^2 * 10^3$) for for $(CuI)_7(HgI_2)_3(As_4Se_3)$ at 123 K.*

Atom	U11	U22	U33	U23	U13	U12
I1	3.9381	3.9381	3.9381	0	0	0
I2	4.2388	4.2388	4.2388	0	0	0
Cd	5.4634	5.4634	5.4634	0	0	0
Cu1	4.2157	4.2157	4.2157	0	0	0
Cu2	3.1534	3.1534	3.1534	-0.1259	-0.1259	-0.1259
Cu3	4.6904	4.6904	4.6904	0	0	0
As1	31.7504	31.7504	31.7504	0	0	0
As2	3.7995	3.7995	3.7995	0	0	0
Se1	3.7995	3.7995	3.7995	0	0	0

***Table A.40:** Selected bond lengths for $(CuI)_7(HgI_2)_3(As_4Se_3)$ at 123 K.*

Atom	Atom	Length/ Å	Atom	Atom	Length/ Å
Cu1	Cu2	2.977	I1	Hg	2.780
I2	Cu1	2.662	Cu	As1	2.940
I2	Cu2	2.488	Cu	As2	2.180

Cu2	I1	2.749	Cu	Se	2.966
Cu1	I1	2.599	As1	As1	2.467
Cu2	I1	2.749	As2	Se	2.516
I1	Cu3	2.589			

Table A.41: *Selected bond angles for $(CuI)_7(HgI_2)_3(As_4Se_3)$ at 123 K.*

Atom	Atom	Atom	Angle/°	Atom	Atom	Atom	Angle/°
Cu1	I2	Cu1	109.471(3)	I1	Hg	I1	105.118(2)
Cu2	I2	Cu2	109.471(2)	I1	Hg	I1	118.580(3)
Cu2	I2	Cu1	70.529(2)	I1	Cu3	I1	111.702(2)
Cu2	Cu1	I1	58.607(1)				
Cu2	Cu1	I2	51.990(1)				
I1	Cu1	I1	111.034(2)				
I1	Cu1	Cu2	109.512(2)				
Cu1	I1	Cu3	34.995(4)				

Table A.42*: Fractional Atomic Coordinates (* 10^4) and equivalent Isotropic Displacement Parameters ($Å^2$* 10^4) for $[(Hg_2I_6)(HgI_2)][Cu(MeCN)_4]$at 123 K.*

Atom	*Wyckoff*	*x*	*y*	*z*	*U(eq)*
Hg1	16e	2939.2(4)	6250	6250	22.85(8)
Hg2	8a	6250	6250	6250	25.46(11)
I3	16f	1250	5431.0(2)	6250	19.87(10)
I4	32h	3948.3(5)	6248.7(2)	5362.5(2)	21.71(8)
I5	16f	6250	5300.3(2)	6250	23.36(12)
Cu6	16f	1250	3793.8(5)	6250	20.7(2)
N9	32h	147(6)	4185(2)	5840(2)	20.7(10)
C6	16f	-564(7)	4383(3)	5606(3)	20.7(11)
C1	32h	-1418(6)	4630(3)	5317(3)	25.2(14)
N2	32h	2369(6)	3382(2)	5860(2)	20.2(10)
C2	32h	3073(6)	3151(3)	5654(3)	19.4(11)
C3	16f	3922(8)	2848(3)	5393(4)	28.7(16)

***Table A.43**: Anisotropic Displacement Parameters ($Å^2 * 10^3$) for $[(Hg_2I_6)(HgI2)][Cu(MeCN)_4]$ at 123 K.*

Atom	U_{11}	U_{22}	U_{33}	U_{23}	U_{13}	U_{12}
Hg1	25.17(16)	28.64(17)	14.75(12)	1.15(13)	0	0
Hg2	23.1(2)	12.53(16)	40.7(3)	0	0	0
I3	21.8(2)	13.68(19)	24.2(2)	0	2.1(2)	0
I4	22.53(19)	26.53(19)	16.06(15)	1.40(15)	2.99(1)	-0.23(1)
I5	27.3(3)	11.97(19)	30.8(3)	0	-2.1(3)	0
Cu6	20.5(5)	19.8(5)	21.8(5)	0	-1.1(4)	0
N9	22(3)	20(2)	20(2)	0.3(18)	0(2)	1.1(19)
C6	16(2)	25(3)	21(3)	-3(2)	0(2)	1(2)
C1	13(3)	32(4)	31(4)	-3(3)	-6(2)	6(2)
N2	22(3)	18(2)	21(2)	0.4(18)	1(2)	0.1(18)
C2	17(3)	20(3)	21(3)	2(2)	-1(2)	-4(2)
C3	22(4)	29(3)	35(4)	9(3)	4(3)	7(3)

***Table A.44**: Selected bond lengths for $[(Hg_2I_6)(HgI_2)][Cu(MeCN)_4]$ at 123 K.*

Atom	Atom	Length/ Å	Atom	Atom	Length/ Å
Hg1	$I3^1$	2.9106(5)	Cu6	N9	1.976(7)
Hg1	I3	2.9105(5)	Cu	N2	1.988(6)
Hg1	$I4^2$	2.6958(5)	Cu6	N24	1.988(7)
Hg1	I4	2.6959(5)	N9	C6	1.152(10)
Hg1	I5	2.5974(6)	C6	C1	1.406(11)
Hg1	$I5^3$	2.5974(6)	N2	C2	1.149(10)
Cu6-	$N9^4$	1.976(7)	C2	C3	1.444(12)

[1]1/4-x,5/4-y,+z; [2]+x,5/4-y,5/4-z; [3]5/4-x,5/[4]-y,+z; 41/4-x,+y,5/4-z

***Table A.45**: Selected bond angles for [(Hg$_2$I$_6$)(HgI$_2$)][Cu(MeCN)$_4$ at 123 K.*

Atom	Atom	Atom	Angle/°	Atom	Atom	Atom	Angle/°
I3	Hg1	I3^1	100.626(19)	N9	Cu6	N2	112.0(3)
I4^2	Hg1	I3^1	105.189(12)	N94	Cu6	N2	103.8(3)
I4	Hg1	I3	105.188(12)	N9	Cu6	N2^4	103.8(3)
I4	Hg1	I3^1	105.309(12)	N9^4	Cu6	N2^4	112.0(3)
I4^2	Hg1	I3	105.309(12)	N2	Cu6	N2^4	111.0(4)
I4^2	Hg1	I3	131.36(3)	C6	N9	Cu6	174.5(7)
I5	Hg2	I4	180.0	N9	C6	C1	179.2(10)
Hg1	I3	I5^3	79.38(2)	C2	N2	Cu6	175.7(7)
N9^4	Cu6	Hg^1	114.5(4)	N2	C2	C3	177.9(8)

11/4-x,5/4-y,+z; 2+x,5/4-y,5/4-z; 35/4-x,5/4-y,+z; 41/4-x,+y,5/4-z

***Table A.46**: Fractional Atomic Coordinates (* 10^4) and equivalent Isotropic Displacement Parameters (Å^2* 10^4) for As$_2$Cu$_4$I$_2$S$_4$ at 123 K.*

Atom	*Wyckoff*	*x*	*y*	*z*	*U(eq)*
I	2i	2539.5(4)	9810.6(8)	635.5(4)	10.37(8)
As	2i	8470.7(7)	1684.9(13)	3583.9(7)	7.81(12)
Cu1	2i	3311.4(9)	2327.8(18)	3642.6(9)	11.44(16)
Cu2	2i	5393.7(13)	6518(2)	1326.0(11)	22.7(2)
S1	2i	6150.7(17)	4612(4)	3929.5(16)	9.1(2)
S2	2i	9255.2(17)	204(3)	6333.2(16)	8.3(2)

Table A.47: *Anisotropic Displacement Parameters ($Å^2 * 10^3$) for $As_2Cu_4I_2S_4$ at 123 K.*

Atom	***U_{11}***	***U_{22}***	***U_{33}***	***U_{23}***	***U_{13}***	***U_{12}***
I	8.92(13)	13.0(2)	9.32(13)	-0.65(12)	2.47(9)	0.33
As	5.23(19)	9.6(3)	8.8(2)	-0.61(19)	1.93(16)	-0.03(1)
Cu1	6.8(3)	13.8(4)	14.0(3)	-0.6(3)	3.0(2)	0.2(2)
Cu2	21.2(4)	32.4(6)	16.2(4)	7.0(4)	7.9(3)	14.2(4)
S1	4.5(4)	12.4(7)	10.7(5)	0.2(5)	2.3(4)	0.8(5)
S2	5.5(4)	10.3(8)	9.4(5)	-0.7(5)	2.5(4)	0.1(4)

Table A.48: *Selected bond lengths for $As_2Cu_4I_2S_4$ at 123 K.*

Atom	Atom	Length/ Å
I	$Cu1^1$	2.6613(8)
I	$Cu2^2$	2.5559(9)
I	Cu2	2.5361(9)
As	S1	2.2356(15)
As	S2	2.2895(14)
As	$S2^3$	2.3199(15)
Cu1	S1	2.2811(15)
Cu1	$S1^4$	2.3094(16)
Cu1	$S2^5$	2.2989(15)
Cu2	S1	2.2510(16)

^{1}+x,1+y,+z; ^{2}1-x,1/2+y,-z; ^{3}2-x,1/2+y,1-z; ^{4}1-x,-1/2+y,1-z; ^{5}1-x,1/2+y,1-z

Table A.49: *Selected bond angles for $As_2Cu_4I_2S_4$ at 123 K.`*

Atom	Atom	Atom	Angle/°	Atom	Atom	Atom	Angle/°
$Cu2^1$	I	$Cu1^2$	114.09(3)	I	Cu2	I7	127.99(4)
Cu^2	I	$Cu2^2$	94.42(3)	S1	Cu2	I7	114.52(5)
Cu^2	I	$Cu2^1$	76.42(2)	S1	Cu2	I	117.39(5
S1	As	$S2^3$	96.24(6)	As	S1	$Cu1^7$	117.53(6)
S1	As	S2	95.01(5)	As	S1	Cu1	112.60(8)
S2	As	$S2^3$	99.90(4)	As	S1	$Cu2^6$	98.73(5)

S1	Cu1	I5	120.24(5)	Cu1	S1	Cu1[3]	108.49(5)
S1	Cu1	I5	107.22(4	Cu2	S1	Cu1[4]	123.10(9)
S1	Cu1	S1[4]	101.54(4)	Cu2	S1	Cu1[3]	94.06(6)
S1	Cu1	S2[6]	115.78(6)	As	S2	As8	105.00(5)
S2	Cu1	I5	105.57(4)	As	S2	Cu1[4]	99.60(6)
S2	Cu1	S1[4]	107.05(5)	Cu1	S2	As8	98.77(6)

[1]1-x,1/2+y,-z; [2]+x,1+y,+z; [3]2-x,1/2+y,1-z; [4]1-x,-1/2+y,1-z; [5]+x,-1+y,+z; [6]1-x,1/2+y,1-z; [7]1-x,-1/2+y,-z; [8]2-x,-1/2+y,1-z